UCSF
UC San Francisco Electronic Theses and Dissertations

Title
Visual motion signals underlying pursuit eye movements in monkeys

Permalink
https://escholarship.org/uc/item/7m66479m

Author
Krauzlis, Richard J.

Publication Date
1991

Peer reviewed|Thesis/dissertation

eScholarship.org Powered by the California Digital Library
University of California

Visual motion signals underlying pursuit eye movements in monkeys: behavior, models, and neural responses in the cerebellum

by

Richard J. Krauzlis

DISSERTATION

Submitted in partial satisfaction of the requirements for the degree of

DOCTOR OF PHILOSOPHY

in

Neuroscience

in the

GRADUATE DIVISION

of the

UNIVERSITY OF CALIFORNIA

San Francisco

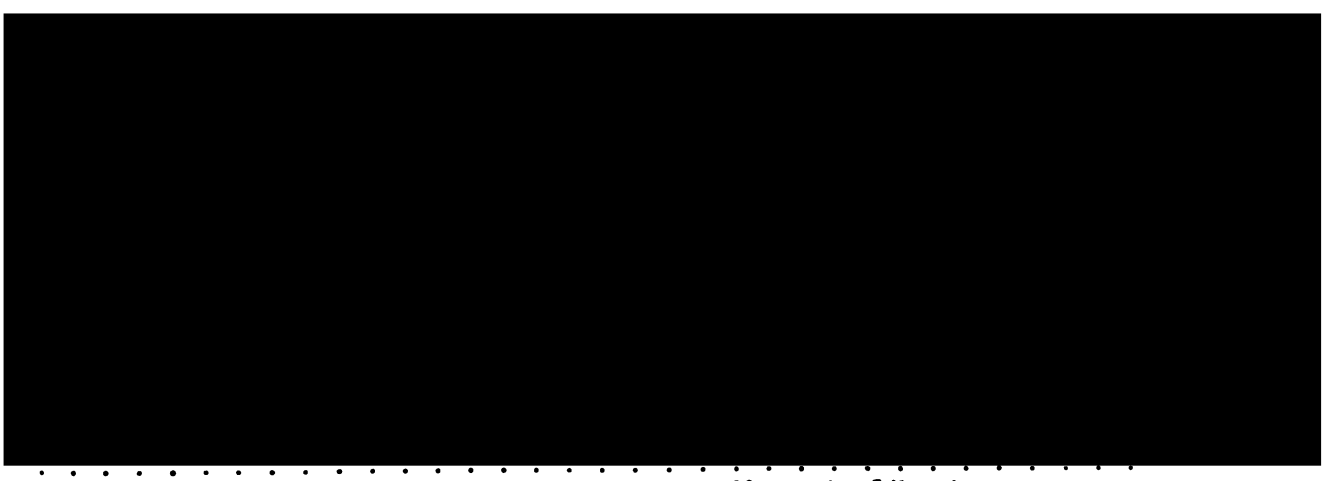

Date University Librarian

Degree Conferred: 12/31/91

Copyright 1991

by

Richard J. Krauzlis

To my parents

They encouraged my curiosity when I was small

and that has made all the difference in my life

Acknowledgements

I would like to thank my graduate advisor, Steve Lisberger, for his invaluable support and critical guidance. I would also like to thank the members of my committee for their helpful comments and for many thoughtful conversations: Roger Nicoll, Mike Stryker, Mike Merzenich and Bill Newsome. I would also like to thank my undergraduate advisor, Carl Olson, without whose influence I probably never would have entered graduate school. I thank the members of the lab for their help, their friendship and for putting up with my sometimes strange behavior: Kay Logan, Sascha duLac, Helen Bronte-Stewart, Dianne Broussard, Terri Pavelko and Josh Schwartz. I would especially like to thank four very close friends: David Perkel, Lee Stone, Alfredo Franco, and Coban Tun. Without their support, I would not have finished this thesis. Finally, I would like to thank Tamar Boursalian, whose presence in my life in the past year has been like a gift from heaven.

Visual motion signals underlying pursuit eye movements in monkeys: behavior, models, and neural responses in the cerebellum

Richard J. Krauzlis

Pursuit eye movements are defined as the ocular tracking of small moving targets against textured visual backgrounds. Pursuit eye movements are well-developed only in primates and involve neural pathways including visual areas in the cerebral cortex and regions of the cerebellum that can directly act to move the eyes. We have examined the visual motion signals underlying pursuit and the neural processing of these signals in alert monkeys using a combination of behavioral experiments, computer simulations, and recordings from isolated units in the cerebellum.

Our results suggest that a specific set of signals is used by the visual system to encode the motion of the target. These visual signals are related to the velocity and the acceleration of the target's image on the retina. A computer model that includes a sensitivity to these visual signals is able to reproduce several distinguishing features of pursuit. In addition, we have demonstrated that these same visual signals may be encoded by neurons in the cerebellum to provide a command to smoothly move the eyes. Recordings in the flocculus and ventral paraflocculus of the cerebellum indicate that each of the visual signals used for pursuit is present in the simple-spike firing rate of Purkinje cells. Furthermore, the output provided by these Purkinje cells displays a spatial organization that is consistent with the reference frame defined by the vestibular pathways in the brainstem. These findings represent an initial attempt to map a general conceptual scheme for the control of pursuit eye movements onto the anatomical substrates for pursuit in the brain.

Table of contents

List of tables and figures

page

Visual motion signals underlying the initiation of pursuit

General Introduction

"In order to understand how the brain works,
you have to study the brain while it's working."[1]

It is bold and perhaps naive to presume that one day we may understand how the assemblage of approximately 100 billion neurons contained within the primate brain accomplishes the constellation of remarkable feats which comprise our "behavior" and yet, that understanding is the goal of behavioral neuroscience. The achievement of this goal can be aided by many approaches, including the use of in vitro preparations and simulations of brain function on the computer. Ultimately, however, the study of how the brain controls behavior requires that we examine the brain in the act -- as it receives, processes and executes the signals that underly the generation of behavior.

In the present work, we have examined the neural control of smooth pursuit eye movements in monkeys. Smooth pursuit is defined canonically as the ocular tracking of small moving targets against textured visual backgrounds. However, behind this austere definition lies a rich set of questions. How is the target defined? How is the motion of the target represented by the activity of neurons in the visual system? How are these sensory signals transformed into commands to move the eyes? How might cognitive factors influence the processing of either the sensory or the motor signals used to produce pursuit? The thesis presented here is that a set of

---

[1] Steve Lisberger, Nature conference on the brain, 1989.

specific signals is used by the visual system to encode the motion of the target. Furthermore, these same visual signals are conveyed by neurons in the cerebellum to provide a command to smoothly move the eyes. Our hope is that a thorough understanding of how these signals are generated and transformed by the brain to produce pursuit eye movements may provide a useful model for understanding the control of voluntary movements in general.

Disbelief is a common reaction to the suggestion that the study of eye movements can provide real insight into the control of complex behaviors. After all, eye movements are so automatic it may seem unlikely that they have much in common with the skillfull movements we most often associate with complex behaviors. However, the ease with which eye movements are performed belies their significance. The control of eye movements seems less complex than other behaviors because they are taken for granted. The accuracy of eye movements is a precondition for normal vision, because movements of the eyes are needed to place the image of objects of interest on the fovea and to keep them there. Since vision is the premier guiding sense in primates, even slight disruptions in the control of eye movements can lead to major disruptions in the performance of many other behaviors. The transformation of signals underlying eye movements therefore reflects a finely tuned process that is fundamental to other, less practiced, movements. Just as the examination of the tools used everyday by members of a foreign culture can provide insights into the structure of their society, so we believe that the study of eye movements may provide real insight into the problems confronted and solved by the brain in the control of behavior.

Study of the control of eye movements also has one important advantage over study of most other kinds of movements. Unlike the control of movements of the arms and legs, the control of eye movements is not confronted with the problem of variable loads. The mass associated with the eyes is not subject to change, since the eyes are not used to pick up objects. The eyes are used to point at objects, but unlike the limbs, the center of mass of the eyes does not change very much when the eyes are pointed. This means that feedback signals from the muscles of the eye play only a small role in the control of eye movements. In studying eye movements, we can therefore concentrate on issues associated with the direct transformation of sensory signals into commands for movement.

In the current work, we use several approaches to examine how visual information related to the motion of the target is used to provide commands for pursuit eye movements. We begin with a study of the general features associated with the performance of pursuit eye movements. In chapter one, we examine the trajectories of eye velocity evoked by several types of target motions. The set of target motions consists of targets initially at rest that then either move at a constant velocity or accelerate smoothly up to some constant velocity. Examination of the time-varying profiles of eye velocity evoked by these target motions allows us to identify three visual motion signals that underly the generation of pursuit eye movements. These visual motion signals are related to the velocity and the acceleration of the target's retinal image.

In the second chapter, we incorporate these visual motion signals into a general model of smooth pursuit eye movements. Through computer simulations we show that the model's ability to replicate some features of pursuit eye movements depends upon the inclusion of visual signals

encoding both image velocity and image acceleration. For example, the ability of the model to reproduce the high frequency oscillations often observed during pursuit requires the inclusion of a sensitivity to image acceleration. The model is also used to mimic the eye movements observed when pursuit is stopped. These features of smooth eye movements are not attributed to visual motion signals, but require the action of non-visual inputs. The role of these inputs in the model suggests alternate interpretations for the non-visual signals observed in extrastriate visual cortex.

In chapters three and four, we present data obtained by recording extracellularly in the flocculus and ventral paraflocculus of the cerebellum. We focused on these regions of the cerebellum, because they represent the most likely candidates for converting visual motions signals into commands for smooth eye movements. In chaper three, we examine the vectors for smooth eye movements defined in this part of the cerebellum. We recorded from Purkinje cells and mossy fibers to determine the spatial organization of the eye velocity and visual signals conveyed by these structures. Our results show that the output of the cerebellar flocculus and ventral paraflocculus are consistent with the reference frame defined by vestibular pathways in the brainstem.

Finally, in chapter four, we examine the visual motion signals conveyed by Purkinje cells in the flocculus and ventral paraflocculus. We recorded from Purkinje cells while the monkey smoothly tracked the same types of target motions that were used to identify the visual motion signals underlying pursuit in chapter one. We then used a distributed network model which incorporates these visual signals to describe the different types of firing rate profiles observed on floccular P-cells. Our results indicate that the firing rate of each P-cell in our sample can be accounted for by a

combination of visual motion signals and eye velocity. The analysis also indicates that each of the visual motion signals used for pursuit is represented in the output of the flocculus.

Our experiments represent an initial attempt to map the anatomical substrates for pursuit in the brain onto a general conceptual scheme for the control of pursuit eye movements. The ability to place the activity of individual cerebellar Purkinje cells in the context of a quantitative model for pursuit is an important step toward achieving a complete understanding of how the brain accomplishes pursuit. The delineation of how other brain regions complement the functions of the flocculus and ventral paraflocculus in the generation of pursuit is likely to provide a general understanding of how pathways from the cerebral cortex to the cerebellum control voluntary movements.

Chapter One

Visual motion signals underlying the initiation of pursuit

Summary and Conclusions

1. We used the monkeys' performance during the natural "open-loop" period of the initiation of pursuit to characterize the dynamics of the visual motion signals that drive pursuit eye movements. These data formed the basis for a model that describes how three types of visual inputs are each converted into commands for pursuit eye acceleration. Each visual input was characterized by examining the eye movement response to a different type of target motion.

2. The dynamics of the initial response to a constant velocity target depend upon how long the target is visible before it starts to move. If there is no delay between the appearance of the target and the onset of its motion, the first 100 ms of pursuit consists of a simple exponential rise in eye velocity that is proportional to image speed. If the motion onset delay is longer than 100 ms, the initial eye movement consists of two phases of eye acceleration. The later phase of eye acceleration occurs 40-100 ms after the onset of pursuit and remains proportional to image speed. The earlier phase occurs 0-40 ms after pursuit onset and has an amplitude that is relatively insensitive to image speed, but that is always larger than that seen when the motion onset delay is 0 ms.

3. The image velocity pathway in our model describes the later phase of eye acceleration evoked by constant velocity targets. The pathway converts the step in image velocity associated with the target motion into a scaled and smoothed step in eye acceleration. Integration of this eye acceleration

command produces a simulated eye velocity response that matches the exponential rise in eye velocity of the later component.

4. The image motion transient pathway describes the early phase of eye acceleration in the response to constant velocity targets. The pathway generates a biphasic eye acceleration command with an amplitude that saturates for image speeds over 15 °/s. Integration of this eye acceleration command produces a transient pulse of eye velocity that reaches a peak at 50-100 ms after the onset of the response.

5. The eye movements evoked by smoothly accelerating targets are only partially accounted for by the pursuit system's sensitivity to image velocity. The additional eye acceleration observed in the response to smoothly accelerating targets is described by the image acceleration pathway in our model. The pathway converts the ramp in image velocity associated with an accelerating target into a smoothed step command for eye acceleration.

6. The description of the effects of image motion on pursuit eye movements provided by our model may be useful for determining which features of pursuit eye movements are due to the processing of visual motion inputs and which are due to other inputs or to properties of the motor output pathways.

Introduction

During ocular tracking of small moving targets, monkeys and humans use a combination of saccadic and smooth pursuit eye movements to keep the retinal image of the target within the high acuity region near the fovea. Saccades are ballistic eye movements that correct position errors by quickly placing the image from stationary or moving targets on the fovea. In contrast, pursuit is a continuous, smooth eye motion that is elicited by moving visual targets and that stabilizes the moving target's image on the retina. During pursuit, any mismatch between the motion of the eye and the motion of the target results in motion of the target's retinal image. Pursuit can therefore be thought of as a negative-feedback system in which visual information about the motion of the target represents an error signal that drives corrective smooth eye movements.

Observations on pursuit eye movements in humans and monkeys have demonstrated that the pursuit system is actually more complex than a simple negative-feedback system. If, as simple models imply, pursuit were driven directly by a visual error signal, eye velocity would be related to image motion. In fact, eye acceleration, not eye velocity, is best related to image motion during smooth pursuit (Lisberger et. al. 1981; Lisberger and Westbrook 1985; Tychsen and Lisberger 1986; Carl and Gellman 1987). If pursuit were a simple negative-feedback system, eye velocity should be zero when the error signal is zero. In fact, when image motion during pursuit is eliminated by stabilizing the target's image on the retina, eye velocity is sustained almost perfectly (Morris and Lisberger 1987). These observations suggest that the basic negative-feedback structure of the pursuit system is

augmented by a form of memory that automatically maintains eye velocity so that it can be adjusted by visual motion inputs.

The neural substrate for pursuit has been identified through a combination of behavioral lesion studies and anatomical tracer experiments. Its primary components consist of pathways from the visual cortex to the cerebellum, which cause smooth eye movements by modulating activity in brainstem pathways to ocular motorneurons. The importance of the visual cortex has been revealed by studying the deficits in pursuit following lesions in extrastriate areas specialized for processing visual motion. Lesions of the middle temporal area (MT) produce at least a transient retinotopic deficit in the initiation of pursuit (Newsome et al. 1985). Ablation of the adjacent medial superior temporal area (MST) produces a more complicated syndrome consisting of a retinotopic deficit in the initiation of pursuit and a directional deficit in the maintenance of pursuit (Dursteler et al. 1987). There is also more recent evidence that the frontal eye fields (FEF) are important for normal pursuit (Lynch 1987; MacAvoy and Bruce 1988; MacAvoy et al. 1988). These cortical areas project to the dorsolateral pontine nuclei (DLPN) and the accessory optic system (AOS) which, in turn, project to widespread regions of the cerebellum, including the flocculus and vermis (Brodal 1978, 1979, 1982; Glickstein et. al. 1980, 1985; Huerta et al. 1986; Kunzle and Akert 1977; Leichnetz 1989; May and Andersen 1986; Langer et al. 1985; Ungerleider et. al. 1984). Neurons in the DLPN, AOS, flocculus, and vermis show activity related to smooth pursuit eye movements and lesions in these regions also cause severe deficits in the ability to generate pursuit (Kase et al. 1979; Lisberger and Fuchs 1978; Miles and Fuller 1975; Miles et. al. 1980; Mustari et al. 1988; Noda and Suzuki 1979; Stone and Lisberger 1990; Suzuki and Keller 1988a,b; Suzuki et al. 1981; Suzuki et al. 1984; Zee et al. 1981).

A major gap in our understanding of pursuit eye movements is how theoretical observations about the system are related to physiological data concerning its neural substrates. Beyond the general acknowledgement that visual motion is required for pursuit and that information about visual motion is evaluated by extrastriate visual areas, there is little information about what types of signals the pursuit system uses and what role particular brain regions play in processing these signals. The difficulty is that there are many possible ways to configure a system that can accomplish pursuit and that the available physiological data do not constrain the possibilities. For example, single-unit recording data from area MST and the cerebellar vermis have been interpreted as supporting a model of the pursuit system in which image motion is used to explicitly construct a neural signal encoding target velocity (Newsome et al. 1988; Suzuki and Keller 1988b). In contrast, recordings from the cerebellar flocculus have been discussed in the context of models in which raw visual signals lead directly to changes in eye velocity (Stone and Lisberger 1990).

In the first two chapters, we define a class of pursuit models that is based directly upon behavioral observations and that is also consistent with several key features of the pursuit system. In the first chapter, we examine the initiation of pursuit and present a quantitative description of the visual signals that drive pursuit eye movements. We develop this description by fitting eye velocity data with a model consisting of parallel pathways tht transform image motion into the observed eye velocity responses. Our analysis indicates that image acceleration, as well as image velocity, are used by the pursuit system. In the second chapter, we incorporate these quantitative descriptions of the visual motion processing for pursuit into a more complete model of the pursuit system. We then use the model to

explore which features of pursuit can be attributed to processing of the three visual motion inputs.

Methods

Preparation of animals

Experiments were conducted on four Rhesus monkeys weighing 5.0 - 8.0 kg. After initial training on a reaction-time task modified from Wurtz (1969), each monkey underwent sterile surgery while anesthetized with halothane. A coil of wire was implanted on the sclera of one eye (Judge et al. 1980) so that eye movements could be monitored with the magnetic search coil technique. Three or four bolts were implanted in the skull to anchor a receptacle for head restraint. During daily recording sessions lasting 2 - 3 hours, each monkey sat in a primate chair with his head fixed to the frame of the chair. A pair of 18 inch square coils were attached to the chair to generate the magnetic fields used to record eye position. The monkey's eye monitor was initially calibrated by having him perform the reaction time task with targets at known positions. Once the system was calibrated, we switched to a window task in which the monkey received rewards every 1500 ms as long as his eye position remained within 2 - 3 degrees of the target.

Presentation of visual stimuli

Visual stimuli were circular spots of light 0.1 to 0.5 degrees in diameter projected onto the back of a tangent screen. Stationary targets were generated by projecting the image of an LED directly onto the screen. Moveable targets were generated by reflecting a light beam off a pair of orthogonal, servo-controlled mirror galvanometers (General Scanning, CCX 650). Command signals for target position were provided by the digital-to-analog converter of

a laboratory computer. Actual target position was measured from feedback signals from the mirror galvanometers. The optical projection system was set up with both the mirror galvanometers and the monkey's eyes 114 cm from the screen to eliminate possible nonlinearities introduced by using a flat tangent screen. The experimental room was dimly illuminated by incandescent lights and the monkey was allowed binocular viewing. Under these conditions, the moveable target was 2.2 log units brighter than our perceptual threshold for detection of a 100 ms flash.

Visual stimuli for pursuit were presented in individual trials like that shown in Fig. 1.1. This paradigm is a modification of the step-ramp trial originally designed by Rashbass (1961). Each trial started when the monkey fixated a central red spot for a duration indicated by the dashed horizontal line along the eye position trace. After a random interval (500-1000 ms), a white target spot appeared at an eccentric position and remained stationary for an additional random interval (300-500 ms). To initiate pursuit, the fixation spot was extinguished and the target began to move. We generated step-ramp target motions with separate stationary and moving spots to avoid unwanted motion that is seen when a single spot is physically stepped away from straight-ahead gaze. Target motion lasted 600 - 800 ms. The monkey was rewarded with approximately 0.1 ml of water or juice at the end of each trial if he maintained his eye position within 2 degrees of the stationary target and within 3 - 4 degrees of the moving target throughout the trial. If his eye position strayed out of these windows, the trial was aborted and he received no reward. The only exception to the fixation requirement was a 300 - 400 ms grace period allowed at the onset of target motion.

Experiments consisted of a series of 1500 to 2500 trials selected in random order from a list of up to 40 trials. The randomization of trials

overcame a natural tendency of the monkeys to guess how the target would move, since the first part of each trial did not contain enough information for the monkey to identify the trial type. In addition, catch trials were also randomly inserted into the series at a lower frequency to eliminate nonspecific anticipatory responses and to verify that anticipatory responses were not contaminating our data. The catch trials required the monkey to maintain fixation of the central spot as an eccentric target flashed on for 300 - 500 ms.

In approximately half of the trials, we presented constant velocity targets using the step-ramp paradigm described above. Targets speeds in the constant velocity trials ranged from 2.5 to 30 ^{o}/s. In the remainder of the trials, we modified the step-ramp trial in one of three ways. First, we changed the duration of the interval when the fixation and target spots are both visible. In our usual step-ramp trial, this interval lasts 300 ms; in these modified trials, this interval ranged in duration from 0 to 1000 ms. Second, instead of having the target immediately assume a constant velocity, we accelerated the target smoothly from rest for 125 ms and then had the target continue at the velocity attained at the end of the period of acceleration. We presented targets accelerating at rates ranging from 45 to 400 ^{o}/s^{2}. Finally, instead of ending the trial with the target moving at a constant speed, we first stopped the target and required the monkey to fixate the stationary target for 300 to 500 ms. In these trials, the target was stepped forward as it stopped, in a manner complementary to the onset of target motion, to eliminate the need for a final corrective saccade at the end of the trial.

In two of the four monkeys, we also presented trials in which we used electronic feedback to generate sustained controlled image motion. Normally, because of the pursuit system's negative-feedback configuration,

the motion of the target's retinal image is equivalent to the target's physical motion only during the 80 to 120 ms period before the monkey's initiates pursuit. We extended this natural open-loop interval by adding the eye position signal obtained from the scleral search coil to the desired image motion. This resulted in a controlled motion of the target's retinal image, regardless of the monkey's eye velocity. We used these open-loop tracking conditions to examine the responses to constant image velocities of 5 to 30 $^{o}/s$ and constant image accelerations of 45 to 120 $^{o}/s^2$. Before each experiment, we calibrated the eye coil using procedures described by Morris and Lisberger (1987) and corrected for any nonlinearities in the monitoring system as necessary.

For each type of trial, we initially set the starting position of the target so that the target moved through the monkey's fixation point as he initiated pursuit. During several practice sessions, we examined the saccades made by the monkey during each trial, determined the size and direction of his saccades, and made fine adjustments in the starting position of the target to eliminate the need for corrective saccades. As a result of this procedure, in most of our records saccades either occurred 250 ms or longer after pursuit initiation or not at all.

Data acquisition and analysis

Experiments were conducted using a computer program that controlled the target motion, monitored the monkey's behavior, and sampled the data. Voltages related to eye position, eye velocity, target position and target velocity were digitized during the experiment at 1 ms intervals and stored on computer disk. The eye velocity signal was obtained by analog differentiation of the eye position voltage (DC to 50 HZ, -20 dB/decade).

Data were analyzed after the experiment using a computer. Records from each trial were displayed on a video screen using an interactive program that allowed the user to place cursors on the data traces. We analyzed our data in two ways, depending upon which features of the responses we wanted to examine. One analysis provided measurements of latency and eye acceleration in individual trials. We inspected each response on the video screen and placed cursors on the eye velocity records at the initiation of pursuit and at the onset of the first saccade. The computer calculated the eye acceleration as the change in eye velocity in 20 ms intervals following the initiation of pursuit and also calculated the average latency to initiate pursuit. Intervals were not included in the analysis if they overlapped the first saccade. A second analysis was used to obtain averaged traces. Each individual trial was again displayed on the screen and inspected. If the pursuit response began with a saccade or if pursuit was interrupted by a saccade occurring earlier than 100 ms after pursuit initiation, the trial was discarded. Approximately 5 to 10% of the trials were discarded because of early saccades. For the remaining trials, we marked the beginning and end of each saccadic eye movement in the eye velocity trace. The computer removed the saccade and replaced it with an eye velocity segment that connected the eye velocity at the beginning and end of the saccade. Trials of the same type were aligned on the onset of target motion and averaged together to obtain the mean and SD for each ms interval of the record.

Generation of modeled responses

Averaged eye velocity responses were further analyzed by developing computer models that replicated quantitative and temporal features of the behavior. The software for generating the modeled responses was written in "C" language and run on a DEC microvax II and on a DECstation 3100.

Elements of the model described by differential equations were implemented as discrete numerical routines in C using "bomol", a block oriented modelling program written by Lance Optican and Herschel Goldstein. After assessing the qualitative performance of different models by testing different combinations of elements and adjusting the parameters by hand, we applied a more objective method for determining parameter values. The output of the model was compared to behavioral data and the values of the parameters were systematically adjusted to obtain a fit which matched the actual data with the minimum error. The error was calculated as the sum of the squared differences between the output of the model and the actual responses, measured for each millisecond sample of data. Optimal parameter values were estimaged using the downhill simplex method of Nelder and Mead (1965), as described by Press et. al. (1988). The simplex method always converges to a solution, although the exact solution depends somewhat upon the initial conditions. For this reason, we ran the optimization procedure numerous times with different initial values and checked that the method converged to the same, or nearly the same, solution. Occasionally, a particular set of initial values would lead to a solution that was quite different and heuristically unreasonable; we discarded these solutions on the assumption that they represented aberrant local minima. To further confirm that the solution was robust, we started the optimization procedure at least one additional time with the initial values set equal to the optimal values obtained from the previous run and checked that the method once again converged to the same set of values.

Results

The upper trace of Fig. 1.1 shows the mean and standard deviation of the eye velocity evoked by 22 presentations of a step change in target velocity from zero to 25 °/s to the right. After a latency of 80 ms, eye velocity increased smoothly, crossed target velocity, and then oscillated about a steady-state velocity of 24.8 °/s. The input to the visual system for the stimulus in Fig.1.1 is shown by the trace labeled "image velocity", which is the difference between target velocity and eye velocity. The trajectory of image velocity emphasizes distinct initiation and maintenance phases in pursuit. Before the onset of pursuit, image motion is large and identical to target motion. During steady-state pursuit, image motion is small and primarily reflects fluctuations in eye velocity. Previous studies have shown that the first 80 ms of the response during the initiation of pursuit are unaffected by visual feedback, because of the latency of visual inputs. Measurements of eye acceleration in this initiation phase therefore provide good estimates of the open-loop response of the system to visual motion inputs that are completely determined by the target motion in the latency period. Our strategy in this chapter was to provide a variety of trajectories of target motion and to analyze the eye acceleration during the initiation phase of pursuit. Our goal was to determine the structure and parameters of models that best describe the open-loop transformation of visual motion inputs into pursuit eye movements.

Two components in the initiation of pursuit

In Fig. 1.1, both the fixation light and the target light were illuminated for at least 300 ms prior to the onset of the ramp target motion. We defined the interval in which the target was visible and stationary as the "motion

onset delay" (MOD). Systematic variation of the MOD revealed that the intiation of pursuit to constant velocity targets could be dissociated into two components. For example, Fig. 1.2A shows schematically the target motion for two trials in which the MOD was 300 ms and 0 ms. When the MOD was 300 ms, both the fixation light and the target light were visible and stationary for 300 ms before the fixation light was extinguished and the target light started to move. When MOD was 0 ms, the fixation light was visible for 300 ms, but the target light was not illuminated until it started to move. Fig. 1.2B shows the effect of changing the MOD on the average eye velocity evoked by target motion at 5, 15, and 30 °/s. Comparison of the eye velocity elicited for MOD = 0 ms (dashed traces) and MOD = 300 ms (solid traces) revealed two differences. First, for this monkey, the latency for the initiation of pursuit was approximately 30 ms longer when the MOD was 0 ms. Second, the initial rate of eye acceleration was larger and there was some overshoot in the response before the eye reached its steady-state velocity when the MOD was 300 ms. In contrast, the initial rate of eye acceleration was lower and there was no overshoot in the transition to steady-state velocity when the MOD was 0 ms.

The existence of two separate components in the initiation of pursuit was clearest in records of eye acceleration. Figs. 1.3A and C show the eye acceleration traces obtained by differentiating the six eye velocity traces shown in Fig. 1.2B. Figs. 1.3B and D show eye acceleration traces from identical experiments with a second monkey. The dashed vertical lines partition the response into an early interval (0 - 40 ms after initiation of pursuit) and a late interval (40 - 100 ms). When the motion onset delay was 300 ms (Fig. 1.3A,B), the eye acceleration in the early interval was nearly independent of image speed, while the eye acceleration in the later interval was proportional to

image speed. In both monkeys, eye acceleration 40 ms after the onset of pursuit was almost as large as that later in the trial. When the motion onset delay was 0 ms (Fig. 1.3C,D), the early phase of eye acceleration was almost absent and the response consisted primarily of a later phase of eye acceleration that was graded with image speed nearly from its onset. The absence of the earlier component of the response caused a large apparent increase in latency for monkey O and only a small increase for monkey J.

Fig. 1.4 quantifies the effect of motion onset delay on eye acceleration in the early and later intervals for monkey J. Each graph plots eye acceleration in the intervals 0 to 40 and 40 to 100 ms after the onset of pursuit, measured from records of eye velocity. In contrast to the data presented in Fig. 1.3, the measurement intervals were aligned with the onset of pursuit, not with the onset of target motion, so that the analysis intervals for the MOD = 0 ms trials were approximately 30 ms later than the same intervals for the MOD = 300 ms trials. The graphs confirm the impression given by inspection of the eye acceleration traces in Fig. 1.3. When the motion onset delay was 300 ms (Fig. 1.4A), the early eye acceleration (open symbols) saturates for image speeds greater than 10 °/s. In contrast, the later eye acceleration (filled symbols) increased with image speed and did not saturate over the range of image speeds tested. When the motion onset delay was 0 ms (Fig. 1.4B), both the early and late eye accelerations increased as a function of image speed and neither showed saturation.

When open-loop tracking conditions were used to prolong the interval of controlled image velocity beyond the normal 80 to 100 ms, the later phase of eye acceleration was sustained and remained proportional to image speed. The traces in Fig. 1.5A compare the responses to steps in target velocity of 10 and 20 °/s under normal closed-loop conditions (solid traces) with responses

to prolonged image motion at the same speed in open-loop conditions (dashed traces). The first two arrows demarcate the normal late phase of eye acceleration. The second and third arrows indicate the interval of additional eye acceleration caused by the extended open-loop conditions. When the image velocity input was prolonged by 100 ms, eye acceleration during the late phase of the initiation of pursuit was maintained at a slightly lower rate for an additional 100 ms . Fig. 1.5B plots eye acceleration as a function of image speed for the late phase of pursuit. Measurements obtained from the interval 40 to 100 ms after the onset of pursuit of closed-loop target motion (closed symbols) were closely matched by measurements from the interval 40 to 200 ms after the onset of pursuit for trials in which the open-loop interval was extended (open symbols). Linear regression of the two sets of data produced nearly identical slopes, but slightly different y-intercepts.

We next examined the effect of different motion onset delays by varying the amount of time that the target was visible before it started to move. The lefthand panels of Fig. 1.6 show families of eye velocity responses for a series of MODs in two monkeys. The traces are aligned on the onset of pursuit to highlight the effect of MOD on initial eye acceleration, although aligning the traces on pursuit onset obscures the effect of MOD on pursuit latency. The numbers to the left of the traces indicate the length of the interval between illumination of the target and the onset of its motion. As before, the initial eye acceleration was modest when the MOD was zero or small. As MOD was increased, the initial eye acceleration was more brisk and there was a tendency for eye speed to overshoot target speed. Figures 1.6B and D plot the magnitude of the average eye accelerations in the first 40 ms of pursuit as a function of the motion onset delay. For both monkeys in which this experiment was performed, the magnitude of the early eye acceleration

was lowest when MOD was zero or small. Early eye acceleration increased smoothly as motion onset delay increased, reached a peak for delays of 100 - 300 ms, and decreased slightly for very large values of MOD.

Quantitative description of the response to steps of target velocity

To describe the eye motion during the initiation of pursuit to step-ramp target motion, we developed a model with two parallel pathways that relate directly to the early and late phases of eye acceleration revealed by our behavioral analysis of the initiation of pursuit. Each pathway contained four functions indicated in the schematic diagram at the top of Fig. 1.7. The input, a step in image velocity, is first delayed to account for the latency to initiate pursuit. Delayed image velocity is scaled by a gain element and conditioned by a filter. The output of the filter represents a command for eye acceleration that is integrated to produce one component of the eye velocity response.

Fig. 1.7A-C describe how the late component was modeled for data from monkey O. Parameters that produced the best fit to the eye velocity responses were obtained using a Simplex algorithm as described in Methods. The solid traces in Fig. 1.7C are eye velocity traces from monkey O in which the late phase of eye acceleration was behaviorally isolated by setting the MOD equal to 0 ms. The data were obtained from trials in which the monkey tracked steps of image speed of 2.5, 5, and 10 °/s. First, the steps in image velocity were scaled by a linear gain function to match the different rates of eye acceleration observed for different image speeds. Next, the signals were passed through a filter, described by a single time constant, that had the step response shown in Fig. 1.7B. Finally, integrating the scaled and filtered step of image velocity reproduced the observed exponential rise in eye velocity. The open circles in Fig. 1.7A are measurements of the average eye acceleration over the open-loop interval from the eye velocity traces (indicated by the two

arrows in panel C). The straight line in Fig. 1.7A shows the best-fit linear gain function that produced the modeled responses shown by the dashed lines in Fig. 1.7C. The initial eye acceleration of the modeled responses (Fig. 1.7A, open symbols) agreed well with the initial eye acceleration in the actual data. Because this pathway produced an eye acceleration command that was a scaled and filtered version of the image velocity input, we will refer to it as the "image velocity" pathway.

Fig. 1.7D-F describe how the early component of pursuit was modeled. The solid traces in Fig. 1.7F were obtained by subtracting the eye velocity obtained with MOD = 0 ms (Fig. 1.7C) from the more robust responses obtained when the motion onset delay was 300 ms. To model the pulsatile shape of the early component of eye velocity, we used a filter that converted the step of image velocity into a biphasic command for eye acceleration. The filter was produced by cascading a differentiator and a second order system and was described by two parameters, the break frequency (ω) and the damping ratio (ζ). The best-fitting parameters for these traces ($\omega = 27.12$, $\zeta = 0.59$) produced a filter with the step-response shown in Fig. 1.7E. The gain element used to scale the input step in image velocity was defined by a compound function, consisting of a linear component and a saturating component. For the data in Fig. 1.7F, the best-fitting parameters described the nearly linear function shown by the continuous line in Fig. 1.7D. The optimal delay was 61.9 ms, approximately 34 ms shorter than the delay for the image velocity pathway.

The dashed traces in Fig. 1.7F show the output of the model generated with these parameters. Because the gain element was nonlinear, the order of the elements affected the performance of the model. It was easier for the optimization routine to find a good fit to the data when the gain element

preceded the filter. This order allowed simple scaling of the filter's step response. Also, because the filter was underdamped and acted as a low-pass differentiator, the gain measured at its output was different from the gain function in Fig. 1.7D. This explains why measurements of eye acceleration from either the behavioral data (Fig. 1.7D, triangles) or the output of the model (Fig. 1.7D, squares) were different from the gain function used in the model. Because this pathway described an eye acceleration related to the onset of target motion, we will refer to it as the "image motion transient" pathway.

We next developed a composite model by summing the outputs of the image velocity and image motion transient pathways and optimized the fit of the composite model to the eye velocity produced in step-ramp trials in which the MOD was 300 ms. The eye velocity elicited during these trials contain both early and late phases of eye acceleration and were matched by simultaneously adjusting the parameters in both pathways. The composite model had no difficulty in fitting the eye velocity responses from step-ramp data with MOD = 300 ms and often appeared to have too many parameters, sometimes resulting in spurious parameter values. We therefore decided to constrain the parameter describing the gain function in the image velocity pathway, by using the regression line describing the relationship between the late component of eye acceleration and image speed. This forced the model to attribute the sustained later eye acceleration to image velocity and not to the image motion transient. We also constrained one parameter controlling the dynamics of the early component (ζ) to remain within the range ($0<\zeta<1$). This guaranteed a filter with a pulse-like output appropriate for the early component. The composite model therefore contained seven free parameters: the delays in the two pathways, the three parameters describing

the gain element for the early component, the break frequency of the image motion transient filter, and the time constant controlling the filtering in the image velocity pathway.

The results of fitting the composite model to eye movements from two monkeys are shown in Fig. 1.8. Fig. 1.8A and D compare the eye velocity produced by velocity steps of 5, 15, and 25 °/s with MOD = 300 ms (solid lines) with the best-fit output of the composite model (dashed lines). The composite model apportioned the response into image velocity and image motion transient components that matched the behavioral dissocation of the early and late phases of eye acceleration. The lower two rows of Fig. 1.8 compare the behaviorally isolated early and late phases of eye acceleration with the outputs of the two pathways of the composite model. The averaged eye velocity responses to velocity steps of 5, 15, and 25 °/s with MOD = 0 ms (solid lines in Fig. 1.8B and E) matched the output of the image velocity pathway in the model (dashed lines). The behaviorally isolated early phase of eye acceleration (solid lines in Fig. 1.8C and F) matched the output of the image motion transient pathway in the model (dashed lines).

Fig. 1.9 summarizes the properties of the nonlinearities and filters in the models that provided the best fits for constant velocity target data in four monkeys. For each monkey, the data set consisted of averaged eye velocity to leftward and rightward step-ramp target motions of 5, 10,15, 20 and 25 °/s. The lefthand graphs for each monkey show gain as a function of image velocity. The open circles in the graphs indicate eye acceleration measured from the late interval of averaged eye velocity. The solid lines represent the linear function determined by linear regression of measurements from the later phase of eye acceleration. Separate functions were determined for leftward and rightward image motion. The gain functions for the model

show a small offset with respect to the behavioral data, because the y-intercept of the linear regression of the behavioral data was not used in the model. The y-intercept, which was usually close to zero, was eliminated in the model both because the slope was the salient parameter related to image velocity gain and because a non-zero y-intercept in the gain function would have produced a constant eye acceleration, even in the absence of any image motion.

The middle column of Fig. 1.9 shows the nonlinear gain elements in the image motion transient pathway for each monkey. With the exception of monkey I, the model provided a best fit in which the early component saturated for image speeds greater than 10-20 °/s. The open triangles show the average eye accelerations produced by the image motion transient pathway, measured from the onset of the modeled early component to its peak. For reasons mentioned before, these measurements did not match the non-linear gain elements in this pathway (solid lines). However, the output of the image motion transient pathway agreed well with the average eye acceleration measured from the isolated early component obtained by subtracting MOD = 0 trials from MOD = 300 trials. Unfortunately, we had the data to make the latter comparison only in monkeys J and O (open squares).

The righthand graph for each monkey shows the step-responses of the filters used in the two components of the model. For clarity, we have shown only the step responses for the filters used in modelling rightward pursuit. The thick lines represent the step-responses of the low-pass filters used in the image velocity pathway; the thin lines represent the step-responses of the filters used in the image motion transient pathway. Step-responses are shown, rather than impulse responses, because the actual inputs to the filters used in the models is a scaled step in image velocity. The properties were

qualitatively similar in the four monkeys, but showed varied quantitative detail. For example, monkey N had a much shorter time constant in his image velocity pathway than either monkey O or monkey J. Values for the parameters of the best-fit models from each monkey are listed in table 1.1.

Pursuit of smoothly accelerating targets

To determine whether the motion onset transient reflected a general sensitivity to visual image acceleration or was only evoked by the abrupt onset of motion, we examined the responses to smoothly accelerating targets. Fig. 1.10 shows the eye and target motion for a trial that began like our standard step-ramp trial, with a fixation spot at straight ahead gaze and an eccentric and stationary target light. However, when the fixation light was extinguished, the target accelerated smoothly at a constant rate of 120 $^{o}/s^{2}$ for 125 ms and then continued at 15 $^{o}/s$, the velocity attained at the end of the acceleration. The pursuit evoked by smoothly accelerating targets was qualitatively similar to that evoked by steps of target speed. After a latency of 120 ms, the eye accelerated for approximately 100 ms before reaching a steady-state velocity of 14.5 $^{o}/s$.

Latencies for initiating pursuit of smoothly accelerating targets were consistently longer than latencies for constant velocity targets. Latencies for initiating optokinetic and pursuit eye movements have been modeled as the combination of a fixed processing delay and the time required for the target to traverse a minimal displacement (Carl and Gellman 1987, Collewijn 1972). We applied this description to our data for pursuit of constant velocity and smoothly accelerating targets. Fig. 1.11A shows latency measurements from monkey O for steps of targt velocity when MOD was 300 ms. Latency was plotted as a function of inverse speed so that it could be related to speed by the equation: latency = α + β(1/speed) In this formulation, α gives the value of the fixed processing delay

ec) which has units of de

ear regression shown by th

ntering targets, latency is

ance acceleration]$^{1/2}$. L

acceleration]$^{1/2}$ therefore

[acceleration]$^{1/2}$, where β

and β = 0.014^{0}. Data from

timated values for α an

step-ramp and smoothly

creased latencies for initia

ably due to the additional

tance and not due to cha

reshold for mimimum di

The eye movements

mbined action of separat

elocity and image acceler

elocity component to an

n attempt to predict the e

elocity, based upon the

athway used to fit the ey

The solid lines in Fig. 1.1

celerating at 64, 120, an

stant then continued a

celeration. Although

ther limited the perio

was always longer than

e velocity responses p

and β, which has units of degrees, gives the minimum displacement. For the linear regression shown by the line in Fig. 1.11A, α = 74.7 ms and $\beta = 0.015^{o}$. For accelerating targets, latency is related to acceleration by the equation: time = [(2 x distance)/acceleration]$^{1/2}$. Linear regression of latency plotted against [2/acceleration]$^{1/2}$ therefore represents the function: latency = α + β'[2/acceleration]$^{1/2}$, where $\beta' = [\beta]^{1/2}$. For the data plotted in Fig. 1.11B, α = 73.4 ms and $\beta = 0.014^{o}$. Data from each of the four monkeys, summarized in Table 1.2, produced values for α and β that were similar, thought not always identical, for step-ramp and smoothly accelerating target motions. This implies that the increased latencies for initiating pursuit of smoothly accelerating targets were largely due to the additional time required for the target to move the minimum distance and not due to changes in the fixed processing time or to changes in the threshold for mimimum displacement.

The eye movements evoked by an accelerating target could reflect the combined action of separate sensitivities of the pursuit system to image velocity and image acceleration or could be simply the response of the image velocity component to an orderly sequence of image speeds. Fig. 1.12 shows an attempt to predict the eye velocity evoked by accelerating targets in one monkey, based upon the best-fitting parameters for the image velocity pathway used to fit the eye movements evoked by steps of target velocity. The solid lines in Fig. 1.12A show the average eye velocities evoked by targets accelerating at 64, 120, and 320 $^{o}/s^{2}$. In each trial, the target accelerated for 125 ms and then continued at a velocity equal to that attained at the end of the acceleration. Although the final speeds and the limited size of the tangent screen limited the period of acceleration, the duration of smooth acceleration was always longer than the open-loop interval. The dashed traces show the eye velocity responses predicted by passing the initial target velocity through

e image velocity pathway
e of target acceleration, th
e larger than that predicte
ween actual and predicte
e eye velocity evoked by
mmed for by the image v
esponse traces scaled as a f

If the apparent sensitiv
e onset of motion, then the
al and predicted response
eleration was lengthened.
sponses to the same target
ditions and with the ope
erged at approximately 1
al feedback began to ha
dicted response, which w
erated with a continuou
were obtained by sub
al eye velocities in Fig
ctual open-loop period a
d of the extended open
esent in the open-loop
as greater than predicte

For one monkey,
ed to the values obta
pparent sensitivity to i
e latency in our simu

the image velocity pathway derived from constant velocity targets. For each rate of target acceleration, the eye velocity evoked by the accelerating target was larger than that predicted by the image velocity pathway. The difference between actual and predicted eye velocity (Fig. 1.12B) represents that portion of the eye velocity evoked by an accelerating image that could not be accounted for by the image velocity pathway. The magnitude of the difference traces scaled as a function of image acceleration.

If the apparent sensitivity to image acceleration were related merely to the onset of motion, then the shape and amplitude of the difference between actual and predicted responses should not change when the period of image acceleration was lengthened. The two solid traces in Fig. 1.12C compare the responses to the same target accelerating at 120 $^{o}/s^{2}$ under normal, closed-loop conditions and with the open-loop period extended by 50 ms. The traces diverged at approximately 100 ms after the onset of pursuit, the time when visual feedback began to have an effect. The dashed trace indicates the predicted response, which was the same for both cases, because it was generated with a continuous acceleration as the input. The traces in Fig. 1.12D were obtained by subtracting the predicted eye velocity from the two actual eye velocities in Fig. 1.12C. The first arrow indicates the end of the natural open-loop period and the second arrow is placed 50 ms later, at the end of the extended open-loop period. The sustained image acceleration present in the open-loop trials resulted in a sustained eye acceleration that was greater than predicted by a sensitivity to image velocity.

For one monkey, we set the parameters for the gain and filter elements equal to the values obtained for the step-ramp data and documented that the apparent sensitivity to image acceleration did not disappear when we varied the latency in our simulation of the image velocity pathway from 0 to 150 ms.

the image velocity pathway derived from constant velocity targets. For each rate of target acceleration, the eye velocity evoked by the accelerating target was larger than that predicted by the image velocity pathway. The difference between actual and predicted eye velocity (Fig. 1.12B) represents that portion of the eye velocity evoked by an accelerating image that could not be accounted for by the image velocity pathway. The magnitude of the difference traces scaled as a function of image acceleration.

If the apparent sensitivity to image acceleration were related merely to the onset of motion, then the shape and amplitude of the difference between actual and predicted responses should not change when the period of image acceleration was lengthened. The two solid traces in Fig. 1.12C compare the responses to the same target accelerating at 120 $^{o}/s^{2}$ under normal, closed-loop conditions and with the open-loop period extended by 50 ms. The traces diverged at approximately 100 ms after the onset of pursuit, the time when visual feedback began to have an effect. The dashed trace indicates the predicted response, which was the same for both cases, because it was generated with a continuous acceleration as the input. The traces in Fig. 1.12D were obtained by subtracting the predicted eye velocity from the two actual eye velocities in Fig. 1.12C. The first arrow indicates the end of the natural open-loop period and the second arrow is placed 50 ms later, at the end of the extended open-loop period. The sustained image acceleration present in the open-loop trials resulted in a sustained eye acceleration that was greater than predicted by a sensitivity to image velocity.

For one monkey, we set the parameters for the gain and filter elements equal to the values obtained for the step-ramp data and documented that the apparent sensitivity to image acceleration did not disappear when we varied the latency in our simulation of the image velocity pathway from 0 to 150 ms.

For each simulation, we computed mean squared error as the sum of the squared difference between each simulated and actual eye velocity point, divided by the number of points. The three lines in Fig. 1.13B plot mean squared error as a function of simulation latency for targets accelerating smoothly at 64, 120, and 180 $^{o}/s^{2}$. In each case, the minimum error was large, even though the latency that produced minimum error depended on image acceleration. The open square shows that the mean squared error was much smaller when the image velocity pathway alone was used to fit the eye velocity evoked by steps in image velocity of 5, 15, and 25 $^{o}/s$ for MOD = 0 ms (Fig. 1.7C). The open triangle shows that the mean squared error was also small when the composite model was used to fit the same steps in image velocity for MOD = 300 ms (Fig. 1.8D). The arrow indicates a latency of 25 ms, the latency used to generate the modeled responses shown in Fig. 1.13A (dashed lines), which do not provide a good fit to actual eye velocity (solid lines).

Quantitative description of the response to accelerating targets

We incorporated a third pathway into the model to describe the eye velocity recorded during the initiation of pursuit for smoothly accelerating targets. The solid traces in Fig. 1.14C show the image acceleration component of the response in monkey J when he initiated pursuit of smoothly accelerating targets of 64, 120, and 320 $^{o}/s^{2}$. These traces were calculated by subtracting the predicted eye velocities from the actual eye velocities evoked by the accelerating targets, as described in Fig. 1.12. To model this component, we used an image acceleration pathway that differentiated and filtered the input ramp in image velocity to produce a smoothed step and then scaled the step to produce the appropriate amplitude eye acceleration. The elements in the image acceleration pathway were described by the same equations as in

the image motion transient pathway, but in this case the filter preceded the gain element. The dashed lines in Fig. 1.14C represent the best-fit output of the image acceleration pathway for the data from monkey J. The response of the filter described by the best-fitting parameters (ω = 75.86, ζ = 0.30) to steps in image velocity is shown in Fig. 1.14A and the gain function is shown in Fig. 1.14B. The open circles show that there was good agreement between the non-linear gain function in the model and the average eye acceleration measured from the difference traces over the open-loop interval (the interval indicated by the arrows in panel C).

Fig. 1.15 summarizes the properties of the best-fit image acceleration pathway for four monkeys. For each monkey, we matched the performance of the image acceleration pathway to traces obtained by subtracting the output of that monkey's image velocity pathway from his eye velocity responses to targets accelerating at 45, 64, 80, 120, 180, 320, and 400 $^{o}/s^{2}$; leftward and rightward trials were fitted separately. All six parameters defined in the pathway were optimized, although the damping ratio (ζ) was constrained as in the optimization of the parameters for the image motion transient pathway. The lefthand graphs in Fig. 1.15 indicate the step-responses of the filters used in the model for each monkey. All of the filters have the same qualitative form, although there was some quantitative variation among monkeys in the properties of the filters. The break frequency (ω) ranged from 25.62 to 75.86, and the damping ratio (ζ) ranged from 0.193 to 0.324. The righthand graphs show the gain elements obtained by optimization in the models. For 3 of 4 monkeys, the magnitude of the response saturated for image accelerations larger than 200 $^{o}/s^{2}$. The open circles are measurements of the average eye acceleration from the difference between actual and predicted eye velocities evoked by accelerating targets. In this case, because

the gain element followed the differentiating filter, there was a good correspondence between the gain elements used in the models and the measurements made from the behavioral data.

Because the models for the image motion transient pathway and the image acceleration pathway had similar forms, we next assessed whether a single pathway could account for both the image motion transient component of the initiation of pursuit to step-ramp target motion and the responses attributed to smooth image accelerations. Our strategy was to assess how well a two component model, consisting of an image velocity pathway and an image motion transient pathway like those shown in Fig. 1.7, could replicate the responses to both constant velocity and smoothly accelerating targets. First, we optimized the parameters of the two component model to fit data from step-ramp trials. We measured the mean squared error of the fit to each step-ramp trial and computed the average error separately for leftward and rightward step-ramp trials. Without changing the parameters, we then tested the performance of the model on the eye velocity data from smoothly accelerating targets, to which it had not been fit. We described the ability of the model to fit the two sets of data by plotting error during step-ramp trials as function of error during smoothly accelerating target trials (Fig. 1.16). The square symbols show the performance of the two pathway model when fit to constant velocity trials, and tested, but not optimized for smoothly accelerating target trials. The points were located close to the abscissa, indicating that the model's fit was good for data from constant velocity targets, but not as good for data from smoothly accelerating targets. We then repeated the analysis, but now optimized the model to fit the data for smoothly accelerating targets, but not constant velocity targets. The performance of the model, shown by circles, showed a good fit to eye velocity

from smoothly accelerating target trials, but a poor fit to constant velocity target data. The triangles show the results from the two component model when its parameters were adjusted to optimize the fit to data from both constant velocity and smoothly accelerating targets. The triangles are not close to either the abscissa or the ordinate, indicating that the model achieved an intermediate quality of fit when forced to fit both sets of data. We concluded that the two component model could not fit both sets of data as well as it could fit either the step-ramp or smoothly accelerating target data alone. Finally, the open diamonds characterize the performance of a model with three pathways: an image velocity pathway, an image motion transient pathway, and an image acceleration pathway. Because this model could use separate pathways to describe both the early component of the initiation of pursuit and the additional responses seen during pursuit of accelerating targets, it provided the best fit for both sets of data.

The termination of pursuit

Fig. 1.17 shows an example of the type of trial we used to examine the termination of pursuit. The trial began as a standard step-ramp trial, but instead of ending with the extinction of the moving visual target, the target stopped for 400 ms at the end of the trial and the monkey was required to fixate it before receiving a reward. When the target speed changed from 20 to 0 °/s the target stepped again to obviate the need for a final corrective saccade. As shown by the image velocity trace, the visual motion associated with this step-ramp-step-stop target motion was an initially constant image motion at the onset of target motion that decreased toward zero as eye velocity matched target velocity, followed by a constant image motion in the opposite direction when the target stopped. An example of one eye velocity response to this target motion is shown immediately above the image velocity trace. The

uppermost trace shows the averaged response from twenty trials, and the dashed lines indicate one standard deviation.

Our results confirm previous observations in humans (Robinson et al. 1986, Luebke and Robinson, 1988) that the termination of pursuit is qualitatively different from the initiation of pursuit. The traces in Fig. 1.18A and B show averaged eye velocity responses for step-ramp-step-stop target motions at speeds of 10 and 20 °/s for rightward (A) and leftward pursuit (B). The traces begin and end with eye velocity equal or close to zero. For the initiation of pursuit, the eye velocity rose briskly and there was some overshoot before it assumed a steady-state value. During the termination of pursuit, the deceleration of the eye was also brisk, but there was no overshoot as the eye approached zero velocity.

The major distinction between the initiation and the termination of pursuit was that the onset reflected nonlinear processing of visual inputs, while the termination of pursuit appeared to be a purely linear process. Fig. 1.18 C and D plot the same data as A and B, but with eye velocity normalized for target speed by multiplying the 20 °/s traces by 0.5 and the 10 °/s traces by 1. Normalization revealed the nonlinear properties of the onset of pursuit. The traces with the larger peaks at the inititation of pursuit are the responses to 10 °/s, reflecting the larger proportional contribution of the image motion transient component at lower image speeds. In contrast, normalization caused the traces for different speeds of target motion to superimpose nearly exactly at the offset of pursuit, indicating that the termination of pursuit scaled approximately linearly with amplitude. As noted by Robinson et. al. (1986), eye velocity during the offset of pursuit can be described as a decaying exponential with a single time constant. We estimated this time constant by measuring the steady-state eye velocity in each trial and determining the

amount of time from the beginning of the offset required to reach 1/e of this value. For both target speeds and for both leftward and rightward pursuit, the time constant was approximately 80 ms.

Discussion

Eye movements as a probe for visual motion processing

We have used the monkeys' performance during the initiation of pursuit eye movements as a probe to characterize the visual motion signals that contribute to pursuit. By examining the first 80 ms of the response, the portion of the response that is uncorrupted by visual feedback, we have directed our analysis at the eye movements evoked directly by the visual motion inputs. Anticipatory effects and cognitive strategies are unlikely to contaminate our results, because stimuli of different speeds and directions were presented in a randomly interleaved fashion (Kowler and Steinman 1979). Furthermore, because the range of eye velocities and accelerations attained by the monkeys in our experiments was well below what is seen during saccadic eye movements or the smooth phases of vestibularly driven eye movements, we believe that the nonlinear properties we have observed reflect the processing of visual inputs for pursuit, rather than limits imposed by the output motor pathways.

In contrast to previous studies, which examined how static properties of the visual stimulus affect the quality of pursuit eye movements, we have described the dynamic transformations that convert visual motion inputs into the trajectories of pursuit eye velocity observed for different target

motions. The target motions used in our study are variations of the step-ramp motion introduced by Rashbass (1961). By presenting stimuli in which target position and target motion required oppositely directed eye movements, Rashbass demonstrated that pursuit is a response to visual motion. Subsequently, it has largely been assumed that the visual motion signal subserving pursuit is image velocity, the difference between target velocity and eye velocity. Furthermore, few studies have addressed the issue of how visual motion is transformed by the pursuit system into the profiles of eye velocity observed during tracking. In the present study, we presented three types of target motion that are variations of the step-ramp target motion used by Rashbass. We conclude that the eye velocity elicited by these three types of target motion cannot be explained by a single simple transformation of image velocity and we suggest that these target motions reveal separate components of visual motion that contribute to pursuit.

The effect of motion onset delay on pursuit initiation

The profile of initial eye acceleration elicited by a constant velocity target depends upon the motion onset delay, defined as the length of time that the target is visible before the onset of its motion. When the target simply appears moving at an unpredictable time (MOD = 0 ms), eye acceleration over nearly the entire first 100 ms of pursuit is proportional to image speed. When the target is visible for at least 50 ms before the onset of its motion (MOD > 50 ms), the earliest eye acceleration (0 - 40 ms after pursuit onset) is larger and is no longer proportional to image speed, but the eye acceleration over a later interval (40 - 100 ms after pursuit onset) remains proportional to image speed.

Our interpretation of the motion onset delay effect is that the visual system in its quiescent state is very sensitive to abrupt changes in image

velocity, but its ability to detect motion is masked when a target first appears in the visual field. We presume that the on-response associated with the appearance of the target produces noise within the population of motion detectors. This masking noise dissipates by 50 - 100 ms, at which time the motion detectors are once again sensitive to image motion onset. The differences in eye acceleration produced by delaying the onset of target motion may be due to differences in adaptation state caused by the amount of time that the bright target spot is visible. Preliminary data suggest that changes in the contrast of the target change the amplitude of the MOD effect (S. Lisberger, personal communication). However, we cannot rule out the possibility that cognitive factors also play a role. In particular, the increase in the amplitude of the earliest eye acceleration over the first several days in monkey O suggests that the use of the motion transient signal is enhanced with practice.

The effect of varying MOD revealed that the initial eye movements evoked by steps in target velocity can be modeled with two separate components related to the onset and the speed of image motion. This helps to understand the previous observations of differences between the early and late phases of eye acceleration during the initiation of pursuit. The magnitude of the early phase of eye acceleration is relatively unaffected by the speed, contrast or size of the moving image (Lisberger and Westbrook 1985). The magnitude of the early component is also isotropic across the visual field, while the magnitude of the later component is larger when the moving image is closer to the center of the field (Lisberger and Pavelko 1989). The consistent differences in their sensitivity to visual parameters suggests that the early and late components of pursuit may reflect two separable processes for evaluating image motion.

Initiation of pursuit of smoothly accelerating targets

The eye velocity generated in response to smoothly accelerating targets was greater than that expected from the measured sensitivity to image velocity. We suggest that this augmented response reflects a sensitivity to image acceleration *per se*, which provides an input to pursuit that sums with the contribution of image velocity. A role for image acceleration in generating pursuit eye movements has been suggested previously (Morris and Lisberger 1985; Lisberger et al. 1987). The advantage of the present analysis is that we have characterized its contribution to the smooth pursuit response during the open-loop period of the initiation of pursuit and are therefore more certain that we are examining properties of the direct visual inputs. Our analysis does not allow us to exclude the possibility that the nervous system is capable of extracting even higher order information about image motion. Instead, it groups all sensitivity to motion of an order greater than velocity into a signal that is attributed to image acceleration.

Signals related to image acceleration have important consequences for the control of movement. In everyday situations, visual targets rarely move at a constant speed. The speed of natural targets often fluctuates and when targets begin to move, their speed increases smoothly because of inertia. The use of image acceleration signals makes it possible to change eye or limb velocity more quickly in these cases and thereby improves the accuracy of motor performance. For pursuit eye movements, a sensitivity to image acceleration can also account for the lack of overshoot in the transition from the initiation of pursuit to steady-state tracking (Krauzlis and Lisberger 1989) and for the high frequency oscillations observed during maintained pursuit (Morris and Lisberger 1985, Krauzlis and Lisberger 1989, Goldreich et al. in press). The emergent properties produced by image acceleration in the

control of pursuit eye movements will be examined in greater detail in the following chapter.

Current models of motion detection in primates, which use an analysis of the power contained within spatial and temporal frequencies of the image (Adelson and Bergen 1985; Watson and Ahumada 1985), do not exclude a sensitivity to image acceleration, but the possibility of determining image acceleration has not been directly tested. In this regard, it is important to note the development of a class of motion stimuli, called drift-balanced stimuli, which are invisible to these motion models, but which lead to a clear perception of motion in human observers (Chubb and Sperling 1988). To account for the ability of humans to detect motion in these displays, Chubb and Sperling suggest a series of additional transformations of the image preceding the standard motion analysis, and include in this series a filter which performs a temporal differentiation of the image. It is possible that the temporal filter required to account for the perception of motion in these drift-balanced displays is related to the temporal filter needed to account for the sensitivity to image acceleration seen in our behavioral experiments.

A preliminary model of the visual inputs for pursuit

The contribution of the image velocity, image acceleration and image motion transient components to the initiation of pursuit can be summarized with a model, as shown in Fig. 1.19. The three components are each processed in a separate pathway of the model. The input to each pathway is image velocity and the output of each pathway is a command for smooth eye acceleration. The three commands for eye acceleration are summed and then integrated to produce the pursuit eye velocity response. The placement of an integrator at this location allows the model to replicate the behavioral observations that visual motion is interpreted by the pursuit system as a

command for eye acceleration (Lisberger et. al. 1981) and that pursuit eye velocity can be maintained in the absence of any image motion (Morris and Lisberger 1987).

The three pathways of the model are active in different combinations during the initiation of pursuit of different target motions, reflecting the different contributions of the three visual motion components. During the initiation of pursuit of a constant velocity targets, the image velocity component makes a sustained contribution to eye acceleration, while the image motion transient component makes a brief contribution only if the motion onset delay is longer than 50 - 75 ms. For smoothly accelerating targets, the image velocity and image acceleration components both make sustained contributions to eye acceleration. The model does not attempt to describe the factors that control how the delay in the onset of target motion influences the contribution of the image motion transient signal.

The pathways in the model describe transformations of an image velocity signal, because this provides a convenient way to focus on how motion signals are related to components of the pursuit eye movement response. We have thereby bypassed the problem of computing image velocity from the temporal pattern of luminance changes present in the retinal image. By employing this simplification, we do not mean to imply that the visual system explicitly encodes image velocity, or that the evaluation of image velocity is a distinct process which precedes the transformations described by the three pathways of our model. On the contrary, it is likely that image velocity is a signal encoded implicitly by the activity of widely distributed sets of neurons and that the transformations described by our model reflect some of the properties of that encoding.

We suggest this model as an initial guideline for examining the functional role of the visual motion signals for pursuit. It is likely that many aspects of the model will have to be amended to account for data not presented in this chapter. For example, in our experiments, in which image speeds were 30 °/s or less, eye acceleration was linearly related to image speed. Other experiments in monkeys (Lisberger and Westbrook 1985) and humans (Carl and Gellman 1987; Tychsen and Lisberber 1986) indicate that this relationship would saturate for image speeds over 60 °/s. We also do not include a sensitivity to offsets in image position, which have been shown to cause eye accelerations during sustained tracking (Morris and Lisberger 1987). Our model describes separate image motion transient and image acceleration components, because with our simple model we were unable to obtain parameters that could account for all of our data. It is possible that the two components are in fact different aspects of a single process that could have been described with a more flexible non-linearity and higher order filters. Also, our model describes fixed contributions of visual motion signals, but the actual contribution of these visual inputs to pursuit may be regulated or changed. Our observations on the offset of pursuit confirm the earlier observations of Robinson et al. (1986) and suggest that, at the very least, the visual inputs used to bring eye velocity to zero are different than the visual inputs used to initiate pursuit. Finally, our description assumes that the problem of identifying and analyzing the motion of the target has been solved. In normal tracking situations, the object of pursuit must be followed across textured backgrounds, often in the midst of motion elsewhere in the visual field that not only complicates the evaluation of the motion of the target, but that also likely influences the evaluation of what should be identified as the object of pursuit.

Using visual motion signals to probe the neural substrates for pursuit

The physiological correlates of the three pathways in our model are unknown. The pathways could correspond to anatomically distinct pathways, to separate populations of neurons, or to the properties of a single population of neurons. We used the three-pathway structure in our model primarily because the properties of the three pathways were determined with data from three different experimental paradigms. The three-pathway structure therefore has the practical advantage of dividing the visual signals into pieces which can be identified and examined in separate experiments.

Some recent experiments have used the target motions described in this study to investigate the relationship between the firing rate of isolated neurons and the visual motion signals related to image velocity, image acceleration, and image motion transient. Preliminary recording data show that the responses of many neurons in area MT are modulated by motion onset delay and that some neurons encode a signal related to image acceleration (Movshon and Lisberger 1990, Movshon et al. 1991, Lisberger and Movshon 1991). A study of Purkinje cell activity in the cerebellum indicates that the output of the ventral paraflocculus/flocculus encodes all three visual motion components, in addition to eye velocity (Krauzlis and Lisberger 1990). These studies suggest that the application of behavioral results, specifically the use of motion onset delay and accelerating targets, may be useful for identifying the signal transformations performed by the anatomical components of the pursuit system.

Table 1.1. Values of parameters used in the models for monkeys J, O, N and I. For the image velocity pathway, τ refers to the time constant of the first-order system, $\tau dy(t)/dt + y(t) = x(t)$, used as a filter, and a refers to the slope of the linear function used as a gain element. For the image motion transient and image acceleration pathways, ω gives the cut-off frequency and ζ gives the damping ratio of the second-order system used as a filter: $(dy^2(t)/dt^2 + 2\zeta\omega dy(t)/dt + \omega^2 y(t) = \omega^2 x(t)$. The values of a, b, and c refer to the coefficients used in the nonlinear gain function: $y = ax + be^{c/x}$. Different gain functions were used in each of the three pathways for rightward and leftward pursuit.

Table 1.1

	Monkey			
	J	O	N	I
image velocity				
τ	0.0200	0.0389	0.0057	0.0354
right				
a	9.3430	8.2870	6.373	15.906
left				
a	7.6180	8.0450	5.986	17.172
image motion transient				
ω	43.027	33.227	41.442	38.934
ζ	0.4990	0.1840	0.8010	0.9000
right				
a	-0.1875	-2.0896	-0.2009	-0.3386
b	10.778	209.058	12.196	65.826
c	-0.4950	-0.0484	-0.3974	-0.0843
left				
a	-0.1404	-0.9517	-0.2321	-0.6136
b	9.3825	92.327	13.041	69.439
c	-0.5093	-0.0598	-0.4501	-0.0809
image acceleration				
ω	75.859	25.617	71.035	63.983
ζ	0.2990	0.3240	0.2210	0.1930
right				
a	0.0031	-0.0215	-0.0112	0.1704
b	76.964	203.048	136.512	144.715
c	-0.0405	-0.0491	-0.0343	-0.0123
left				
a	-0.0202	0.2016	0.0575	0.1728
b	188.494	137.181	258.807	95.749
c	-0.0250	-0.0695	-0.0307	-0.0256

Table 1.2. Values of parameters describing latency to initiate pursuit. Latency was modeled for each of the four monkeys as the sum of a fixed delay (α) and the time required to traverse a minimum displacement (β).

Table 1.2

	Monkey			
	J	O	N	I
step-ramp				
mean latency (ms)	72.6 ± 3.7	74.7 ± 1.6	78.8 ± 2.7	92.7 ± 4.3
α	67.6	73.2	77.1	87.7
β	0.054	0.015	0.018	0.024
smooth accelerations				
mean latency (ms)	81.4 ± 6.1	88.9 ± 6.7	111.3 ± 7.6	113.3 ± 8.5
α	67.1	73.4	92.2	94.2
β	0.012	0.014	0.021	0.023

Figure 1.1. Example of pursuit eye movement evoked by a target moving at a constant velocity of 25 °/s. Dashed line with position traces indicates when fixation LED was illuminated. Middle traces show the eye velocity response and image velocity from a single trial. Top trace shows average eye velocity from 22 presentations of the target motion. Dashed lines surrounding top solid trace indicate 1 standard deviation. Upward deflections indicate rightward motion.

Fig. 1.1

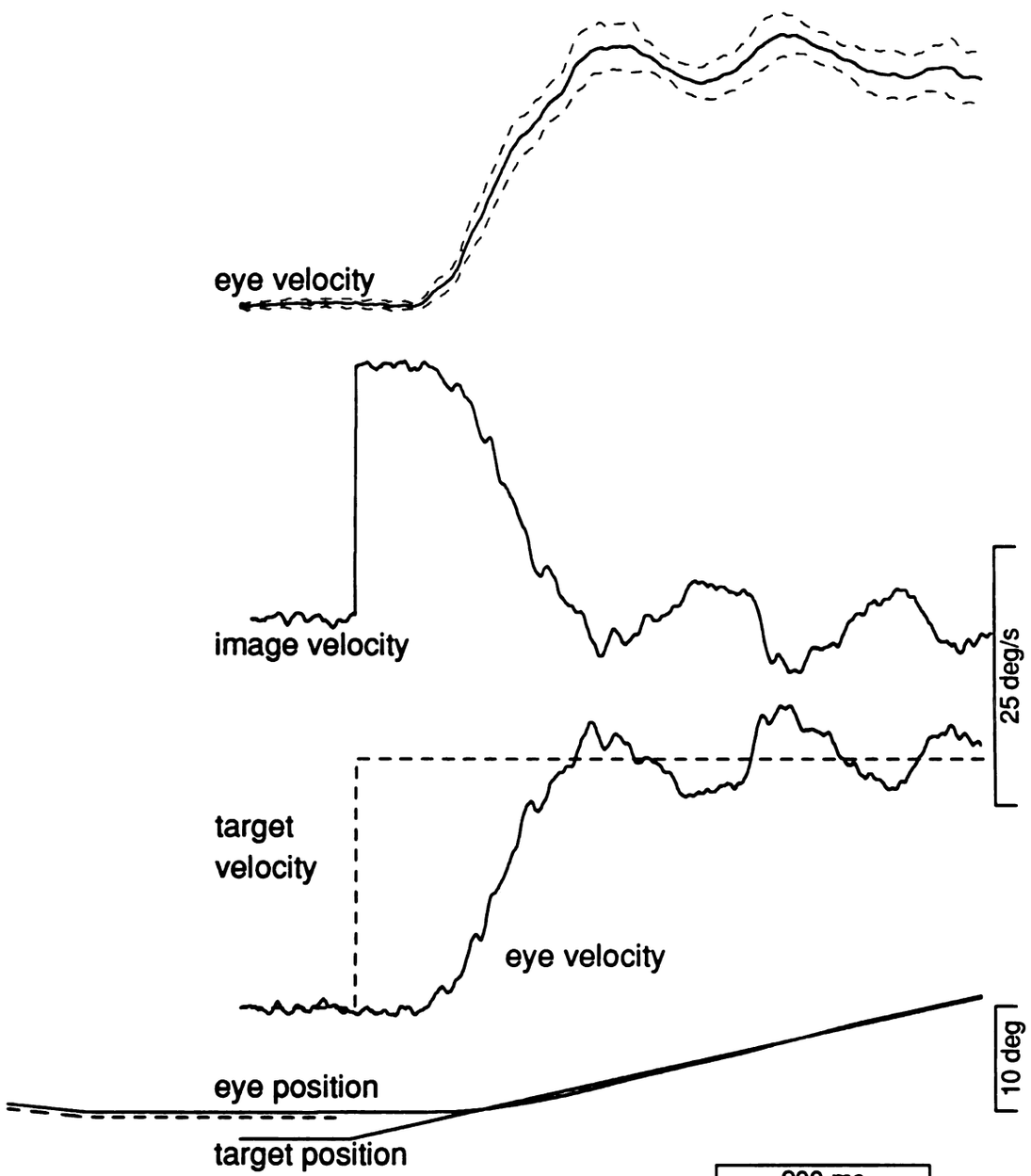
eye velocity
image velocity
25 deg/s
target
velocity
eye velocity
10 deg
eye position
target position
200 ms

Figure 1.2. The effect of motion onset delay. A: Schematic diagram showing difference between two MODs. When MOD = 300 ms, both LED and target light are illuminated for 300 ms before onset of target motion (top). When MOD = 0 ms, target is not seen before onset of its motion (bottom). Dashed line indicates that mirror galvantometer is moving, but shutter is not open. B: Sample averaged eye velocity responses to three constant velocity targets with a MOD of 0 ms (dashed traces) or 300 ms (solid traces). Downward pointing arrow indicates onset of target motion.

Fig. 1.2

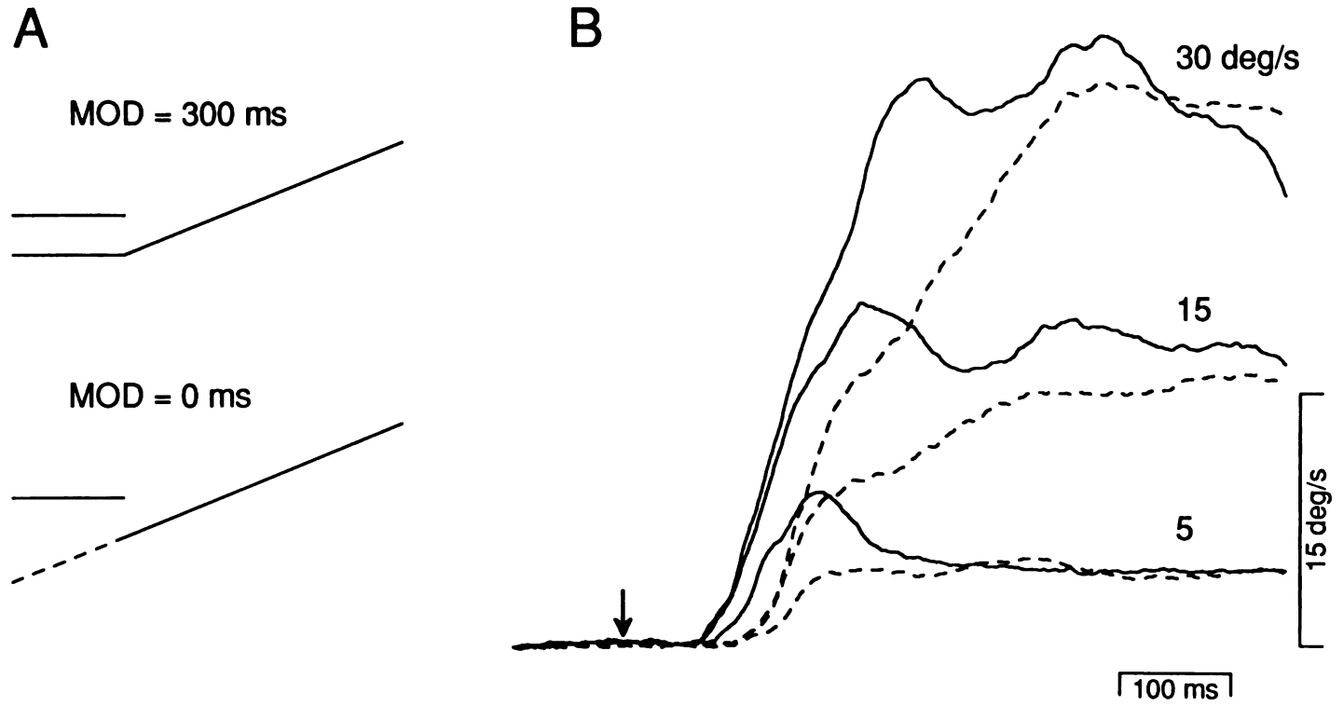

Figure 1.3. Effect of motion onset delay on eye acceleration for two monkeys. A : Acceleration traces from monkey O obtained by differentiating averaged eye velocity trace for constant velocity targets of 5, 15, and 30 °/s presented with a motion onset delay of 300 ms. C : Acceleration traces from monkey O's responses to same target speeds, but presented with a motion onset delay of 0 ms. B and D : Analagous acceleration traces obtained with data from monkey J. For each trace, the first vertical dashed line is placed at the initiation of pursuit for the MOD = 300 ms case. The second and third vertical lines are placed 40 ms and 100 ms after the onset of pursuit, respectively. All traces are aligned with the onset of target motion.

Fig. 1.3

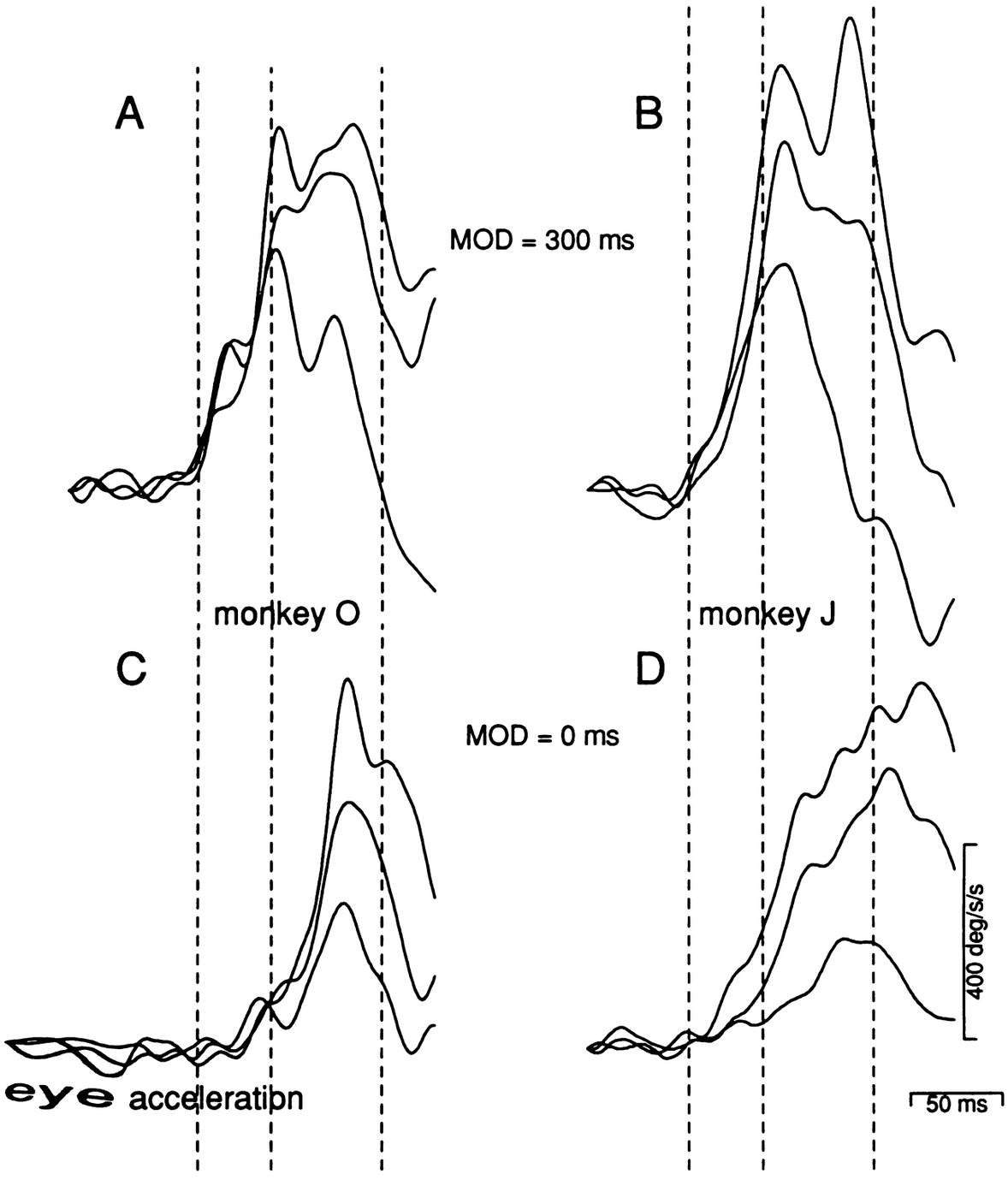
A
B
MOD = 300 ms
monkey O
monkey J
C
D
MOD = 0 ms
400 deg/s/s
50 ms
eye acceleration

Figure 1.4. Quantification of MOD effect on eye acceleration for monkey J. A : Average eye acceleration measured over two intervals for responses to constant velocity targets with MOD = 300 ms. Open symbols are measurements of average eye acceleration from 0-40 ms after the onset of pursuit; closed symbols are measurements from 40-100 ms after the onset of pursuit. Circles are measurements from rightward pursuit; squares from leftward pursuit. For each measurement, early and late intervals were aligned with the onset of pursuit of individual trials. Bars indicate one standard deviation. B : Measurements of average acceleration in early and late intervals for responses to constant velocity targets with MOD = 0 ms. Symbol conventions are same as in A.

Fig. 1.4

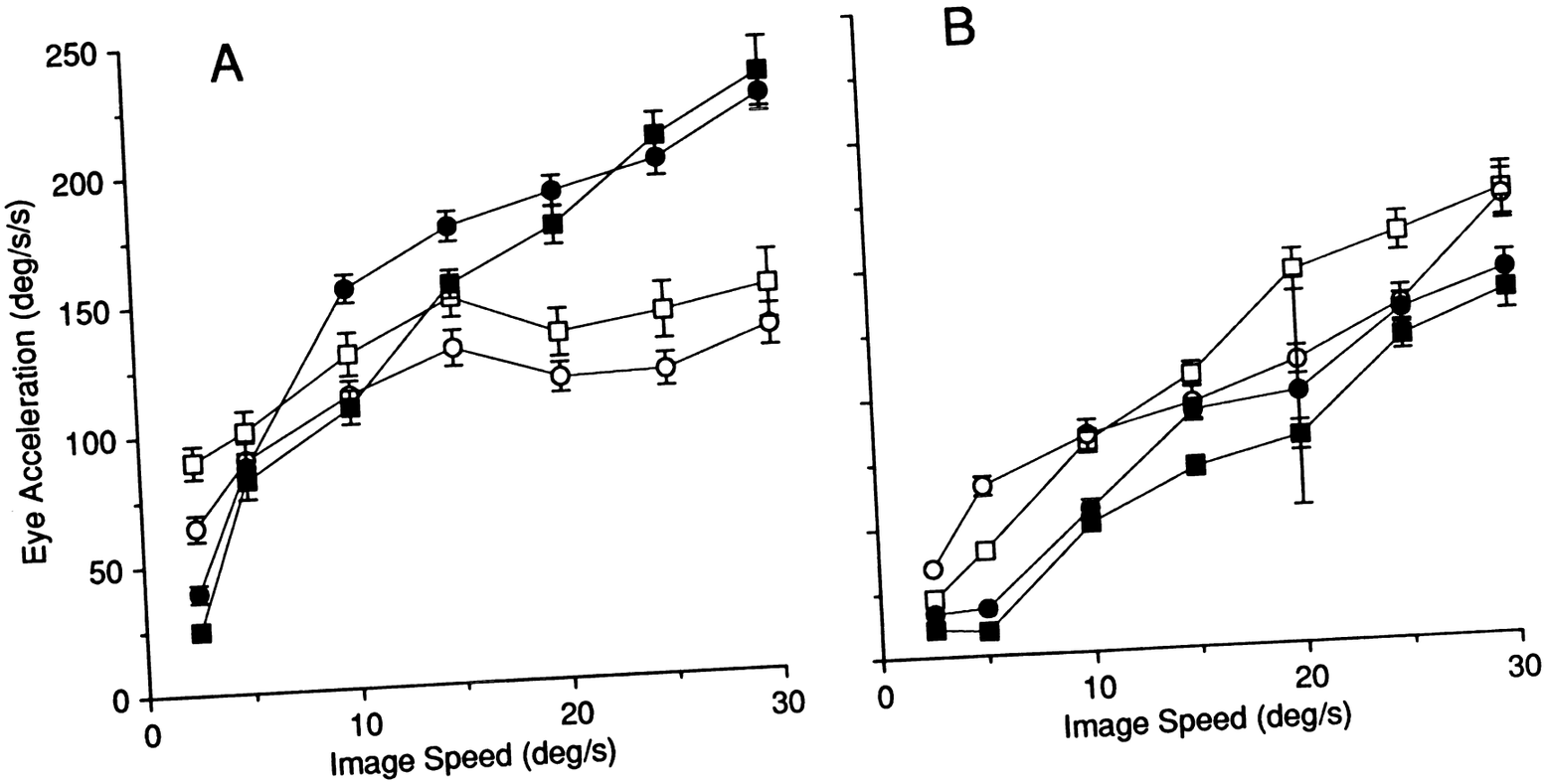
A
B
250
200
150
100
50
0
Eye Acceleration (deg/s/s)
0
10
20
30
Image Speed (deg/s)
0
10
20
30
Image Speed (deg/s)

Figure 1.5. Comparision of eye acceleration evoked by closed-loop and open-loop constant velocity targets. A : Averaged eye velocity responses to two constant velocity targets either under normal closed-loop tracking conditions (solid lines) or using electronic feedback to prolong the interval of controlled image velocity by 100 ms (dashed lines). The arrows are placed 40, 100, and 200 ms after the onset of pursuit. B : Measurements of average eye acceleration from traces like those shown in A. Closed symbols show average acceleration over an interval 40-100 ms after the onset of pursuit for closed-loop tracking. Open symbols show average acceleration over an interval 40-200 ms from responses to targets presented under open-loop conditions. Solid line indicates linear regression of closed-loop data (slope = 8.69, y intercept = 14.27, r = 0.99); dashed line indicates regression of open-loop data (slope = 8.28, y intercept = 4.04, r = 0.99).

Fig. 1.5

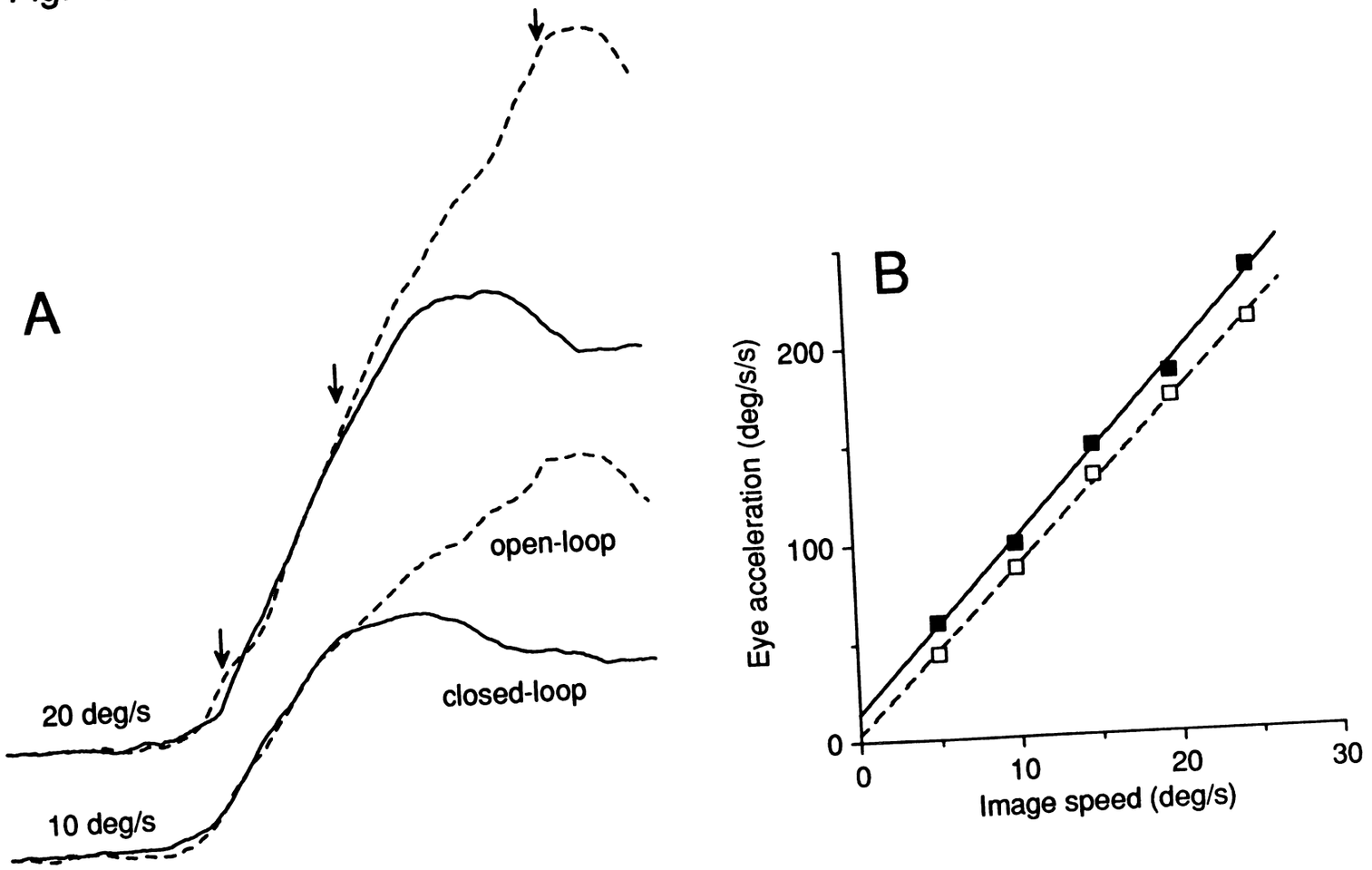
A
20 deg/s
10 deg/s
open-loop
closed-loop
B
Eye acceleration (deg/s/s)
200
100
0
0
10
20
30
Image speed (deg/s)

Figure 1.6. The effect of systematic changes in motion onset delay. A and C : Averaged eye velocity responses to a constant velocity target of 5 °/s for a series of motion onset delays. The number to the immediate left of each trace indicates in ms how long the target was visible before it started to move. Dashed vertical lines indicate an interval 0-40 ms after the onset of the eye movement response. Traces are aligned on the onset of the eye movement response. A is data from monkey O; C is data from monkey J. B and D : Measurements of average eye acceleration for responses from a series of motion onset delays over the interval 0-40 ms. Circles are measurements from rightward eye movements shown in A and C. Squares are measurements from similar leftward eye movements (traces not shown).

Fig. 1.6

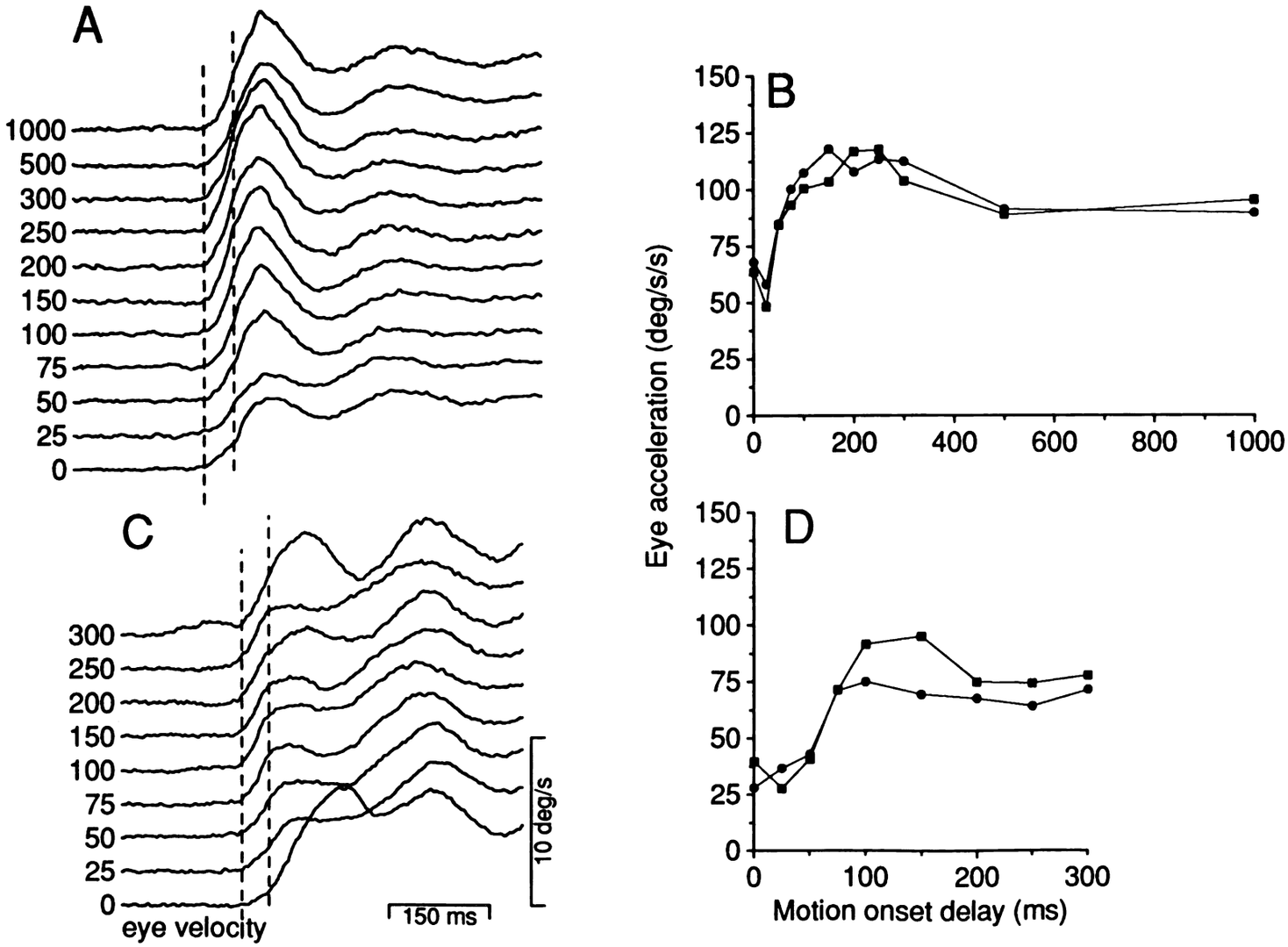
A
1000
500
300
250
200
150
100
75
50
25
0
B
150
125
100
75
50
25
0
0
200
400
600
800
1000
Eye acceleration (deg/s/s)
C
300
250
200
150
100
75
50
25
0
10 deg/s
150 ms
eye velocity
D
150
125
100
75
50
25
0
0
100
200
300
Motion onset delay (ms)

Figure 1.7. Modelling the early and late phases of eye acceleration evoked by constant velocity targets. The diagram (top) shows the flow of signals in both pathways. The input in both cases is a step in image velocity, which is delayed, scaled by a gain element, and then filtered. The box labelled "integ." performs a mathematical integration to convert the eye acceleration command produced by the filter into a simulated eye velocity response. A : Linear gain element used in the image velocity pathway to generate simulated traces shown in C. Line shows actual gain element, symbols are measurements of eye acceleration from either the actual (circles) or simulated (squares) eye velocity traces. B : Step-response of the filter used in the image velocity pathway. The filter was a first order system: $\tau dy(t)/dt + y(t) = x(t)$, with τ equal to 32 ms. C : Comparison of actual (solid) and simulated (dashed) eye velocity responses to constant velocity targets of 2.5, 5, and 10 °/s with a MOD of 0 ms. Arrows are placed at 100 and 165 ms after the onset of target motion. D : Non-linear gain element used in the image motion transient pathway (solid line) and measurements from actual (circles) or simulated (squares) eye velocity traces. The gain function was described by the equation: $y = ax + be^{c/x}$. E : Step-response of the filter used in the image motion transient pathway. The filter was a second order system: $d^2y(t)/dt^2 + 2\zeta\omega dy(t)/dt + \omega^2 y(t) = \omega^2 x(t)$. F : Comparison of behaviorally isolated early component (solid) and simulated (dashed) eye velocity responses to constant velocity targets (2.5, 5, and 10 °/s). The early component was obtained by subtracting the eye velocity responses obtained with a MOD of 0 ms (traces shown in C) from responses obtained with a MOD of 300 ms. Arrows are placed at 80 and 165 ms after the onset of target motion. Simulated eye velocity in F reaches a peak at about 170 ms. This corresponds to when the

step response in E crosses zero, because the step-response in E is a command for eye acceleration which is integrated to produce the pulses of eye velocity shown in F.

Fig. 1.7

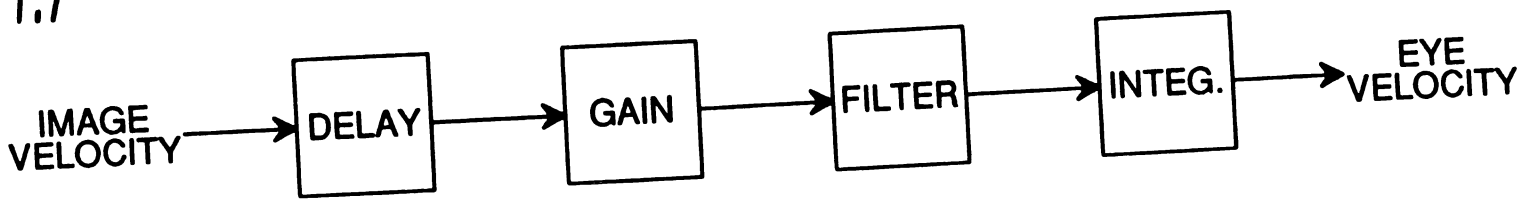
IMAGE VELOCITY
DELAY
GAIN
FILTER
INTEG.
EYE VELOCITY

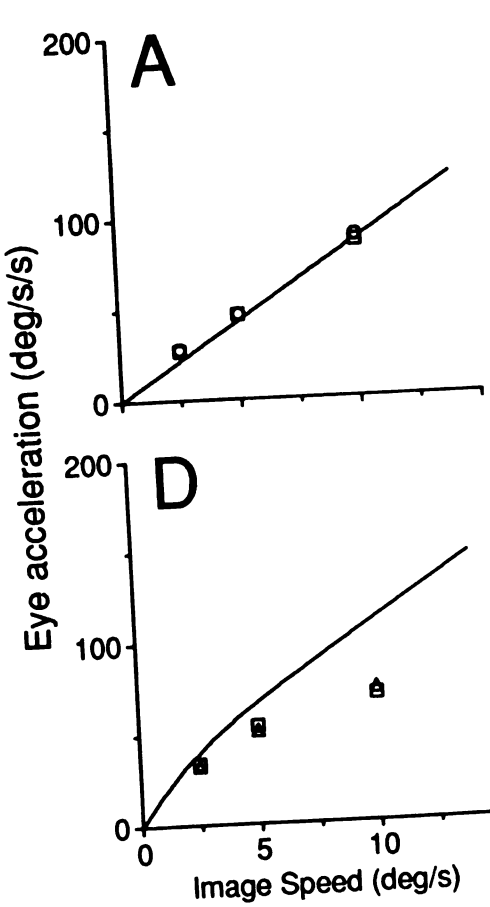
A
200
100
0
Eye acceleration (deg/s/s)
D
200
100
0
0
5
10
15
Image Speed (deg/s)

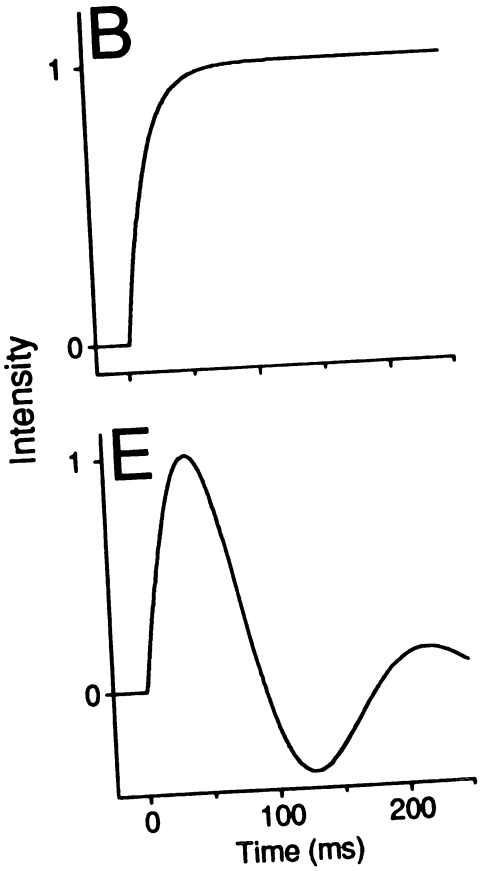
B
1
0
Intensity
E
1
0
0
100
200
Time (ms)

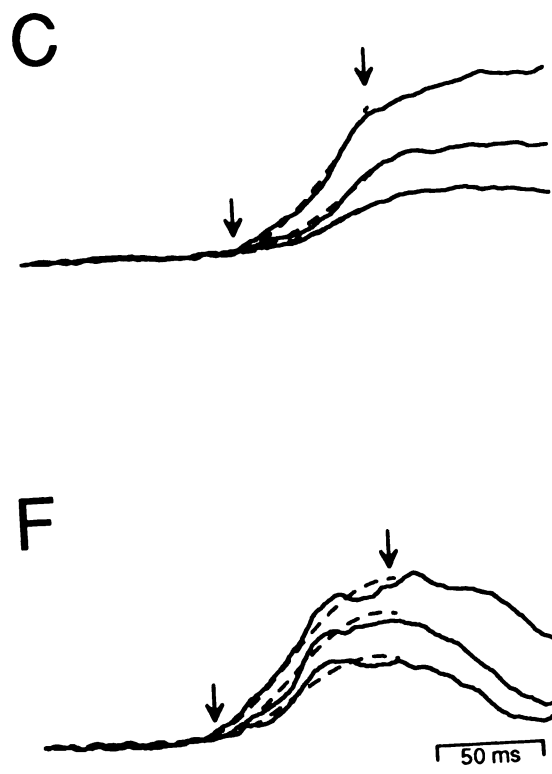
C
F
5 d/s
50 ms

62

Figure 1.8. Fitting image velocity and image motion transient pathways simultaneously to eye velocity responses. A : Comparison of actual (solid) and simulated (dashed) eye velocity responses to constant velocity targets (5, 15, and 25 °/s) presented with a MOD of 300 ms. B : Comparison of eye velocity responses to constant velocity targets presented with a MOD of 0 ms (solid) with the output of the image velocity pathway (dashed), using the same parameters as in A. C : Comparison of behaviorally isolated early component (solid) with the output of the image motion transient pathway (dashed), using same parameters as in A. Traces for the early component were obtained as in Fig. 1.7. D-F : Similar data and simulations from monkey O.

Fig. 1.8

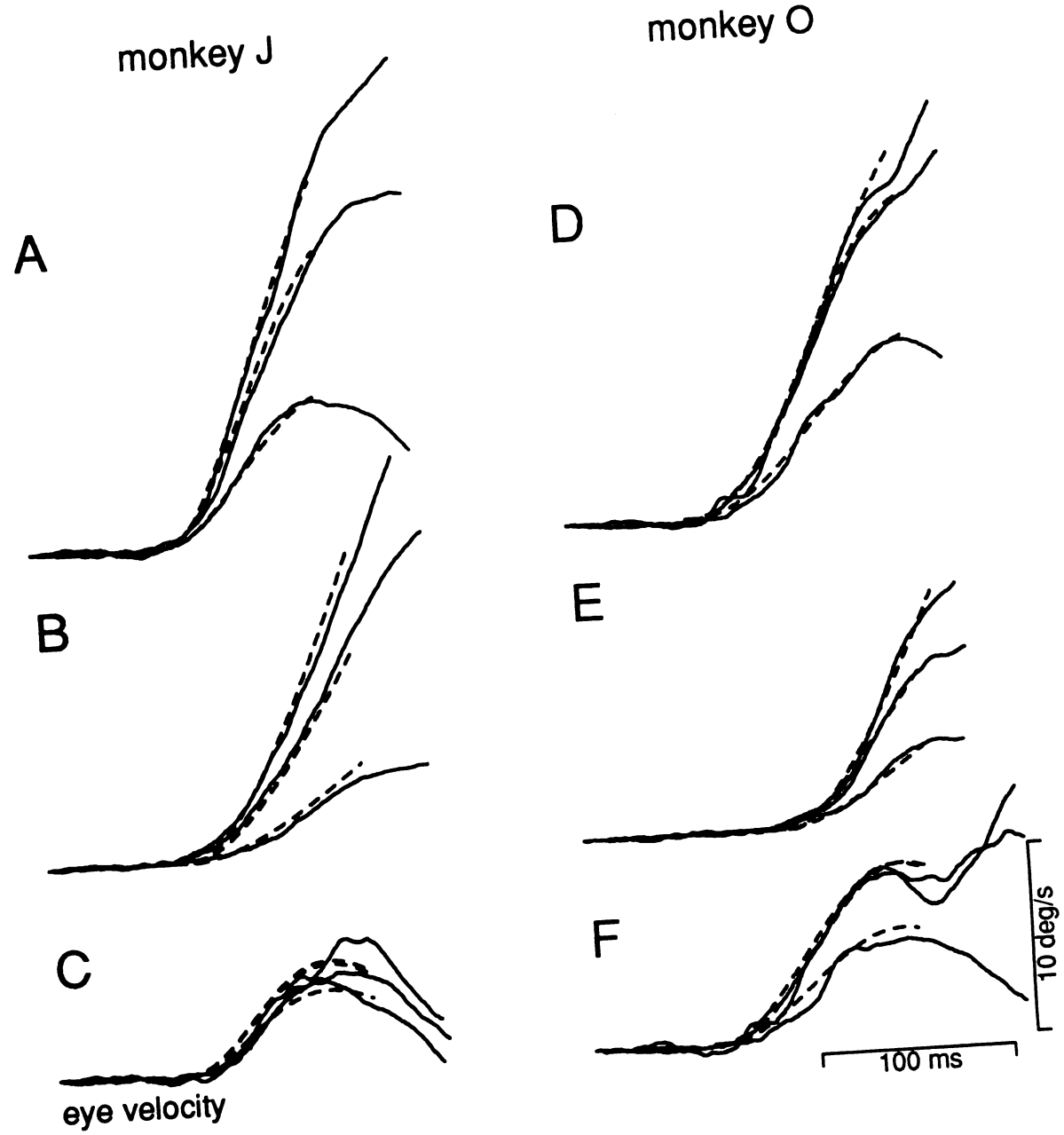

Figure 1.9. Summary of model parameters used to fit eye velocity responses to constant velocity targets from four monkeys. Each row displays parameters from a single monkey. First column shows gain elements used in the image velocity pathways (solid line) and measurements of the later phase of eye acceleration (circles). Second column shows gain elements used in the image motion transient pathway (solid line) and measurements of the early phase of eye acceleration, measured from either the simulated (triangles) or behaviorally isolated early componets (squares). Third column shows step responses of the image velocity (thick lines) and image motion transient (thin lines) pathways.

Fig. 1.9

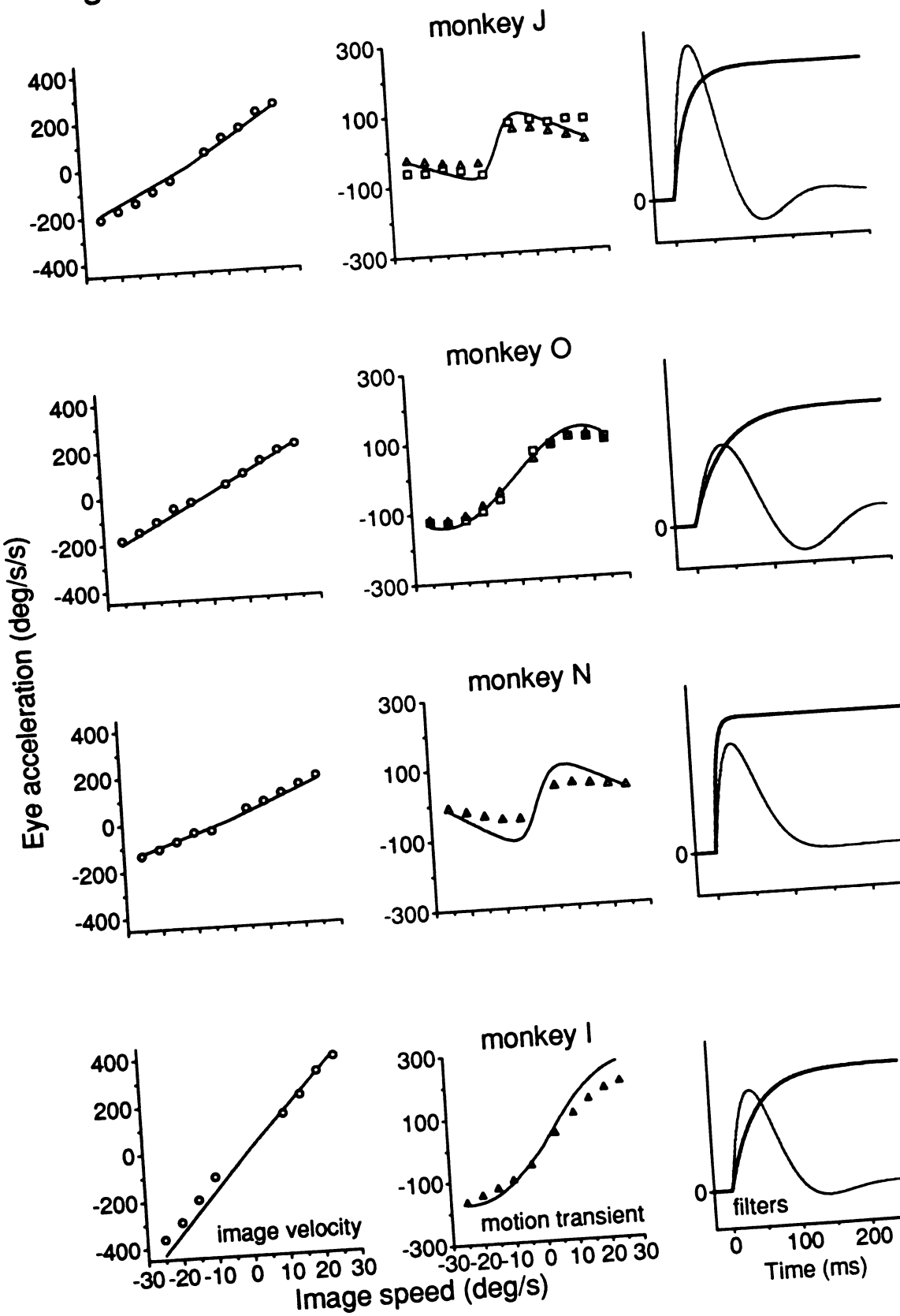
monkey J
monkey O
monkey N
monkey I
400
200
0
-200
-400
300
100
-100
-300
Eye acceleration (deg/s/s)
image velocity
motion transient
filters
-30 -20 -10 0 10 20 30
Image speed (deg/s)
0 100 200
Time (ms)

Figure 1.10. Example of an eye velocity response evoked by a smoothly accelerating target. Dashed line with position traces indicates illumination of fixation LED. Cropped upward deflection in eye velocity occuring approximately 250 ms after the onset of the response represents a saccadic eye movement.

Fig. 1.10

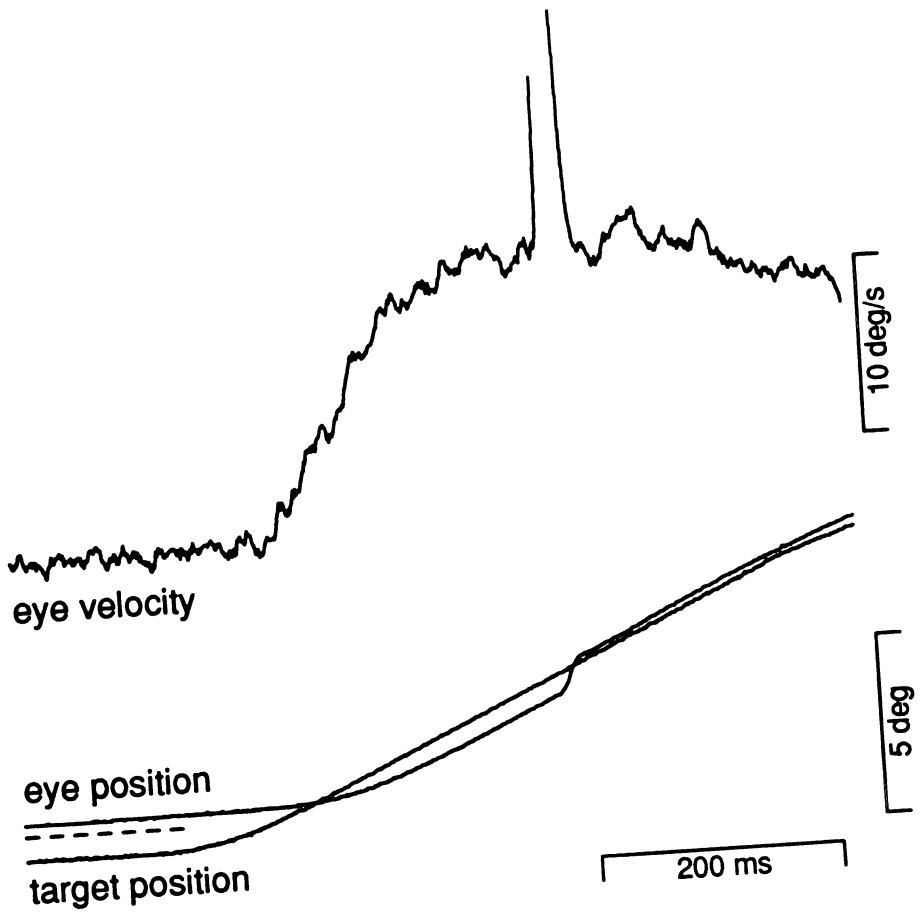
10 deg/s
eye velocity
5 deg
eye position
target position
200 ms

Figure. 1.11 Latency measurements for monkey O for constant velocity (A) and smoothly accelerating (B) targets. Each symbol represents the average latency to initiate pursuit for one speed or rate of acceleration. Lines show results of linear regression of the data.

Fig. 1.11

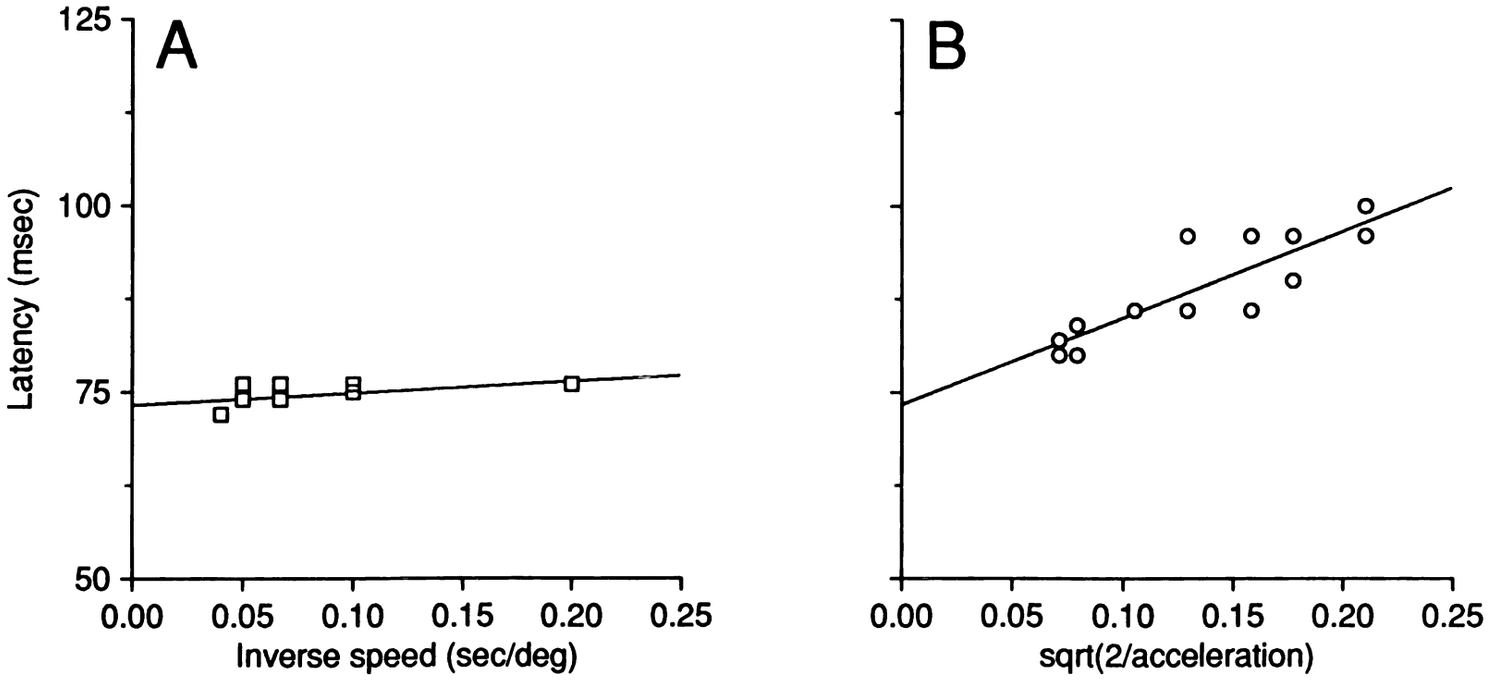
A
125
100
75
50
Latency (msec)
0.00
0.05
0.10
0.15
0.20
0.25
Inverse speed (sec/deg)
B
0.00
0.05
0.10
0.15
0.20
0.25
sqrt(2/acceleration)

Figure 1.12. Predicting responses to accelerating targets using the image velocity pathway. A : Comparison of actual response to smoothly accelerating target (solid) and response predicted by using ramp in image velocity as input to the image velocity pathway (dashed). Parameters used to generate predicted responses were same as those described in Fig. 1.9. B : Difference traces obtained by subtracting predicted traces from actual eye velocity traces in A. C : Comparison of predicted response to smoothly accelerating target to actual eye velocity response under either normal closed-loop conditions or using electronic feedback to extend the open-loop period by 50 ms. D : Difference traces obtained by subtracting predicted trace from the two actual eye velocity responses shown in C. The difference obtained from the open-loop eye velocity response deviated from the closed-loop trace at approximately 162 ms, indicated by the first arrow, and continues to increase in amplitude. The second arrow indicates 212 ms, the time when the effect of prolonged image motion would be expected to end.

Fig. 1.12

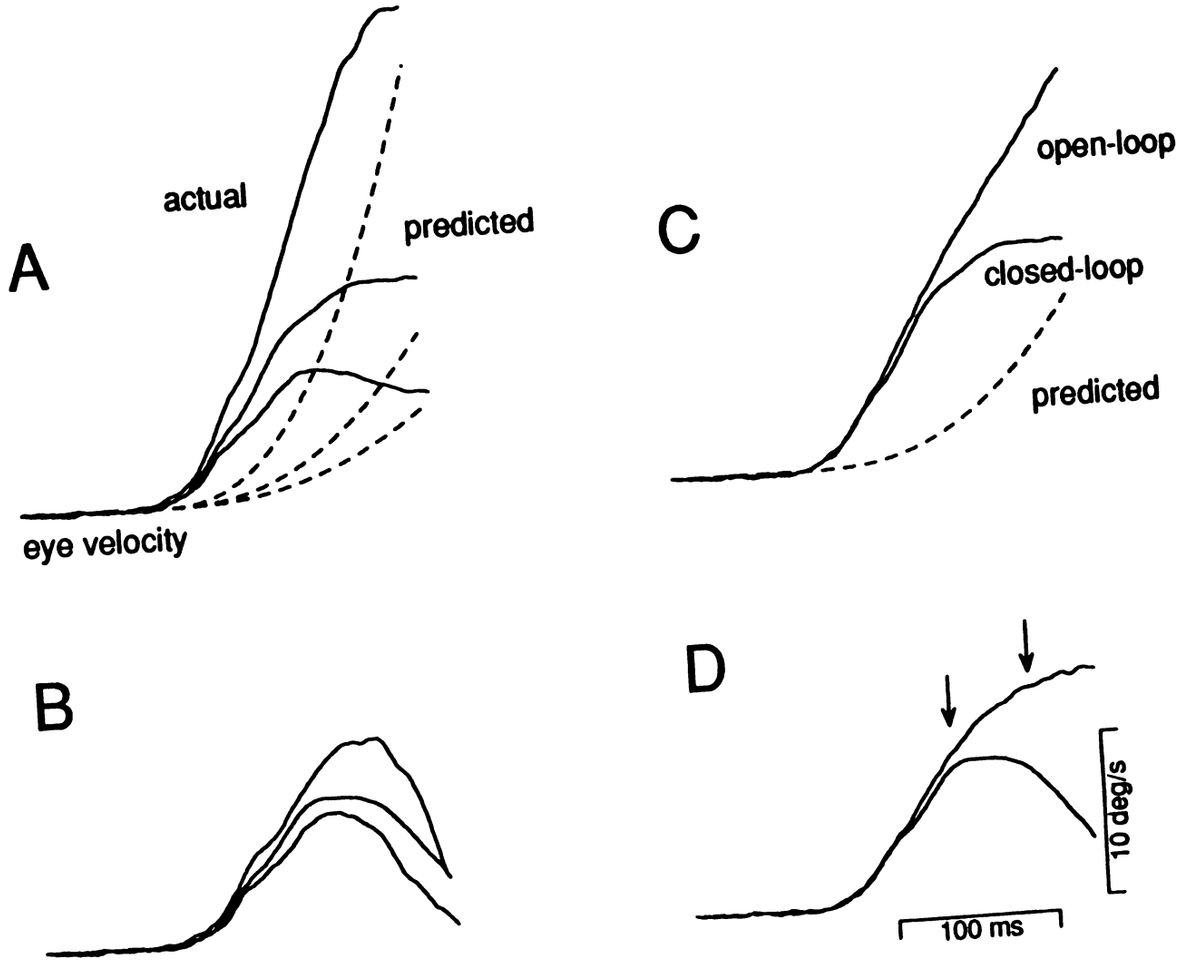
A
actual
predicted
eye velocity
B
C
open-loop
closed-loop
predicted
D
10 deg/s
100 ms

Figure 1.13. Effect of using different latencies to generate predicted responses to accelerating targets. Traces on the left compare actual (solid) and predicted (dashed) responses to a smoothly accelerating target, using a latency of 25 ms to generate the predicted responses. Graph on the right shows how error of predicted response changed as a function of simulation latency. Error was measured as the sum of the squared difference between each simulated and actual eye velocity point, divided by the number of points. The three lines plot error separately for three smoothly accelerating targets (64, 120, and 180 $^{o}/s^{2}$). The square indicates the error associated with the simulated late component of pursuit shown in Fig. 1.7C. The triangle indicates the error associated with the composite model's fit to constant velocity targets presented with a MOD of 300 ms shown in Fig. 1.8D. The arrow indicates a simulation latency of 25 ms.

Fig. 1.13

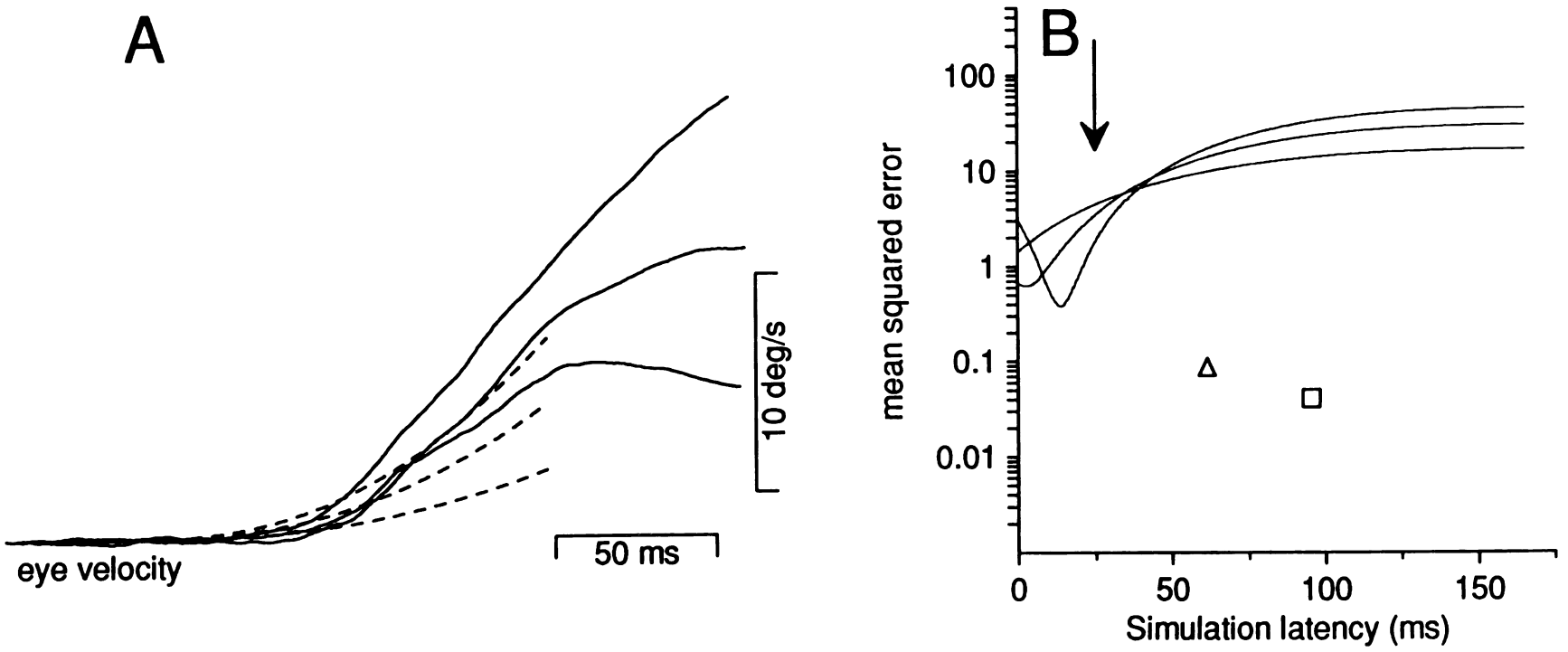
A
eye velocity
50 ms
10 deg/s
B
mean squared error
100
10
1
0.1
0.01
0
50
100
150
Simulation latency (ms)

Figure 1.14. Modeling the additional eye acceleration evoked by smoothly accelerating targets. The diagram on top shows the flow of signals in the model, which is identical to image velocity and image motion transient pathways, except that the order of the filter and gain elements is reversed. A : Step-response of the filter used in image acceleration pathway. Filter behaves as a low-pass differentiator. B : Gain element used in the image acceleration pathway (solid line) and average eye acceleration over the open-loop period (circles) measured from difference traces shown in C. C : Comparison of difference traces (solid) and output of the image acceleration pathway (dashed). Difference traces were obtained by subtracting output of the image velocity pathway from the actual response to smoothly accelerating targets. Arrows indicate open-loop interval.

Fig. 1.14

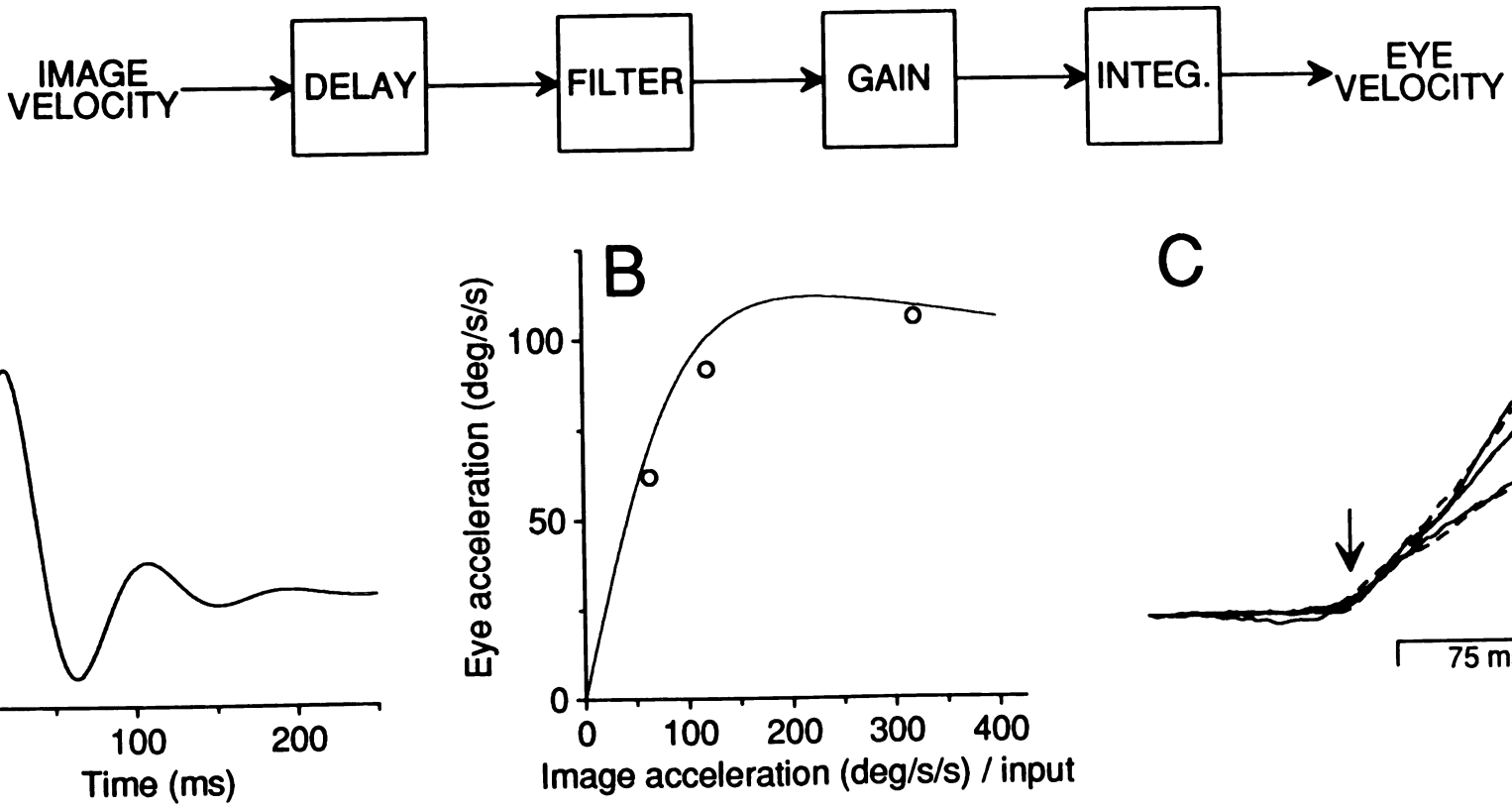
IMAGE VELOCITY
DELAY
FILTER
GAIN
INTEG.
EYE VELOCITY
A
Intensity
0
0
100
200
Time (ms)
B
Eye acceleration (deg/s/s)
100
50
0
0
100
200
300
400
Image acceleration (deg/s/s) / input
C
10 deg/s
75 ms

Figure 1.15. Summary of parameters used in image acceleration pathway for four monkeys. Each row shows parameters from a single monkey. Left column shows step-responses of filters. Right column shows the gain elements (solid line) and average eye acceleration from difference traces (circles) measured over the open-loop interval.

Fig. 1.15

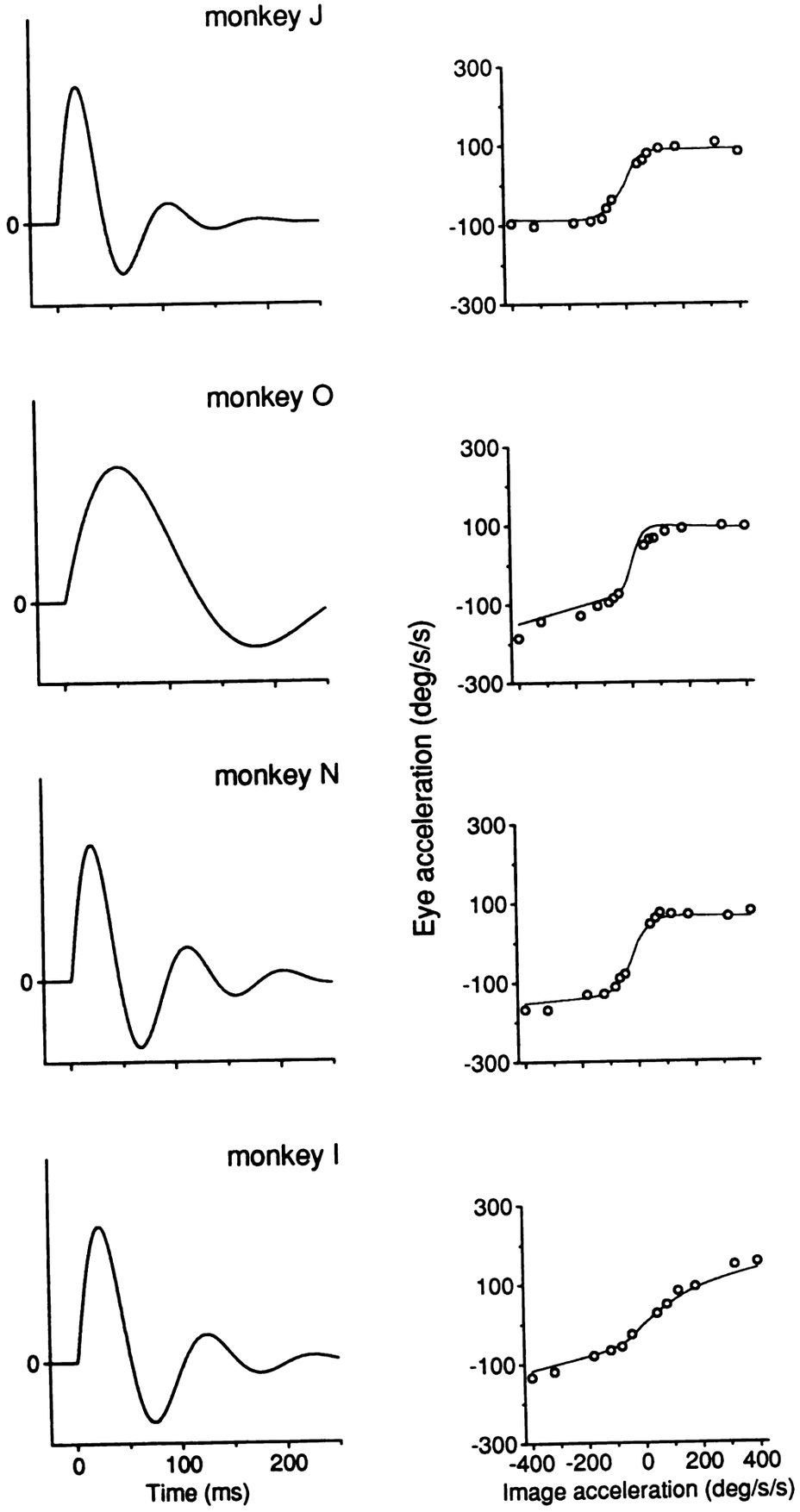
monkey J
monkey O
monkey N
monkey I
0
300
100
-100
-300
Eye acceleration (deg/s/s)
0
100
200
Time (ms)
-400 -200 0 200 400
Image acceleration (deg/s/s)

Figure 1.16. Errors associated with simulated responses produced by models with two or three pathways. Each of the four graph shows the error produced with simulations for data from one monkey. Each point compares the error of the fit to responses evoked by constant velocity targets with the error of the fit to responses to smoothly accelerating targets. Different filled symbols represent errors associated with a different set of parameter values, using a model consisting of an image velocity and an image motion transient pathway. Squares show errors associated with parameters optimized to constant velocity targets. Circles show errors with parameters optimized to smoothly accelerating targets. Triangles show errors with parameters optimized to both. Open diamonds show errors associated with parameters optimized to fit both, but using a three pathway model that includes an image acceleration pathway. For each monkey, each symbol represents the average error for five constant velocity trials (5, 10, 15, 20, 25 $^{o}/s$) or five smoothly accelerating trials (45, 64, 80, 180, 320 $^{o}/s^2$). There are two of each symbol for each monkey, because leftward and rightward trials were treated separately.

Fig. 1.16

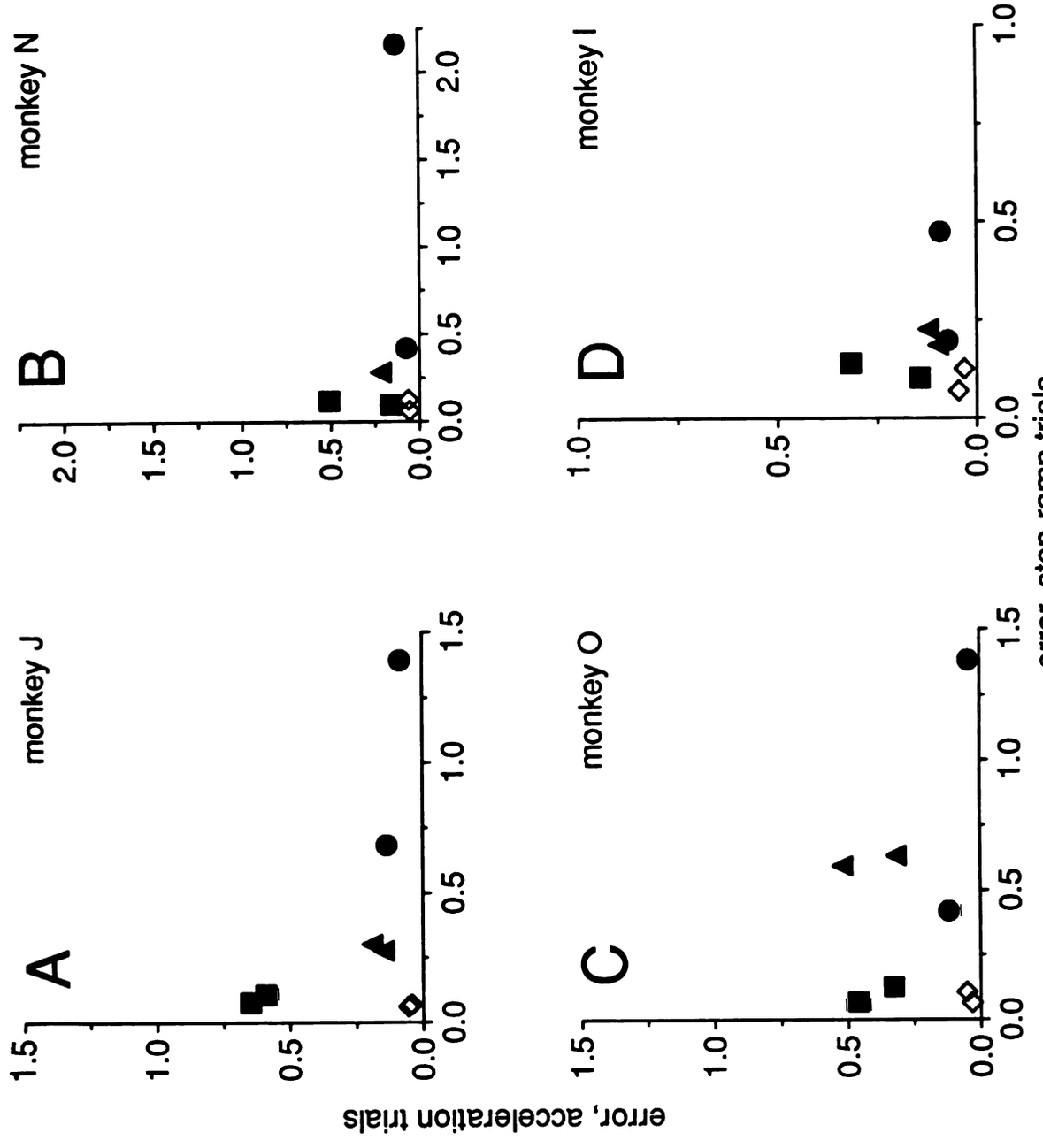
A
monkey J
B
monkey N
C
monkey O
D
monkey I
error, acceleration trials
error, step-ramp trials

Figure 1.17. Target motion used to examine the termination of pursuit. Position traces on bottom show how a 20 °/s constant velocity target steps forward and stops at the end of the trial. Middle traces show the image velocity associated with this target motion and an individual eye velocity response. Top trace shows averaged eye velocity response from monkey O to presentation of the target motion. Dashed lines indicate one standard deviation. Responses consistently showed a brief twitch immediately before the decay in eye velocity, as can be seen in the averaged trace. This twitch was in the same direction as the target motion and may have been a response to the final step used to eliminate corrective saccades.

Fig. 1.17

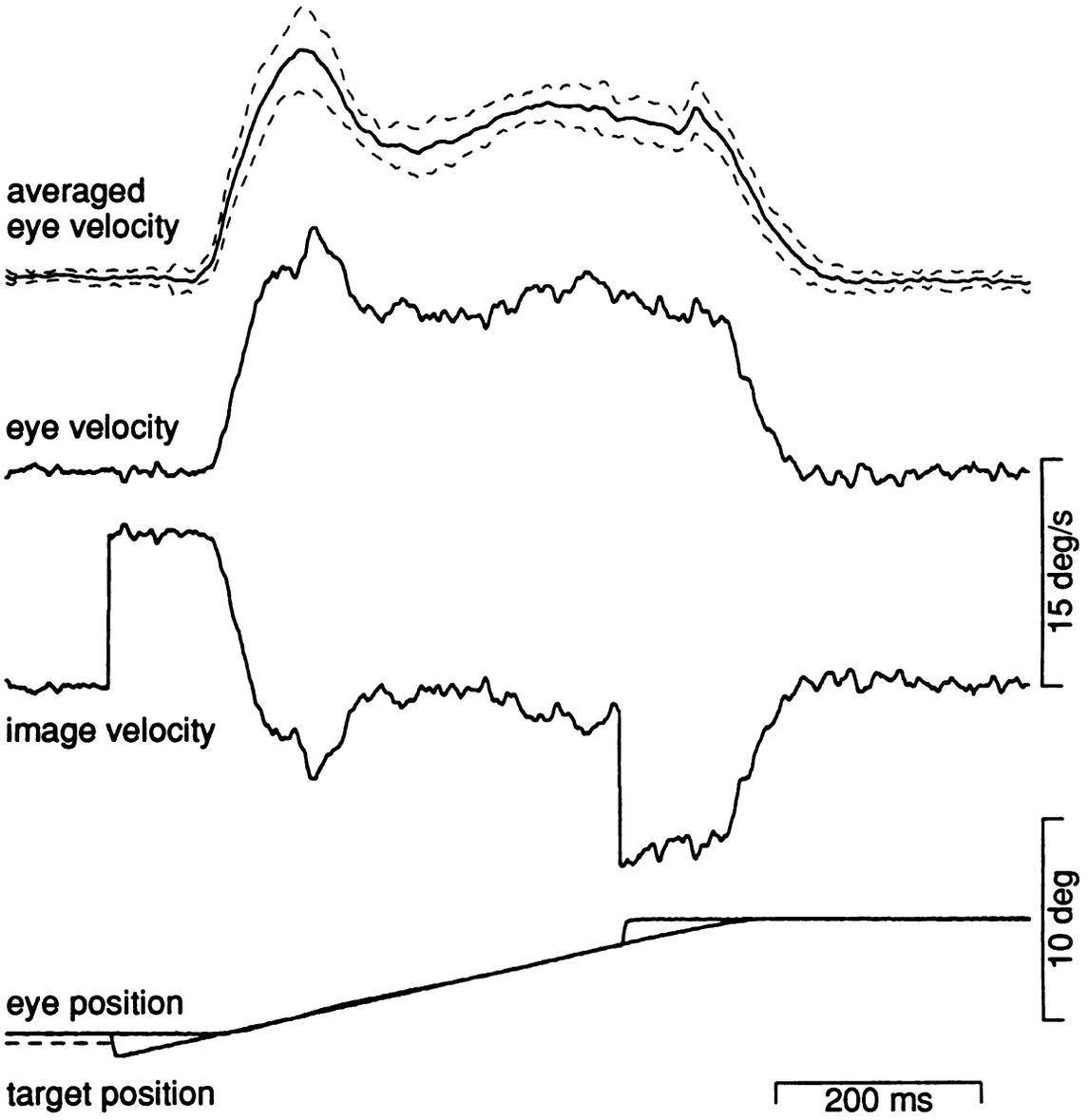
averaged
eye velocity
eye velocity
image velocity
15 deg/s
10 deg
eye position
target position
200 ms

Figure 1.18. Offset of pursuit scaled linearly with speed. A and B : Averaged eye velocity responses to two target speeds (10, 20 °/s) presented as shown in Fig. 1.16, for rightward (A) and leftward (B) directions. C and D : Superimposition of traces shown in A and B achieved by linear scaling.

Fig. 1.18

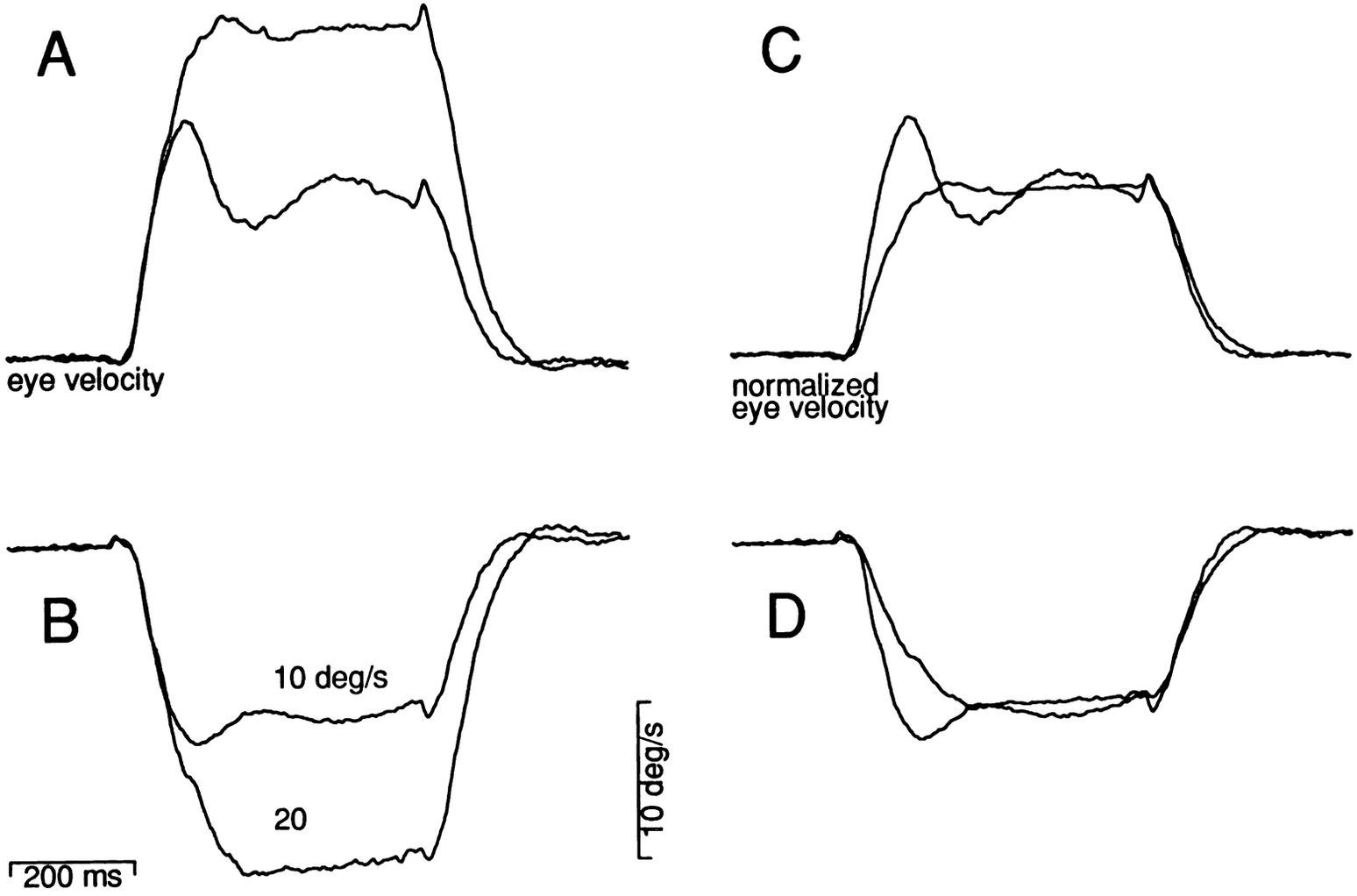
A
eye velocity
C
normalized
eye velocity
B
10 deg/s
20
200 ms
10 deg/s
D

Figure 1.19. Summary diagram of the model describing the visual inputs underlying the initiation of pursuit. Components are described using Laplace notation.

Fig. 1.19

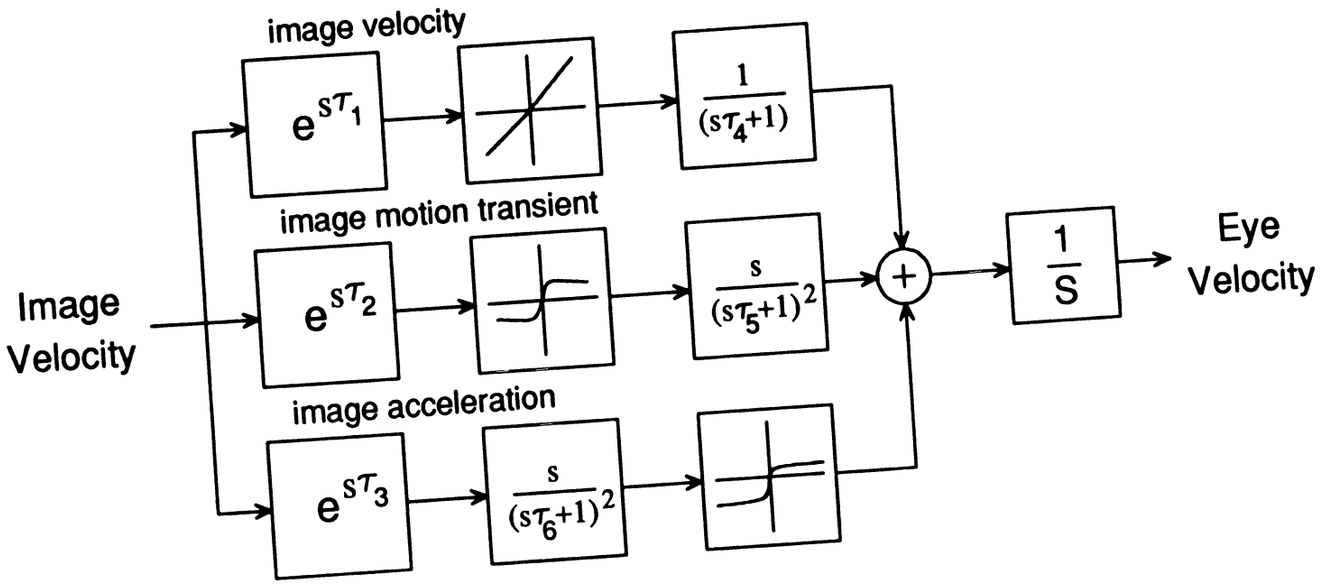
image velocity
image motion transient
image acceleration
Image Velocity
$e^{s\tau_1}$
$e^{s\tau_2}$
$e^{s\tau_3}$
$\frac{1}{(s\tau_4+1)}$
$\frac{s}{(s\tau_5+1)^2}$
$\frac{s}{(s\tau_6+1)^2}$
+
$\frac{1}{S}$
Eye Velocity

Chapter Two

A model of pursuit eye movements based on behavioral observations

Summary and conclusions

1. We developed a class of model that reproduces several properties of the pursuit system revealed by recent behavioral and physiological experiments. The basic form of the model is a negative-feedback system that considers visual motion to represent a command for eye acceleration. A mathematical integrator placed within the feedback loop converts the visual motion signals into changes in eye velocity and maintains eye velocity in the absence of image motion.

2. We began with a description of the properties of the visual motion inputs for pursuit, based upon our analysis of the initiation of pursuit described in chapter one. These visual motion inputs are included in the model as three separate parallel pathways that are sensitive to image velocity, image acceleration, and an image motion transient.

3. The properties of visual motion processing can account for many of the features of both the initiation and the maintenance of pursuit. For example, the sensitivity to image acceleration included in the model reproduces the high frequency oscillations in eye velocity sometimes observed during pursuit and matches the system's response to higher frequency target motions. Also, the variation in the trajectory of pursuit eye velocity observed in different monkeys or in one monkey on different trials can be accounted for by changes in the sensitivities to the three visual motion inputs.

4. Visual motion inputs cannot reproduce the change in eye velocity observed at the termination of pursuit. To account for this aspect of pursuit eye movements, we introduced a pre-motor circuit that supplants the mathematical integrator. The pre-motor circuit can switch between two modes: a nearly perfect integrator and a very leaky integrator. In the first mode, the circuit performs the same function as the mathematical integrator used previously. In the second mode, the circuit produces an output that decays exponentially. The time constant of the decay can be set to match the smooth changes in eye velocity observed at the termination of pursuit.

5. The mode of operation of the pre-motor circuit is governed by an input that acts through a "soft switch". The function of this switch is consistent with evidence, provided by electrical stimulation at different sites in the brain, that the pursuit system contains a "switch". The role of the input that controls the switch parallels the functions ascribed to area MST. Changing the value assigned to this input affects both the initiation and the maintenance of smooth pursuit, similar to the effects observed after MST lesions.

6. The results of our simulations indicate that the three visual motions signals included in the model reflect important aspects of the processing underlying pursuit. Our results also provide alternate interpretations concerning the role of non-visual signals in the generation of pursuit. The issues raised by the model suggest specific questions about how individual neural structures participate in the genesis and control of pursuit eye movements.

Introduction

Study of pursuit eye movements has provided a wealth of data about both the dynamics of the pursuit movements and the role of particular brain structures in generating pursuit. The variety and saliency of these observations place strict constraints on the organization of the neural systems underlying pursuit. The construction of models that attempt to embody these constraints can provide a useful tool for highlighting unresolved issues in the control of pursuit eye movements and for focusing investigation of the brain structures needed for pursuit. However, over the past several years the description of novel properties in the pursuit system has largely outpaced the development of quantitative models. The information currently available about pursuit eye movements suggests three major criteria that candidate models of the pursuit system should satisfy. First, the model should be able to replicate the dynamics of pursuit eye velocities produced during tracking of the target motions used most often to assess smooth pursuit behavior -- ramps of constant target speed and sinusoidal target motion. Second, the model should be able to reproduce the exaggerated pursuit eye movements produced by behavioral manipulations or electrical stimulation, as well as the deficient performance caused by lesions. Finally, because the organization of the pursuit system is believed to be largely conserved across primates, a single class of model should be able to account for the pursuit behavior of both monkeys and humans.

Recent models of pursuit have focused on the first criterion -- replicating the trajectory of eye velocity observed during pursuit tracking. The principle challenge has been to define a model that can both match the

initial rise in eye velocity at the initiation of pursuit and reproduce the correct frequency of oscillations in eye velocity that often occur during maintained pursuit. One class of model, developed by Robinson et al. (1986) to fit data from human subjects, succeeds in reproducing both the initiation of pursuit and the steady-state oscillations by segregating control over these two phases of pursuit. The trajectory of eye velocity at the initiation of pursuit is driven by the visual inputs, whereas oscillations during steady-state are controlled by an internal feedback loop. The observed frequency of steady-state oscillations observed in humans can be reproduced by adjusting the total delay around the internal feedback loop.

A second class of model accomplishes similar goals using visual signals related to image acceleration, as well as image velocity (Morris and Lisberger 1985; Lisberger et al. 1987, Krauzlis and Lisberger 1989). One version of this model (Krauzlis and Lisberger 1989) is based upon analysis of the first 100 ms of pursuit eye velocity evoked by steps and ramps of target velocity in monkeys. As shown in Fig. 2.1, the model includes three pathways that allow non-linear processing of visual signals related to image velocity, image acceleration, and an image motion transient. This model also provides independent control over the dynamics of the initiation and maintenance of pursuit, because the initiation of pursuit is controlled by the image velocity and image motion transient pathways, while steady-state pursuit is dominated by the image acceleration pathway (Krauzlis and Lisberger 1989).

Recent experiments in monkeys have provided data that discriminate between the two classes of models. It was observed that when the delay in visual feedback is increased, the frequency of spontaneous oscillations in eye velocity is reduced (Goldreich et al. in press). This suggests that the oscillations are a consequence of visual feedback and not due to an internal

feedback loop. Preliminary simulations of the two classes of models showed that the Krauzlis and Lisberger model (1989) could reproduce the observed changes in oscillation frequency, while the Robinson et al. (1986) model could not. These results indicate that the models based upon multiple visual inputs (Morris and Lisberger 1985, Krauzlis and Lisberger 1989) more accurately describe the organization of the pursuit system.

There are other features of normal pursuit that are not reproduced by either class of model. For example, most models of pursuit predict that at the termination of pursuit, when the target abruptly stops as the eye is moving at a constant velocity, the eye should respond to the ensuing visual motion just as it does at the initiation of pursuit. In fact, eye velocity at the termination of pursuit does not display the overshoot and ringing that are characteristic of the initiation of pursuit, but usually returns smoothly to zero (Robinson et al. 1986; Luebke and Robinson 1988). The absence of ringing cannot be attributed to an asymmetry in the dynamics of pursuit for decelerations versus accelerations, since decelerations of the eye during pursuit do produce overshoot and ringing if they do not bring eye velocity near zero (Luebke and Robinson 1988). These and other observations have led to the suggestion that pursuit may contain a "switch" that marks the transition between fixation and pursuit tracking. For example, spontaneous oscillations in eye velocity occur frequently during pursuit, but are rarely observed during fixation (Robinson et al. 1986). It has also recently been shown that the pursuit system can respond to target motions with frequencies as high as 6 Hz, but only if the target motions are presented after pursuit has been initiated (Goldreich et al. in press).

An additional challenge is to design a model with components that can easily reproduce the abnormal pursuit eye movements observed in

behavioral lesion and stimulation experiments. The retinotopic deficits in pursuit seen after lesions of the middle temporal visual area (MT) could be modeled as the creation of a scotoma for visual motion (Newsome et. al., 1985), with the result that the pursuit system no longer has access to visual error signals from a localized portion of the visual field. However, lesions in the medial superior temporal sulcus (area MST) cause deficits in pursuit eye movements toward the side of the lesion that are not as easily explained (Dursteler et al. 1987, Dursteler and Wurtz 1988). It has also been shown that stimulation at some brain sites always evokes a smooth pursuit eye movement (Ron and Robinson 1973; Belknap and Noda 1987; MacAvoy et al. 1988), while stimulation at other sites produces a smooth eye movement only if pursuit has already been initiated (May et. al., 19nn; Komatsu and Wurtz, 1989). The conditional effects of electrical stimulation of pursuit pathways may be a further consequence of a "switch" in pursuit.

The goal of the present chapter is to provide evidence that the class of model presented in chapter one can replicate the observed dynamics of pursuit using a structure that is consistent with the known biology of the system. We first describe how the three visual motion pathways can replicate the observed trajectories of eye velocity during the initiation and maintenance of pursuit. We next document that the model can reproduce the spontaneous oscillations in a manner that is consistent with the observations of Goldreich et al. (in press). Finally, we introduce a modification that allows the model to switch between pursuit and fixation and to replicate the eye velocity observed at the termination of pursuit. We will show that the model is applicable to humans as well as monkeys, and that the inclusion of a switch in the model can provide a functional

explanation for the effects observed after stimulating or ablating the visual pathways that provide inputs for pursuit.

Methods

Acquisition of pursuit eye velocity data

Averaged eye velocity traces shown in this paper are derived from the same set of data as presented in chapter one. Detailed methods of how these data were obtained were described in the Methods section of that chapter.

Construction and simulation of models

The software for implementing the models was written in "C" language and run on a DEC microvax II and on a DECstation 3100. The model was initially described as a block diagram consisting of a set of functions and differential equations. The block diagram was converted into a set of discrete numerical routines in C programming language using "bomol", a modeling program written by Lance Optican and Herschel Goldstein. The code describing the model was incorporated as a subroutine into an interactive program that was used to run simulations of the model, to adjust parameters in the model, to make measurements of the model's performance, and to compare model simulations directly with eye velocity data.

Individual parameters in the model were adjusted in one of two ways. For clarity, the two methods will be referred to throughout the paper as "optimized" and "adjusted by hand". When parameters were "optimized", the user marked some or all of the parameters and specified a set of eye velocity data to which the model was to be matched. The program then iteratively adjusted the marked parameters to provide a least-squares fit to the

data. As described in the previous paper, parameter values were adjusted using the downhill simplex method of Nelder and Mead (1965). During this automatic procedure, all unmarked parameters were held fixed at their initial values. When parameters were "adjusted by hand", the user assigned values directly to individual parameters. Adjustment by hand was used for two purposes. First, parameters were usually adjusted by hand before they were optimized to improve the efficiency and reliability of the fitting algorithm. Second, adjustment by hand was used to assess the role of individual parameters.

The program also provided several functions for characterizing the performance of the model's output. One function measured the error of the model's fit to the eye velocity data. Error was quantified as the sum of the squares of the difference between actual and simulated eye velocity at each ms in the selected interval, divided by the number of milliseconds. A second function measured the amplitude and frequency of the model's output for sinewave inputs. An interval of the simulated eye velocity was selected and the program calculated the amplitude, frequency and phase shift of the best-fitting sinewave. Finally, the program provided outputs that showed the simulated eye velocity from the model, the signals present at different nodes in the model, the functions in the gain elements, and the step-responses of the filters.

Results

Weighting of visual motion inputs required for realistic pursuit eye velocity

Fig. 2.2 shows the results of adjusting the parameters in the model to match the first 80 ms of pursuit eye velocity for monkey J. The details of how the parameter values for the gain functions and filters were obtained were described in the first chapter. The solid traces in Fig. 2.2A show the average eye velocity responses for the first 80 ms during the initiation of pursuit of targets moving at constant velocities of 5, 15, and 25 °/s rightward (upward deflected traces) and leftward (downward deflected traces). The solid traces in Fig. 2.2B show the average eye velocity to targets smoothly accelerating at 64, 120, and 320 °/s^2. The dashed traces show the simulated responses obtained by optimizing the parameters in the three visual motion pathways of the model to fit these first 80 ms of data as described in the methods section. The image velocity pathway contained the linear gain element (G_v) shown in Fig. 2.2C and a filter (H_v) with the step-response shown in Fig. 2.2D. The image motion transient pathway used the saturating gain function (G_t) shown in Fig. 2.2E and a filter (H_t) with the step-response shown in Fig. 2.2F. Finally, the image acceleration pathway contained the saturating gain function shown in Fig. 2.2G (G_a) and a filter with the step-response shown in Fig. 2.2H (H_a).

We began by testing the emergent properties of the models with parameters that were optimized to match the open-loop eye velocity measured from the first 80 ms of pursuit. We provided the model with the same inputs as before, but ran the simulation for a total of 450 ms to produce a simulated eye velocity that displayed the effects of eye velocity feedback. In both the model and the monkey, the eye velocity beyond the first 80 ms of

pursuit showed the effects caused by eye velocity negative feedback (dashed lines in Fig. 2.1) and therefore revealed the closed-loop behavior of the system. As shown in Fig. 2.3 for monkey J, the parameters that were optimized to match open-loop pursuit provided only a rough fit to closed-loop eye velocity. The solid traces in Fig. 2.3A show the average eye velocity obtained during pursuit of constant velocity targets moving at 5, 15, and 25 °/s and the dashed traces show the simulated eye velocities obtained using the best-fit parameters from open-loop pursuit. Fig. 2.3B shows average eye velocities and simulated eye velocities obtained with steps in target acceleration of 64, 120, and 320 °/s^2. For both constant velocity and accelerating targets, the initiation of pursuit was accurately modeled, but the simulated eye velocities tended to be lower than the actual eye velocity during steady-state and they showed pronounced ringing in the transition from initiation to steady-state tracking.

We improved the closed-loop performance of the model by optimizing the parameters for the gain elements in the three motion processing pathways, while holding the filter parameters fixed. Fig. 2.3C compares average and simulated eye velocities to steps in target velocity with the new parameters and Fig. 2.3D shows data for steps in target acceleration. A few distinct changes in the gain elements allowed the model to produce these improved simulated eye velocities. For the image velocity pathway (Fig. 2.3E), the optimized gain element (thick line) was described by the equation: $y = ax + be^{c/x}$, and deviated slightly from the linear gain element derived from the initiation of pursuit (thin line). In particular, the gain function for closed-loop pursuit had slightly different slopes and showed an additional reduction in gain around 0 °/s of image velocity. For the image motion transient pathway, the gain element used to match closed-loop pursuit (Fig. 2.3F, thick

line) had the same shape as the gain element for open-loop pursuit (thin line), but had a lower peak. For the image acceleration pathway, the two gain elements (Fig. 2.3G) saturated at about the same rate of image acceleration, but the gain element for closed-loop pursuit (thick line) had a substantial reduction in gain around 0 $^{o}/s^{2}$ of image acceleration.

Fig. 2.4 shows the results of modeling the eye velocity for the other three monkeys. We made a separate model for each monkey and first optimized the parameters based upon the first 80 ms of eye velocity evoked by constant velocity and smoothly accelerating images. We then held the filter elements fixed and optimized the parameters in the gain elements to achieve best fits to closed-loop pursuit eye velocity. Figs. 2.4A, C, and E show simulated (dashed) and actual (solid) eye velocities evoked by steps in target velocity of 5, 15, and 25 $^{o}/s$. Figs. 2.4B, D, and F show simulated and actual eye velocities for targets that smoothly accelerated at rates of 64, 120, and 320 $^{o}/s^{2}$. In each case, despite the different profiles of eye velocity exhibited by different monkeys for identical stimuli, the model was able to generate good matches to the data. In particular, the model was able to match the initial rise in eye velocity at the onset of pursuit and achieve a realistic transition to steady-state eye velocity with either modest overshoot in eye velocity (Figs. 2.4A and B), no overshoot (Figs. 2.4C and D), or large overshoot (Figs. 2.4E and F).

Changes in the properties of the gain functions used to match closed-loop pursuit did not seriously affect the ability of the model to match open-loop pursuit. We measured the mean squared error of the model's fit to averaged eye velocity during the initiation of pursuit (0 to 80 ms) and during the entire trial (0 to 450 ms). We then compared the errors of the fits produced with parameters matched to either to open-loop or to closed-loop data. Mean squared error was defined as the sum of the squares of the

difference between actual and simulated eye velocity at each ms in the analysis interval, divided by the number of milliseconds. The four graphs in Fig. 2.5 present the results from the four monkeys. Each symbol plots the error during the initiation of pursuit against the error over the entire trial. The open circles show the errors obtained with the model fit to the first 80 ms of pursuit (open-loop) and the filled squares show the errors obtained with the model fit to the entire trial (closed-loop). The dashed lines have a slope of one, indicating the case of equal error for both conditions. For each monkey, the open-loop model provided much better fits to the initiation of pursuit than to the entire trial, as indicated by the fact that the circles are clustered to the left of the dashed lines. The models fit to closed-loop pursuit provided a much better fit over the entire trial with a small increase in error during initiation, as indicated by the fact that the squares are clustered just above the dashed lines.

The differences in the gain elements for open-loop and closed-loop pursuit was likely caused by the differences in the range of image motion signals presented to the optimization algorithm. The histograms in Fig. 2.6 show the relative frequency of image velocity signals and image acceleration signals that occurred during the simulations shown in Figs. 2.2 and 2.3. During the initiation of pursuit (Fig. 2.6B and D), the distribution of image motion signals was characterized by peaks at the constant velocities and smooth accelerations used in our experiments. The image velocity signals during pursuit initiation (Fig. 2.6B) also showed a plateau between -5 and 5 ^{o}/s due to the smaller image velocities produced by the smoothly accelerating targets. In contrast, when the frequency of image velocity and image acceleration was measured over the entire trial, the histograms (Fig. 2.4A and C) showed a large peak around 0. The range of image motion signals that

increased in frequency during closed-loop pursuit matched the range of image motion signals that were most affected by the dead-zones shown in Fig. 2.3E-G. For example, the dead-zone in the gain function for the image acceleration pathway (Fig. 2.3G) had its largest impact on image accelerations below 50 $^{o}/s^{2}$. Comparison of Figs. 2.6C and D shows that while most image accelerations during closed-loop pursuit were below 50 $^{o}/s^{2}$, these small image accelerations were not present during the initation of pursuit.

We documented the performance of the model by measuring its output when stimulated by sinewaves of different amplitudes and frequencies. As shown diagramatically in Fig. 2.7A, for each sinewave input, we measured the gain of the model's performance by dividing the amplitude of the model's sinusoidal output (A2) by the amplitude of the sinusoidal input (A1). We determined the phase of the model's performance by measuring the delay (d) between the peak in the input sinewave and the peak in the output of the model. This delay was converted to a relative phase measurement by dividing it by the period of the input sinewave (T) and expressing this fraction in terms of degrees. Because the image motion transient pathway did not contribute to steady-state performance of the model, we eliminated the contribution of this pathway to avoid spurious phase shifts that would otherwise be contributed by this pathway.

Applying this analysis to the models used for monkey J demonstrated two major points. First, because of the nonlinearities in the three visual pathways, the response of the models depended on the amplitude of the input, as well as the frequency. The four different types of lines in Figs. 2.7B to E correspond to different input amplitudes ranging from 1.0 to 10.0 $^{o}/s$ peak velocity. To provide a basis for evaluating these measurements, gain and phase measurements made directly from monkey J, that have been

presented previously (Fig. 8 of Goldreich et al. in press), are shown by symbols superimposed on the graphs. The open circles and triangles show data for rightward and leftward pursuit, respectively. The amplitude of the sinewave target motion used to obtain these measurements was $\pm$ 8 °/s.

Second, the stability of the model's behavior required that the gain functions for the image velocity and image accelerations contain additional reductions for values near zero. The effect of these "dead-zones" is shown in Fig. 2.7 by comparing the behavior of the model fit to the initiation of pursuit (Figs. 2.7B and C) with the behavior of the model fit to the entire trial (Figs. 2.7D and E). The gain of the model without the dead-zones (Fig. 7B) was much larger than one for low frequencies, regardless of amplitude. For higher frequencies, the gain showed a large dependence on the amplitude of the input, as shown by the divergent paths taken by the different types of lines in Fig. 2.7B. Including the dead-zones in the gain elements of the model (Fig. 2.7D) both eliminated the very large gains for low frequencies and reduced the amplitude-dependence of the gain at higher frequencies. The phase of the model in the absence of the dead-zones (Fig. 2.7C) did not match the experimentally measured phase lags and, in particular, had an unrealistically large phase lag at low frequencies. For the model that included the dead-zones (Fig. 2.7E), the phase lag was less than 45° for low frequencies and increased monotically for higher frequencies in a way that provided a much better match to the phase lags measured directly for monkey J.

Contribution of visual motion signals to features of pursuit eye velocity

ROLE OF THE THREE VISUAL MOTION COMPONENTS DURING PURSUIT OF CONSTANT VELOCITY TARGETS. The three visual motion processing pathways had disparate effects on the simulated eye velocity produced by the model during both the initiation of pursuit and steady-state pursuit. Fig. 2.8

illustrates the signal transformations performed by the three pathways during pursuit of a 20 °/s constant velocity target. The traces in Fig. 2.8 represent signals at different nodes in the model during the simulation. The trace in the first column shows image velocity, which provided the input to the three visual pathways. In the second column, the top, middle and bottom traces show the individual outputs from the image velocity, image motion transient, and image acceleration pathways, respectively. These traces show how the gain elements and filters transformed image velocity into three separate commands for eye acceleration. In the model shown in Fig. 2.1B, these three signals were summed, integrated to produce a command for eye velocity, and then low-pass filtered by the oculomotor output pathway. However, for illustrative purposes, the third column in Fig. 2.8 shows the components of eye velocity that would have been produced if each eye acceleration command had been integrated and passed through the oculomotor output pathway separately. These traces show that the image velocity pathway was responsible for most of the model's output. The image motion transient pathway contributed an early pulse of eye acceleration that had its maximal effect within the first 100 ms of the output. As shown by the dashed vertical lines, the contribution of the image acceleration pathway began at twice the latency for the other two pathways, because image acceleration did not occur when the target started to move, but only after the eye started to move. The image acceleration pathway acted in the opposite direction as the image velocity and image motion transient pathways, braking eye velocity during the transition to steady-state tracking, because it was responding to the decrease in image velocity.

The role of the three pathways can also be illustrated by eliminating the contribution from one pathway and observing the performance of the

reduced model. The three sets of traces in Fig. 2.9 compare the normal performance of the model during pursuit of a 20 constant velocity target (dashed line) with its performance when the gain in one of the three pathways was set by hand to equal zero (solid lines). When the contribution of the image velocity pathway was eliminated (Fig. 2.9A), the majority of the visual inputs driving eye velocity was abolished, so the initiation of pursuit was severely compromised and the eye never reached an appropriate steady-state velocity. When the image motion transient pathway was lesioned (Fig. 2.9B), the earliest eye acceleration was lessened, but eye velocity reached target velocity and there was a smooth transition from the initiation of pursuit to steady-state tracking. When the image acceleration pathway was lesioned (Fig. 2.9C), the initiation of pursuit was unaffected, but there was a large overshoot in the transition to steady-state eye velocity. This indicates that the image acceleration pathway acted as a brake on eye velocity as the speed of the eye approached the speed of the target. This allowed the model to use a high gain in the image velocity pathway to produce a brisk initiation of pursuit without suffering from an excessive overshoot in eye velocity.

VARIATION IN THE TRAJECTORY OF PURSUIT EYE VELOCITY. The variations observed in the eye velocity evoked on individual trials by the same target motion can be accounted for by changes in the gains of the three visual motion pathways. The uppermost solid trace in Fig. 2.10 displays the averaged eye velocity to fourteen presentations on one day in monkey J of target motion at a constant of 10 °/s and the dashed trace superimposed on the eye velocity trace shows the simulated eye velocity produced by a model with parameters optimized to fit these data. The surrounding dashed lines represent one standard deviation of the eye velocity data. We then matched the output of the model to the fourteen individual eye velocity traces that

were used to generate the averaged trace. We held all parameters in the model fixed at the values used to fit the average and multiplied the output of each pathway by a different scaling factor. The traces labelled A, B, and C show eye velocities for four individual trials (solid lines) and the best-fit simulated eye velocities (dashed lines) obtained with the optimized scaling factors. Scaling the outputs of the three pathways was able to account for the varying amounts of ringing and overshoot in the four eye velocity traces. The two graphs in Fig. 2.10 display the distribution of scaling factors applied the three pathways used to match the eye velocity from all fourteen trials. The points marked by letters correspond to the four eye velocity traces shown to the left. Scaling of different pathways was associated with particular features of eye velocity. For example, trace A had the highest image acceleration gain and showed oscillations that were increasing in amplitude. Trace B had a lower image acceleration gain and showed oscillations that were decreasing in amplitude. Trace C had a large image motion transient gain and showed a large overshoot, while trace A had a small image motion transient gain and no overshoot.

We next assessed whether the changes in the gains required to fit individual trials occurred gradually over the course of the 1 - 2 hours during a single experiment or if changes like those shown in Fig. 2.10 occurred between consecutive trials. We optimized the parameters in the model to match the averaged eye velocity recorded during pursuit of targets moving at constant velocities of 5, 10, 15, 20 and 25 °/s. The individual eye velocity records used to calculate these averages were obtained in an experiment which lasted about 2 hours, during which time the monkey performed slightly over 1300 trials. Contained within this sequence of trials were the constant velocity target motions, presented in randomized order and directed

either rightward or leftward, as well as several other target motions used as catch trials. Holding the parameters fixed at the values matched to the averaged traces, we optimized a scaling factor at the output of each pathway to match the eye velocity recorded on consecutive experimental trials. The three graphs in the left half of Fig. 2.11 plot the values of the scaling factors obtained for each of the three pathways as a function of trial number. As the dispersion of the data in each plot indicates, the values of the scaling factors required to match the individual eye velocity records varied widely from trial to trial. To provide an example of this trial-to-trial variation, the traces in the right half of Fig. 2.11 show an example of four experimental trials that occurred consecutively. The scaling factors required to match the output of the model (dashed lines) to the recorded eye velocity (solid lines) for these sample trials are indicated in the graph by connecting lines. These traces show that both the scaling factors and the eye velocity records could show large changes from one trial to the next. For example, the eye velocity evoked by the 25 °/s leftward target motion in trail #297 evoked little overshoot in eye velocity, but did evoke high frequency oscillations with a large amplitude. On the very next trial, a target moving at 15 °/s rightward evoked a slight overshoot with no high frequency oscillations.

For monkey O, we had data from experiments performed on different days that allowed us to compare the eye velocity records evoked by the same target motions over the course of two months. In particular, we recorded his eye movements on the very first day he tracked target motions presented in our experimental paradigm, as well as on the second day and on several subsequent days. We analyzed these data by optimizing the parameters in the model to match the averaged eye velocity records obtained on an experiment performed 22 days after the first experiment. These eye velocity records and

model parameters are the same as those used in Fig. 2.4 to characterize the mature pursuit behavior of monkey O. We held the parameters in the model fixed and optimized a scaling factor at the output of each pathway to match the data obtained on days preceding and following day #22. For each day, we matched the model to averages of eye velocity recorded during pursuit of targets moving at constant velocities of 5, 10, 15, 20 and 25 °/s. In addition, for day #0, we generated separate averages for the data obtained during the first and second halves of the experiment.

The graphs in the left half of Fig. 2.12 plot the values of the scaling factors obtained for each of the three pathways as a function of experimental day. Unlike the results obtained from individual trials in the well-trained monkey (Fig. 2.11), the scaling factors showed gradual changes while monkey O was learning the task. Initially, neither the image motion transient or image acceleration pathways were required to match his eye velocity. As shown by the uppermost trace in the right half of Fig. 2.12, the eye velocity (solid line) evoked by a target moving at 15 °/s displayed an onset that occurred at the same time as on later days (lower traces), but showed a much slower rise in eye velocity. The model reproduced this behavior using just the image velocity pathway (dashed line). In addition, as shown by the two superimposed data points in the graphs for day #0, there were no differences in the results obtained with data from the first and second halves of the experiment. For the data obtained on day #1, the model used the image acceleration pathway and assigned a larger gain to the image velocity pathway. These changes were reflected in the faster rise in eye velocity shown by the eye velocity and modeled traces shown for day #1. In contrast, the image motion transient pathway was not used by the model until day #8. The invocation of the image motion transient pathway provided the slightly

faster rise in eye velocity observed on day #8 as compared to day # 1. It is possible that the changes attributed to the image motion transient pathway occurred sometime during the week between the experiments performed on days #1 and #8. Finally, after day #8, both the averaged eye velocity records and the scaling factors used in the model were relatively constant.

OSCILLATIONS DURING STEADY-STATE PURSUIT. The gains of the visual motion pathways controlled the amplitude of the oscillations in simulated eye velocity produced by the model during steady-state. Fig. 2.13 shows how changes in the gain of the image velocity and image acceleration pathways affected the amplitude of steady-state eye velocity oscillations. The image motion transient pathway affected the amplitude of initial ringing, but it did not contribute during continuous pursuit, because its contribution to eye velocity was restricted to the first 50 to 100 ms of the model's output. Fig. 2.13A shows that changes in the gain of the image velocity pathway affected the transition of simulated eye velocity to steady-state, but did not have a large effect on steady-state oscillations. The parameters used for these simulations were adjusted to exaggerate the amplitude of the oscillations. The numbers to the left of each trace indicate the factor by which the output of the image velocity pathway was scaled. When the image velocity gain was reduced by hand to one-half or one-quarter of its normal value (lowest two traces), the initial rise in eye velocity was blunted, while when the image velocity gain was increase by 50% (highest trace), there was an overshoot in eye velocity. In both cases, however, the amplitude and frequency of steady-state oscillations were approximately the same, contrary to the behavior predicted by a linear model (Goldreich et al. in press). The apparent differences in frequency shown by the traces in Fig. 2.13A were due to the larger ringing present when the gain of the image velocity pathway was

increased. For example, in the highest trace, the excessive overshoot in eye velocity prolonged the transition to steady-state oscillations, but the frequency of steady-state oscillations was 5.5 Hz, just slightly lower than the 5.6 Hz oscillations produced when the gain of the image velocity pathway was multiplied by 0.25 (lowest trace). Likewise, the amplitude of the steady-state oscillations in the highest and lowest traces were nearly identical (1.67 and 1.61 °/s, respectively).

Changes in the gain of the image acceleration pathway had pronounced effects both on the transition to steady-state and on steady-state oscillations. When the image acceleration gain was one-quarter of its normal value (lowest trace in Fig. 2.13B), there was a large overshoot in eye velocity and negligible steady-state oscillations. When image acceleration was increased by hand by 50% (uppermost trace in Fig. 2.13B), the overshoot in eye velocity was reduced and the steady-state oscillations were very pronounced. The frequency of oscillations was the same for each case (5.5 Hz), but the amplitude of oscillations increased from essentially 0 °/s in the lowest trace to 3.3 °/s in the highest trace.

To further document the different roles played by the image velocity and image acceleration pathways in defining the behavior of the model, Fig. 2.14 shows plots describing the response of the model to sinusoidal inputs. The measurements shown in these plots were obtained in the same way as for the data presented in Fig. 2.7C and D. However, here we compared the response of the normal model with responses in which the contribution of image acceleration and image velocity had been altered. We used a single amplitude input with a peak velocity of 2.5 °/s and multiplied the output of the image velocity or acceleration pathway by 0, 0.5, or 1.5. When the gain of the image velocity pathway was altered (Fig. 2.14A), there were large changes

in the response of the system for frequencies below 5 Hz, but only small changes above this frequency. For example, when the image velocity pathway gain was lowered, the gain of the system was much lower at low frequencies and the phase lag was reduced. In contrast, when the contribution of the image acceleration pathway was altered (Fig. 2.14B), the response of the system was nearly unchanged for frequencies below 2 Hz, but there were large changes for higher frequencies. For example, increasing the gain in the image acceleration pathway amplified the system's response to inputs with frequencies near the frequency at which the output showed a phase shift of -180°. Increasing the gain of the image acceleration pathway also dramatically reduced the system's phase lag. When the contribution of the image acceleration pathway was eliminated, the model reached a phase shift of -180° at 2.5 Hz, compared to 5.0 Hz in the intact model.

The frequency of steady-state oscillations depended upon the total delay through the image velocity and image acceleration pathways. Fig. 2.15 demonstrates the effect of increasing the total delay by imposing additional delays in eye velocity feedback in the model. The lowermost trace in Fig. 2.15 shows the simulated eye velocity produced by the model with the same parameters used in Fig. 2.14, which included a delay of 65 ms in the visual pathways. The traces above it were produced by imposing additional delays in the external feedback loop (dashed line in Fig. 2.1) by the amount indicated alongside each trace. As the imposed delay was increased, the period of oscillation increased, as would be expected of a negative feedback system (Goldreich et al. in press). In addition, the oscillation amplitude also increased, as the larger additional delays made the model less stable.

The effect of imposed delay on oscillation period was measured in the models for each of the four monkeys. The graph in Fig. 2.16 plots the major

oscillation period observed during steady-state output of the model against the additional delay imposed in eye velocity feedback, using the parameters that matched eye velocity during closed-loop pursuit. Each line shows the results for one monkey. For each monkey, there was a progressive increase in oscillation period as the imposed delay was increased. In one case (monkey I), there was an abrupt increase in oscillation period for additional imposed delays of 100 to 120 ms. This abrupt change occurred when the pathway primarily responsible for the steady-state oscillations switched from the image acceleration pathway (shorter imposed delays) to the image velocity pathway (longer imposed delays). The other three monkeys did not show such an abrupt change, but for each monkey, the slope of the curves was less steep for shorter imposed delays than it was for longer imposed delays.

Features of pursuit not replicated by visual motion processing

We next examined several properties of pursuit eye movements that cannot be accounted for by the model shown in Fig. 2.1B. In this section of the paper, we will first discuss two features of pursuit eye velocity that could not be reproduced by the three visual motion pathways. In the following section, we will suggest how the model shown in Fig. 2.1B can be modified to account for these features.

In humans and monkeys, it has been observed that steady-state pursuit eye velocity is not always equal to target velocity (e.g., Collewijn and Tamminga 1984, Fetter and Buettner 1990, Lisberger et al. 1981, Meyer et al. 1985, Robinson et al. 1986). The steady-state gain of the pursuit system, defined as eye velocity divided by target velocity, can be either greater than or less than one, but on average tends to be slightly less than one. However, the model shown in Fig. 2.1B always exhibits a steady-state gain close to one. The traces in Fig. 2.17 compare the normal output of the model (solid line), using

parameters from monkey J, with the output of the model when the contribution of the visual motion pathways was reduced to 0.75, 0.5 and 0.25 times its normal value (dashed lines). Although the initial eye acceleration was diminished when the visual inputs were reduced, eye velocity still climbed toward a steady-state value that matched target velocity. As long as eye velocity memory was able to properly sustain eye velocity, even grossly reduced visual inputs were eventually sufficient to generate a steady-state output with a gain of one.

The model also cannot replicate the decay in eye velocity observed at the termination of pursuit. If eye acceleration at the termination of pursuit were driven by the same visual motion inputs as at the initiation of pursuit, eye velocity should show overshoot and ringing when the eye stops. The solid lines in Fig. 2.18 show the averaged eye velocity generated in response to a target that moved at 5 ^{o}/s for 500 ms either rightward (upper traces) or leftward (lower traces) and then stopped. The parameters in the three visual pathways were adjusted so that the output of the model (dashed lines) matched the first 575 ms of the eye velocity trace, an interval which ended at the time indicated by the two arrows in Fig. 2.18A. When the model was then allowed to respond to the image motion caused by the stopping of the target, it showed overshoot and ringing. In particular, because the stopping of the target caused image motion in the direction opposite to eye velocity, the offset of pursuit for rightward tracking resembled the initiation of pursuit for leftward tracking, and vice versa. Making simple changes in the visual motion signals that contributed to the offset of pursuit could not make the model match the observed decay in eye velocity. Fig. 2.18B shows the model's response when the image motion transient pathway was prevented from contributing to eye velocity at the offset of pursuit and Fig. 2.18C shows the

model's response when only the image velocity pathway was allowed to contribute to eye velocity at the offset of pursuit. In neither case did the output of the model match the observed trajectory of eye velocity.

The traces shown in Fig. 2.18 are individual cases in which the use of visual inputs failed to match the termination of pursuit, but there may be general reasons for this failure. The trajectory of eye velocity at the termination of pursuit always had approximately the same shape -- it was simply scaled by the amplitude of steady-state eye velocity. In contrast, the trajectory of eye velocity during the initiation of pursuit showed great variation for different target motions, an effect reproduced in the model by using nonlinear processing of visual motion inputs. It might be possible to match the termination of pursuit by assuming that the gain functions changed from the nonlinear functions required to match the initiation of pursuit to linear functions during steady-state pursuit. However, this solution seems unlikely, since the model required nonlinear gain functions during steady-state pursuit as well as during initiation. Even the gain element in the image velocity pathway, which was initially described with a linear function, must have nonlinear properties in order for the model to generate realistic steady-state outputs.

A proposed circuit for implementing eye velocity memory

We now propose a simple circuit that can reproduce the features of pursuit shown in Figs. 2.17 and 2.18. The ability to generate steady-state eye velocity that does not equal target velocity (Fig. 2.17) indicates that eye velocity memory does not always act like a perfect mathematical integrator. One possible mechanism for achieving a variable integration relies on the principle that the "leaky" integration performed by a function can be improved by the use of positive feedback. A first-order system, $\tau^2 dy(t)/dt +$

$\tau y(t) = x(t)$, is an example of a function that performs a leaky integration. When provided with a pulse as an input, the output of a first-order system is a step increase that decays exponentially to zero (Fig. 2.19A). The "leakiness" of the integration is determined by the time constant, τ. Adding a positive feedback loop, whose gain is controlled by G, makes the integrator less leaky. As shown in Fig. 2.19B, this circuit can approximate a perfect integrator if G is set equal to $1/\tau$. If G is less than $1/\tau$, the output will decay with an effective time constant given by the formula: $\tau_e = 1/[(1/\tau) - G]$. If G is greater than $1/\tau$, the output of the circuit will not decay, but instead will increase exponentially.

A seredipitous aspect of using a leaky integrator to accomplish eye velocity memory is that the time constant, τ, of the first order system can be chosen to match the decay in eye velocity at the offset of pursuit. We exploited this feature to account for the data shown in Figs. 2.17 and 2.18. For example, we set τ equal to 60 ms, which approximated the time constant of the exponential decay in eye velocity observed at the offset of pursuit (Fig. 2.18). When we then set G equal to 16.67, the circuit shown in Fig. 2.19B converted eye acceleration commands into commands for pursuit eye velocity like the mathematical integrator used previously. We could also increase or decrease G so that the steady-state gain of the model was greater than or less than one. If G was then set equal to zero, the output of eye velocity memory decreased exponentially with a time constant of 60 ms, mimicking the observed decay in eye velocity.

Fig. 2.20 shows how we incorporated this circuit into our model. A key feature of the modified model was that it now included a "soft switch", represented by the multiplicative junction preceding the leaky integrator H_i. The gain element G_S determined the amplitude of the signal labelled "*b*" in

Fig. 2.20. Signal *b*, in turn, determined the amplitude of the input to the leaky integrator (signal "*c*") by scaling both eye velocity positive feedback and the output of the visual motion pathways (signal "*a*"). During normal pursuit, G*s* was set equal to one so that the signal *b* did not change the inputs to the leaky integrator. At the offset of pursuit, G*s* was set equal to zero, so that the signal *b* eliminated all inputs to the leaky integrator. The multiplicative junction was placed just before the leaky integrator so that it could both change the gain of eye velocity feedback and prevent visual motion inputs from affecting eye velocity. The outputs of the visual motion pathways were summed with eye velocity positive feedback so that a single multiplicative junction could be used. A more complicated version of this model might provide separate switches for the visual motion and the eye velocity inputs to the leaky integrator.

We set the parameters τ_i , the time constant of the leaky integrator, and G_{evf}, the gain of eye velocity feedback, equal to values that allowed the model to replicate the offset of pursuit. Figs. 2.21A and B show averaged eye velocity traces to step-ramp-step-stop trials with ramps of 5, 10, and 20 °/s for rightward and leftward target motion. We set G_S equal to 1 and set τ_i equal to 58.6 ms so that the decay of the leaky integrator would match the offset of pursuit after passing through the first-order model of the output motor pathways. For τ_i equal to 58.6 ms, we calculated that G_{evf} should be set equal to 17.1 to make eye velocity memory a nearly perfect integrator. We next adjusted the gain and filter elements in the three visual motion pathways as described before (Figs. 2.3 and 2.4) to match the output of the model to the monkey's eye velocity from the initiation of pursuit through steady-state (400 ms after onset of eye motion). We then ran the simulation for a total of 1000 ms to match the duration of the monkey's eye velocity, but set G_S equal to

zero at the time indicated by the arrow. As shown by Figs. 2.21A and B, the output of the model provided a good match to the decay in eye velocity observed at the offset of pursuit. Figs. 2.21C and D show the simulated eye velocities normalized for target speed. The output of the model showed nonlinear behavior during the initiation of pursuit, but linear behavior during the offset of pursuit.

Fig. 2.22 displays the activity of five signals in the model during a simulation of the offset of pursuit like that shown in Fig. 2.21. We show three signals in the interior of the model (signals a, b and c in Fig. 2.20) that illustrate the interactions introduced to the model by the new premotor circuit, as well as the input (target velocity) and the output (eye velocity). We have already described the transformation of signals in the three visual motion pathways (Fig. 2.8) and their summed contribution is shown by the dashed trace superimposed on signal *a*. At the beginning of the trial, the step in target velocity generated an input to the leaky integrator (*c*) that was identical to the eye acceleration command (*a*), because the switch signal (*b*) was equal to one. The first 180 ms of the switch signal is shown with a dashed line, because its effect on the model's output was the same if it became equal to one at any time prior to the increase in signal *a*. The earliest portion of signals *a* and *c* was dominated by the eye acceleration command provided by the visual motion pathways, as indicated by the dashed portion of signal *a*. After the transition to steady-state pursuit, the amplitude of signal *a* was determined predominantly by eye velocity feedback. Also, during steady-state pursuit signal *c* was identical to signal *a* because the switching signal *b* was equal to one. However, after the target stopped the switching signal *b* became equal to zero, and signals *a* and *c* were no longer the same. The premotor circuit therefore made it possible to dissociate the dynamics of the initiation

and steady-state pursuit from the dynamics of the offset of pursuit. The trajectory of eye velocity during pursuit initiation and steady-state pursuit was controlled by the properties of the three visual motion pathways, while the trajectory of eye velocity at the offset of pursuit was controlled by the filtering imposed by the leaky integrator.

Discussion

We have presented a model of pursuit eye movements that matches the trajectory of pursuit eye velocity at the initiation of pursuit, during steady-state tracking, and at the termination of pursuit. Similar to our previous model (Krauzlis and Lisberger 1989), this model contains three non-linear pathways that are sensitive to different aspects of image velocity and image acceleration. Since the structure of the model is substantially different from that of several previous models, we will first compare the design of our model to that of other models of pursuit. We will then discuss several properties exhibited by the model that it was not designed to produce, but that are also consistent with features of pursuit.

Comparison with other models of pursuit

Early descriptions of pursuit succeeded in defining the features which distinguish smooth tracking eye movements from saccadic eye movements. Rashbass (1961) showed that pursuit eye movements are evoked primarily by the motion of the target's retinal image, whereas saccades are a response to the position of the retinal image. Subsequently, it has been demonstrated that humans can use position information to guide pursuit eye movements (Pola and Wyatt 1979), but under normal tracking conditions retinal position has only minor effects on pursuit eye velocity (Morris and Lisberger 1987). The

basic configuration of the pursuit system is therefore a negative-feedback system driven by image velocity, the difference between eye velocity and target velocity. However, because of the large delay in visual processing, the output of such a simple negative-feedback system often displays unstable oscillatory behavior. The actual organization of the pursuit system must therefore be more complicated, and one goal of pursuit models has been to devise strategies for overcoming the threat to stability posed by the basic negative-feedback configuration of the system.

One strategy, suggested by Young et al. (1963) is for the pursuit system to sample its input in a manner analagous to the way that the saccadic system samples target position. However, Robinson (1965) demonstrated that pursuit eye movements respond to target motion in a continuous manner, in contrast to the behavior of saccadic eye movements. The more robust solution proposed by Young et al. (1968, 1971) and elaborated by Robinson (1971) was to introduce an internal positive feedback loop that conveys a copy of the eye velocity signal being forwarded to the output motor pathways. By adding this efference copy signal to image velocity, the model constructs an internal analogue of physical target velocity. If the dynamics of the internal positive-feedback loop are set to match the dynamics of the external negative-feedback loop, the oscillations caused by visual feedback are completely eliminated.

In contrast, the model we have presented does not eliminate the oscillations caused by visual feedback, but instead controls their amplitude through the use of nonlinear functions in the visual input pathways. In particular, the use of dead-zones in the gain functions of the image velocity and image acceleration pathways permits the model to have a high sensitivity to visual motion when image velocity is large -- for example, at the initiation

of pursuit -- but a low sensitivity during steady-state pursuit when image velocity is small. The reduction in sensitivity during steady-state prevents the output of the model from breaking into undamped oscillatory behavior. Although we have shown that this strategy can produce realistic pursuit, there is no direct evidence demonstrating that the pursuit system has a reduced sensitivity for small visual inputs. Responses to small amounts of image velocity have been documented (Morris and Lisberger 1987), but the responses were not compared to larger amounts of image motion. It is also possible that the pursuit system may employ a more complicated strategy in regulating the use of visual inputs and that our assumption of fixed gain elements is itself invalid. For example, it is possible that the amplitude of the visual input signals is scaled continuously by other cognitive or motor variables. The ability of subjects to generate anticipatory pursuit eye movements is consistent with this idea.

We have designed our model to control the oscillations caused by external negative feedback, rather than eliminate them, because oscillations do occur during pursuit tracking and they occur in a manner which is consistent with them being caused by visual feedback. The oscillations produced by the model are of the same frequency, between 5 and 6 Hz, and amplitude, 2 to 3 degrees, as those observed in the pursuit eye velocity of monkeys. Furthermore, because the oscillations in the model are caused by visual feedback, changing the delay in visual feedback changes the frequency of steady-state oscillations -- as the delay in visual feedback is increased, the frequency of oscillations decreases. In experiments performed in monkeys, imposing additional delay in visual feedback produced the same relationship between imposed delay and oscillation frequency (Goldreich et al. in press). Models that construct an internal analog of target velocity can be extended so

that they too produce oscillations of the correct frequency and amplitude. For example, the model of Robinson et al. (1986) includes an additional internal negative feedback loop that allows the model to reproduce the 3.8 Hz oscillations observed in human pursuit. However, because the oscillations are caused by internal feedback, the frequency of oscillations does not decrease as the delay in visual feedback is increased.

A general difference between the models presented by Young et al. and Robinson et al. and the models we have presented here and previously (Morris and Lisberger 1985; Lisberger et al. 1987; Krauzlis and Lisberger 1989) is that we attribute much of the dynamics of pursuit to the processing of the visual inputs for pursuit, rather than to properties of the output motor pathways. For example, the image velocity and image motion transient pathways control the initial trajectory of eye velocity produced by targets moving at a constant speed. The use of two pathways to produce this initial response is consistent with the observation that there are two phases of eye acceleration during the initiation of pursuit of constant velocity targets. The earliest phase of eye acceleration, occupying the first 0 to 40 ms of the eye movement response, is relatively insensitive to the speed, contrast or retinal location of the moving visual stimulus. In contrast, the subsequent 40 to 60 ms of the eye movement response is sensitive to each of these parameters (Lisberger and Westbrook 1985). The image acceleration pathway in the model plays two roles during the initiation of pursuit. During the initiation of pursuit to smoothly accelerating targets, the image acceleration pathway augments the contribution of the image velocity pathway, which would otherwise be insufficient to match the observed eye movement. The image acceleration pathway also has the property of acting as a brake whenever eye velocity changes rapidly. This effect is especially important during the

transition from the initiation of pursuit to steady-state pursuit of constant velocity targets, when the action of the image acceleration pathway prevents eye velocity from grossly overshooting target velocity.

The model presented here also includes a "pre-motor" circuit for eye velocity memory that allows it to replicate the smooth decay in eye velocity observed at the termination of pursuit. The key feature of this circuit is that it includes a "switch" that regulates how effectively the circuit integrates visual motion inputs into commands for pursuit eye velocity. During the initiation and maintenance of pursuit, the gain of this switch is set equal to one, allowing visual inputs to contribute to pursuit and permitting feedback of eye velocity to accomplish integration. At the termination of pursuit, the gain of the switch goes to zero, making the integrating circuit very leaky and preventing visual inputs from changing eye velocity. The decay in eye velocity from the integrating circuit when it is leaky allows the model to mimic the trajectory of eye velocity at the termination of pursuit.

Properties of the model provided by the circuit for eye velocity memory

The circuit for eye velocity memory was designed to reproduce the smooth transition to zero eye velocitiy observed at the termination of pursuit, but it also allows the model to mimic the effects observed after stimulating or ablating the visual pathways known to be important for pursuit eye movements. For example, the switch included in the model can account for the conditional effects of electrical stimulation. Stimulation at sites in the model produces different effects during fixation than during pursuit, depending upon whether the site stimulated is upstream or downstream of the multiplicative junction. For example, Fig. 2.23 shows the effects of stimulating at three different sites in the model during steady-state pursuit (Fig. 2.23 A to C) or during fixation (D to F). Each traces shows the activity of

an individual signal in the model, using the same format as presented in Figs. 2.20 and 2.22. During maintained pursuit, increasing the activity of each of the three signals shown leads to an acceleration of the eye, as indicated by the deviation of the solid eye velocity trace away from the dashed eye velocity trace (Fig. 2.23 A to C). However, during fixation, only increases in activity of signal c leads to an acceleration of the eye (D to F). Similarly, stimulation at some brain sites causes an eye acceleration whether the monkey is fixating or tracking, while stimulation at other sites causes an eye acceleration only if pursuit has been initiated. This correspondence invites speculation about the possible anatomical location of a switch for pursuit. Stimulation of the dorsolateral pontine nuclei, which convey information from extrastriate visual areas including MT and MST to the cerebellum, causes an eye acceleration only if pursuit has been initiated (May et al. 1986). In contrast, stimulation of the flocculus or ventral paraflocculus produces an acceleration of the eye during fixation or during pursuit (Ron and Robinson 1973, Belknap and Noda 1987). This suggests that the switch is located between the pontine nuclei and the cerebellum. However, there are other routes by which visual inputs may contribute to pursuit, such as projections from extrastriate areas to other nuclei in the pons and brainstem (Brodal 1980). It is possible that the different effects of stimulation in the DLPN and in the cerebellum are a secondary consequence of effects mediated by these other pathways.

The circuit for eye velocity memory suggests a new interpretation for the role of area MST in generating pursuit. The properties of the switching gain, G_S, in the model are similar to the properties of neurons in the dorsal and lateral parts of area MST. These neurons increase their activity during pursuit and this activity is maintained even when image motion has been eliminated (Newsome et al. 1988). The persistent increase in activity reflects

"extra-retinal" inputs, which Newsome et al. suggested were a motor corollary signal related to eye velocity. They further suggest that this extra-retinal signal may be combined with visual signals to produce a neural correlate of target velocity. This interpretation is consistent with the models proposed by Young et al. (1963) and Robinson et al. (1971, 1986) which explicitly reconstruct a neural signal encoding target velocity. For example, changing a single gain element in the model of Robinson et al. (1986) can reproduce the directional pursuit deficits observed in humans after some unilateral cerebral lesions (Leigh 1989). While our model does not contradict this interpretation, it does suggest another viewpoint -- that the extra-retinal activity observed in area MST may reflect sensory or cognitive signals related to the decision to generate pursuit.

The behavior of the model when the gain of the switch, G_S, is decreased or increased, is consistent with the altered pursuit eye movements observed when area MST is either lesioned or electrically stimulated. In the normal case in the model, $G_S = 1$, so the gain of the visual inputs is determined by the gain elements in the three visual motion pathways and the time constant of eye velocity memory is determined by G_{evf} and τ_i. When G_S is less than one, as shown by the three lower traces in Fig. 2.24, pursuit initiation is deficient and steady-state eye velocity is less than target velocity. This combined effect on both the initiation and maintenance of pursuit eye velocity is similar to the effects caused by lesions of MST. When G_S is made greater than one, the effect on the behavior of the model depends upon the current eye velocity. The different trajectories of eye velocity in Fig. 2.25A demonstrate that increasing G_S by a constant amount causes an eye acceleration that is proportional to eye velocity for three amplitudes of stimulation. Each line shows the eye accelerations caused by one amplitude

of stimulation, indicated by the numbers to the right. The graph in Fig. 2.25B shows that, for each amplitude of stimulation, the amplitude of eye acceleration was related to eye velocity. This dependency on eye velocity is similar to the dependency observed with electrical stimulation of area MST (Fig. 6 of Komatsu and Wurtz 1989).

Because our model only considers eye movements in one dimension, it does not address the directional nature of the MST deficit. However, the model could be extended into two dimensions to reproduce the effect of an MST lesion. There is evidence that the neural substrate for pursuit eye velocity memory is organized into horizontal and vertical channels (Stone and Lisberger 1990, Chapter 3). The horizontal channel, at least, likely operates in a push-pull fashion mediated by paired bilateral circuits. If the switching input shared this paired organization, reducing one of the paired inputs would cause an imbalance in the circuit for horizontal eye velocity memory and produce a directional deficit.

The model also suggests a mechanism for recovery from lesions of MT (Newsome et al. 1985) that does not require changes in the inputs provided by visual cortex. Changes in the gain of the switch, G_S, and the gain of eye velocity feedback, G_i, can be used to compensate for lesions of the visual motion pathways. Fig. 2.26 A shows the activity of five signals in the model during pursuit of a target moving at a constant 20 °/s, similar to the data shown in Fig. 2.22 except that the eye velocity and target velocity traces have been superimposed. The traces in Fig. 2.26B show the effect of reducing the outputs of the visual motion pathways to 0.5 times their normal values. The reduction in gain of the visual inputs is reflected in the reduced amplitude of both signals *a* and *c*, resulting in a diminished initiation of pursuit. In Fig. 26C, we have adjusted the gain elements G_{evf} and G_S to compensate for the

reduced visual inputs. Increasing G_S from 1.0 to 2.0 allows the multiplicative junction to amplify the deficient visual inputs to their previous amplitude. A matching decrease in G_{evf} is required to prevent eye velocity memory from becoming unstable. The model therefore suggests a mechanism for recovery from visual motion deficits that does not require rescue of the original visual motion pathways.

Matching the pursuit performance of human primates

To demonstrate that the model can describe pursuit eye movements in humans, as well as monkeys, we matched our model to the data on human pursuit presented by Robinson et al. (1986). Because the method used by Robinson et al. to analyze the trajectory of eye velocity eliminates much of the detail required for our optimization procedure, we could not directly match our model to the eye velocity data that they present. Instead, we ran simulations of the Robinson et al. (1986) model, using the parameters given in their paper, to reproduce the four eye velocity traces shown in Fig. 9 of their paper. These simulations, which represent a reasonable facsimile of the actual pursuit eye velocity produced by human subjects, are shown by the dashed traces in Fig. 2.27A. We matched the performance of our model to these data by determining a new set of vaules for the gain functions and filters, as described above for the data from monkeys. The gain elements used in the image velocity, image motion transient, and image acceleration pathways to produce these simulations are shown in Figs. 2.27B, C and D respectively. The step responses of the filters in these pathways are shown in Figs. 2.27E, F and G. The outputs of the model produced with the new parameters, shown by the solid traces in Fig. 2.27A, provide a good match to the output from the model of Robinson et al. In particular, the output of the model matches the initial rise of the dashed traces and shows steady-state

oscillations at a frequency (3.6 Hz) that is close to that observed in human pursuit.

Unresolved issues concerning the generation of pursuit eye movements

The model presented in this chapter raises several unresolved issues concerning the generation of pursuit eye movements. First, what is the function of the non-visual signals used for pursuit? Our model suggests that these signals facilitate or gate the use of visual information, but that they do not form part of the basic command for pursuit eye movements. In contrast, other models of pursuit suggest that these signals represent a copy of the eye velocity command used to move the eye. By combining these efference copy signals with visual information encoding image velocity, the brain may construct a neural signal representing target velocity. A further possibility is that the non-visual signals have a function that is more complex than the simple toggle switch role described in our model, but a function that is less rigidly defined than the eye velocity feedback role suggested by other models. For example, the non-visual signals could represent the output of a mechanism that uses multiple sensory and cognitive inputs to construct an internal model of target motion. The role of such a mechanism might depend upon the richness of the inputs to which it had access. The mere appearance or identification of a target might elevate the output of the mechanism from some minimal level and facilitate the use of direct visual inputs by the pursuit system. In this capacity, the mechanism would resemble the switch described in our model. However, if the motion of the target could be recognized as a pattern, the mechanism might provide a predictive input to the pursuit system which could effectively supplant the role of direct visual inputs. In this case, the mechanism would resemble the eye velocity or target velocity signals described in other models. To

distinguish among these alternatives, it is important to identify more precisely the information provided by the non-visual signals. Do the signals really encode eye velocity? Are the signals influenced by inputs from other modalities that provide information about the motion of the target? Do the signals show modulation that is related to the predictability of the target motion?

A second issue raised by the model concerns the role of eye velocity feedback in pursuit. In our model, feedback of eye velocity is used to lengthen the time constant of a leaky integrator in order to produce a circuit that can mimic the role of a mathematical integrator. In other models, as mentioned above, eye velocity feedback is used to construct a neural analog of target velocity. In both cases, feedback of eye velocity is used to make the system less dependent on continuous sensory feedback. However, the implications with respect to the anatomy of the pursuit system are quite different. Our model is consistent with the function proposed for the cerebellar flocculus. The identification of eye velocity and visual motion signals on Purkinje cells has led to the suggestion that the flocculus plays two roles in the generation of pursuit. First, through feedback connections with the brainstem, the flocculus may act like the positive feedback loop in the pre-motor circuit of our model (Miles et al. 1980, Lisberger and Fuchs 1978a, Stone and Lisberger 1990). Second, by receiving visual inputs, the flocculus may convert visual motion inputs into commands for eye acceleration (Stone and Lisberger 1990), similar to node *a* in our model (Fig. 2.20). In contrast, the suggestion that feedback of eye velocity is used to reconstruct target velocity implies that the feedback signals are conveyed to the cerebral cortex. One difficulty with this suggestion is that the anatomical pathways that would mediate this feedback are unclear. This scheme also provides no functional interpretation for the

role of the cerebellar flocculus, a structure which is known to be critical for normal pursuit eye movements.

Finally, the model raises an important issue by virtue of what it does not describe. The input to the model is assumed to be target velocity, but no attempt is made to describe how the brain defines the target or quantifies its motion. The importance and complexity of this issue are underscored by the fact that most objects of ocular pursuit appear in rich three-dimensional environments that are very different from the featureless backgrounds used in our experiments. How the brain parses the motion contained in such complicated visual environments and determines which portions to provide as inputs for pursuit eye movements remains an open and vital question.

Figure 2.1. Diagram of the transformations performed in the model. The input to the model is defined as target velocity. At the retina, the difference between target velocity and eye velocity (dashed line) gives image velocity, which provides the input to three parallel pathways. The input to each pathway is first delayed ($e^{s\tau}$), and then scaled by a gain element (G) and filtered (H). The subscripts indicate which visual motion signal each pathway processed: image velocity (v), image motion transient (t), or image acceleration (a). G_a was described by the equation, $y = ax + be^{c/x}$. G_t was described by the equation, $y = ax + b(1/(1+e^{cx}) - 0.5)$. Different values for the coefficients were allowed for positive and negative values of x. G_v was initially described by the equation, $y = ax$, but was subsequently described by the same equation as G_t for reasons described in the text. H_v was a first-order system, $H(s) = 1/s\tau + 1$. H_t and H_a were differentiators cascaded with a second-order system, $H(s) = s/(s\tau + 1)^2$. The parameters describing the transfer functions for H_t and H_a will be given by the damping ratio z and the cut-off frequency w. H_i was a mathematical integrator. H_p was a first-order system, $H(s) = 1/s\tau + 1$. The feedback delay was normally set equal to zero.

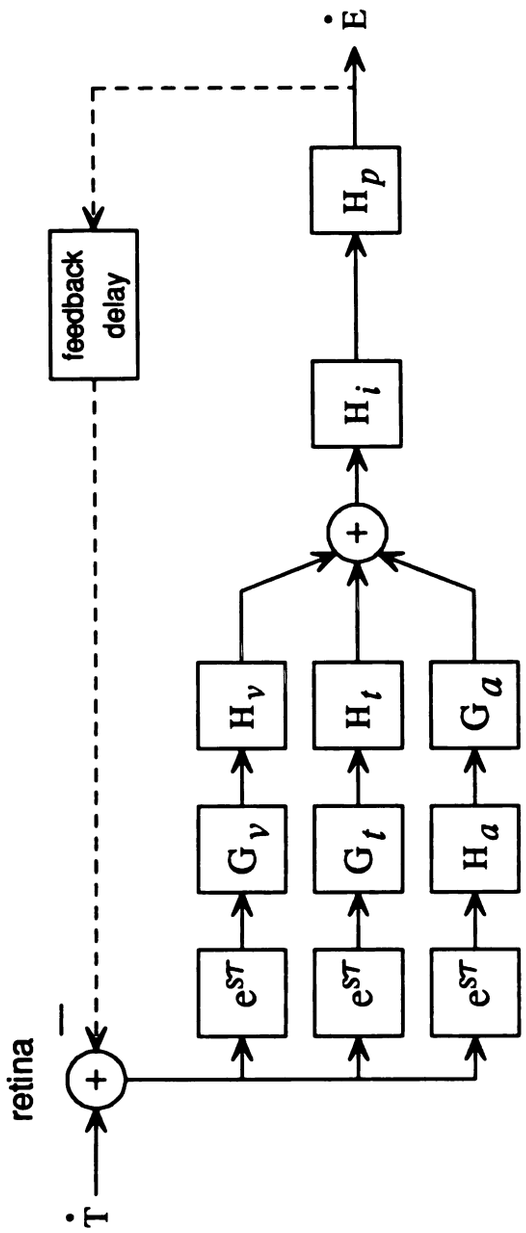

Fig. 2.1

Figure 2.2. Determining the parameters for visual motion processing based upon open-loop pursuit for one monkey. A: Comparison of actual (solid) and fitted (dashed) eye velocity responses to constant velocity targets moving at 5, 15, and 25 °/s rightward (upward deflecting) and leftward (downward deflecting). B: Comparison of actual and fitted eye velocity responses to targets smoothly accelerating at 64, 120, and 320 °/s^2. C: Gain element (G_v) used in the image velocity pathway. D: Step-response of the filter (H_v) used in the image velocity pathway. E: Gain element (G_t) used in the image motion transient pathway. F: Step-response of the filter (H_t) used in the image motion transient pathway. G: Gain element (G_a) used in the image acceleration pathway. H: Step-response of the filter (H_a) used in the image acceleration pathway.

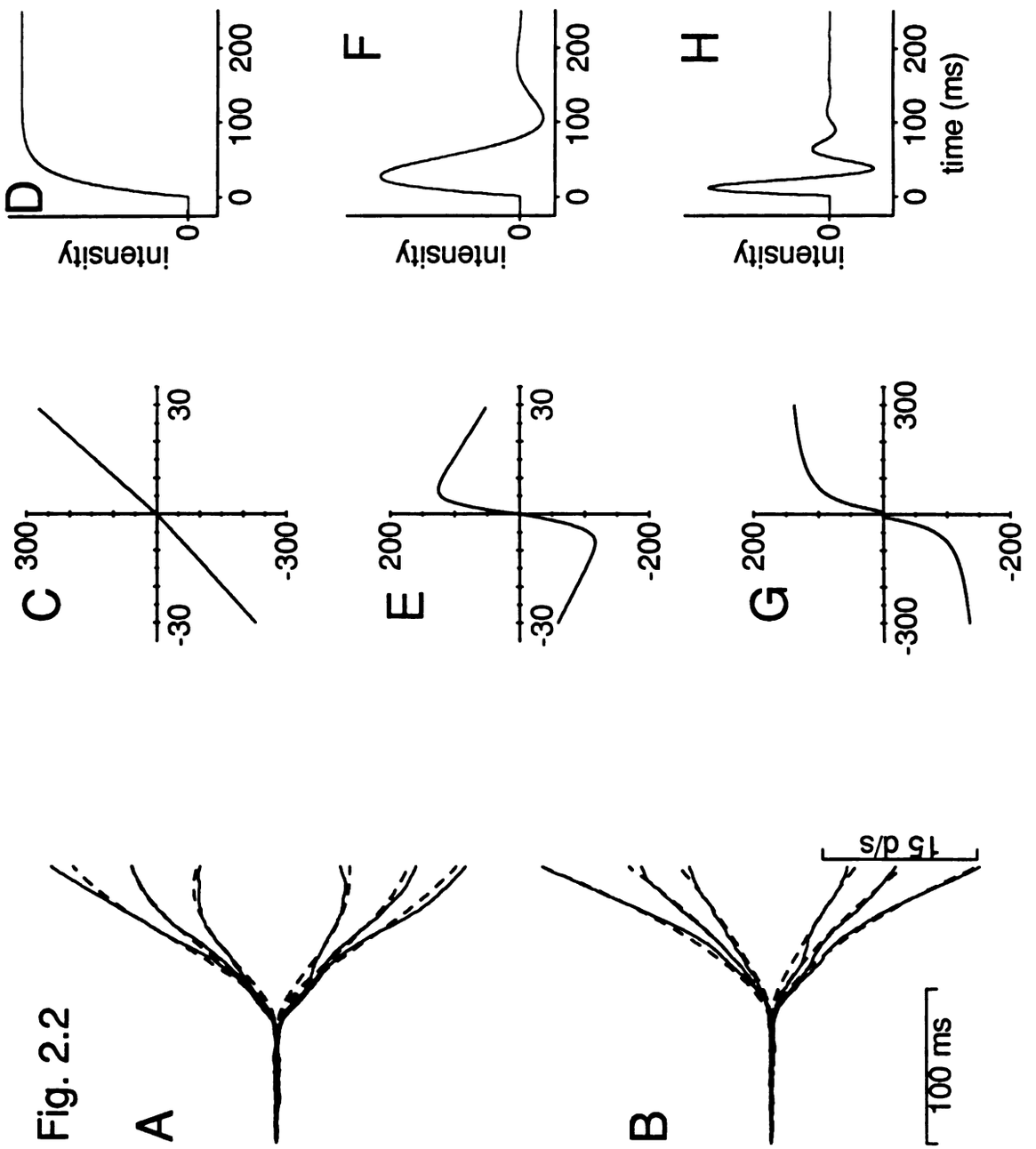
A
B
15 d/s
100 ms
C
300
30
-30
-300
D
intensity
0
0
100
200
E
200
30
-30
-200
F
intensity
0
0
100
200
G
200
300
-300
-200
H
intensity
0
0
100
200
time (ms)

Fig. 2.2

Figure 2.3. Adjusting visual motion pathways to match closed-loop pursuit. A: Comparison of actual (solid) and fitted (dashed) eye velocity responses to constant velocity targets of 5, 15, and 25 $^{o}/s$, using open-loop parameters in visual motion pathways. B: Actual and fitted eye velocity responses to constant velocity targets, using parameters optimized based upon closed-loop data. C: Comparison of actual and fitted eye velocity responses to targets accelerating smoothly at 64, 120, and 320 $^{o}/s^{2}$, using open-loop parameters. D: Actual and modelled eye velocity responses to smoothly accelerating targets, using optimized closed-loop parameters. E-F: Gain elements used in the image velocity (E), image motion transient (F) and image acceleration (G) pathways, comparing functions based upon open-loop (thin lines) and closed-loop (thick lines) data.

Fig. 2.3

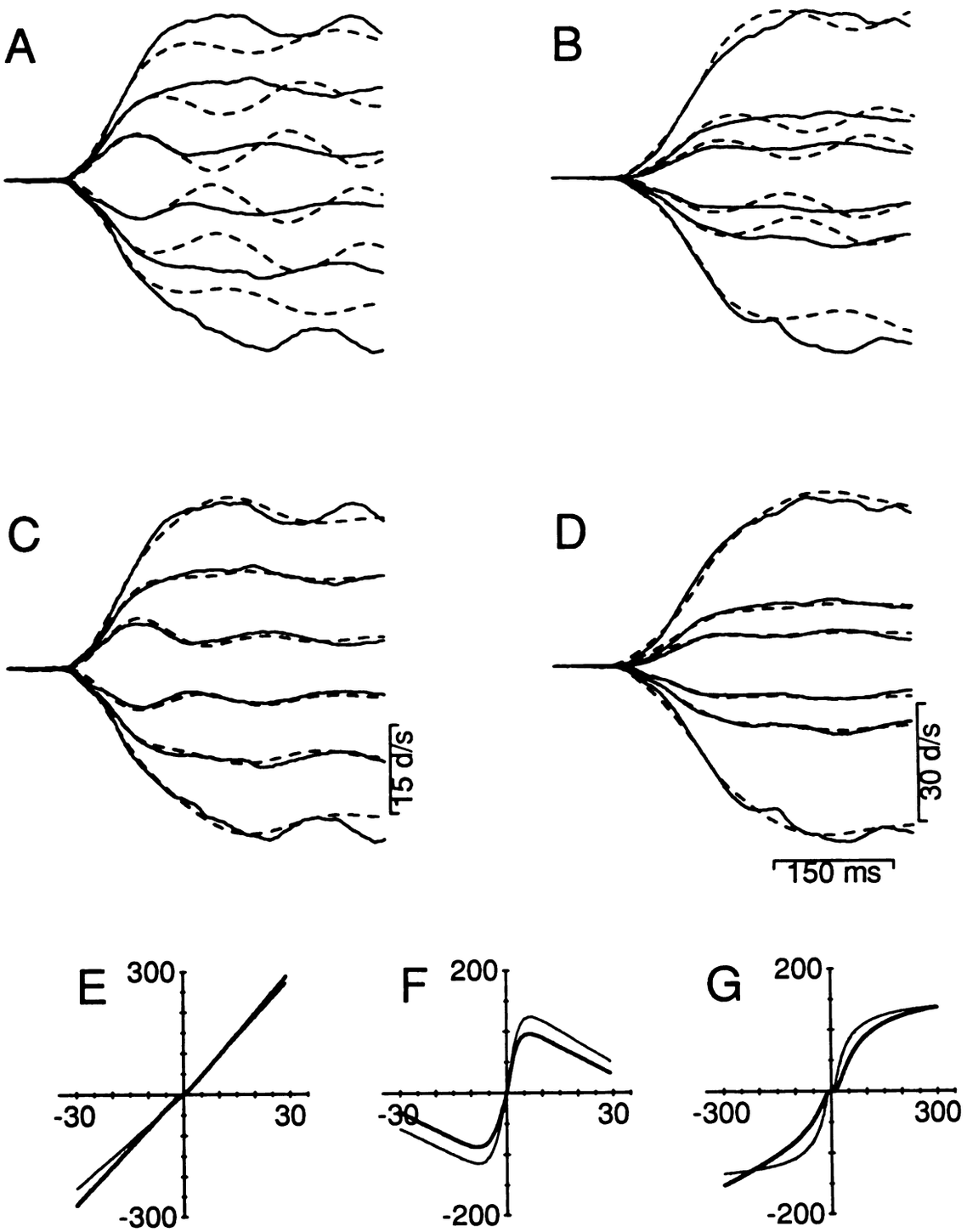
A
B
C
D
15 d/s
30 d/s
150 ms
E
300
-30
30
-300
F
200
-30
30
-200
G
200
-300
300
-200

Figure 2.4. Comparison of actual and modelled eye velocity responses for three other monkeys. A, C, E: Averaged eye velocity responses (solid lines) and modelled responses (dashed) to constant velocity targets of 5, 15, and 25 $^{o}/s$. B, D, F: Averaged eye velocity responses and modelled responses to targets accelerating at 64, 120, and 320 $^{o}/s^{2}$. Each row represents data from one monkey.

Fig. 2.4

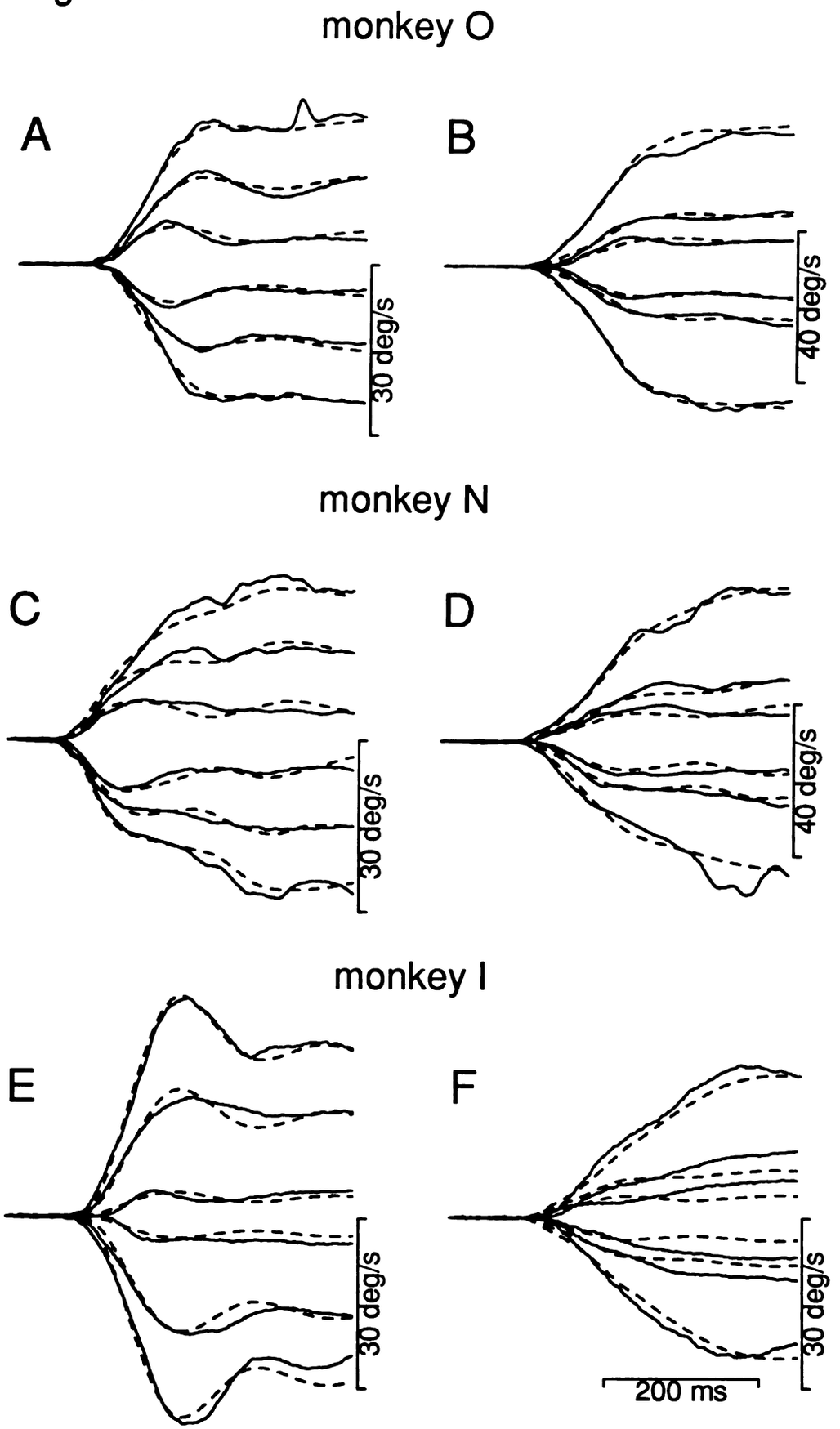
monkey O
A
B
30 deg/s
40 deg/s
monkey N
C
D
30 deg/s
40 deg/s
monkey I
E
F
30 deg/s
30 deg/s
200 ms

Figure 2.5. Accuracy of the models' fit to either closed-loop or open-loop pursuit. Each graph shows data obtained from a different monkey. Each point plots the mean squared error of the model's fit to the initiation of pursuit against that the error measured over the entire trial, using parameters based upon either open-loop data (open circles) or closed-loop data (filled squares).

Fig. 2.5

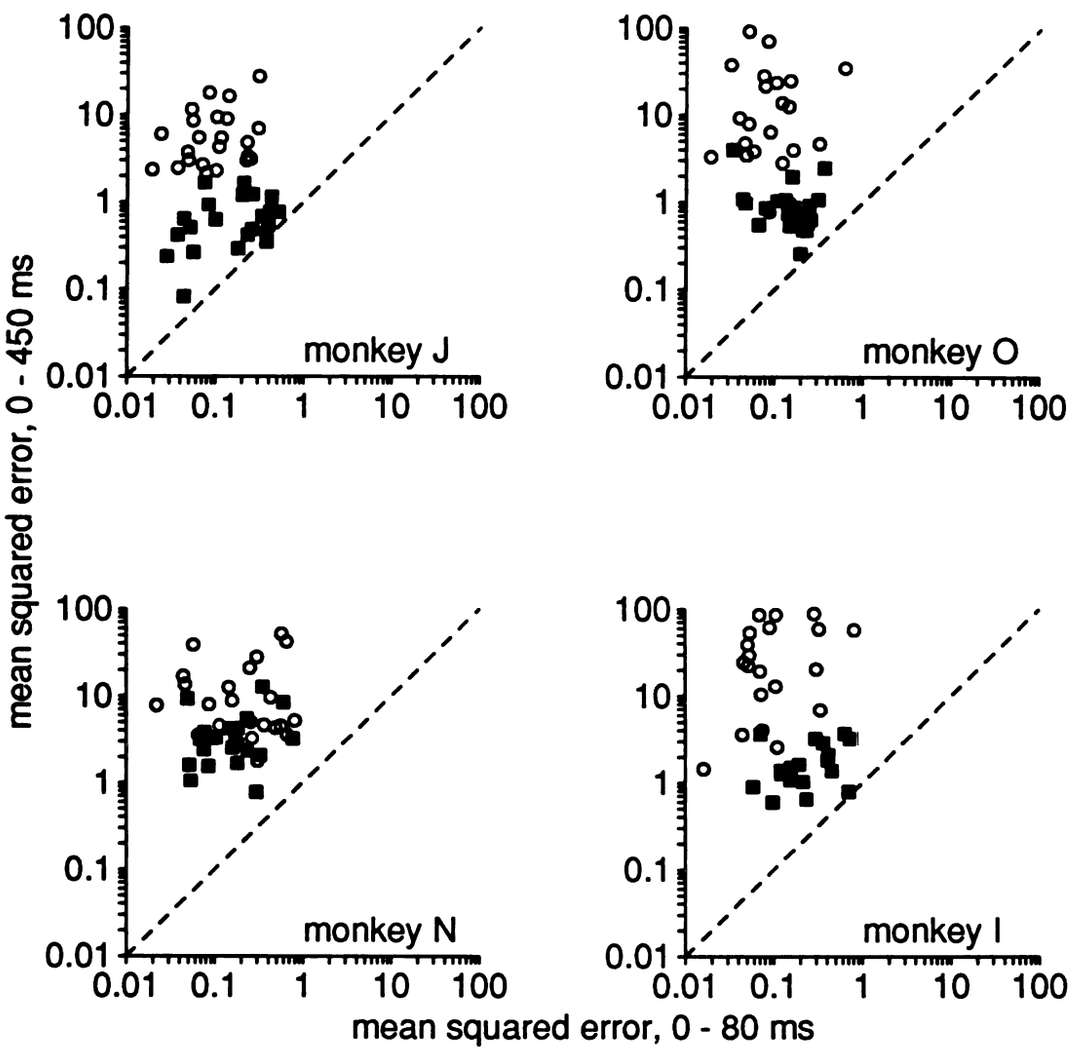
100
10
1
0.1
0.01
0.01 0.1 1 10 100
monkey J
monkey O
monkey N
monkey I
mean squared error, 0 - 450 ms
mean squared error, 0 - 80 ms

Figure 2.6. Histograms of relative frequency for image velocity and image acceleration signals. Graphs in top row show distribution of frequencies of occurrence for the image velocity (A) and image acceleration (C) signals during the performance of an entire trial lasting 450 ms. Graphs in bottom row show frequencies for image velocity (B) and image acceleration (D) when only the first 80 ms are considered.

Fig. 2.6

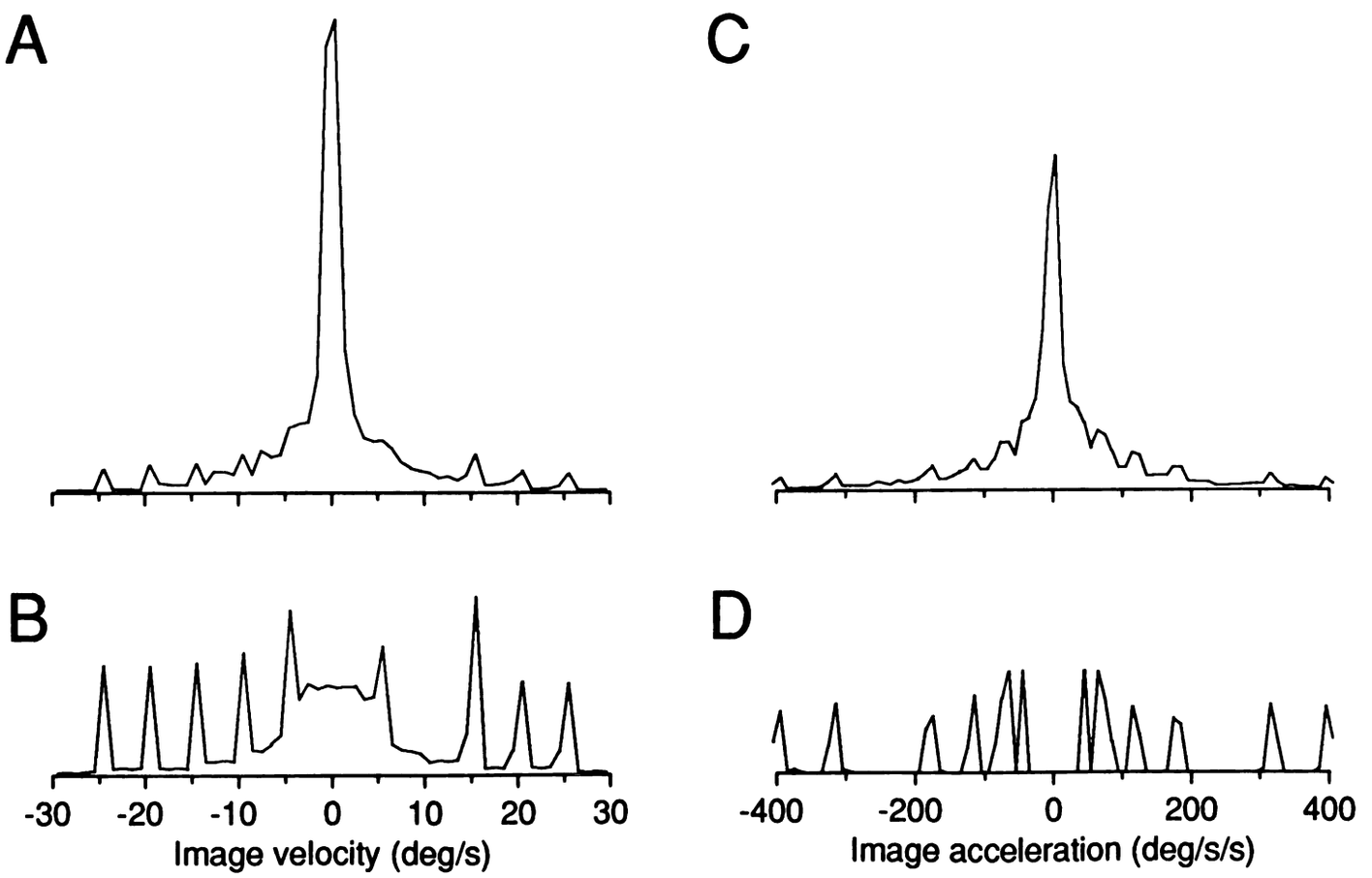
A
C
B
D
-30
-20
-10
0
10
20
30
Image velocity (deg/s)
-400
-200
0
200
400
Image acceleration (deg/s/s)

Figure 2.7. Bode plots obtained from the model with parameters used to fit the eye velocities from monkey J. A: Diagram explaining how the gain and phase of the model's output was measured. B: Graph showing the gain of the model's output for inputs as a function of input frequency, using parameters matched to open-loop pursuit. The four types of lines indicate 4 different amplitudes of input sinewaves, as indicated in the inset. The open symbols superimposed on the graph are data reproduced from Goldreich et al. (in press). D: Graph showing the gain of the model's output as a function of frequency, using parameters matched to closed-loop pursuit. C: Graph showing the phase of the model's output as a function of frequency, using parameters matched to open-loop pursuit. Negative values indicate that the output followed the input in time. E: Graph showing the phase of the model's output, using parameters matched to closed-loop pursuit.

Fig. 2.7

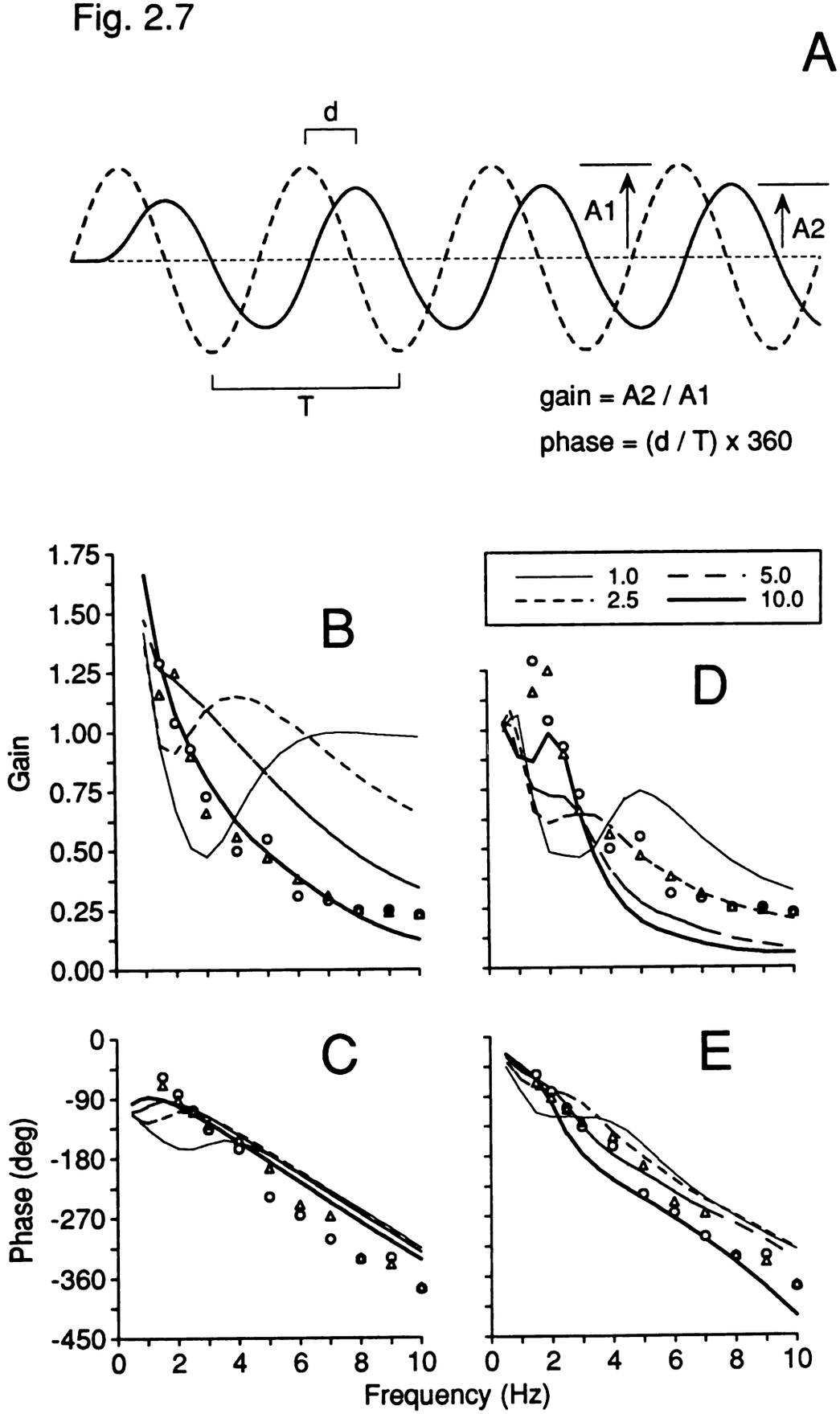
A
d
A1
A2
T
gain = A2 / A1
phase = (d / T) x 360
B
D
C
E
1.0
2.5
5.0
10.0
Gain
Phase (deg)
Frequency (Hz)
1.75
1.50
1.25
1.00
0.75
0.50
0.25
0.00
0
-90
-180
-270
-360
-450
0
2
4
6
8
10

Figure 2.8. Processing of signals in the three visual motion pathways. The traces in successive columns display how image velocity (first column) is transformed to produce the eye velocity observed at the output of the model (last column). The three rows in the second column show the result of non-linear scaling and filtering of the image velocity signal by the image velocity, image motion transient, and image acceleration pathways, respectively. The third column shows the components of eye velocity that are contributed by each of the three pathways. The first vertical dashed line indicates the onset of the response. The second vertical dashed line indicates one latency period later, which marks the onset of the contribution from the image acceleration pathway.

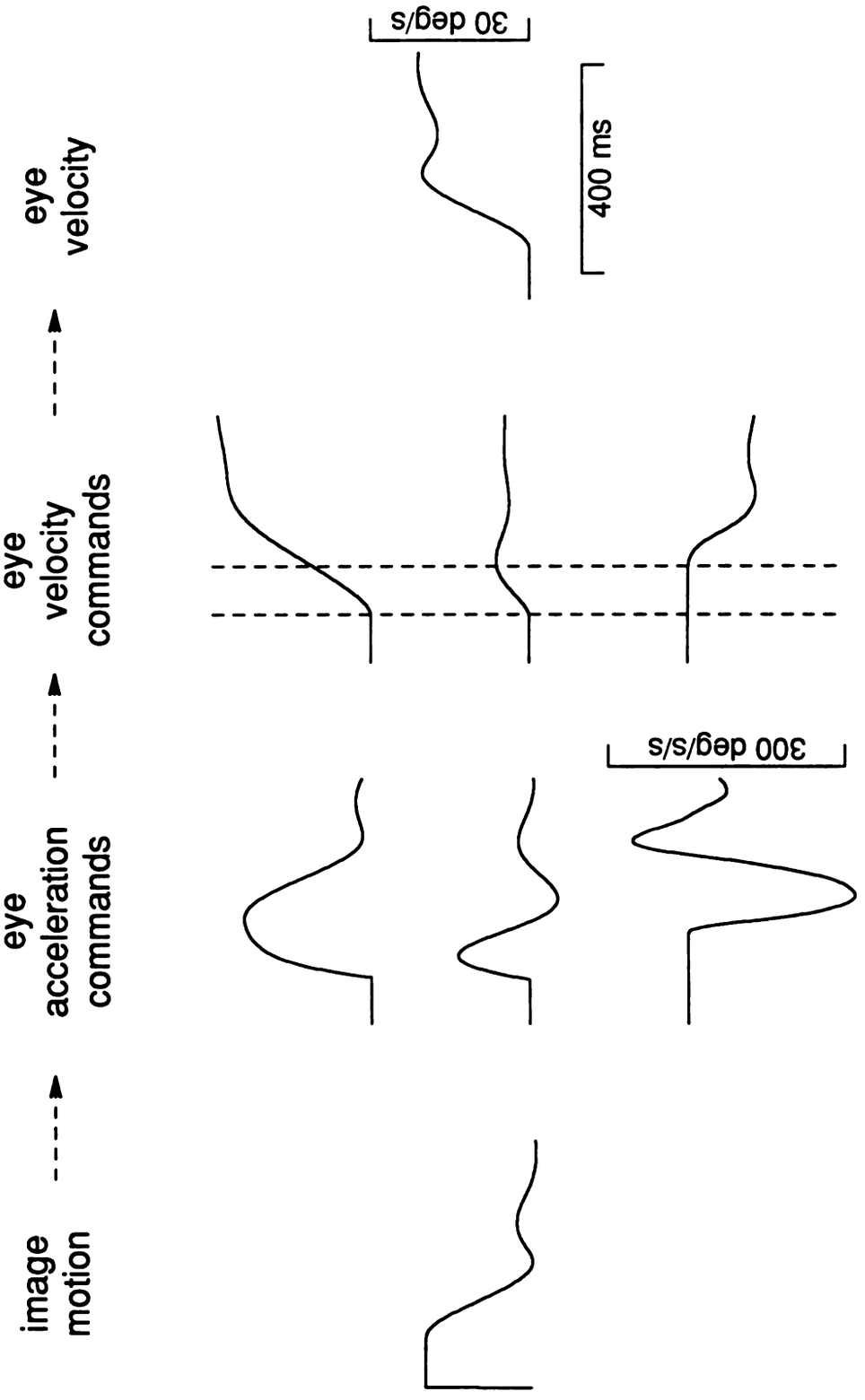
image motion
eye acceleration commands
eye velocity commands
eye velocity
300 deg/s/s
30 deg/s
400 ms

Fig. 2.8

Figure 2.9. Effects of lesioning one of the three visual motion pathways. The dashed traces in A, B, and C show the output of the intact model. Solid lines indicate the outputs of the model when the contribution of the image velocity pathway (A), the image motion transient pathway (B), or the image acceleration pathway (C) was eliminated.

Fig. 2.9

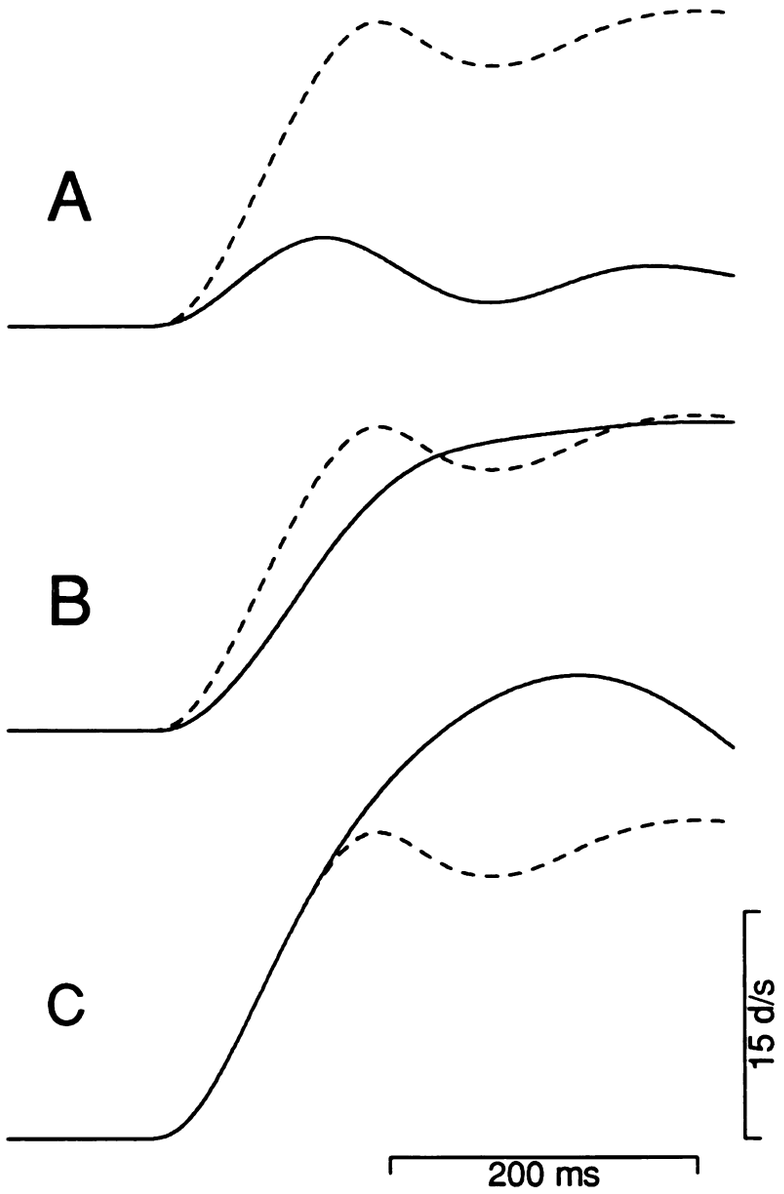

Figure 2.10. Matching the variation in pursuit eye velocity by changing the gain of the visual motion inputs. Top left traces compare average response (solid line) and modeled response (short dash) to a target moving at 15 °/s. Dashed lines surrounding the two traces indicate 1 standard deviation. A-C: Solid lines show three individual eye velocity responses, which were among the fourteen responses used to produce the averaged trace. Dashed trace indicates modelled responses. Graphs on the right show how the gains in the visual motion pathways used to provide a best-fit to the averaged response were scaled so that the model would provide a best-fit to individual responses. Each point marks one pair of scaling factors. For the three pairs of values corresponding to the traces shown in A, B and C, the points have been replaced with the appropriate letters.

Fig. 2.10

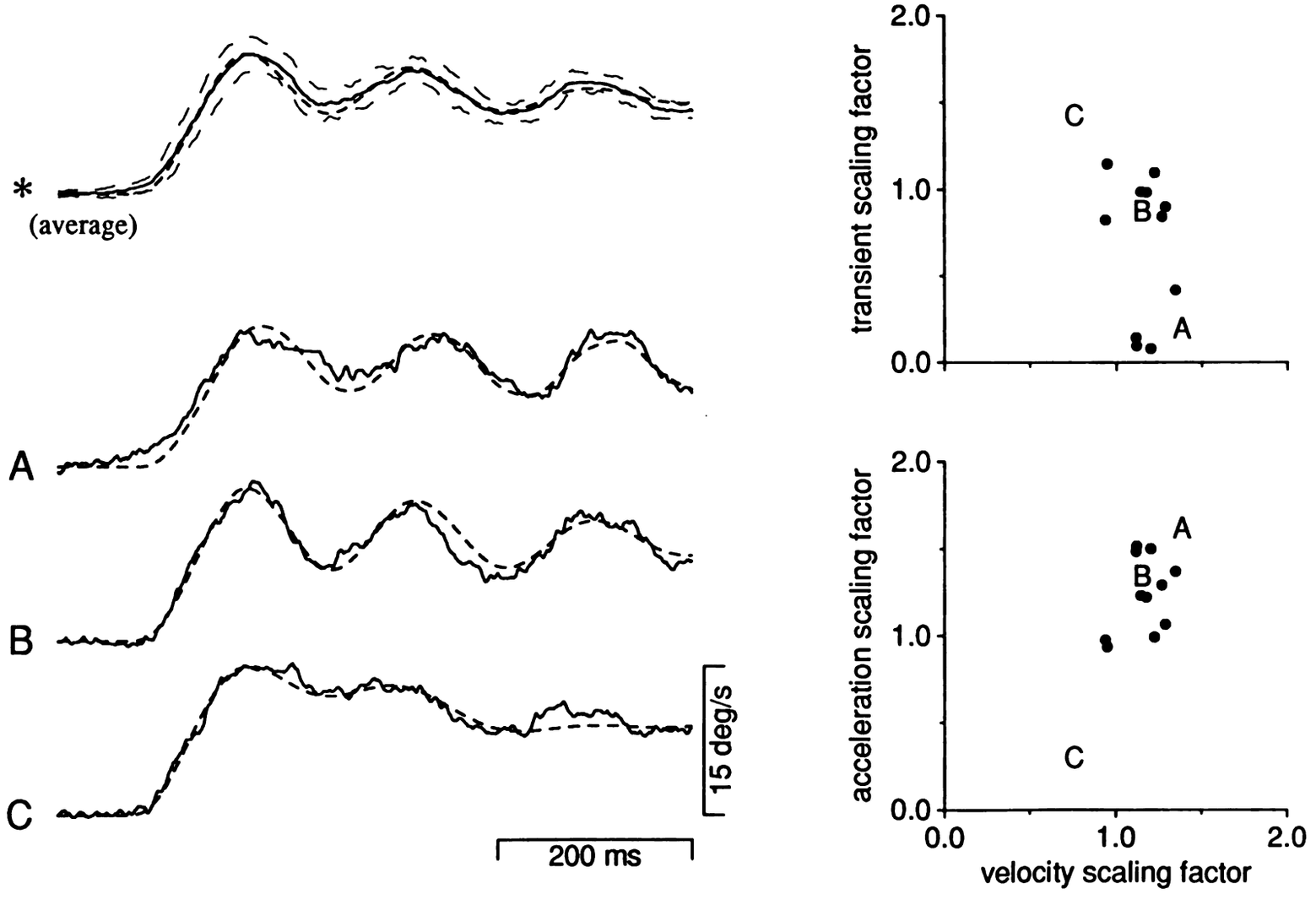
*
(average)
A
B
C
15 deg/s
200 ms
transient scaling factor
2.0
1.0
0.0
C
B
A
acceleration scaling factor
2.0
1.0
0.0
A
B
C
0.0
1.0
2.0
velocity scaling factor

Figure 2.11. Matching the variation in pursuit eye velocity on a trial-to-trial basis. The three graphs to the right plot the scaling factors obtained after optimization of consecutive trials in one experiment. The graphs show the scaling factors applied to the image motion transient pathway (top), the image acceleration pathway (middle), and the image velocity pathway (bottom) as a function of trial number. The traces to the right compare eye velocity records obtained on trials #297, 298, 300 and 303 (solid lines) with the output of the model produced with the best set of scaling factors (dashed lines). The location of these traces in the context of the experiment is indicated in the graphs by connecting the points which represent the scaling factors for these trials. The target motion presented which evoked the eye velocities shown in the four samples were 25 °/s leftward (#297), 15 °/s rightward (#298), 20 °/s leftward (#300) and 20 °/s rightward (#303).

Fig. 2.11

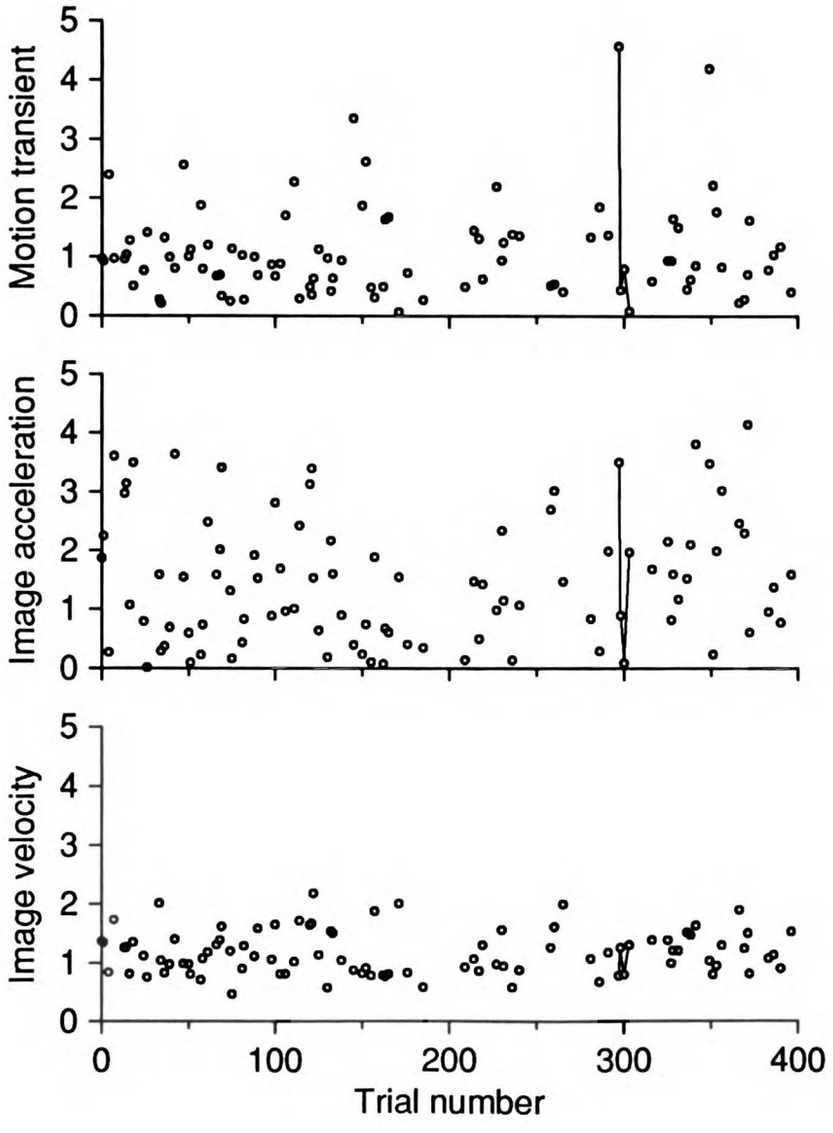
Motion transient
Image acceleration
Image velocity
0
1
2
3
4
5
0
100
200
300
400
Trial number

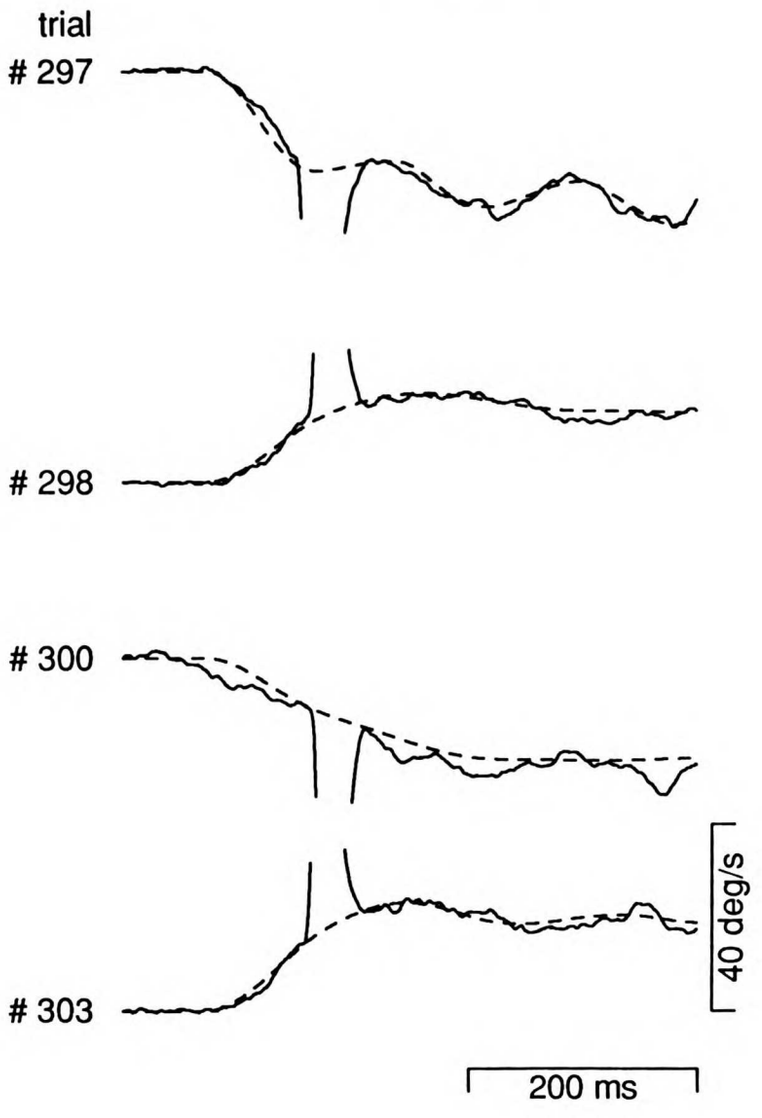
trial
297
298
300
303
40 deg/s
200 ms

Figure 2.12. Matching the variation in pursuit eye velocity recorded over several weeks. The three graphs to the right plot the scaling factors obtained after optimization of averaged data obtained during experiments on several different days. The solid traces to the right compare the averaged eye velocity evoked by a target moving at a constant velocity of 15 ^{o}/s on the first experimental day (day #0), the second day (day #1), the ninth day (day #8), and the fifty-sixth day (day #55). The dashed traces show the output of the model obtained with the optimized scaling factors for each day. The traces shown for day #0 represent the averaged data obtained during the first half of the experimental session.

Fig. 2.12

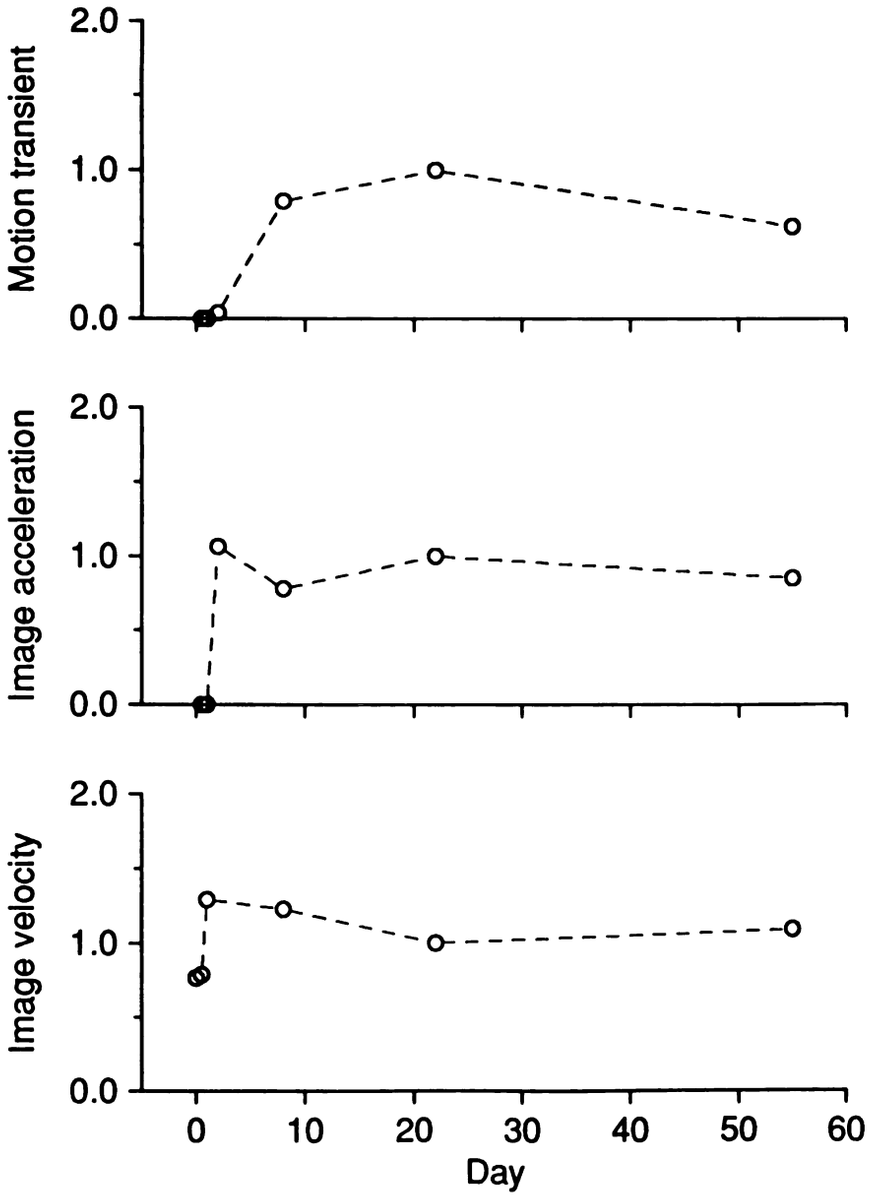
Motion transient
Image acceleration
Image velocity
2.0
1.0
0.0
0
10
20
30
40
50
60
Day

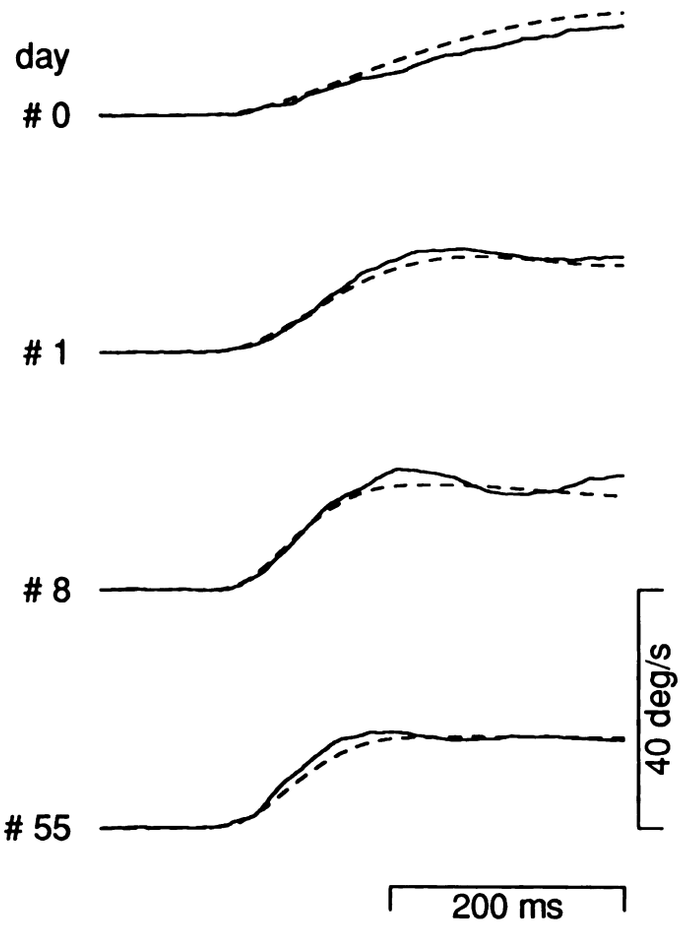
day
0
1
8
55
40 deg/s
200 ms

Figure 2.13. The role of image velocity and image acceleration pathways in controlling the amplitude of oscillations in the model. A: Effect of increasing or decreasing the gain of the image velocity pathway. The number beside each trace indicates the amount by which the gain of the image velocity pathway was multiplied. B: Effect of changing the gain of the image acceleration pathway.

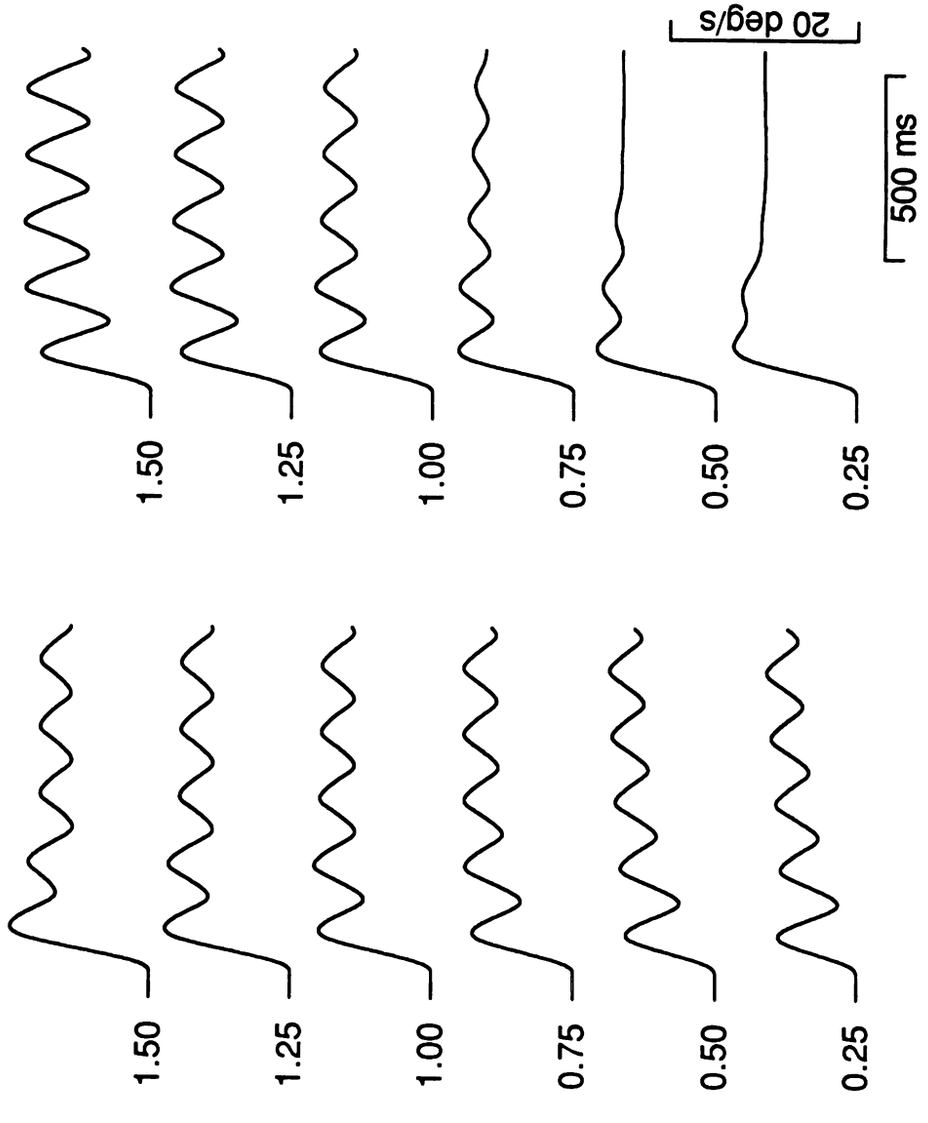

Fig. 2.13

Figure 2.14. Changes in Bode plots caused by changing the gain in the image velocity and image acceleration pathways. The four graphs show Bode plots obtained with the model used to fit the data from monkey J, but after changing the gain of either the image velocity pathway (A) or the image acceleration pathway (B). Each type of line shows the responses obtained after scaling the gain in one pathway by some factor, as indicated in the inset.

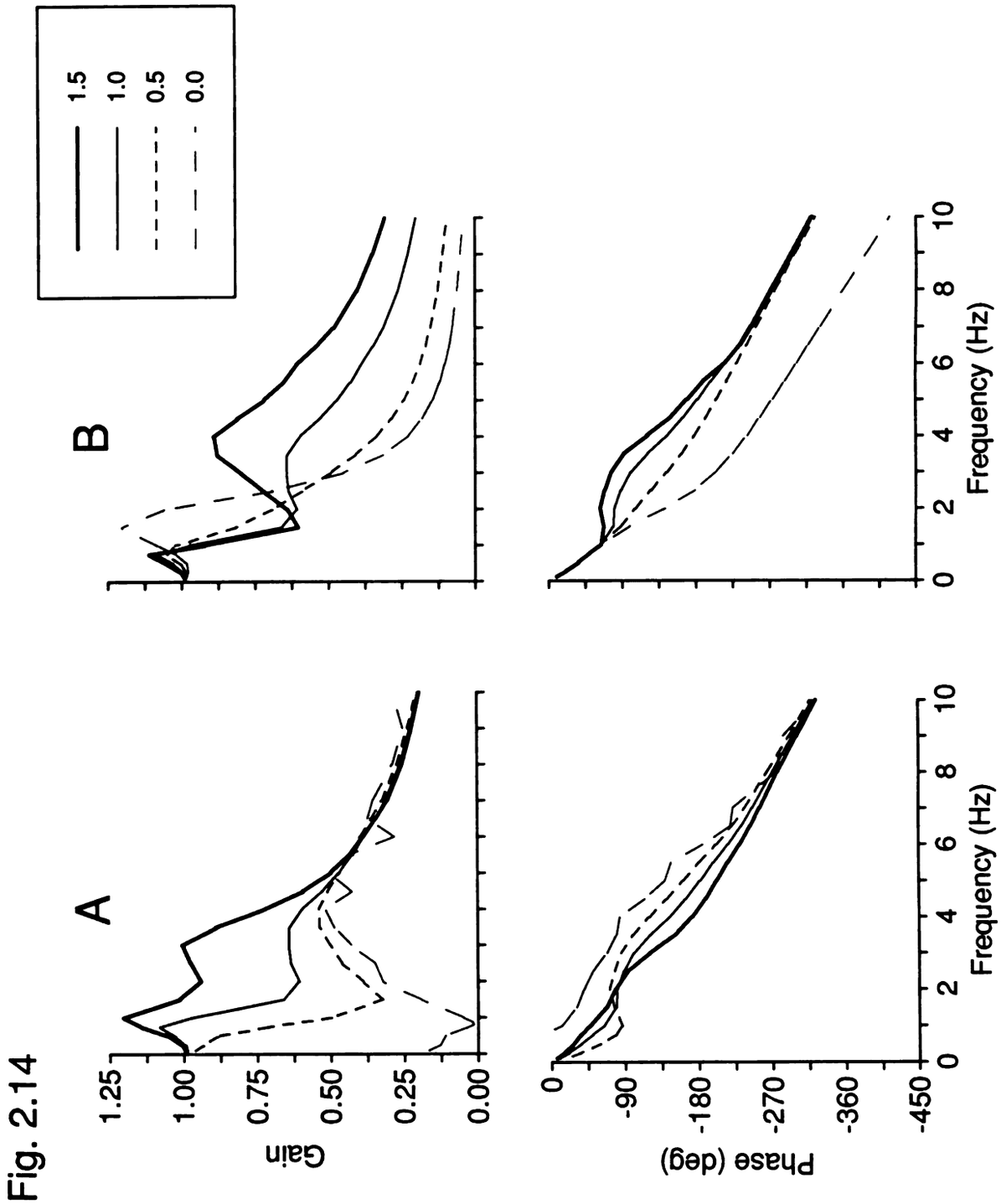
A
B
1.5
1.0
0.5
0.0
Gain
1.25
1.00
0.75
0.50
0.25
0.00
Phase (deg)
0
-90
-180
-270
-360
-450
0
2
4
6
8
10
Frequency (Hz)
Frequency (Hz)

Fig. 2.14

Figure 2.15. Effect of increasing the delay in visual feedback. Each trace indicates the output of the model for a 10 °/s target motion with a different delay imposed in the visual feedback. The number beside each trace indicates the time (in ms) that was added to the delay in visual feedback for all three visual motion pathways.

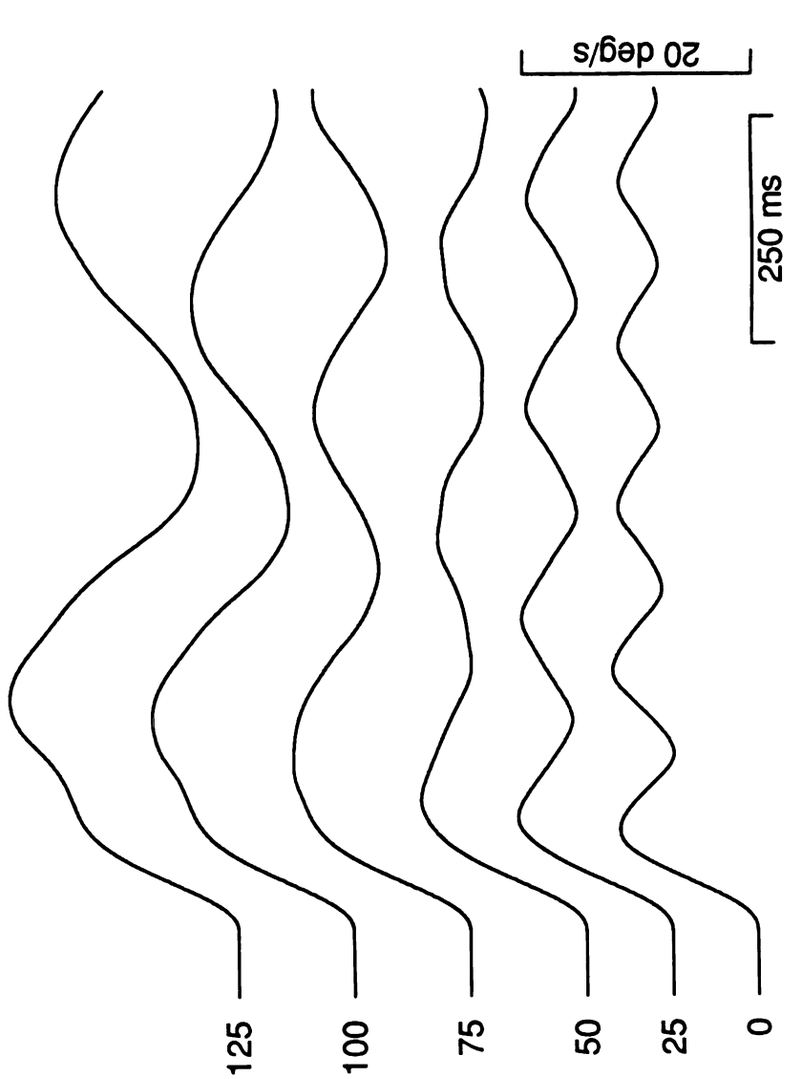

Fig. 2.15

Figure 2.16. Relationship between imposed delay and oscillation period. The graph plots the period of oscillations observed during the steady-state output of the model as a function of imposed delay. Each line in the graph shows the results obtained with the model used to match the data from one of the four monkeys.

Fig. 2.16

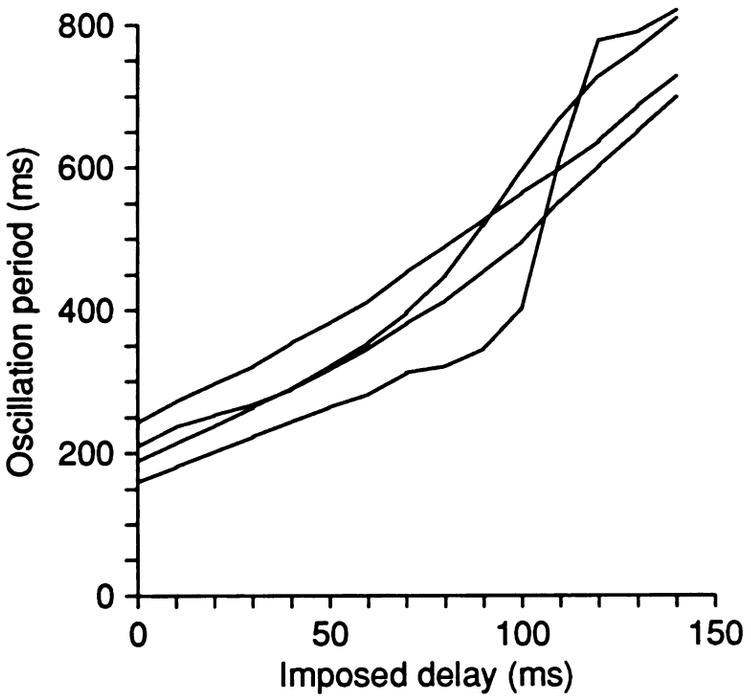
800
600
400
200
0
Oscillation period (ms)
0
50
100
150
Imposed delay (ms)

Figure. 2.17. Effect of lesioning all three visual motion pathways. The solid line indicates the output of the intact model for a target moving at a constant velocity of 20 °/s. The superimposed dashed lines show the reduced output of the model caused by multiplying the output of each of the three visual pathways by 0.75, 0.5, or 0.25. In each case, the output of the model approaches a steady-state value close to 20 °/s.

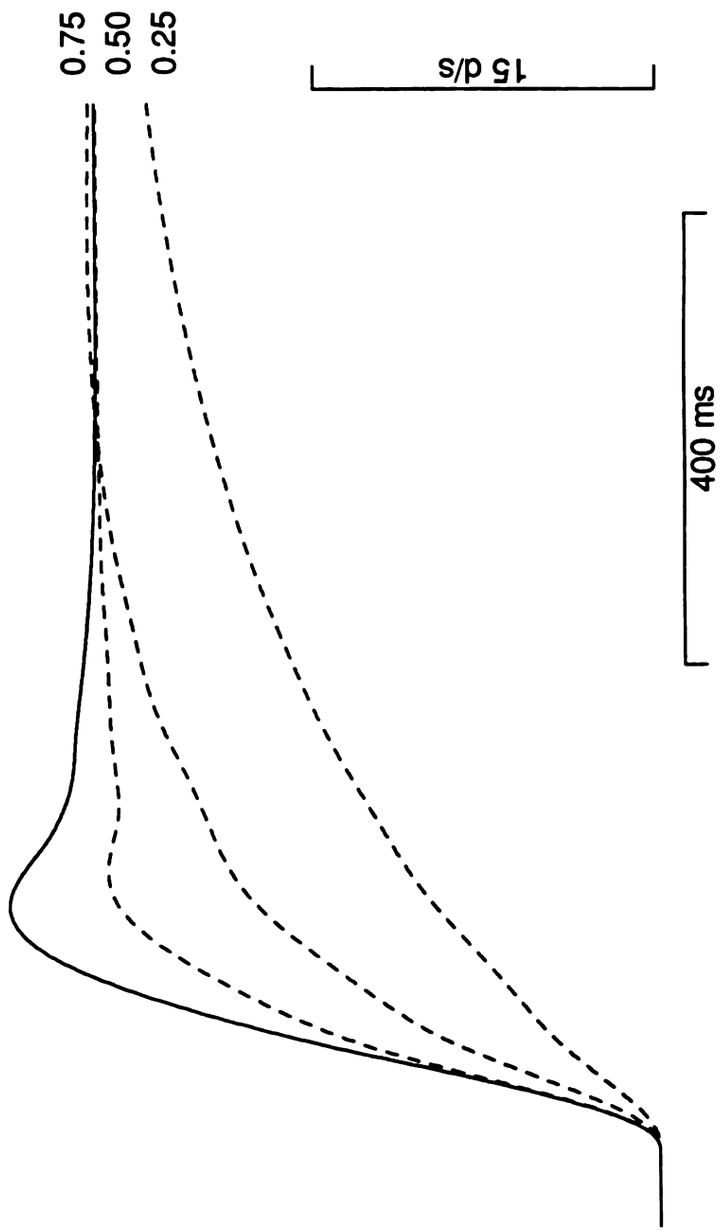

Fig. 2.17

Figure 2.18. Visual motion pathways cannot mimic the offset of pursuit. The solid traces in A, B and C show the average recorded eye velocity during presentation of a step-ramp-step-stop target motion during rightward (top) and leftward (bottom) pursuit. The superimposed dashed lines indicate the outputs of the model when presented with this target motion. A: The output of the model produced at the termination of pursuit (indicated by arrows) when its behavior is governed by the same parameter values as at the initiation of pursuit. B: The output of the model at the termination of pursuit observed when the contribution from the image motion transient pathway is eliminated at the beginning of the termination of pursuit. C: The output of the model when the contribution from both the image motion transient and image acceleration pathways is eliminated at the termination of pursuit.

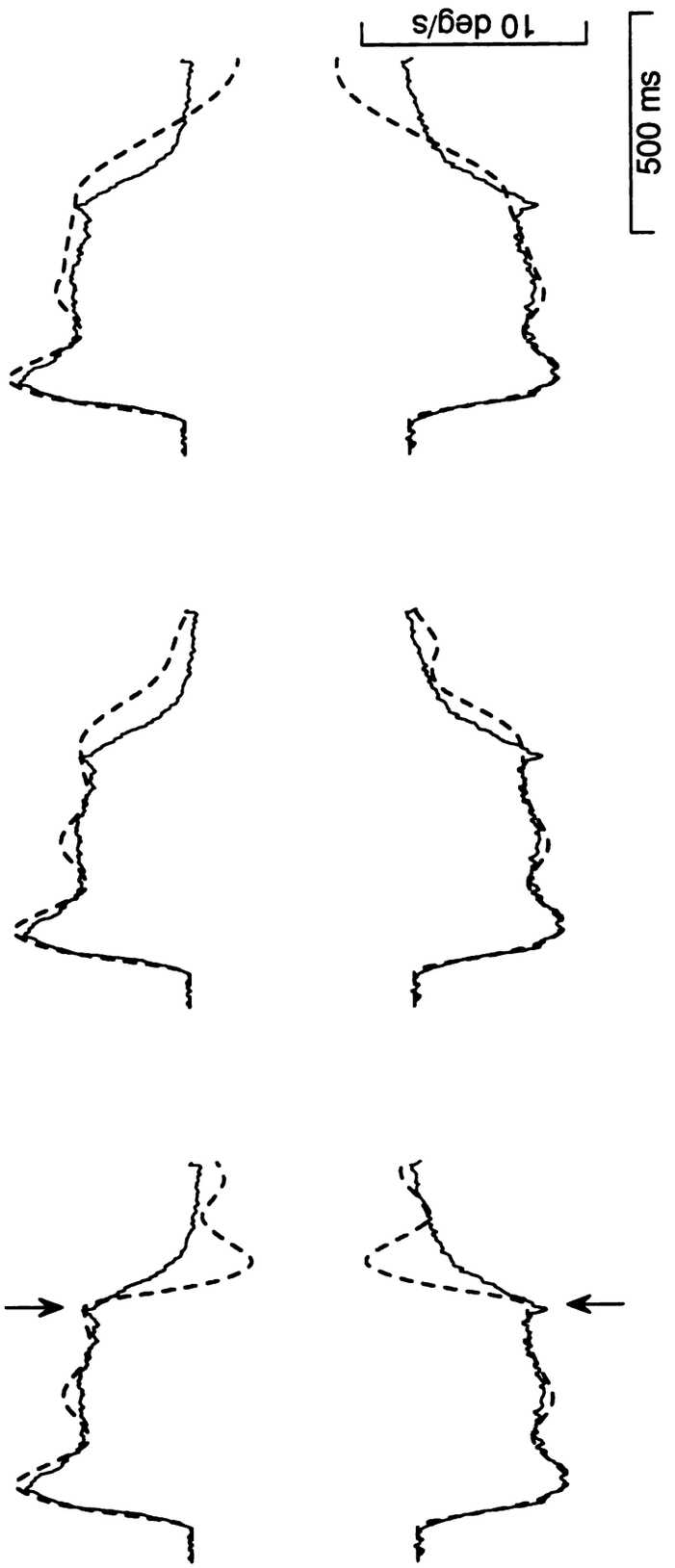

Fig. 2.18

Figure 2.19. A circuit for implementing eye velocity memory. A: An pulse is passed through a first-order system to produce a filtered version of the input pulse. The exponential rise and decay of the filtered step is determined by the time constant τ. B: The output of the first-order system is added back to its input after being multiplied by a factor *G*. Depending on the value of *G*, the output of this circuit is either a filtered pulse (lower dashed line), an integrated pulse (solid line), or an exponentially increasing output (upper dashed line).

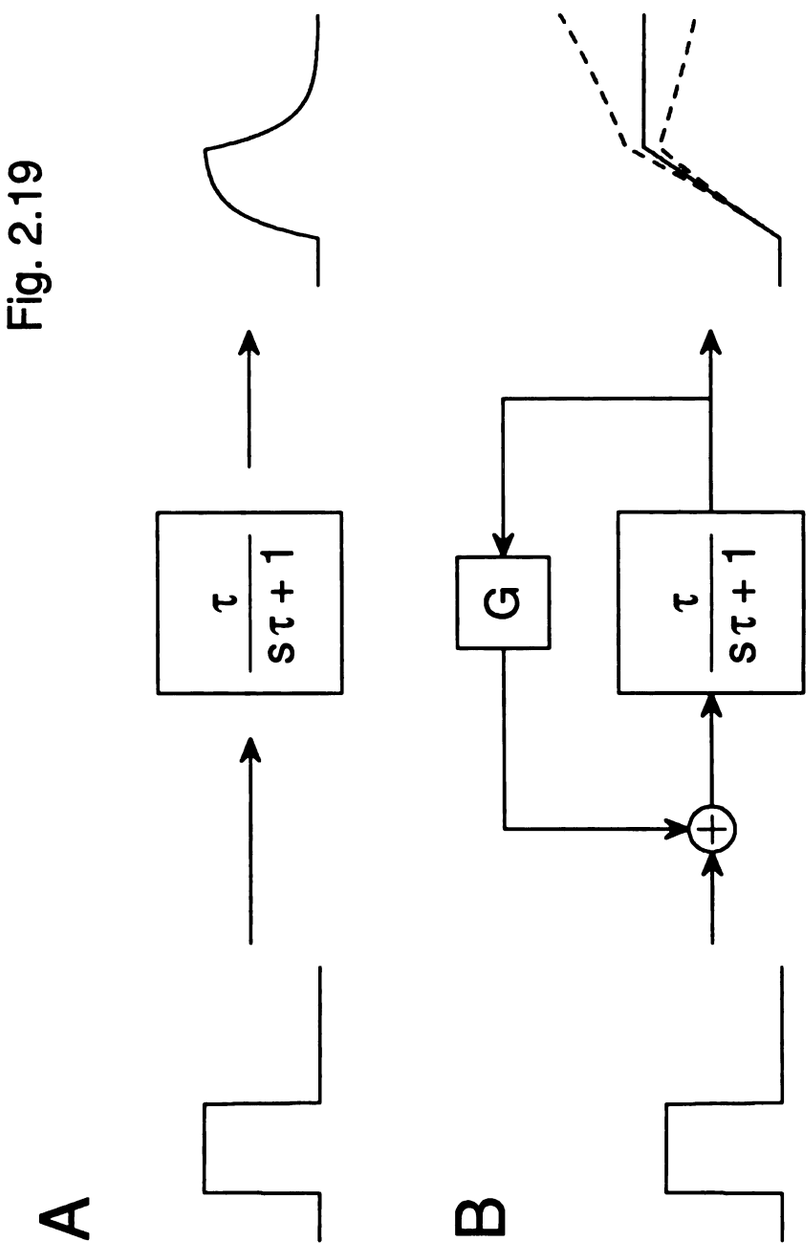

Fig. 2.19

Figure 2.20. Diagram of the model including the new circuit for eye velocity memory. H_i is a "leaky" integrator described by a first-order system, H(s) = $\tau/(s\tau + 1)$. G_S and G_{evf} are a linear gain elements. In practice, the value of G_S was assigned directly, so the summing junction preceding G_S is purely conceptual. The "X" preceding H_i indicates that the input to H_i is first multiplied by Gs. The letters *a*, *b*, and *c* identify signals in the model located at three different locations associated with the circuit.

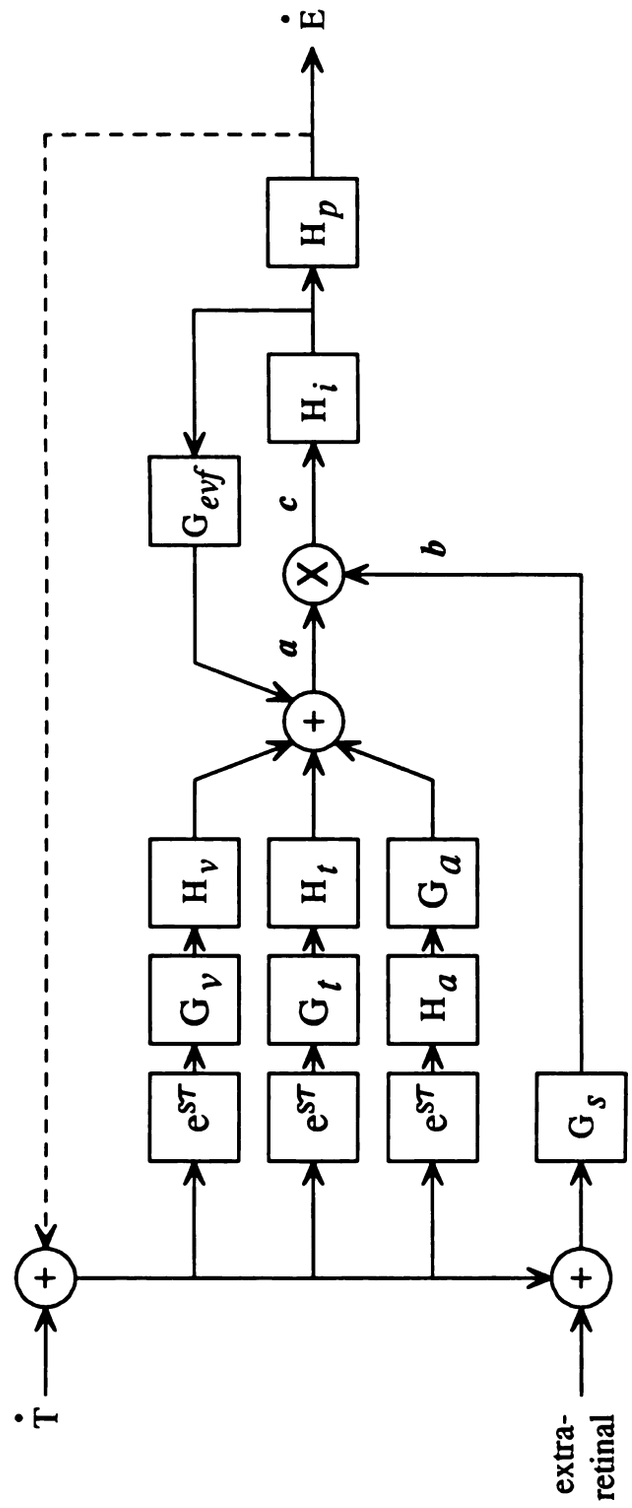

Fig. 2.20

Figure 2.21. Modeling the termination of pursuit. A-B: Comparison of averaged eye velocity responses (solid lines) and modeled responses (dashed) to constant velocity targets of 5, 10 and 20 °/s that moved for 500 ms and then stopped. Arrow indicates when Gs in the model was set equal to zero; the target motion stopped 75 ms before the arrow. C-D: The modeled responses shown in A-B have been scaled so that their steady-state values superimpose.

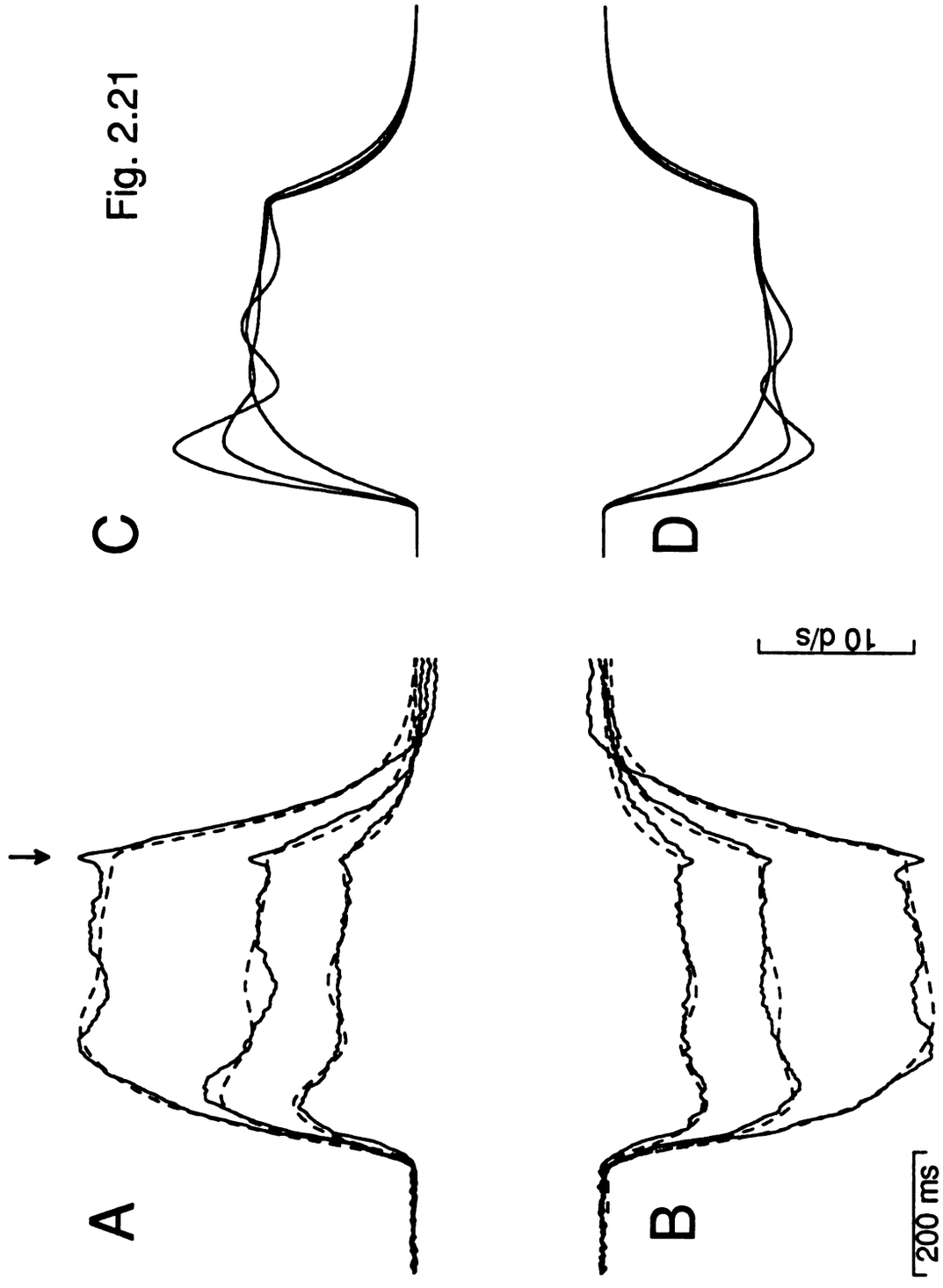

Fig. 2.21

Figure 2.22. Activity of signals in the model during the initiation and termination of pursuit. The three rows of traces show signals from the model as a function of time. The top trace shows the step in target velocity that provided the input to the model. The bottom traces shows the eye velocity output produced by the model. The middle three traces show the activity of three signals associated with the circuit for eye velocity memory, identified by the letter labels used in Fig. 20. The dashed line shown with signal *a* indicates the portion of signal a that was contributed by the sum of the three visual motion pathways. The early part of signal *b* is dashed, because the performance of the model was not effected by exactly when the value of signal *b* becomes equal to one, as long as it preceded the initiation of pursuit.

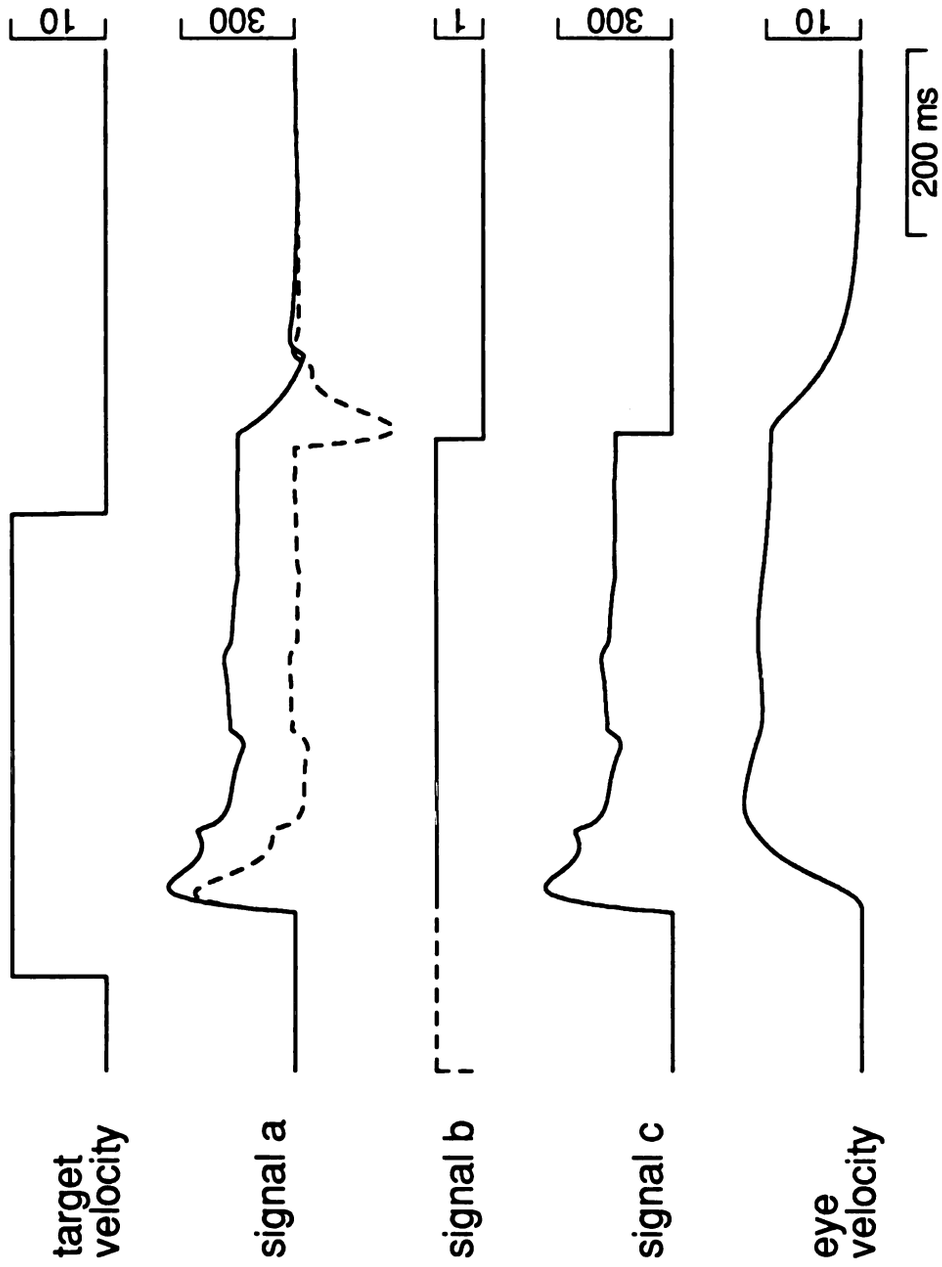
10
300
1
300
10
target velocity
signal a
signal b
signal c
eye velocity
200 ms

Fig. 2.22

Figure 2.23. Stimulation at sites in the model during fixation and during pursuit. A-F: Effect on the model caused by multiplying one of three locations in the model -- *a*, *b* or *c* -- by 1.2 for 100 ms. In each case, the stimulation began 300 ms after the beginning of the trial. The dashed lines indicate the results obtained in the absence of any stimulation. A-C: Results obtained when stimulation occurred in conjunction with the presentation of a 20 °/s target motion ("pursuit"). D-F: Results obtained when stimulation occurred in the absence of any target motions ("fixation"). The four traces in each part of the figure show the simulated eye velocity produced by the model and the activity present at the three locations in the model indicated by the letter labels *a*, *b*, and *c* in Fig. 20.

Fig. 2.23

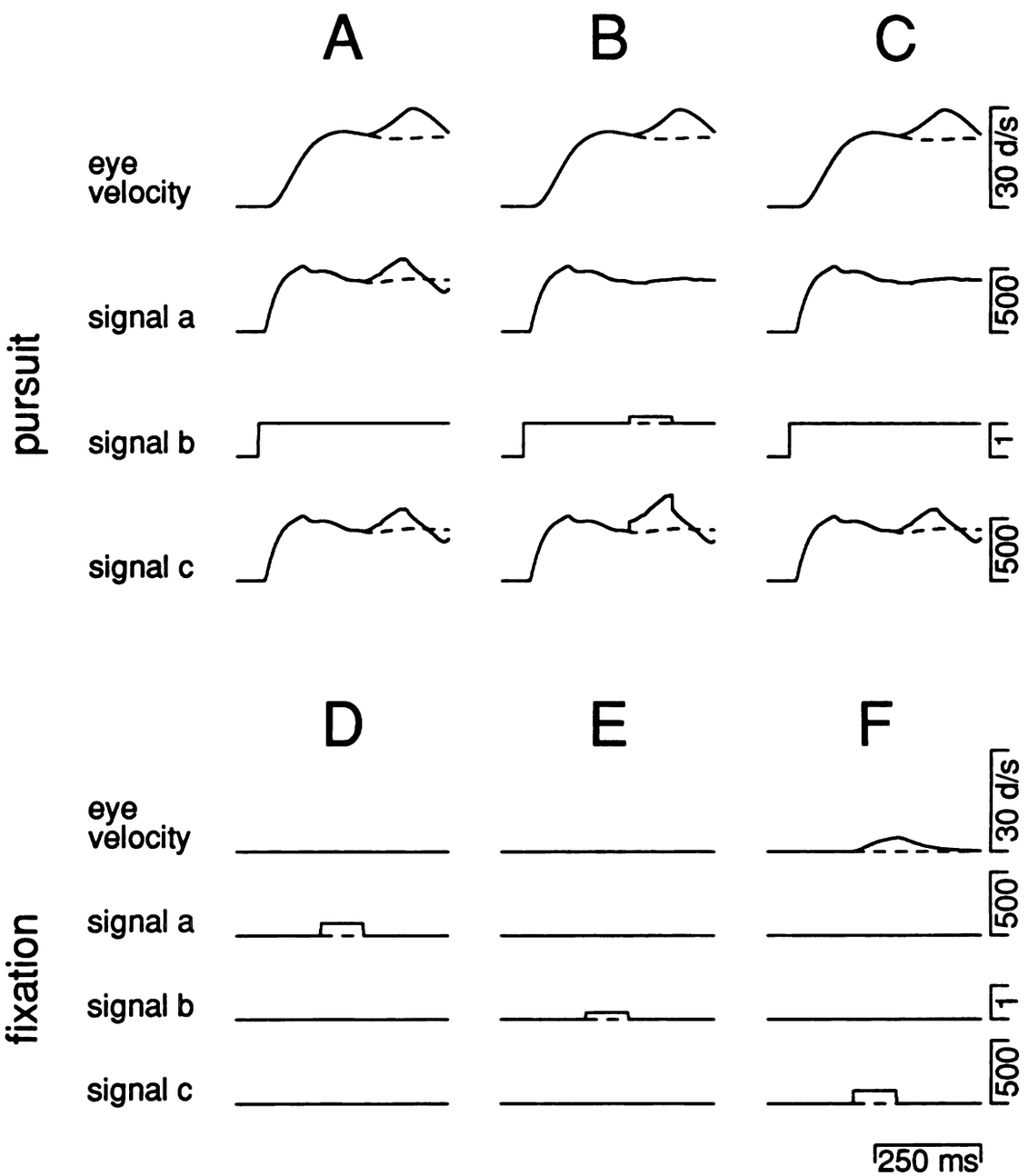
A
B
C
eye velocity
30 d/s
signal a
500
pursuit
signal b
1
signal c
500
D
E
F
eye velocity
30 d/s
signal a
500
fixation
signal b
1
signal c
500
250 ms

Figure 2.24. Effect of decreasing the value of G_S. Solid lines indicate the averaged eye velocity response to a target moving at a constant velocity of 20 °/s. Superimposed dashed line indicates the output of the model using optimized parameters. Dashed traces show the outputs obtained from the model when G_S was set to four different values, as indicated by the numbers to the right of each trace.

Fig. 2.24

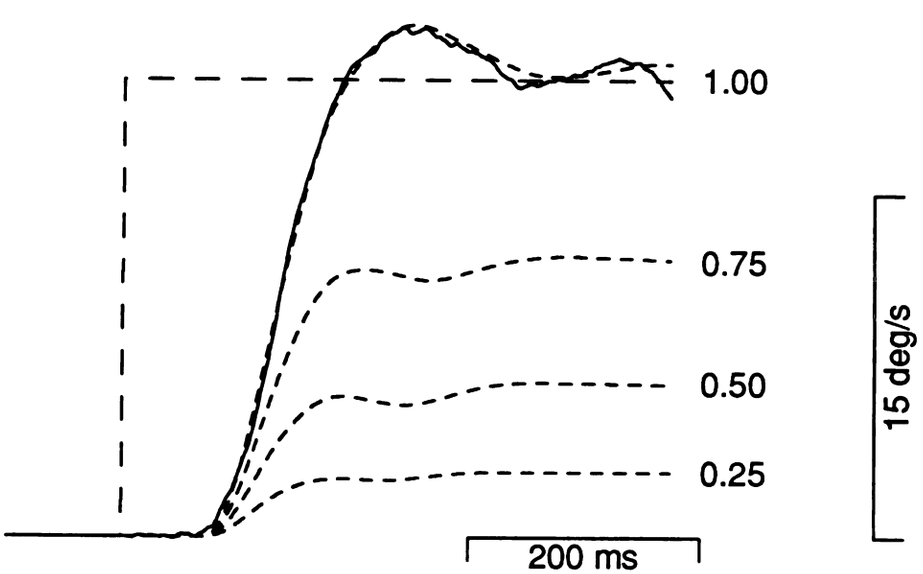

Figure 2.25. Effect of increasing the value of G_S. A: Three dashed traces on top indicate the output of the model for steps in target velocity of 5, 10 and 20 $^{o}/s$. The superimposed solid traces indicate the output of the model produced when the value of G_S is changed from 1.0 to 1.2 for a 100 ms period starting 300 ms after the onset of the target motion. The solid trace below the eye velocity traces shows the value of G_S as a function of time. B: Graph plotting the amplitude of eye acceleration caused by changing G_S, shown as a function of eye velocity at the time of stimulation. Each line indicates the results obtained when G_S was increased by 0.10, 0.25, or 0.50, as indicated by the numbers to the right of each line. Eye acceleration was measured as the average change in eye velocity over the 100 ms period coincident with the period of stimulation.

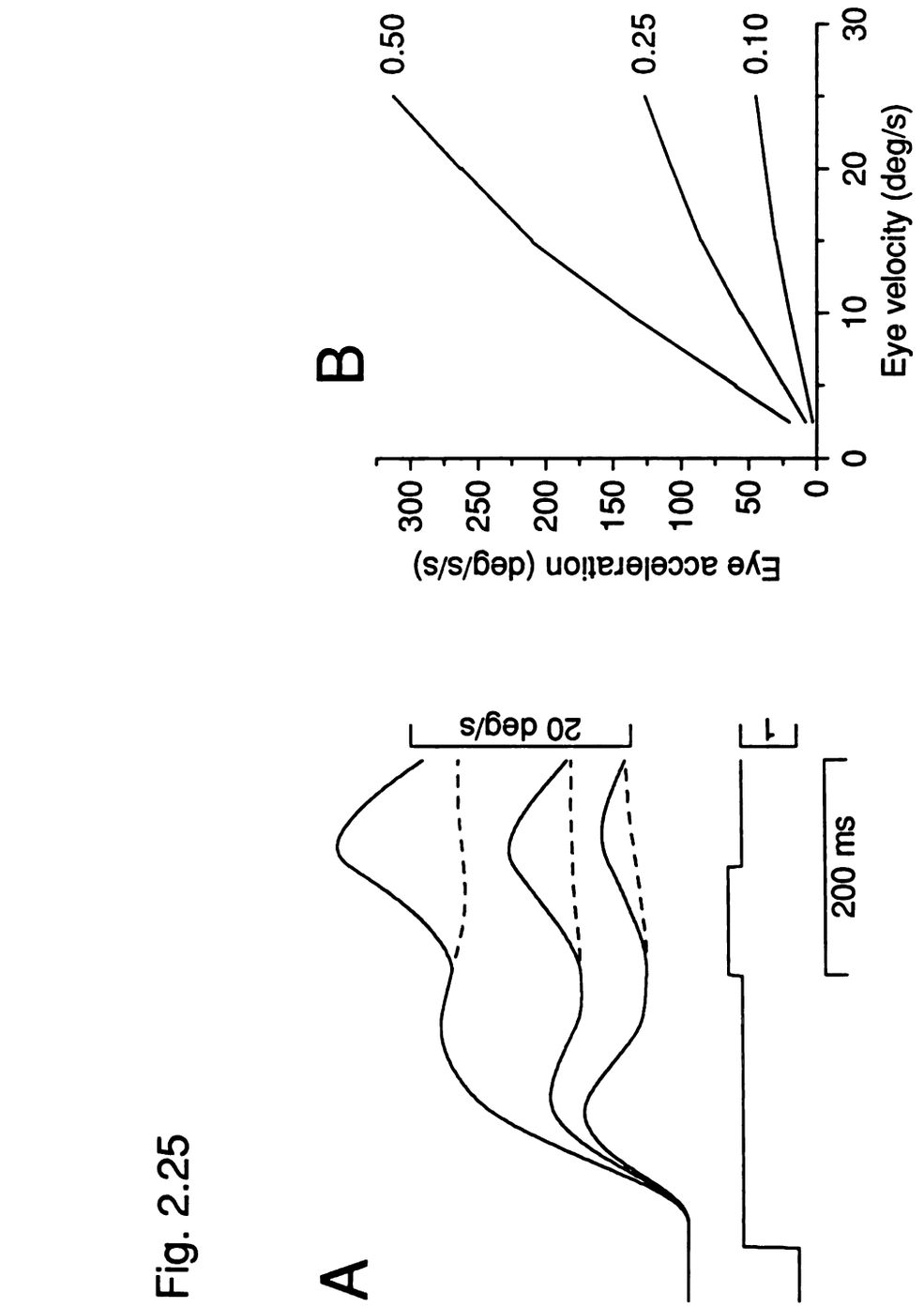
A
20 deg/s
200 ms
B
Eye acceleration (deg/s/s)
300
250
200
150
100
50
0
0.50
0.25
0.10
0
10
20
30
Eye velocity (deg/s)

Fig. 2.25

Figure 2.26. Recovery from "lesions" of the visual motion pathways. The top two pairs of traces show the step in target velocity provided as the input to the model (dashed line) superimposed on the output of the model (solid line). The lower three rows show the activity of three signals in the model, identified by the letter labels shown in Fig. 2.20. For signal *a*, the dashed line indicates the contribution of the sum of the three visual motion pathways. A: The set of traces show the normal output of the model and the normal activity of signals in the model. B: The set of traces show the change in the behavior of the model caused by multiplying the output of each of the three visual motion pathways by 0.5. The amplitude of eye velocity, signal *a*, and signal *c* are each reduced. C: The "recovery" in the behavior of the model caused by increasing G_S from 1.0 to 2.0 and by decreasing G_{evf} from 17.0 to 8.5. The output of the model is restored to its "normal" trajectory (top solid trace), as is signal *c*. The amplitude of signal *a* remains at its lower "lesioned" value, but the amplitude of signal *b* is at twice its "normal" value.

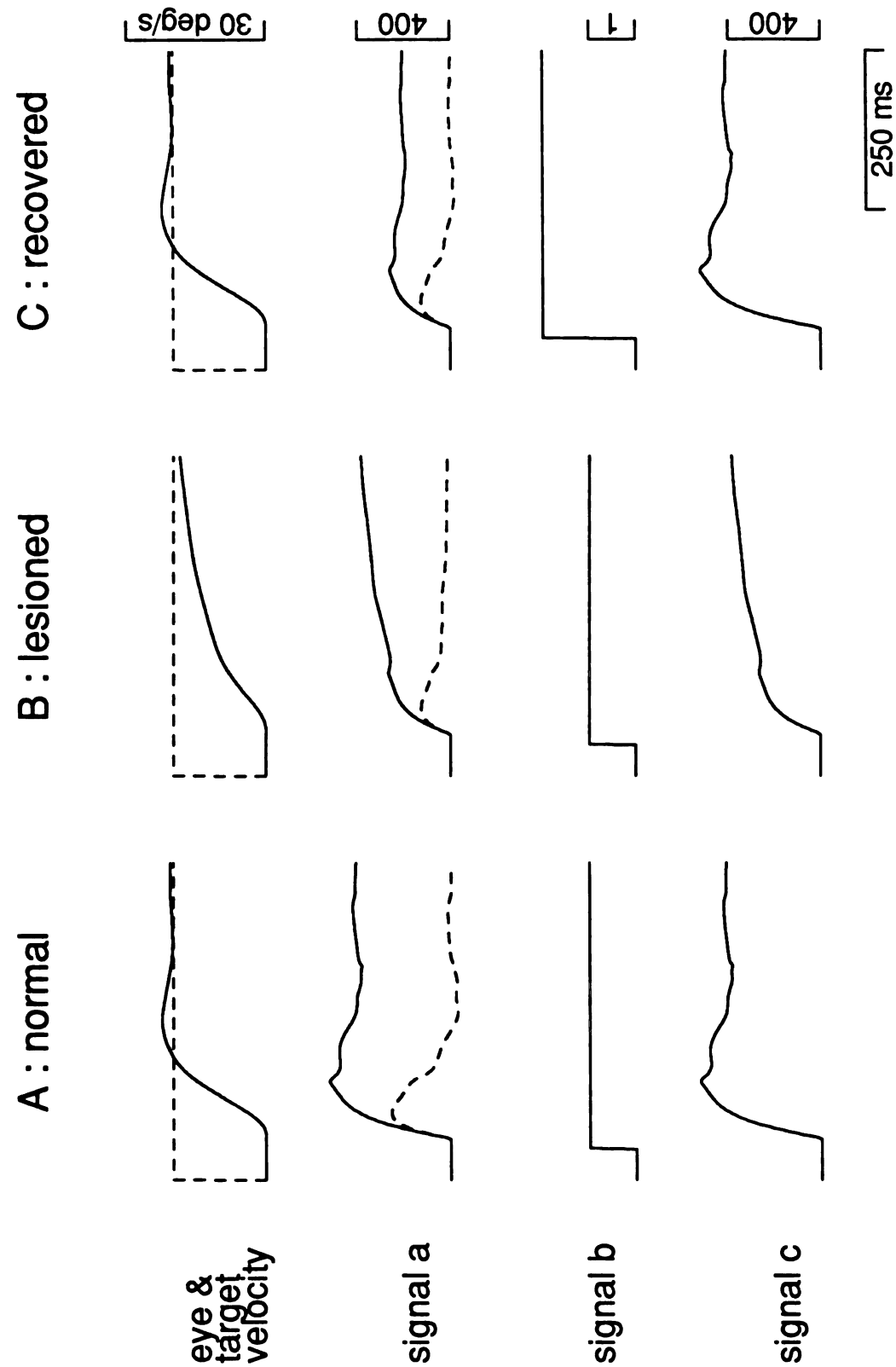
A : normal
B : lesioned
C : recovered
30 deg/s
400
1
400
250 ms
eye & target velocity
signal a
signal b
signal c

Fig. 2.26

Figure 2.27. Modeling the pursuit eye movements of human subjects. A: Comparison of the output from the Robinson et al. (1986) model (dashed traces) and the output of the model presented in this chapter, using optimized parameters in each of the three visual motion pathways. The responses of the models for four different target velocities is shown, as indicated by the numbers next to each pair of traces. B-G: Gain elements and step-responses of filters described by the parameters used in the model. B: Gain element (G_v) used in the image velocity pathway. C: Gain element (G_t) used in the image motion transient pathway. D: Gain element (G_a) used in the image acceleration pathway. E: Step-response of the filter (H_v) used in the image velocity pathway. F: Step-response of the filter (H_t) used in the image motion transient pathway. G: Step-response of the filter (H_a) used in the image acceleration pathway.

Fig. 2.27

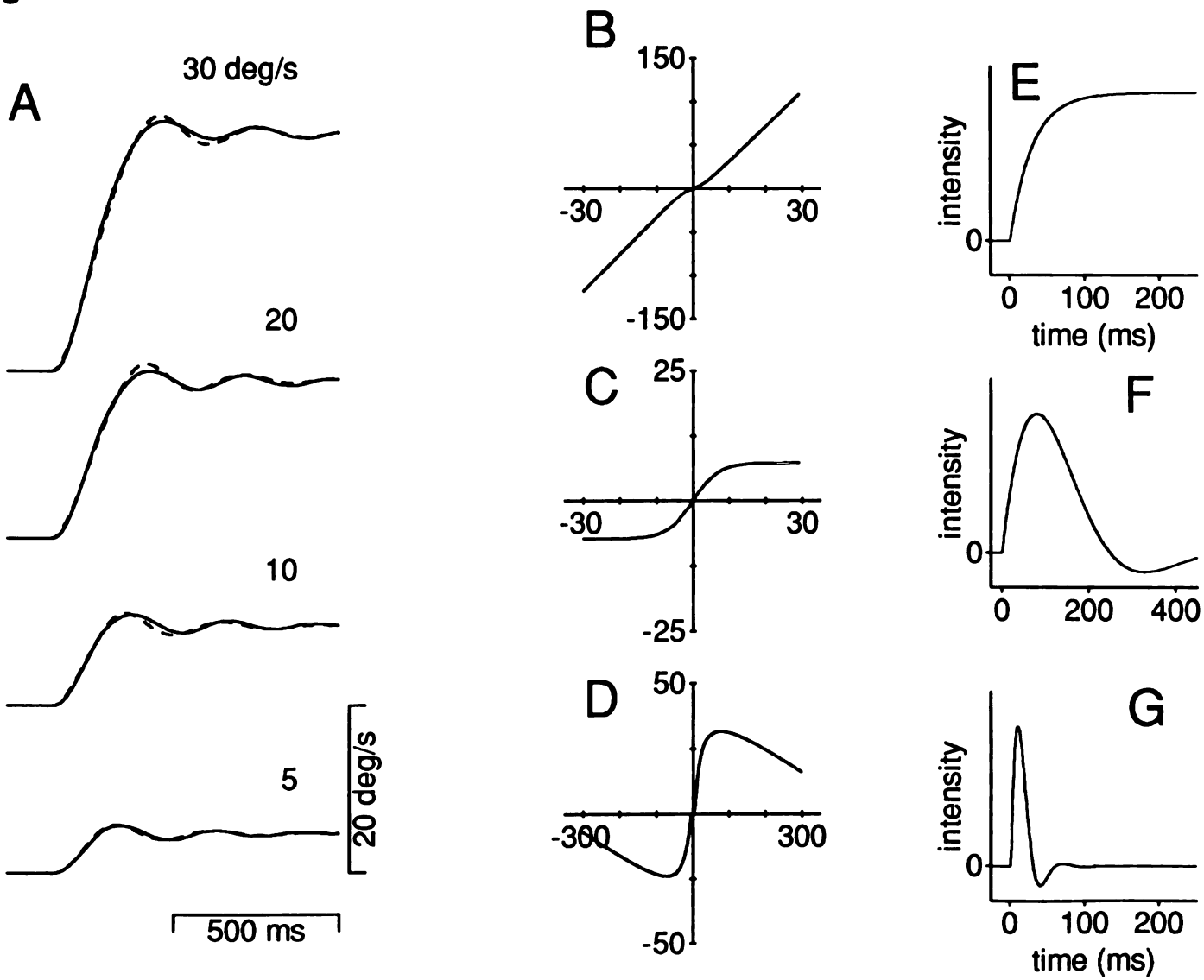
A
30 deg/s
20
10
5
20 deg/s
500 ms
B
150
-30
30
-150
C
25
-30
30
-25
D
50
-300
300
-50
E
intensity
0
0
100
200
time (ms)
F
intensity
0
0
200
400
G
intensity
0
0
100
200
time (ms)

Chapter Three

Vectors for smooth eye movements encoded in the flocculus and ventral paraflocculus of the monkey cerebellum

Summary and conclusions

1. We recorded from Purkinje cells and mossy fibers to determine the spatial organization of the eye velocity and visual signals conveyed by the cerebellar flocculus and ventral paraflocculus. By measuring the modulation in firing rate during sinusoidal tracking along different axes, we determined the best directions for the eye velocity signals conveyed by each unit. By measuring the modulation in simple-spike firing rate during pursuit of step-ramp target motions, we determined separate best directions for the eye velocity and visual signals conveyed by Purkinje cells.

2. Based upon their best directions, Purkinje cells were divided into two classes. Horizontal Purkinje cells preferred eye movements or visual motion directed to the same side as the recording site. Vertical Purkinje cells preferred motion directed downward and approximately 10° contralateral.

3. Purkinje cells displayed very broad tuning for the direction of eye movements and visual motion. The average half-maximum bandwidth of the tuning curves was nno, closely approximating a cosine tuning function. Horizontal and vertical Purkinje cells showed no differences in the shapes of their tuning functions.

4. In contrast to the Purkinje cells, oculomotor mossy fibers had best directions that clustered around the four cardinal directions. The mossy fibers also exhibited tuning for direction that was approximately 40° narrower than that shown by Purkinje cells.

5. Our results indicate that both the eye velocity and visual tuning of floccular Purkinje cells in the primate are consistent with the reference frame defined by vestibular pathways in the brainstem. Horizontal P-cells show tuning that matches the direction of head motion detected by the ipsilateral semicircular canal, while vertical P-cells show tuning that matches the ipsilateral posterior canal.

6. The differences between the tuning exhibited by the mossy fiber inputs and by the outputs conveyed by Purkinje cells suggests that a spatial transformation occurs within the cerebellar flocculus. In addition, although only horizontal and vertical Purkinje cells were found in the present study, the near-orthogonality and the broadness of their tuning makes it possible for the two populations to effectively encode all directions of smooth eye movements.

Introduction

The initiation and planning of movements depends on inputs provided to the nervous system by sensory organs such as the retina and the skin, while the implementation of movements requires an output that specifies the precise pattern of muscle activation. The control of movement therefore requires that sensory inputs converge to a single reference frame compatible with the musculature. The spatial dimensions of sensory and motor reference frames can be represented and compared with vectors. By measuring the vectors expressed by neurons and determining the coordinate system defined by these vectors, it may be possible to delineate the steps by which these spatial transformations are accomplished. In the present study, we have examined the coordinate system defined by the cerebellar flocculus in the primate, a structure that is a critical for mediating visual interactions with the vestibular system (Miles 1990, Precht et al. 1984, Waespe and Henn 1984). Because the relationship of the flocculus to the output motor pathways is well-defined, we can focus on how the flocculus transforms its input signals to match the constraints imposed by its targets.

Data from several species indicate that the organization of the flocculus embodies a reference frame that is shared by the vestibular sense organs and the output pathways of the oculomotor system. The foundation for this shared reference frame is the close correspondence between the planes of motion detected by the three semicircular canals and the axes of rotation defined by the pulling directions of the three pairs of extraocular muscles (Szentagothai 1950). Both anatomical and theoretical considerations suggest that some cross-coupling between the three channels is necessary (Robinson

1982, Simpson and Graf 1981), but to a first approximation each canal is linked, via subdivisions of the vestibular nucleus, to one set of extraocular muscles (e.g., Cohen et al. 1964, Flurr 1970, Ito et al. 1976ab, Szentagothai 1950). For example, primary afferents from the horizontal canal, which convey signals related to ipsilateral head rotations about the vertical axis, project to the medial vestibular nucleus. The medial vestibular nucleus, in turn, exerts an excitatory influence on the ipsilateral medial rectus and the contralateral lateral rectus and an inhibitory influence on the ipsilateral lateral rectus and the contralateral medial rectus. The pulling directions of these muscles act to rotate the eye about an axis that is closely aligned with the axis of rotation sensed by the horizontal canal. A similar principle of organization couples the anterior and posterior canals to the superior and inferior recti and the inferior and superior oblique muscles (for reviews, see Goldberg and Fernandez 19nn). In each case, the organization of the primary vestibular pathways matches the inputs from one of the three canals to the set of muscles that share their spatial axis.

The organization of the flocculus reflects the tripartite organization of the primary vestibular pathways. In non-primate species, the flocculus is divided into distinct zones whose anatomy and physiology conform to the reference frame defined by the semicircular canals and the extraocular muscles. These zones are oriented perpendicular to the long axis of the folia, and each projects differentially to a distinct division of the vestibular nuclear complex (Gerrits and Voogd 1989, Voogd et al. 1987, Balaban et al. 1981). The targets of the projections are consistent with the directions of eye movements evoked by electrical stimulation within each zone. In the cat, for example, the middle floccular zone projects to the medial vestibular nucleus (Sato et al. 1982, Sato et al. 1988) and stimulation of this zone causes ipsilaterally-directed

horizontal eye movements (Sato and Kawasaki 1984). There is some disagreement about the exact organization of these zones within the flocculus (e.g. see discussion of Gerrits and Voogd 1982), but the data from both rabbits and cats demonstrate a topographical relationship between the anatomical zones in the flocculus and the vestibular pathways in the brainstem.

It has been shown that the visual inputs to the flocculus in non-primates conform to the shared vestibular-oculomotor reference frame. Visual inputs are conveyed to the flocculus by climbing fibers from the inferior olive (Groenewegen and Voogd 1977, Gerrits and Voogd 1982, Gerrits and Voogd 1989, Sato et al. 1982) and by mossy fibers arising from several brainstem nuclei, including the nucleus reticularis tegmenti pontis (NRTP) and perhaps the vestibular nuclei (Maekawa et al. 1981, Sato et al. 1983, Gerrits and Voogd 1989). Each of these sources of visual inputs to the flocculus, in turn, receives its primary visual input from nuclei of the accessory optic system (AOS). The striking property of neurons in the AOS of the rabbit and cat is their preference for visual stimuli that indicate movement of the subject in the environment (for reviews, see Simpson et al. 1979, Simpson 1984, Grasse and Cynder 1990). Neurons in these nuclei respond selectively to the motion of large textured patterns and the preferred directions of motion are closely aligned with the directions of head motion detected by the semicircular canals. The mapping of visual inputs to the flocculus in correct spatial register can therefore be accomplished simply by connecting each AOS neuron to the appropriate floccular zone.

In primates, the spatial organization of the signals conveyed by the flocculus has not been directly studied. Electrical stimulation in the flocculus can evoke horizontal and vertical eye movements, but there is no clear evidence of zonal organization (Ron and Robinson 1973, Balaban and

Watanabe 1984, Belknap and Noda 1987). There is also some anatomical evidence that the climbing fiber projections to the flocculus (Brodal and Brodal 1981, 1982) and the projections from the flocculus to the vestibular nuclei (Balaban et al. 1981; Broussard and McCrea, submitted) display a zonal organization like that observed in non-primates. Recordings from the flocculus indicate that there are two classes of Purkinje cells (P-cells) which are distinguished by their preferences for horizontal or vertical eye movements (Miles et al. 1980, Stone and Lisberger 1990). However, because the directional tuning of the eye velocity signal on P-cells has not been measured, the spatial organization of these output signals is not known. In addition, the primate flocculus may receive visual inputs that do not conform to the reference frame defined by the semi-circular canals. In primates, the flocculus is critical for the performance of smooth pursuit eye movements, which permit tracking of small targets over textured backgrounds (Takemori and Cohen 1974, Zee et al. 1981). The local analysis of motion in the visual field underlying smooth pursuit is very different from the analysis of full-field visual motion accomplished by the AOS of non-primates. The additional visual signals necessary for generating pursuit are provided from visual areas in the cerebral cortex (Newsome et al. 1985, 1988) and most likely reach the flocculus by projections through the pontine nuclei (Brodal 1978, 1979, 1982; Glickstein et al. 1972, 1980, 1985; Langer et al. 1985), a pathway that appears to be less prominent in non-primates. Because all directions of motion are represented in these cortico-pontine visual pathways (Maunsell and Van Essen 1983, Albright 1984, Mikami et al. 1986, Suzuki and Keller 1984, Mustari et al. 1988, Thier et al. 1988), the visual signals for pursuit must be adapted to match the more restricted spatial organization of the floccular targets.

In this chapter, we present single-unit recording data from the primate flocculus that provide some clarification of these issues. Our report consists primarily of a description of the directional tuning of signals recorded from floccular P-cells. As described by several previous investigators, the simple-spike firing rate of most floccular P-cells reflects a combination of eye velocity, head velocity and visual motion inputs (Miles and Fuller 1975; Lisberger and Fuchs 1974, 1978; Noda and Suzuki 1979a,b; Miles et al. 1980; Waespe and Henn 1981; Buttner and Waespe 1984; Noda 1987; Markert et al. 1988; Stone and Lisberger 1990). The strength of the eye velocity signal can be determined by measuring the modulation in simple-spike firing rate as the subject pursues the continuous motion of a small visual target. The strength of the visual signal can be determined by having the subject initiate pursuit of a target that moves at a constant velocity. At the initiation of pursuit, floccular P-cells show a transient increase or decrease in simple-spike firing rate that is caused by visual inputs (Stone and Lisberger 1990). In the present experiments, we have used these two tracking behaviors to assess the directional tuning of the eye velocity and visual motion signals. We have found that the distributions of preferred directions for both the eye velocity and the visual motion signals on floccular Purkinje cells are aligned with the spatial orientation of the semicircular canals.

Methods

Preparation of animals

Experiments were conducted on four Rhesus monkeys weighing 5.0 - 8.0 kg. After initial training on a reaction-time task modified from Wurtz (1969), each monkey underwent sterile surgery while anesthetized with

halothane. A coil of wire was implanted on the sclera of one eye (Judge et al. 1980) so that eye movements could be monitored with the magnetic search coil technique. Three or four bolts were implanted in the skull to anchor a receptacle for head restraint. During daily recording sessions lasting 2 - 3 hours, each monkey sat in a primate chair with his head fixed to the ceiling of the chair. A pair of 18 inch square coils were attached to the chair to generate the magnetic fields used to record eye position. The monkey's eye monitor was initially calibrated by having him perform the reaction time task with targets at known positions. Once the system was calibrated, we switched to a window task in which the monkey received rewards every 1500 ms as long as his eye position remained within 2 - 3 degrees of the target.

After the animal was trained in the behavioral paradigms, it was prepared for single-unit recording. In a second surgical procedure, we implanted a stainless steel cylinder over a hole trephined in the skull. The cylinder was placed stereotaxically 11 mm lateral of the midline along the interaural line and tilted back 26^{o} of the coronal plane. The cylinder was capped securely, cleaned daily and filled with isotonic saline and antibiotic ointment (chloramphenicol 1%) to prevent infection.

Presentation of visual stimuli

Visual stimuli were circular spots of light 0.1 to 0.5 degrees in diameter projected onto the back of a tangent screen placed 114 cm in front of the monkey. Stationary targets were generated by projecting the image of an LED or fiber optic light beam onto the screen. Moveable targets were generated by reflecting a light beam off a pair of orthogonal, servo-controlled mirror galvanometers (General Scanning, CCX 650). Command signals for target position were provided by the digital-to-analog converter of a laboratory computer. Actual target position was measured from feedback signals from

the mirror galvanometers. The optical projection system was set up with both the mirror galvanometers and the monkey's eyes 114 cm from the screen to eliminate possible nonlinearities introduced by using a flat tangent screen. The experimental room was dimly illuminated by incandescent lights and the monkey was allowed binocular viewing. Under these conditions, the moveable target was 2.2 log units brighter than our perceptual threshold for detection of a 100 ms flash.

Presentation of vestibular stimuli

The monkey, chair, and attached magnetic field coils were set on a Contraves-Goertz turntable (20 ft-lb peak torque). Because the monkey's head was fixed to the chair in the stereotaxic plane, motion of the turntable provided passive stimulation of the horizontal semicircular canals. We measured angular head velocity with a tachometer and measured angular head position with a precision potentiometer attached to the shaft of the the turntable.

Single-unit recording

Recordings were made with glass-insulated platinum-iridium microelectrodes manufactured in our laboratory. The electrodes were mounted on an adjustable stage that attached to the recording cylinder and driven through the dura with a hydraulic microdrive (). Extracellular unit activity was passed through a standard head stage (), amplified (bandpass 100 Hz - 10 kHz) and converted into trigger pulses with a window discriminator.

The electrode typically travelled 2.5 to 3.5 cm through cerebral cortex and cerebellum en route to the cerebellar flocculus. Entry into the cerebellum was marked by a large increase in background activity. The flocculus was identified within the cerebellum by the presence of activity related to eye movements. We identified P-cells by their simple-spike waveform (large

negativity followed by a small positivity) and the characteristic presence of a complex-spike. P-cells could often be heard in the midst of background activity and isolated by careful and repeated movements of the electrode. Once isolated, P-cells could be held for up to one hour. We identified mossy fibers by their brief, triphasic (positive-negative-positive) or biphasic (positive-negative) waveforms. In contrast to P-cells, mossy fibers were often isolated unexpectedly and were difficult to hold for longer than 5 minutes.

Behavioral paradigms

Once isolated, activity of each unit was recorded during a sequence of behavioral conditions. We first tested the responsiveness of the unit with the sinusoidal tracking tasks used previously to identify P-cells and oculomotor mossy fibers in the flocculus (Lisberger and Fuchs 1978a; Miles et al. 1980, Stone and Lisberger 1990). 1) With the head stationary, the monkey tracked a sinusoidally moving target (0.5 Hz, $+10^{o}$). The monkey was rewarded after each interval of 1500 ms during which his eye position remained within 2^{o} of the moving spot. This behavior allowed us to measure the unit's sensitivity to eye velocity. 2) The monkey tracked the same sinusoidally moving target, but the turntable was moved exactly with the visual target. This paradigm required the monkey to cancel his vestibuloocular reflex and allowed us to measure the unit's sensitivity to head velocity. 3) The monkey fixated a stationary spot. By systematically placing the spot at different locations on the tangent screen, we could assess the unit's sensitivity to eye position.

After initial tests, most units were studied in two experiments. In the first experiment, the monkey tracked a sinusoidally moving target as described above, but after 10 - 15 cycles of accurate tracking the orientation of target motion was rotated by 30^{o}. The target motion at each orientation was sinusoidal (0.5 Hz, $\pm 10^{o}$) and centered on a point corresponding to straight

ahead gaze. We recorded from each P-cell during a total of six orientations of target motion. If the target motions are viewed as having swept across the face of a clock, the six orientations of target motion corresponded to axes placed at 12 to 6 (vertical), 1 to 7, 2 to 8, 3 to 9 (horizontal), 4 to 10, and 5 to 11 o'clock.

In the second experiment, we used a modification of the step-ramp trial originally designed by Rashbass (1961). Each trial started when the monkey fixated a central red spot. After a random interval (500-1000 ms), a white target spot appeared at an eccentric position and remained stationary for an additional random interval (300-500 ms). To initiate pursuit, the fixation spot was extinguished and the target began to move at a constant speed of 30 ^{o}/s. We generated step-ramp target motions with separate stationary and moving spots to avoid unwanted motion that is seen when a single spot is physically stepped away from straight-ahead gaze. Target motion lasted 600 - 800 ms. The monkey was rewarded with approximately 0.1 ml of water or juice at the end of each trial if he maintained his eye position within 2 degrees of the stationary target and within 3 - 4 degrees of the moving target throughout the trial. If his eye position strayed out of these windows, the trial was aborted and he received no reward. The only exception to the fixation requirement was a 300 - 400 ms grace period allowed at the onset of target motion.

We presented step-ramp targets moving in twelve directions. The target motions were presented in a series of 300 - 400 trials selected in random order from a list of twelve trials. Randomizing the order in which the trials were presented overcame a natural tendency of the monkeys to guess how the target would move, since the first part of each trial did not contain enough information for the monkey to identify the trial type. In addition, catch trials were also randomly inserted into the series at a lower frequency to

eliminate nonspecific anticipatory responses and to verify that anticipatory responses were not contaminating our data. The catch trials required the monkey to maintain fixation of the central spot as an eccentric target flashed on for 300 - 500 ms.

Data acquisition and analysis

Experiments were conducted using a computer program that controlled the target motion, monitored the monkey's behavior, and sampled the data. Voltages related to eye position, eye velocity, target position and target velocity were digitized during the experiment at 1 ms intervals and stored on computer disk. The eye velocity signal was obtained by analog differentiation of the eye position voltage (DC to 50 HZ, -20 dB/decade).

Data were analyzed after the experiment using a computer. Records from each trial were displayed on a video screen using an interactive program that allowed the user to place cursors on the data traces. In the eye velocity traces, we marked the beginning and end of each saccadic eye movement in the eye velocity trace. The computer removed the saccade and replaced it with an eye velocity segment that connected the eye velocity at the beginning and end of the saccade. For data from sinusoidal tracking, traces from at least 8 cycles were aligned on the zero crossings and averaged. For data from step-ramp trials, if the pursuit response began with a saccade or if pursuit was interrupted by a saccade occurring earlier than 100 ms after pursuit initiation, the trial was discarded. Approximately 5 to 10% of the trials were discarded because of early saccades. For the remainder, trials of the same type were aligned on the onset of target motion and averaged together to obtain the mean and SD for each ms interval of the record. For both sinusoidal and step-ramp data, firing rate was calculated by averaging the reciprocal of the

interspike intervals, using a method described previously (Lisberger and Pavelko 1986).

Results

The data in this paper are based on extracellular recordings from 120 Purkinje cells in both flocculi of two monkeys. Fifty P-cells had firing rates that were more strongly modulated during horizontal than during vertical eye movements. All but one of these P-cells were identified as horizontal "gaze velocity" P-cells, according to the criteria of Lisberger and Fuchs (1978) and Stone and Lisberger (1990). Fig. 3.1 shows averages of the firing rate recorded from a typical horizontal gaze velocity P-cell recorded in the left flocculus. The vertical dashed lines indicate peak leftward eye and head velocity. During sinusoidal pursuit, the modulation in the firing rate was largest during leftward, i.e. ipsilateral, eye velocity (Fig. 3.1A). The sensitivity to eye velocity measured from these data, defined as the modulation in firing rate divided by the modulation in eye velocity, was 2.28 spikes/s per deg/s. When the monkey's head was moved passively with the same motion as the target spot, a condition that requires cancellation of the VOR, the modulation in firing rate was maximal during leftward head velocity (Fig. 3.1B). Typical of gaze velocity P-cells, the sensitivity to head velocity sensitivity (2.47 spikes/s per ^{o}/s) was similar to the sensitivity to eye velocity.

The firing rates of the remaining P-cells were more strongly modulated during vertical eye movements. We did not systematically assess the sensitivity to head velocity of the vertical P-cells, although for some we noted a modest response during head movements directed toward the side opposite the recording site. As suggested by Stone and Lisberger (1990), this modest

response may be due to activation of the vertical canals, consistent with the view that these P-cells are the vertical homologues of the horizontal gaze velocity neurons.

Fig. 3.2 summarizes the responses of our sample of P-cells in the tracking conditions used to identify them as gaze velocity P-cells. Fig. 3.2A plots the sensitivity to head velocity as a function of the sensitivity to eye velocity for the 44 horizontal P-cells from which we recorded during both sinusoidal pursuit and cancellation of the VOR. The dashed line represents the behavior expected if the sensitivities to eye and head velocity were exactly equal. The actual data lie close to the line, but the sensitivity to head velocity (1.70 ± 0.84 spikes/sec per °/sec, SD) was on average slightly greater than the sensitivity to eye velocity (1.51 ± 0.78 spikes/sec per °/sec, SD). Fig. 3.2B shows the distribution of sensitivities to eye velocity for the 65 vertical P-cells. The mean sensitivity of the vertical P-cells to eye velocity was 1.48 spikes/s per °/sec (SD = 0.75).

Directional preferences of P-cells during sinusoidal pursuit

To assess the directional preferences of floccular P-cells, we first studied their firing rate during sinusoidal pursuit along six different axes. The axes along which the target traversed are indicated by the orientations of the double-headed arrows to the left of each trace in Fig. 3.3. In each case, the target moved sinusoidally ($\pm$10 deg, 0.5 Hz) through straight-ahead gaze. To simplify presentation of these experiments, we will refer to the axes of motion by the corresponding pairs of hour locations on the clock. Each of the traces to the right represent the average firing rates recorded from one P-cell over 10-15 cycles during pursuit along one of the six axes. The firing rate traces are aligned by the vertical dashed lines according to vertical and horizontal eye velocity. The left dashed lines indicate the peak upward eye

velocity; the right lines indicate peak downward eye velocity. Peak horizontal eye velocity is also indicated by the dashed lines, but of necessity changes sign in the upper and lower halves of the figure (small arrows).

The firing rate of the P-cell shown in Fig. 3.3 changed smoothly as the axis of tracking was rotated. The firing rate during vertical tracking (6 o'clock - 12 o'clock) was modulated $\pm$55.26 spikes/sec from a baseline firing rate of 100.50 spikes/sec. Tracking along the 1 o'clock - 7 o'clock axis and the 5 o'clock - 11 o'clock axis produced similar modulations in firing rate (51.22 and 49.11 spikes/s, respectively). However, the modulation in firing rate during horizontal tracking showed a slight bias for rightward eye velocity (13.56 spikes/sec).

The modulation in firing rate for different axes of tracking is summarized by the polar plot in Fig. 3.3B. The dashed line indicates the mean firing rate during tracking in each direction. This P-cell showed a slightly higher mean firing rate during vertical tracking (100.50 spikes/s) than during horizontal tracking (88.70 spikes/s). The solid line shows how the modulation in firing rate changed as a function of direction of tracking. For each direction of tracking, we calculated the "preferred" response by adding the amplitude of modulation to the mean firing rate and calculated the "non-preferred" response by subtracting the amplitude of modulation from the mean firing rate. For each trace in Fig. 3.1A, we therefore obtained two data points, 180 degrees apart, for the polar plot in Fig. 3.3B.

We next fit a smooth function to the data representing the modulation in simple-spike firing (filled circles in Fig. 3.3B). The fitted function allowed us to characterize the shape of tuning exhibited by each P-cell and to interpolate between the twelve directions presented in the experiments. The polar plot in Fig. 3.3C shows again the responses plotted in Fig. 3.3B, with the

best-fit tuning function superimposed. The data points were fitted with a Gaussian function, $y = a + be^{-(x-x')^2/(2c^2)}$, where a represents the baseline firing rate, b represents the amplitude of modulation and c represents the variance of the Gaussian. The function has a maximum value of (a + b) at the direction x'. Best-fitting parameters were determined with an iterative optimization algorithm (Nelder and Mead, 1965) to produce the tuning curve shown by the solid line in Fig. 3.3C. The P-cell's best direction, given by the value of x', is represented in Fig. 3.3C by an arrow pointing from the origin of the polar plot to the peak of the tuning curve. This P-cell had a best direction of 170.87°. The tuning curve also provided a measure of the strength of the P-cell's tuning for direction. We defined a "directionality index", defined as 1 - worst/best, where "best" is the amplitude of the curve for the preferred direction and "worst" is the amplitude of the curve in the non-preferred direction. The directionality index equals 0 if the unit shows no tuning for direction and equal 1 if the unit is completely suppressed in the non-preferred direction. The P-cell illustrated in Fig. 3.3 had a directionality index of 0.75. We also calculated a half-maximum bandwidth for the tuning curve obtained with data from each P-cell. To calculate the half-maximum bandwidth, we determined the range in degrees over which the modulated portion of the tuning curve exceeded half of its maximum value. The half-maximum bandwidth for the P-cell presented in Fig. 3.3 was 167.83°.

The distribution of best directions from our sample of P-cells is shown in Fig. 3.4. Data from each of the three flocculi are presented separately. Figs. 3.4A and B show the best directions obtained from the 65 units recorded in the left flocculus of monkey O. Each line in Fig. 3.4A is a vector that represents the best direction for one P-cell, using the same format as in Fig. 3.3C, but omitting axes and arrowheads for clarity. The length of each vector

is proportional to the directionality index of the unit. Fig. 3.4B shows the data from the same P-cells in histogram format. Both the clustering of best directions in Fig. 3.4A and the bimodal distribution in Fig. 3.4B indicated that the P-cells recorded from this flocculus could be divided into two main groups: a set of horizontal units that prefer tracking directed ipsilaterally and a set of vertical units that prefer tracking down and slightly contralateral. We categorized each P-cell based on its preferred direction: P-cells with preferred directions within 30° of ipsilateral (240 to 300°) were defined as "horizontal", P-cells with preferred directions within 30° of down (150 to 210°) were defined as "vertical". These directional intervals are indicated in Fig. 3.4B by the horizontal bars over the histogram. The average best direction for the 33 horizontal P-cells was 272.19° (SD = 10.96). The average best direction for the vertical P-cells was 170.10° (SD = 10.31), approximately 10° oblique and contralateral of down. In addition, there were 4 units that were not classified as either horizontal or vertical. These units preferred horizontal pursuit in the contralateral direction, but as can be seen by the length of the vectors representing these units (Fig. 3.4A), they tended to be less strongly selective for the direction of tracking.

The distribution of best directions measured from the 44 units in the right flocculus of monkey O (Fig. 3.4C and D) was a mirror image of the best directions observed in the left flocculus (Fig. 3.4A and B). Once again, the best directions of the population clustered around two primary directions. Horizontal P-cells (best directions: 60 to 120°) preferred eye movements directed rightward, i.e., ipsilaterally. Vertical P-cells (best directions: 150 to 210°) preferred eye movements directed downward and slightly contralateral. The average best direction for the horizontal P-cells was 90.33° (SD = 12.42) and the average best direction for the vertical P-cells was 185.24° (SD = 10.74).

To confirm that the oblique preferred axes for the vertical P-cells shown in Figs. 3.4A to D was a general phenomenon and not an idiosyncratic feature of monkey O, we recorded from 11 vertical P-cells in a second monkey. The distribution of best directions measured from P-cells recorded in both flocculi of monkey U are shown in Fig. 3.4E-F. In combining data obtained from the two sides, we have presented the data obtained from P-cells in the right flocculus as though were from the left flocculus. For units recorded in the right flocculus, we rotated the best directions 180° around the vertical axis, so that the best directions shown in Fig. 3.4E represent the mirror images of their actual best directions. The distribution of best directions were also clustered around a best direction (mean $\pm$ SD = 173.80 $\pm$ 13.87°) that was slightly contralateral of exactly down.

We next assessed whether the best direction associated with our population of vertical P-cells was significantly different than exactly down or 180°. We pooled all of the best directions from all four flocculi, adjusting the data obtained from the right flocculi, as described above, to make them comparable with data obtained from the left flocculi. Calculation of the t value for the population of 63 vertical P-cells indicated that the mean best direction (172.52°) was significantly different from exactly down ($p<0.001$). Calculation of separate t values for data obtained from each individual flocculus indicated a significant difference in one case (left flocculus of monkey O, $p < 0.001$), but not in the other cases.

Directional preferences of P-cells during step-ramp tracking

To distinguish between the preferred directions of the eye velocity and visual signals on floccular P-cells, we recorded the activity of 52 P-cells during pursuit of targets that started from rest and then moved at a constant velocity, the step-ramp target motion introduced by Rashbass (1961). Fig. 3.5 shows

how we used this target motion to separately measure visual- and eye velocity-related simple-spike responses. The bottom two traces in Fig. 3.5 show the target position and the monkey's eye position as a function of time. Initially, the monkey fixated a stationary spot, indicated by the dashed line, as an eccentric target spot appeared at an unpredictable time. When the fixation spot was extinguished, the eccentric target spot moved at a constant speed of 30 °/s. After a latency of approximately 80 ms, the monkey's eye velocity increased smoothly and matched the velocity of the target. As indicated by the trace in the middle of Fig. 3.5, the average simple-spike firing rate that accompanied this behavior consisted of a transient overshoot in firing rate, followed by a lesser sustained increase in firing rate. It has been previously demonstrated (Stone and Lisberger 1990) that the transient overshoot is related to the visual motion caused by the onset of target motion, while the sustained increase is related to steady-state eye velocity.

We dissociated the transient visual response from the sustained eye velocity response by assuming that the modulation in firing rate observed during steady-state tracking was due only to eye velocity. The sensitivity to eye velocity of the P-cell was calculated by dividing the average change in firing rate during steady-state pursuit (450 to 750 ms after target motion onset, shown by the two arrows in Fig. 3.5) by the average eye velocity over this same interval. The sensitivity to eye velocity of the P-cell shown in Fig. 3.5 was 1.23 spikes/sec per deg/sec. We then estimated the component of the P-cell firing rate driven by eye velocity by multiplying eye velocity by the sensitivity to eye velocity on a millisecond time scale over the entire trial. This produced an estimate of the "eye velocity component" of the simple-spike firing rate, shown superimposed on the simple-spike firing rate trace in Fig. 3.5. Separate eye velocity components and sensitivities to eye velocity

were calculated for each of the twelve directions of tracking. The difference between the actual firing rate and the estimated eye velocity component represents the estimated visual component of simple-spike firing rate, shown by the trace at the top of Fig. 3.5. The sensitivity to visual motion of the P-cell was calculated by measuring the average firing rate attributed to the visual component over a 100 ms interval beginning with the onset of the eye movement (indicated by the dashed vertical lines), and then dividing the average firing rate by the speed of the image motion. The visual sensitivity of this P-cell was 2.87 spikes/sec per °/sec.

For each P-cell, we recorded the simple-spike firing rate during tracking of step-ramp targets moving in 12 different directions and calculated the eye velocity and visual components for each direction. The presentation of each target was identical to that shown in Fig. 3.5, except that the direction of the target motion was randomly selected from a set of directions spaced at 30° intervals. In each case, the target started from a position slightly offset from straight-ahead gaze and moved at 30 °/s toward an eccentric location that corresponded to one of the twelve hour locations on the face of a clock. The estimated eye velocity and visual components for all twelve directions from one vertical P-cell are shown in Fig. 3.6. In each pair of superimposed traces, the smoother trace represents the estimated eye velocity component and the noisier trace represents the estimated visual component. The arrow to the left of each pair of traces indicates the direction of the target motion that elicited the responses. Summing each pair of components would reconstitute the simple-spike firing rate recorded during pursuit in that direction. Comparison of the paired traces indicated that the estimated eye velocity and visual components changed in unison for pursuit in different directions. For this P-cell, the firing rate related to both components was increased during

downward tracking and decreased below the baseline firing rate during upward tracking. During horizontal pursuit, both the visual and eye velocity components of the response showed a preference for rightward pursuit. To construct tuning curves for each P-cell, we quantified the amplitude of the eye velocity and visual components of the firing rate for each direction of tracking. The amplitude of the eye velocity component was determined by measuring the average firing rate of the estimated eye velocity component during steady-state pursuit (450 to 750 ms). The amplitude of the visual component was determined by measuring the average firing rate of the estimated visual component during the first 100 ms of the initiation of pursuit.

The amplitudes of the eye velocity and visual components changed smoothly as a function of direction and were summarized with polar plots like that shown at the bottom of Fig. 3.6. Each open square represents the end-point of a vector. The length of the vector shows the magnitude of the eye velocity (left plot) or visual (right plot) component and the direction of the vector indicates the direction of tracking. We fitted these data with a Gaussian function to obtain the smooth curve superimposed on the data, just as was done with the sinusoidal data (Fig. 3.3C). The eye velocity and visual components had similar best directions, as indicated by the single arrow in each plot, and both best directions were slightly contralateral of exactly down (eye velocity: 163.70, visual: 159.80). The directional tuning for both components was very broad: the half-maximum bandwidths were 211.72 and 165.17, respectively.

For the population of P-cells, the best directions for both the eye velocity (Fig. 3.7A) and visual (Fig. 3.7B) components of the response were clustered around the same two primary directions that were observed in the

data obtained from sinusoidal tracking. Each line in Figs. 3.7A and C is a vector indicating the best direction of either the eye velocity (Fig. 3.7A) or visual (Fig. 3.7C) component of the response from one P-cell. The lengths of the lines are proportional to the directionality index obtained from each tuning curve. Figs. 3.7 B and D show the same data in histogram format. The data were obtained from recordings in both flocculi of monkey O. In combining data obtained from the two sides, we have presented the data obtained from P-cells in the right flocculus as though were from the left flocculus. For units recorded in the right flocculus, we rotated the best directions 180° around the vertical axis, so that the best directions shown in Fig. 3.7 represent the mirror images of their actual best directions. As we did for the data obtained during sinusoidal pursuit (Fig. 3.4), we categorized the eye velocity and visual responses for each P-cell as either horizontal (preferred direction: 225 to 315°) or vertical (preferred direction: 135 to 225°). For the eye velocity component of the response, the average preferred direction was 274.30° (SD = 14.54) for the horizontal P-cells and 166.53° (SD = 20.72) for the vertical P-cells. For the visual component of the response, the average preferred directions were 269.69° (SD = 12.90) and 165.52° (SD = 19.85), for the horizontal and vertical P-cells, respectively.

Although the best directions for the eye velocity and visual components were similar on average in our sample, they were not tightly correlated on single P-cells. The graph in Fig. 3.8A plots the best directions determined for the visual component as a function of the best directions for the eye velocity component. To convey a sense of how strongly each unit was tuned for direction, the P-cells are represented by different symbols according to their directionality index. Units with a DI for the eye velocity component above 0.5 are shown with open circles, units with a DI for both components

above 0.5 are shown with closed circles, and the one unit with both below 0.5 is shown with an open triangle. The best directions tend to covary, but are not very well described by linear regression, as shown by the scatter of points around the dashed line (slope: 0.83, y intercept: 19.69, SE: 58.08). For comparison, we also plotted the best directions determined from data obtained with sinusoidal tracking as a function of the best directions of the eye velocity component from step-ramp trials. As shown in Fig. 3.8B, these data cluster more tightly along the regression line (slope: 0.865, y intercept: 23.23, SE: 17.20).

Tuning functions of P-cells

As shown by the graphs in Fig. 3.9, the shapes of the tuning functions were generally uniform across our population of P-cells. The histograms in the left half of Fig. 3.9 show the distribution of values from the directionality index (DI = 1 - worst/best). All three distributions were unimodal and centered between 0.5 and 1.0, indicating that both the eye velocity and visual signals recorded from our sample of P-cells were strongly tuned for motion along their preferred axes. For the data obtained during sinusoidal pursuit (upper left graph), the distribution had a mean value of 0.73 (SD = 0.20), but was skewed toward a value of 1.0. As seen in the data obtained from step-ramp trials, the eye velocity components (middle graph) were more strongly tuned for direction than the corresponding visual components (lower graph). The mean directionality index for the estimated eye velocity component was 0.71 (SD = 0.27); the mean value for the visual component was 0.51 (SD = 0.22).

The histograms in the right half of Fig. 3.9 show the distribution of half maximum bandwidths. The distributions were each centered near 180°, indicating that in most cases the tuning properties of individual P-cells could

be well-described by a cosine or sine function. For the functions fit to data from sinusoidal pursuit, the distribution of half-maximum bandwidths showed a peak just above 180° (mean ± SD = 184.13° ± 60.74). The visual components measured from step-ramp trials (mean ± SD =166.90°±59.85) tended to be more narrowly tuned than the eye velocity components (mean ± SD =181.50°±54.97). The peak in the histogram at 360° includes 9 P-cells which showed little directional tuning and which were not included in the calculation of average values.

Preferred directions of P-cells during tracking about different eye positions

If the directional tuning of P-cells is determined by the pulling directions of the extraocular muscles, the preferred directions should change when the eye is rotated in the orbit so that the pulling directions of the extraocular muscles are changed. For 9 P-cells, we therefore assessed the effect of eye position on the preferred direction for sinusoidal tracking. In these experiments, the monkey tracked a target that moved ± 5 degrees sinusoidally at 0.5 Hz, either horizontally or vertically. In four separate conditions, the sinusoidal target motion was offset so that the monkey's mean eye position was shifted away from straight ahead gaze into each of the four quadrants. We found that the modulation of simple-spike firing rate could be influenced by the monkey's eye position, but different P-cells showed different effects. Fig. 3.10 shows data from one P-cell whose simple-spike firing rate during sinusoidal pursuit was strongly effected by eye position. The pairs of traces in Fig. 3.10A show the average firing rate recorded during horizontal (hor) and vertical (ver) tracking. The traces are aligned on the dashed vertical line, which indicates peak downward and leftward eye velocity. The mean offset of eye position away from straight-ahead gaze is indicated in x and y coordinates by the numbers above each pair of traces.

When the mean eye position was located in the right quadrant, either above (+15, +10) or below (+15,-10) the horizontal meridian, the simple-spike firing rate increased during rightward tracking. When the mean eye position was located in the left quadrant (-15,+10 and -15,-10), the simple-spike firing rate increased during leftward tracking. Smaller changes in simple-spike firing rate also occurred during vertical tracking in different quadrants. These changes in firing rate observed for the P-cell shown in Fig. 3.10A are summarized by the diagram in Fig. 3.10B. Each arrow depicts a vector that describes the sensitivity to eye velocity during tracking in one quadrant. The x and y components of each vector were determined from the values of the sensitivity to eye velocity during horizontal and vertical tracking, respectively. The position each vector's tail indicates the mean position of the eye during tracking.

To allow comparison with data obtained from other P-cells, we transformed the vector plot shown in Fig. 3.10B into a pair of plots like those shown in Figs. 3.10C and D. For each of the four vectors placed in eccentric quadrants in Fig. 3.10B, we measured how the amplitude and the direction of the vectors describing the sensitivity to eye velocity changed relative to the vector placed at straight-ahead gaze. Fig. 3.10C plots the changes in amplitude of the four eccentric vectors and Fig. 10D plots the changes in the directions of the vectors. The data points in Fig. 10C all have a value greater than zero, indicating that the sensitivity to eye velocity was larger at all four eccentric positions than it was at straight ahead gaze. The data points in Fig. 3.10D are positive for leftward mean eye positions (-15,+10 and -15,-10), but are negative for rightward mean eye positions (+15,-10 and +15,+10). These data points indicate that the vectors in the left half of Fig. 3.10B were rotated clockwise,

while the vectors in the right half were rotated counterclockwise, relative to the vector placed at straight-ahead gaze.

The two graphs in Fig. 3.11 show data obtained in the same way from all 9 P-cells. Some of the P-cells showed a pattern of change in their sensitivity to eye velocity that was similar to that displayed by the unit shown in Fig. 3.11. However, at least one P-cell showed the converse pattern of change. Also, the changes in sensitivity to eye velocity did not conform to a prediction based on consideration of how the pulling directions of the extraocular muscles change with changes in eye position. For example, the dashed lines in Fig. 3.11 show how the amplitude and the direction of the activation of the contralateral superior oblique muscle would change for the four eccentric eye positions used in this experiment (based on data from Robinson 1975). Since the preferred directions of the vertical P-cells are most closely aligned with the pulling direction of this muscle, it might be expected that changes in the sensitivity to eye velocity of vertical P-cells would be yoked to the kinematic constraints of this muscle. However, the data shown in Fig. 3.11 do not confirm this prediction.

Directional tuning of oculomotor mossy fibers

We also recorded from 45 mossy fibers that discharged in relation to pursuit eye movements. These included 26 mossy fibers whose discharge was virtually a neural analog of eye position and 19 mossy fibers whose discharge reflected a combination of eye position and eye velocity signals. Mossy fibers which primarily encode eye position or eye velocity may represent two distinct populations of afferents to the flocculus (Stone and Lisberger 1989). However, the two types of mossy fibers showed nearly identical properties with respect to directional tuning and we present them as a single population. For the majority of units (n = 35), we assessed directional tuning by recording

from the isolate mossy fiber during sinusoidal pursuit, using the same methodology as shown for the P-cell in Fig. 3.3. For 10 units, we obtained data about directional tuning by recording during the performance of step-ramp trials, like that shown in Fig. 3.5. When data from step-ramp trials was used, we measured only the firing rate during the steady-state portion of the trial, as was done to compute the eye velocity component of the response of P-cells.

In contrast to the best directions observed in our sample of P-cells, the preferred directions of mossy fibers were clustered around four cardinal directions. Each line in Fig. 3.12A shows the best direction of one mossy fiber, using the same vector description as presented in Figs. 3.4 and 3.7. We divided the population of mossy fibers into four classes, as shown by the histogram in Fig. 3.12B. The average best directions of the four classes were 6.76^{o} (SD = 4.98), 94.71^{o} (SD = 5.79), 179.51^{o} (SD = 8.59), and 272.75^{o} (SD = 6.53), for the up (n = 7), right (n = 12), down (n = 13), and left (n = 13) mfs, respectively.

Mossy fibers tended to be more selective for eye movements in their preferred direction than P-cells. As shown by the histogram in Fig. 3.13A, the distribution of directionality indices for the population of mossy fibers had a peak near 1.0 (mean $\pm$ SD = 0.93 $\pm$ 0.12). The peak in the histogram near 1.0 reflects the fact that the majority of mossy fibers were often completely suppressed during tracking in the non-preferred direction. Mossy fibers also tended to have tuning functions that were about 40^{o} more narrow than those measured for P-cells. The mean half maximum bandwidth for the population of mossy fibers was 140.19^{o} (SD = 34.71).

Discussion

We have recorded from floccular Purkinje cells to determine the spatial organization of the eye velocity and visual signals conveyed by the flocculus. By observing the modulation in simple-spike firing rate during sinusoidal tracking along different axes in the frontal plane, we determined how the firing rate of each P-cell varied as a function of eye movement direction. In addition, by using step-ramp target motions, we were able to distinguish between the directional tuning of the eye velocity and visual motion components of simple-spike firing. Our results show that both the eye velocity and visual tuning of floccular Purkinje cells in the primate are consistent with the reference frame defined by primary vestibular pathways in the brainstem.

The coordinate system defined by floccular Purkinje cells

The vectors defined by the eye velocity and visual signals of floccular Purkinje cells are compatible with a coordinate system based on either the planes of motion detected by the semicircular canals or the pulling directions of the extraocular muscles. Our population of P-cells fell into two distinct classes: horizontal cells which preferred eye movements directed toward the ipsilateral side and vertical cells which preferred eye movements directed downward. The two classes of P-cells have been observed by several previous investigators (Miles et al. 1980, Stone and Lisberger 1990), but our results show that the signals conveyed by these two classes of P-cells are not exactly horizontal and vertical. In particular, both the eye velocity and visual signals on vertical P-cells are rotated approximately 10° toward the contralateral side. The four polar plots in Fig. 3.14 compare the preferred directions of the P-cells

observed in the present study (upper plots) with the preferred directions of head motion detected by the ipsilateral semicircular canals (lower left) and with the pulling directions of the extraocular muscles (lower right). The directions shown for the semicircular canals and extraocular muscles are based upon the data of Simpson et al. (1986a,b). For vertical P-cells, the slight rotation of the preferred directions away from vertical means that the output signals are aligned both with the plane of motion detected by the ipsilateral anterior canals (Fig. 3.14, lower left) and with the pulling directions of the ipsilateral inferior rectus and the contralateral superior oblique (Fig. 3.14, lower right). The signals conveyed by the horizontal P-cells are aligned with both the ipsilateral horizontal canal and with the ipsilateral lateral rectus and the contralateral medial rectus.

The vectors defined by the output of the flocculus imply that a transformation must occur either in the projections to the flocculus or in the flocculus itself, because the eye velocity and visual motion inputs to the flocculus do not share this spatial organization. Neurons in the two pathways which may provide visual inputs to the flocculus are directionally selective, but do not have biases for the directions shown by floccular P-cells. One possible source of visual inputs to the flocculus, the dorsolateral portion of the pontine nuclei, contains a population of neurons in which all directions of motion are represented (Suzuki and Keller 1984, Mustari et al. 1988, Thier et al. 1988). These neurons are likely candidates for providing the visual inputs used for pursuit, because they receive visual inputs from areas of cortex known to be important for processing of visual motion (Brodal 1978; Glickstein et al. 1972, 1980, 1985), respond well to the small visual stimuli that are important for pursuit (Suzuki and Keller 1984, Mustari et al. 1988, Thier et al. 1988), and project directly to the portions of the flocculus in which we

recorded (Brodal 1979, 1982; Langer et al. 1985). A second possible source of visual inputs are the nuclei of the accessory optic system. A minority of neurons in these nuclei also respond well to the small moving stimuli that are effective in eliciting smooth pursuit (Westheimer and Blair 1974; Hoffman et al. 1988; Hoffman and Distler 1989; Mustari and Fuchs 1989, 1990) and may provide inputs to the flocculus through projections to the nucleus reticularis tegmenti pontis (Brodal 1980b, Brodal 1982), which also receives direct cortical inputs (Brodal 1980a). A similar transformation is required of the eye movement inputs to the flocculus, since the best directions for our sample of oculomotor mossy fibers were clustered around the four cardinal directions -- up, down, left and right. Previous studies of the oculomotor mossy fibers in the flocculus have also found all four cardinal directions represented (Lisberger and Fuchs 1978b, Miles et al. 1980, Stone and Lisberger 1989). A major function of the flocculus may be to convert these visual motion and eye velocity inputs into a format that is compatible with the reference frame defined by the floccular targets.

Comparison of the spatial organization of the primate flocculus with that observed in non-primates

The functional organization of our population of P-cells is consistent with the organization observed in the flocculus of the rabbit and cat. In the rabbit and cat, the flocculus inhibits pathways associated with the ipsilateral and anterior canals, but does not directly influence pathways related to the ipsilateral posterior canal (Ito et al. 1977, Baker et al. 1972, Hirai and Uchino 1984). Consistent with these results, we did not observe a population of P-cells whose output would be aligned with the ipsilateral posterior canal. We did record from a small number of vertical P-cells with visual or eye velocity signals that preferred upward motion, but they were much less selective for

direction than the larger population of P-cells that preferred downward eye movements.

In the cat and the rabbit, the flocculus is organized as a set of distinct zones, each of which is matched to one component of the reference frame defined by the semicircular canals. The directional tuning of the horizontal and vertical P-cells we have studied are consistent with a zonal organization, but because we did not reconstruct the exact location of our recording sites, we cannot provide direct evidence for such an organization. It is likely that most of our recording sites were located in the rostral folia of the flocculus, folia which are more correctly referred to as part of the ventral paraflocculus (Voogd et al. 1987, Gerrits and Voogd 1989). This suggests that a common spatial organization may be present throughout the floccular complex, including the caudal folia of the flocculus proper and the more rostral folia located in the ventral paraflocculus. At least in the cat and rabbit, these two regions share inputs from the vestibular nuclei and the dorsal cap of Kooy, but the ventral paraflocculus receives a visual projection from the pontine nuclei that the flocculus does not (Gerrits and Voogd 1989). The common pattern of organization may therefore reflect the effect of the shared inputs. In particular, since the termination pattern of the climbing fibers coincides with the delineation of floccular zones, it is possible that the identity of zones in the flocculus is determined by the climbing fiber inputs.

Functional aspects of floccular organization in the primate

The flocculus of the primate plays a critical role in generating smooth pursuit eye movements, an eye movement behavior that is absent or poorly developed in non-primates. Both the eye velocity and visual signals observed on floccular P-cells are important for the control of pursuit. The eye velocity signals on P-cells are believed to encode a motor corollary signal used

to sustain eye velocity during pursuit (Lisberger and Fuchs 1978a, Miles et al. 1980, Stone and Lisberger 1990). This signal may reflect the activity of a feedback loop formed by projections from the flocculus to the vestibular nuclei and projections to the flocculus from the vestibular nuclei and the nucleus prepositus (Langer et al. 1985a,b; Broussard and McCrea). The motor corollary activity mediated by these pathways is believed to sustain eye velocity during pursuit. The visual signals conveyed by the flocculus represent commands for eye acceleration during pursuit. By changing the simple-spike firing rate of floccular P-cells, visual inputs can modulate the level of activity in the feedback loop and thereby produce changes in pursuit eye velocity.

Our data indicate that the feedback loop formed by the flocculus is organized into horizontal and vertical channels. For pursuit eye movements in the horizontal plane, the direction and amplitude of pursuit eye velocity should depend upon the balance of activity between the populations of horizontal P-cells in the two flocculi. At present, it is unclear how the balance of activity in the two populations is coordinated, although the mirror symmetry observed in the directional tuning suggests the two flocculi may operate in a push-pull fashion. Further information about the connections of the central vestibular neurons to which the flocculus projects is needed to clarify this issue. Visual inputs to the flocculus, conveyed primarily by descending cortical projections through the pontine nuclei (Brodal 1978; Glickstein et al. 1972, 1980, 1985), can be viewed as signals which cause accelerations of the eye by shifting this balance of activity. It is also possible that non-visual signals from cortex may play a role in regulating the activity in these neural circuits, since extra-retinal signals have been recorded in the cortical areas that provide these inputs. The directional asymmetries in

pursuit observed after some cortical lesions (Dursteler et al. 1987) could be caused by disrupting the balance influenced by these cortical inputs.

For pursuit eye movements in the vertical plane, the command for eye velocity provided by the flocculus is asymmetric, since the populations of vertical P-cells on both sides encode downward eye movements. The functional implications of this asymmetry are unclear. It has been observed in behavioral experiments that the average acceleration of the eye over the first 100 ms of the initiation of vertical pursuit is lower than that produced during horizontal pursuit of the same target motion (Lisberger and Pavelko 1989). It is possible that these lower eye accelerations during vertical pursuit are due to the absence of P-cells encoding upward eye velocity. Since eye velocities in the preferred direction can excite P-cells over a larger range of firing rates than eye velocities in the non-preferred direction can inhibit P-cells, the dynamic range of eye velocities encoded in each flocculus is biased. For horizontal pursuit, the biased encoding provided by the horizontal P-cells in one flocculus is complemented by the horizontal P-cells in the other flocculus. For vertical pursuit, P-cells from the two sides have the same bias. The narrower dynamic range provided by the pooled output of vertical P-cells from the two sides may restrict the range of eye accelerations generated during vertical pursuit. This line of reasoning would also suggest that eye accelerations during downward pursuit should be larger than those during upward pursuit.

The absence of a signal encoding upward eye velocity might seem to imply that the outputs from the flocculus are insufficient to properly encode eye velocity for pursuit. However, because floccular P-cells have very broad tuning curves and because the best directions for the two populations of P-cells are nearly orthogonal, the encoding of eye velocity by the flocculus is

both efficient and complete. The graphs in Fig. 3.15 show schematically how the choice of preferred directions and tuning curves affects the encoding of eye movements. The plots in the upper row (A to D) show four possible pairs of tuning curves. Each tuning curve shows how activity in one channel would change as a function of the direction of eye movement. The four graphs in the bottom row (E to H) display for each pair of tuning curves the hypothetical activity in one channel plotted against the activity in the second channel. If one considers an eye movement vector sweeping around the clock in each graph in the upper row, the rotation of the vector can be described by the paths shown by the functions plotted in the graphs in the lower row. If the vector is pointing straight up and then rotated clockwise, it moves along the paths through the points labeled upward (U), rightward (R), downward (D), leftward (L) and back to upward. If the output of the two channels is to provide a robust encoding of eye velocity, each direction should be mapped to a unique point. To minimize ambiguity, the points should also be as distant from each other as possible. For optimal encoding with two channels, the plots of activity should therefore describe a circle, a situation which occurs when the two channels are exactly orthogonal to each other and diplay cosine tuning functions. If the two channels are not orthogonal to each other (B and F, C and G), or if the tuning functions are more narrowly tuned (D and H), very different directions may be encoded by similar ratios of activity in the two channels. The encoding of eye velocity and visual signals by the flocculus is very close to matching this description, deviating only enough from orthogonality so that the preferred direction of the vertical channel matches the spatial axis of the posterior semicircular canal.

Figure 3.1 Identification of a typical horizontal gaze velocity P-cell. A: Average simple-spike firing rate of a horizontal P-cell during sinusoidal pursuit eye movements. Vertical dashed line indicates peak leftward eye velocity. Target moved sinusoidally ±10 at 0.5 Hz. B: Average simple-spike firing rate during cancellation of the vestibulo-ocular reflex. Vertical dashed line indicates peak leftward head velocity. Target and chair moved together ±10 at 0.5 Hz. In both A and B, a single cycle is repeated twice for clarity.

Fig. 3.1

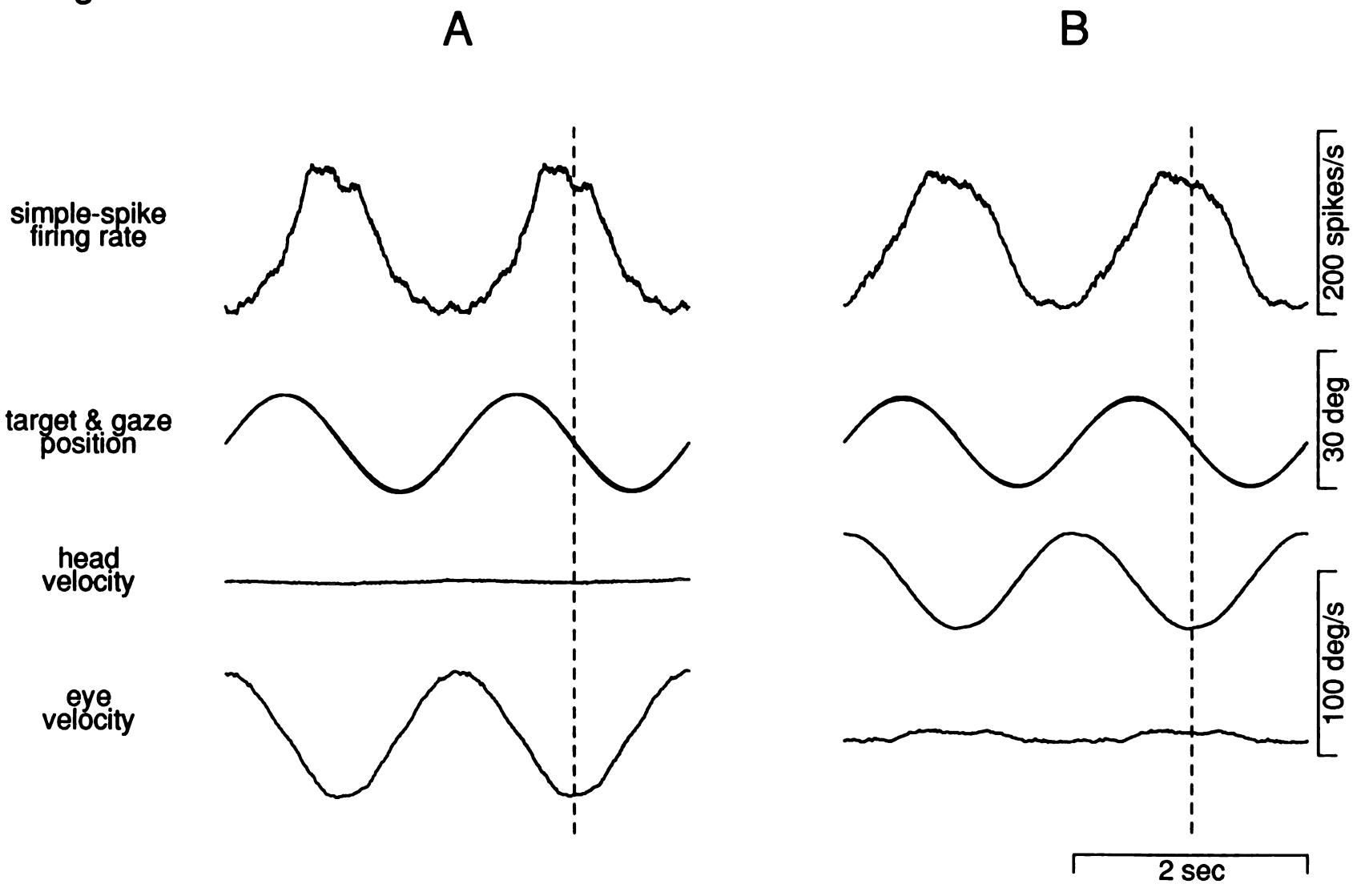
A
B
simple-spike firing rate
target & gaze position
head velocity
eye velocity
200 spikes/s
30 deg
100 deg/s
2 sec

Figure 3.2 Sensitivities to eye and head velocity. A: Graph plotting the sensitivity to head velocity as a function of sensitivity to eye velocity for our population of horizontal P-cells. Each open square represents a pair of measurements made from data for one P-cell. The dashed line indicates a slope of one. B: Histogram showing the distribution of sensitivities to eye velocity for our population of vertical P-cells.

Fig. 3.2

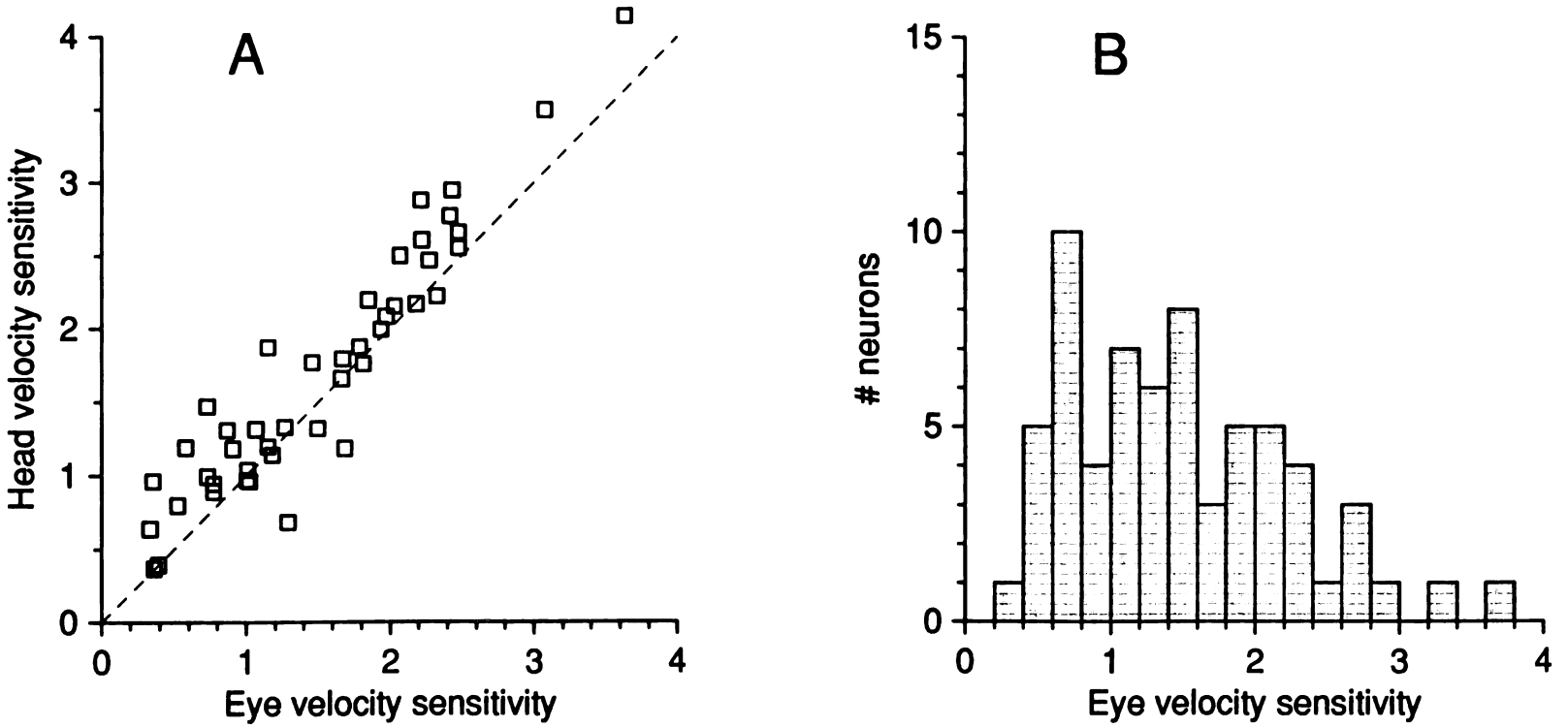
A
Head velocity sensitivity
Eye velocity sensitivity
0
1
2
3
4
B
neurons
Eye velocity sensitivity
0
5
10
15

Figure 3.3 Directional tuning measured during sinusoidal pursuit. A: Averages of simple-spike firing rate recorded from one P-cell during sinusoidal pursuit along six different axes. The axis of motion in each case is indicated by the arrow to the left of the trace. The traces are aligned with the dashed vertical lines. In the upper half of A, the left and dashed line indicates peak rightward and upward eye velocity, and the right dashed line indicates peak leftward and downward eye velocity. In the lower half, the left line indicates peak leftward and upward eye velocity, and the right line indicates peak rightward and downward velocity. B: Polar plot showing the amplitude of modulation of simple-spike firing rate during different directions of sinusoidal pursuit. Open squares indicate the dc offset of simple-spike firing rate. Filled circles indicate the amplitude of modulation of simple-spike firing rate. C: Polar plot showing amplitude of modulation as in B, with tuning curve superimposed. The arrow indicates the best direction for this P-cell, given by the maximum of the tuning function.

Fig. 3.3

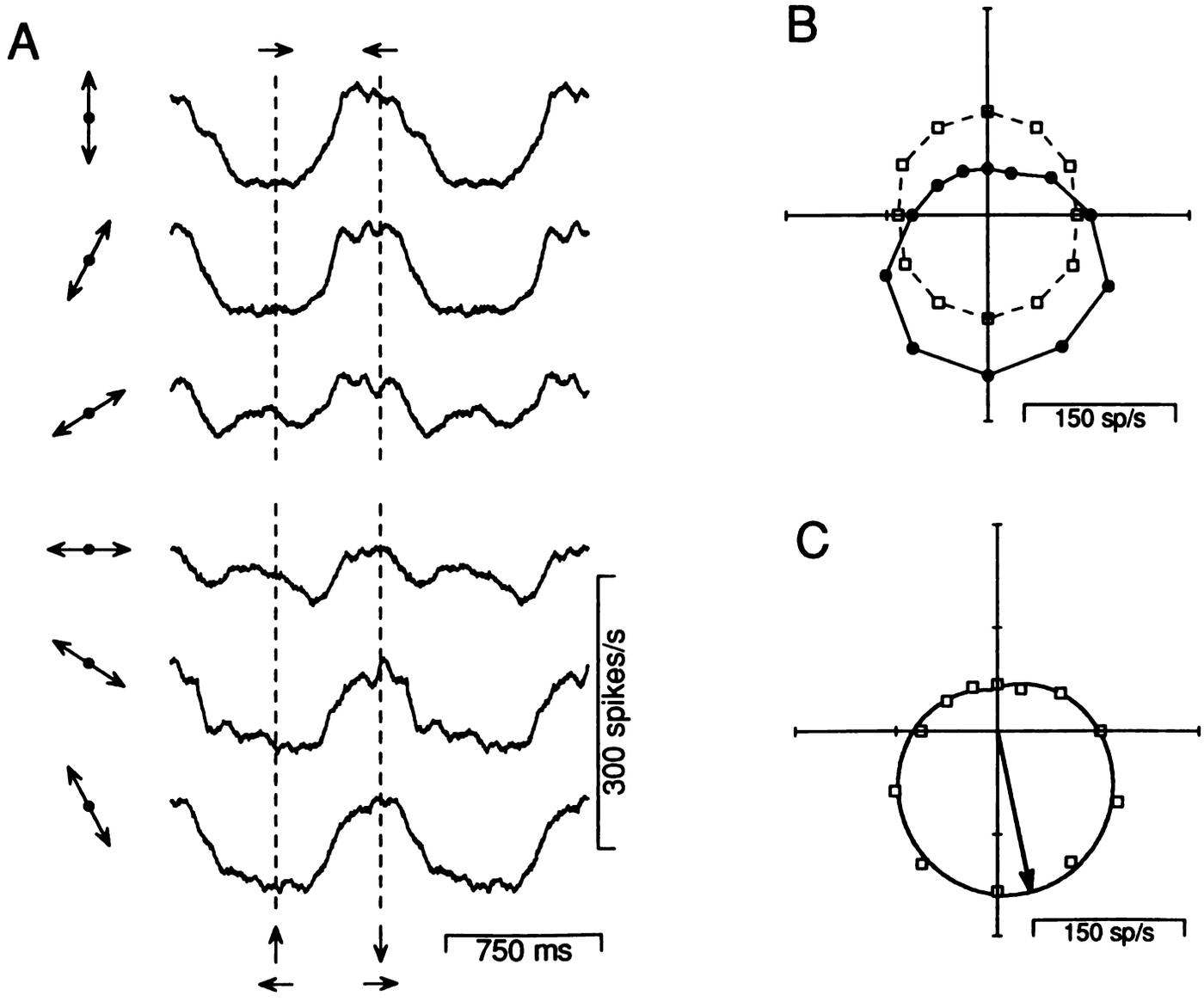

Figure 3.4 Distribution of best directions for P-cells measured during sinusoidal pursuit. A, C, E: Polar plots showing distribution of best directions. Each line represents a vector pointing in the best direction of one P-cell. The length of each line is proportional to the directionality index (DI = 1 - worst/best). B, D, F: Histograms showing the distribution of best directions for the same data as shown in A, C and E. A-B: Data obtained from the sample of P-cells in the left flocculus of monkey O. C-D: Data obtained from the right flocculus of monkey O. E-F: Data obtained from the flocculi of a second monkey.

Fig. 3.4

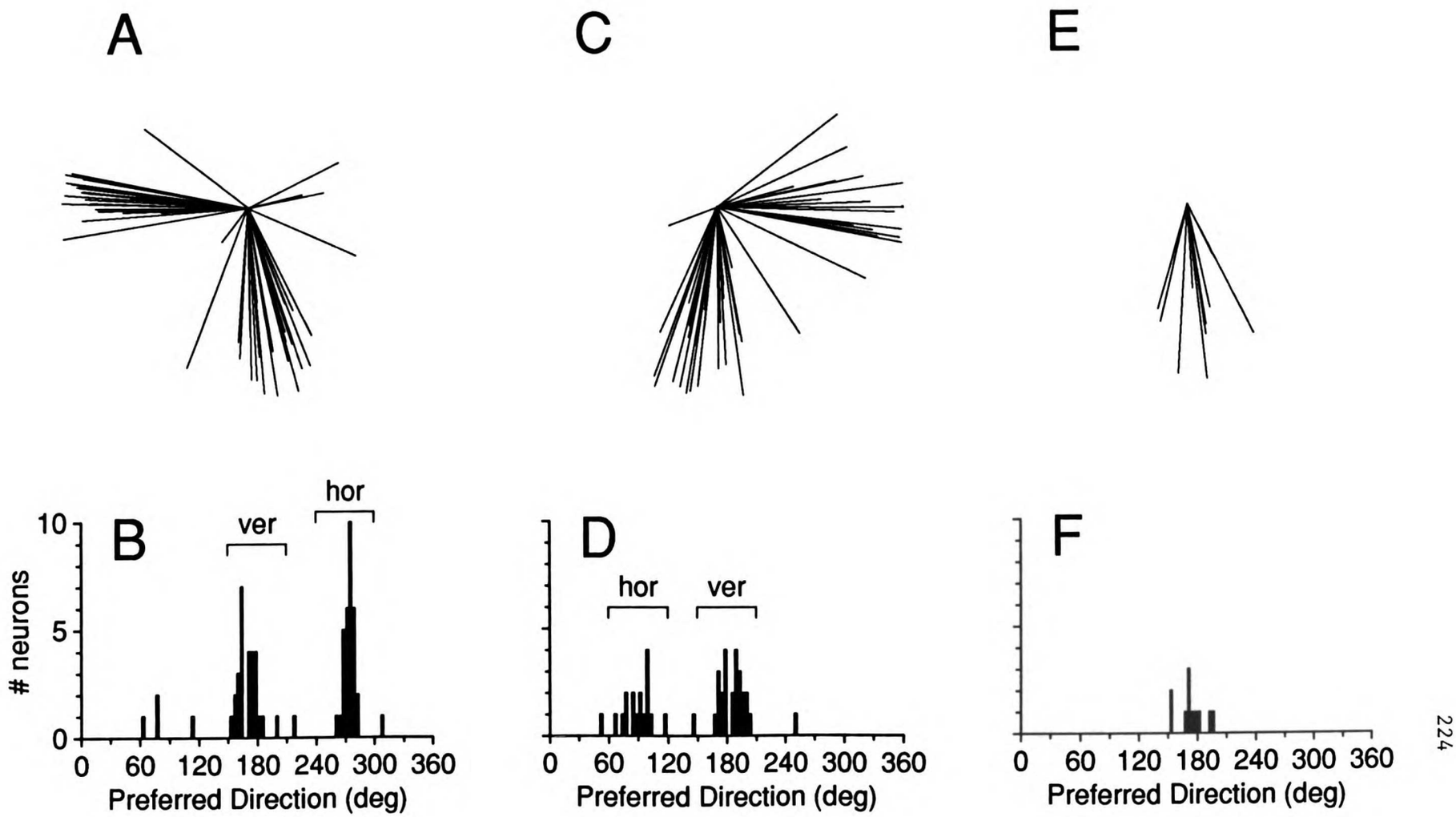
A
C
E
B
ver
hor
10
5
0
neurons
0 60 120 180 240 300 360
Preferred Direction (deg)
D
hor
ver
0 60 120 180 240 300 360
Preferred Direction (deg)
F
0 60 120 180 240 300 360
Preferred Direction (deg)

Figure 3.5 Step-ramp trial used to dissociate eye velocity and visual components of simple-spike firing rate. Lowest traces show target and eye position as a function of time. Dashed line indicates position of stationary LED used as fixation target at the beginning of trial. Eye velocity trace shows average from approximately 20 presentations of the constant velocity motion of the target, aligned on the onset of target motion. Arrows are placed at 450 and 750 ms after the onset of target motion, and demarcate the interval used to calculate the sensitivity to eye velocity. The horizontal dashed line superimposed on trace representing the visual component indicates 0 spikes/s. The two vertical dashed lines indicate 100 and 200 ms after the onset of target motion, the interval used to calculate the sensitivity to visual motion.

Fig. 3.5

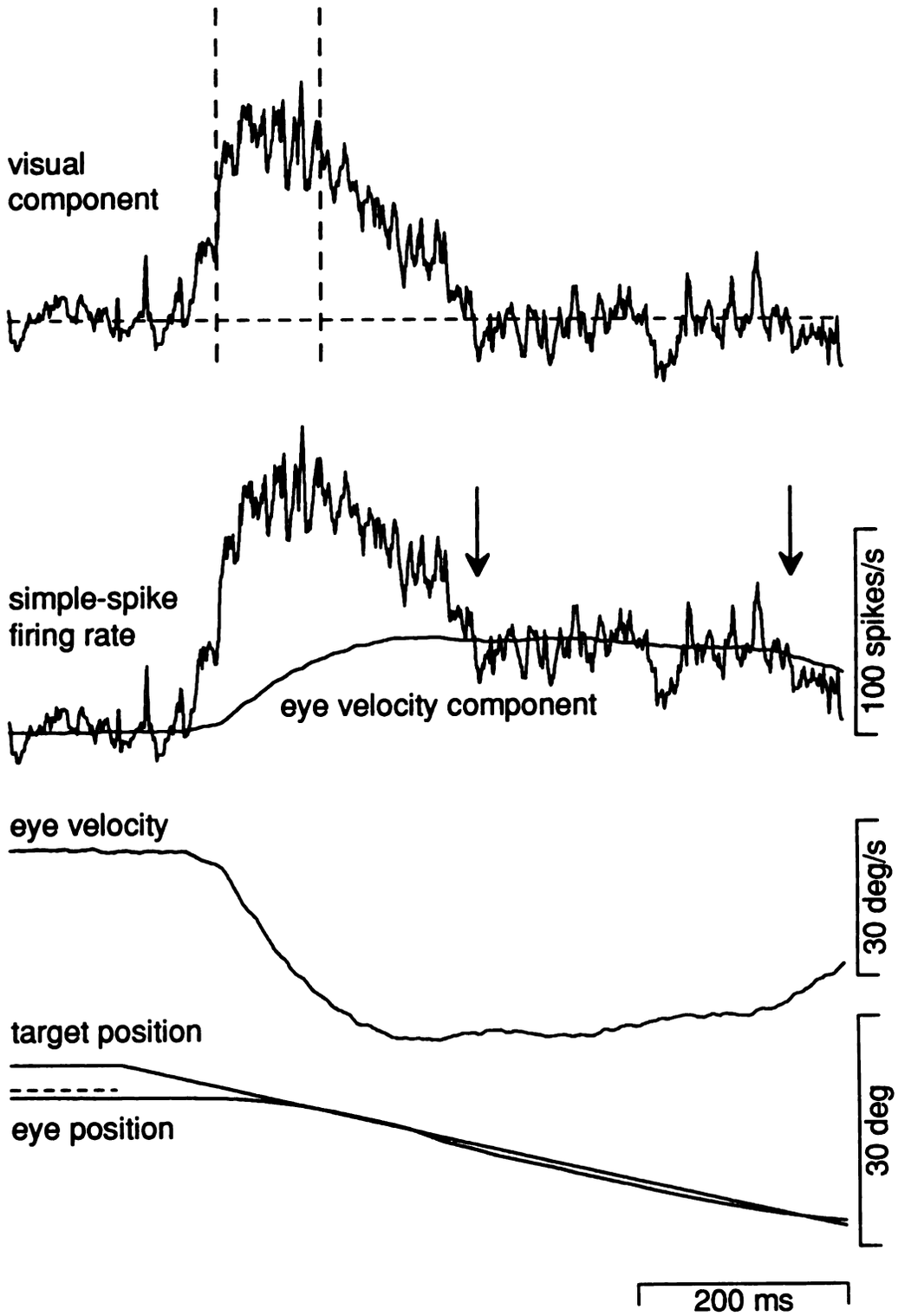
visual
component
simple-spike
firing rate
eye velocity component
100 spikes/s
eye velocity
30 deg/s
target position
eye position
30 deg
200 ms

Figure 3.6 Directional tuning of eye velocity and visual components. Each pair of traces shows the eye velocity component (smooth trace) and the visual component (noisier trace) of simple-spike firing rate calculated for one P-cell for pursuit of a step-ramp target motion in one direction. The direction that elicited each pair of components is indicated by the arrow to the left of each pair. The polar plots at the bottom of the figure show estimates of the amplitudes of the eye velocity component (left) and the visual component (right) as a function of the direction of motion. Each open square represents a measurement made from one step-ramp trial. The continuous functions superimposed on the graphs show the tuning curves fitted to the data. The arrow in each polar plot indicates the direction corresponding to the maximum value of the tuning curve.

Fig. 3.6

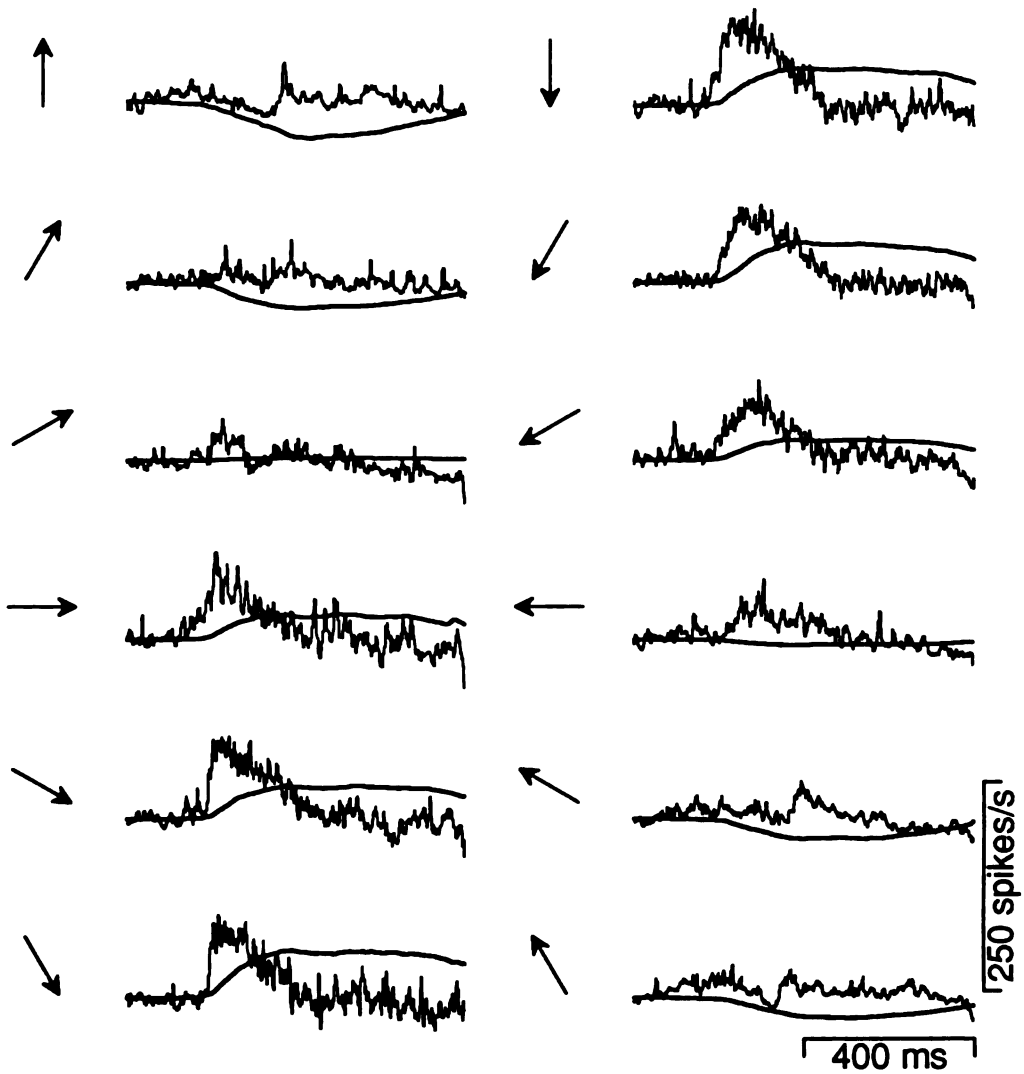

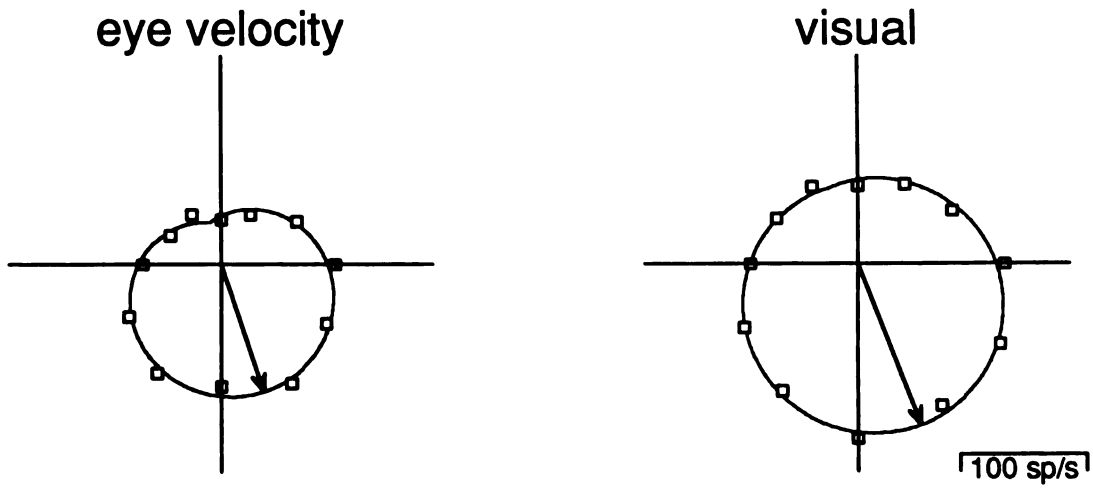

Figure 3.7 Distribution of best directions for the eye velocity and visual components. A, C: Polar plots showing distribution of best directions for eye velocity (A) and visual components (C). Each line represents a vector pointing in the best direction of one P-cell. The length of each line is proportional to the directionality index (DI = 1 - worst/best). B, D: Histograms showing the distribution of best directions for the eye velocity (B) and visual (D) components, using the same data as shown in A and C.

Fig. 3.7

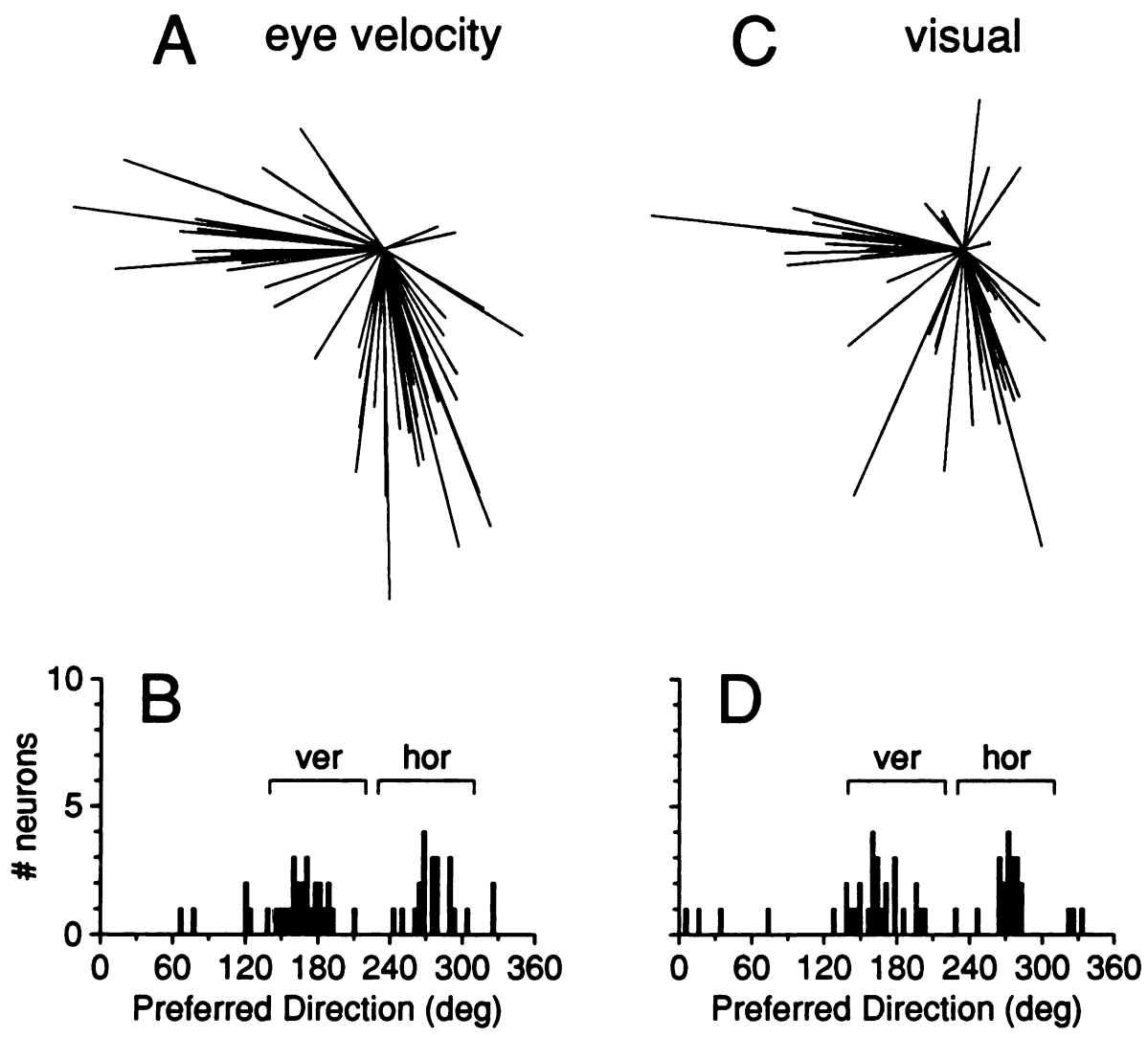
A
eye velocity
C
visual
B
D
ver
hor
ver
hor
10
5
0
neurons
0 60 120 180 240 300 360
Preferred Direction (deg)
0 60 120 180 240 300 360
Preferred Direction (deg)

Figure 3.8 Correlation between best directions of the eye velocity and visual components. A: Graph showing the best directions of the visual components plotted as a function of the best directions of the eye velocity components. Each symbol represents a pair of measurements made from one P-cell. Different symbols indicate different values of the directionality index (DI = 1 - worst/best): filled circles, DI for both components > 0.5; open circles, DI for eye velocity > 0.5; open triangle, DI for both components < 0.5. B: Graph plotting the best direction calculated from data obtained during sinusoidal pursuit as a function of the best direction for the eye velocity component calculated from data obtained during tracking of step-ramp target motions.

Fig. 3.8

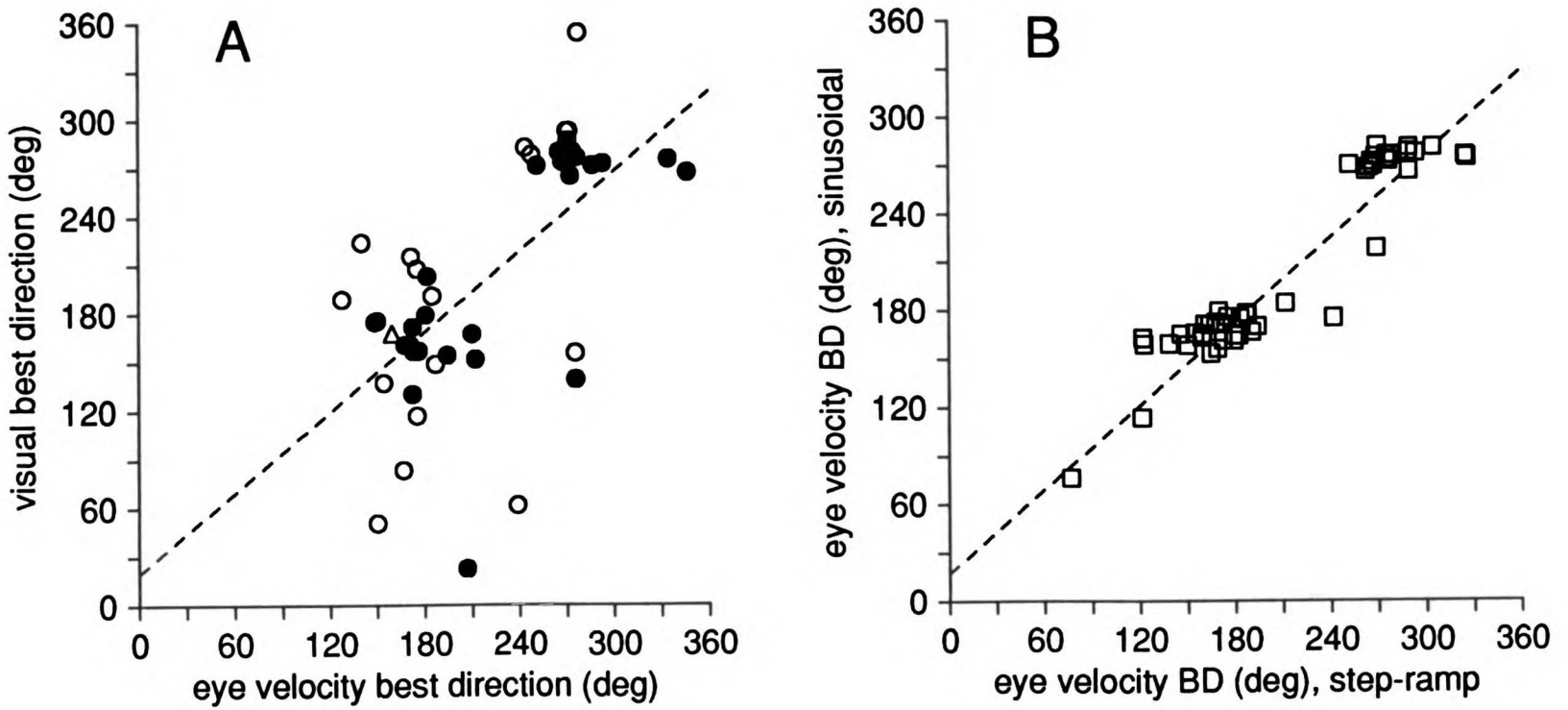
A
visual best direction (deg)
eye velocity best direction (deg)
0
60
120
180
240
300
360
B
eye velocity BD (deg), sinusoidal
eye velocity BD (deg), step-ramp

Figure 3.9 Tuning functions of P-cells. A, C and E: Histograms showing the distribution of values of the directionality index for the sample of P-cells. B, D and F: Histograms showing the distribution of values of the half-maximum bandwidth. A-B: Values calculated from data obtained during sinusoidal tracking. C-D: Values calculated from eye velocity components measured during step-ramp tracking. E-F: Values calculated from the visual components measured during step-ramp tracking.

Fig. 3.9

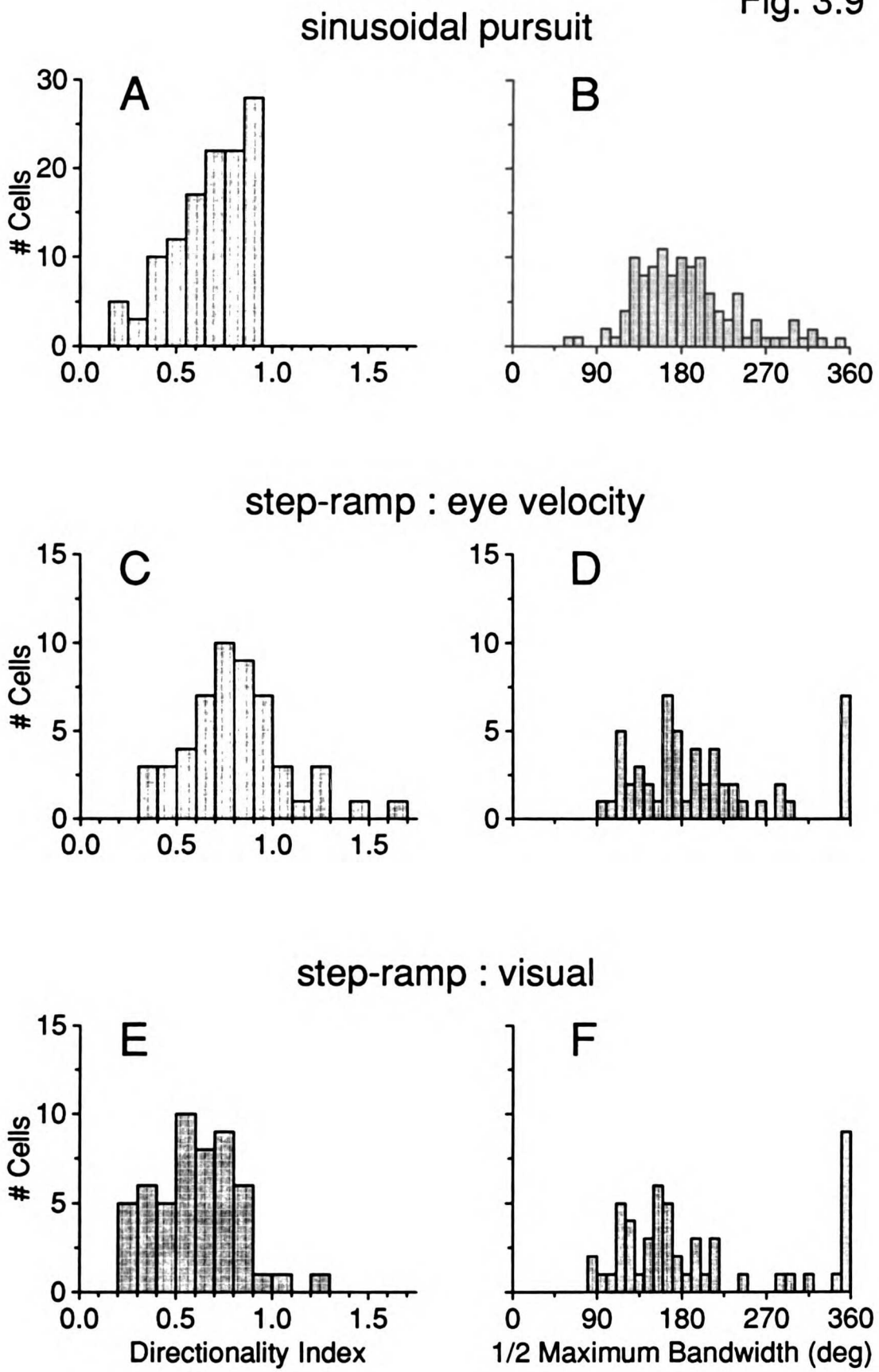
sinusoidal pursuit
A
B
Cells
30
20
10
0
0.0
0.5
1.0
1.5
0
90
180
270
360
step-ramp : eye velocity
C
D
15
10
5
0
step-ramp : visual
E
F
Directionality Index
1/2 Maximum Bandwidth (deg)

Figure 3.10 Changes in direction tuning for one P-cell with changes in eye position. A: Each pair of traces shows the average simple-spike firing rate recorded during vertical (ver) and horizontal (hor) sinusoidal tracking. The pair of numbers above each set of traces indicate the horizontal and vertical location, respectively, of mean eye position. In each case, the target moved sinusoidally $\pm 5^{o}$ at 0.5 Hz. The dashed vertical line indicates peak downward and leftward eye velocity. B: Arrows indicate the best direction of the sensitivity to eye velocity of the P-cell in polar coordinates for different eye positions. The numbers atop each arrow indicate the mean eye position associated with each best direction. C: Changes in the amplitude of the sensitivity to eye velocity plotted as a function of mean eye position. D: Changes in the best direction of the sensitivity to eye velocity. Changes in amplitude and direction are calculated with respect to the vector determined for straight-ahead gaze (0,0).

Fig. 3.10

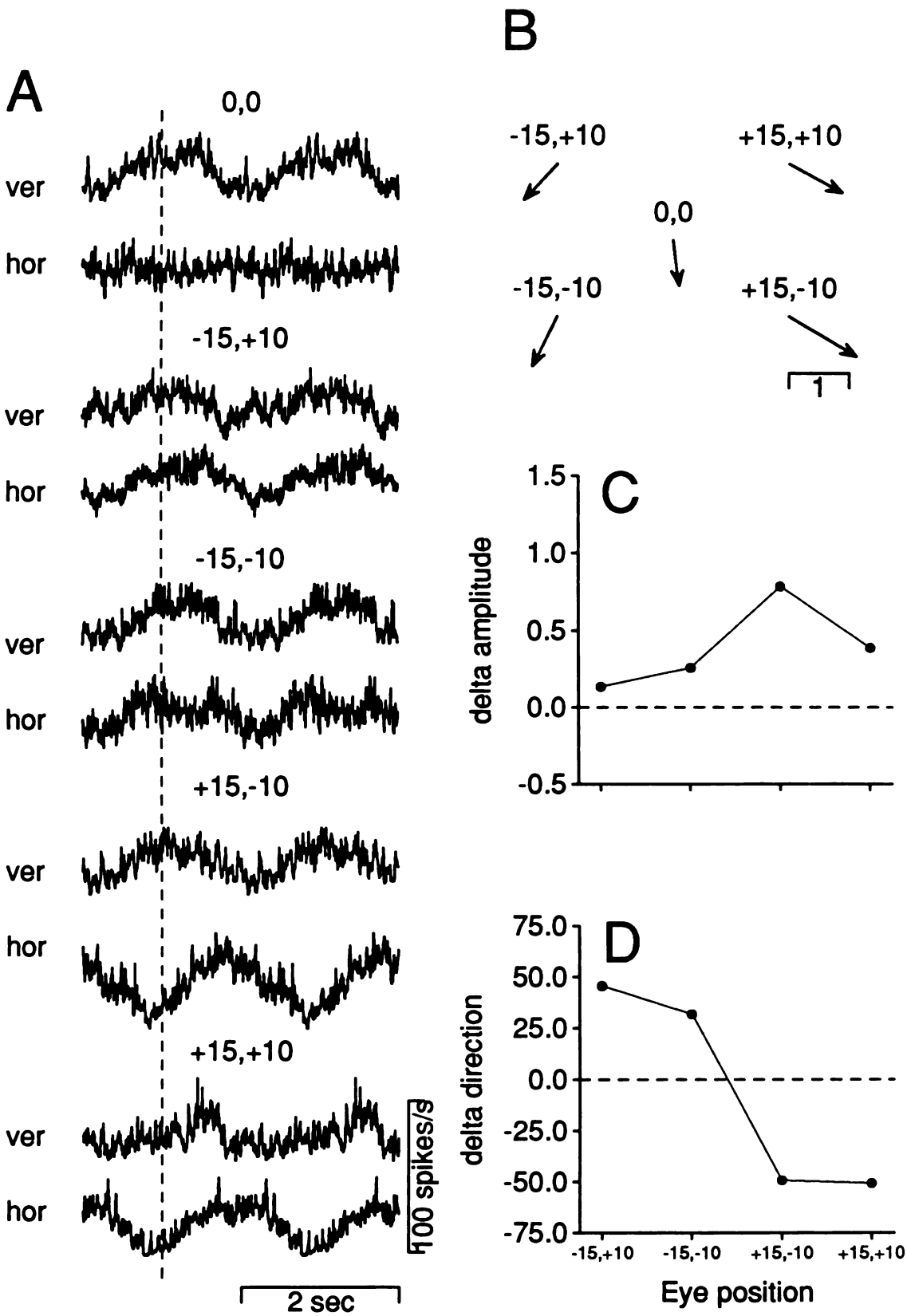
A
0,0
ver
hor
-15,+10
ver
hor
-15,-10
ver
hor
+15,-10
ver
hor
+15,+10
ver
hor
100 spikes/s
2 sec
B
-15,+10
+15,+10
0,0
-15,-10
+15,-10
1
C
delta amplitude
1.5
1.0
0.5
0.0
-0.5
D
delta direction
75.0
50.0
25.0
0.0
-25.0
-50.0
-75.0
-15,+10
-15,-10
+15,-10
+15,+10
Eye position

Figure 3.11 Changes in best directions for different eye positions. Solid lines indicate the changes in amplitude (top graph) and the changes in the direction (lower graph) of the eye velocity sensitivities caused by changes in mean eye position. Each line indicates measurements made from one P-cell, like those illustrated in Fig. 3.10. The dashed lines indicate changes predicted in amplitude and direction, based on the analysis of Robinson (1975).

Fig. 3.11

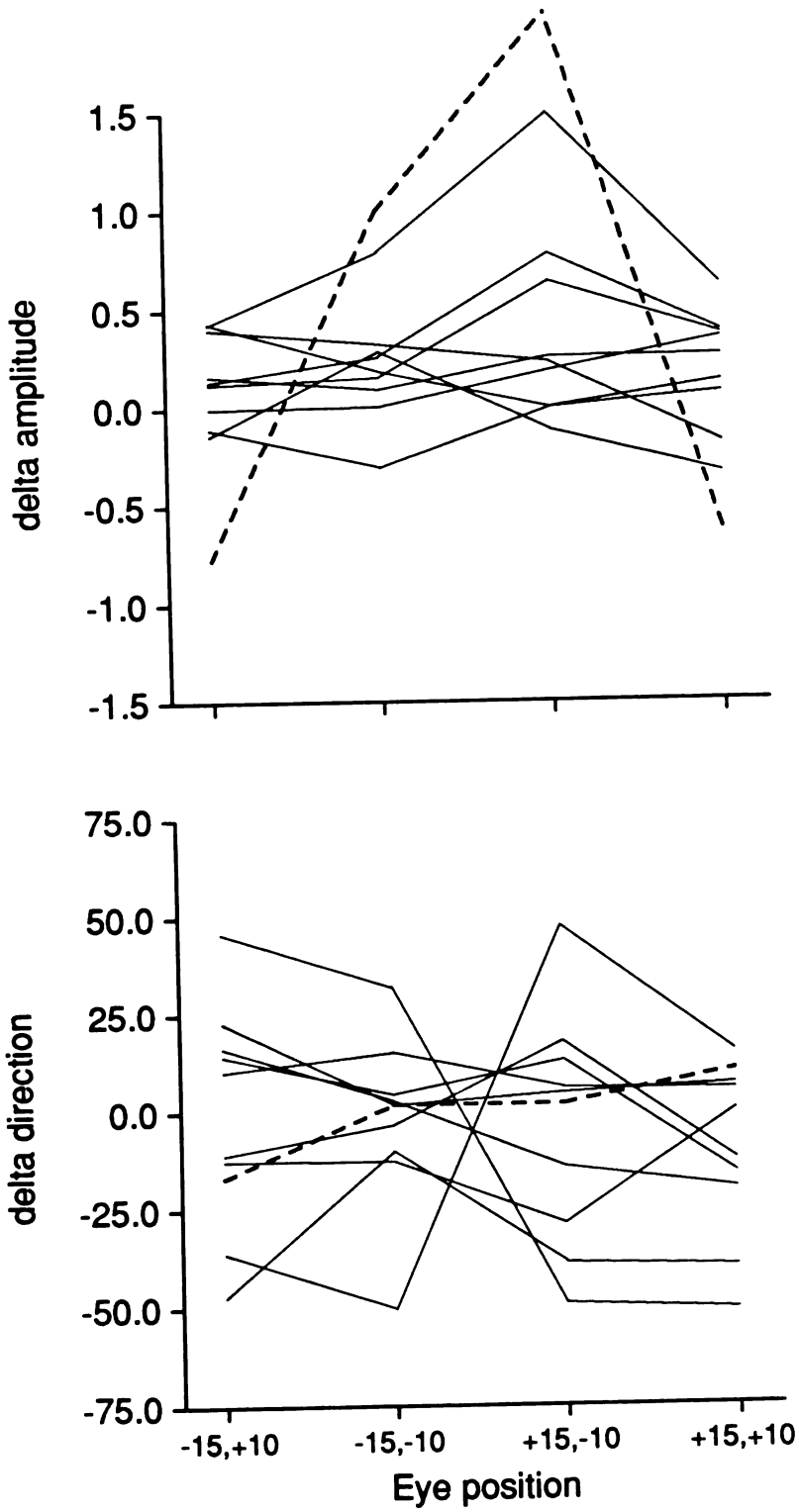
1.5
1.0
0.5
0.0
-0.5
-1.0
-1.5
delta amplitude
75.0
50.0
25.0
0.0
-25.0
-50.0
-75.0
delta direction
-15,+10
-15,-10
+15,-10
+15,+10
Eye position

Figure 3.12 Distribution of best directions for oculomotor mossy fibers. A: Polar plots showing distribution of best directions for our population of oculomotor mossy fibers. Each line represents a vector pointing in the best direction of one mossy fiber. The length of each line is proportional to the directionality index (DI = 1 - worst/best). B: Histograms showing the distribution of best directions for the population of mossy fibers, using the same data as shown in A.

Fig. 3.12

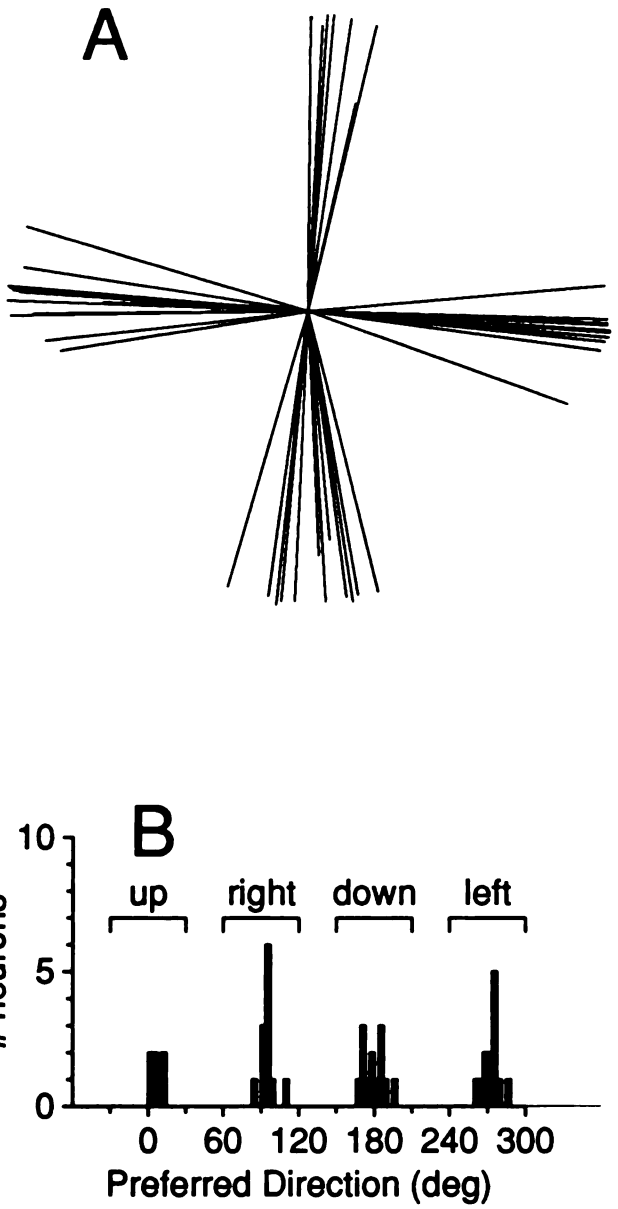
A
B
10
5
0
neurons
up
right
down
left
0
60
120
180
240
300
Preferred Direction (deg)

Figure 3.13 Tuning functions of mossy fibers. A: Histogram showing the distribution of values of the directionality index for the sample of mossy fibers. B: Histogram showing the distribution of values of the half-maximum bandwidth.

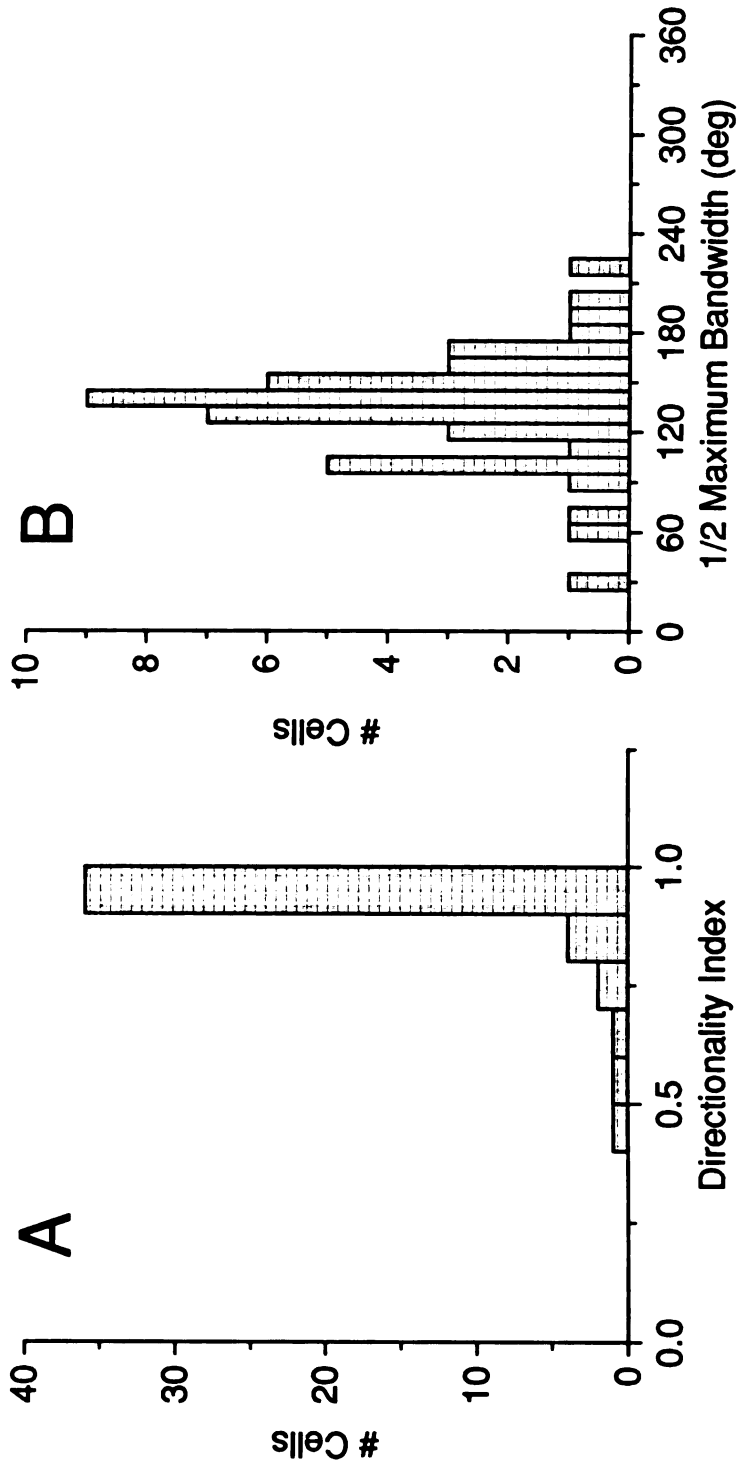
A
Cells
40
30
20
10
0
0.0
0.5
1.0
Directionality Index
B
Cells
10
8
6
4
2
0
0
60
120
180
240
300
360
1/2 Maximum Bandwidth (deg)

Fig. 3.13

Figure 3.14 Comparison of the best directions obtained in the present study with the best directions associated with the semicircular canals and the extraocular muscles. Each circle is a polar plot displaying the best directions for data obtained in the present study (top row) or based upon measurements made previously (lower row). Top row: Each arrow is a vector pointing in the average best direction for a population of P-cells. The four pairs of arrows in the "eye velocity" plot indicate the average best directions obtained from three separate flocculi and from the eye velocity components obtained during step-ramp trials. The single pair of arrows in the "visual" plot indicate the average best directions obtained during step-ramp trials. Bottom row, left: Arrows indicate the planes of motion detected by the horizontal (H), posterior (P), and anterior (A) semicircular canals. Bottom row, right: Arrows indicate the pulling directions of the ipsilateral lateral rectus (LRi), contralateral medial rectus (MRc), ipsilateral inferior rectus (IRi), contralateral superior oblique (SOc) mucles. Best directions for semicircular canals and extraocular muscles based upon the data of Simpson et al. (1986a,b).

Fig. 3.14

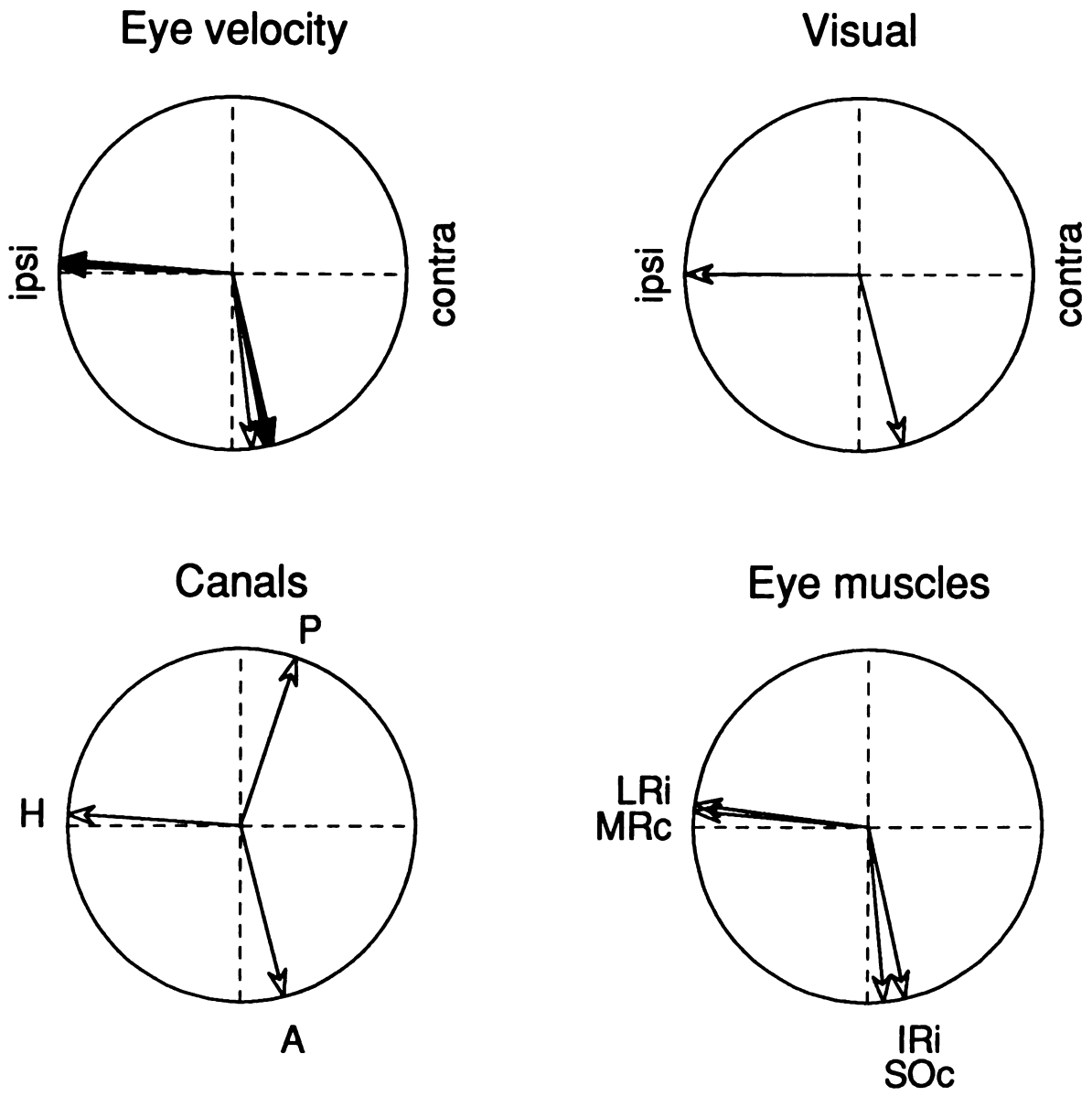
Eye velocity
ipsi
contra
Visual
ipsi
contra
Canals
P
H
A
Eye muscles
LRi
MRc
IRi
SOc

Figure 3.15 Encoding of direction of eye movements by two populations of cells. A-D: Each graph is a polar plot showing a pair of hypothetical tuning curves. Each curve is described by the equation: $y = a + be^{-(x-x')2/(2c2)}$. For A-D, a = 10 and b = 165. For A-C, c = 80; for D, c = 45. The best directions (x') were set to be either 90° (A, D) apart, 135° (B) apart or 180° (C) apart. E-H: Each graph is matched to the pair of tuning curves directly above. In each graph, the amplitude of one tuning curve is plotted as a function of the amplitude of the second tuning curve in the pair, for all possible directions of motion. Locations are labelled on the curves for directions corresponding to up (U), down (D), right (R) and left (L).

Fig. 3.15

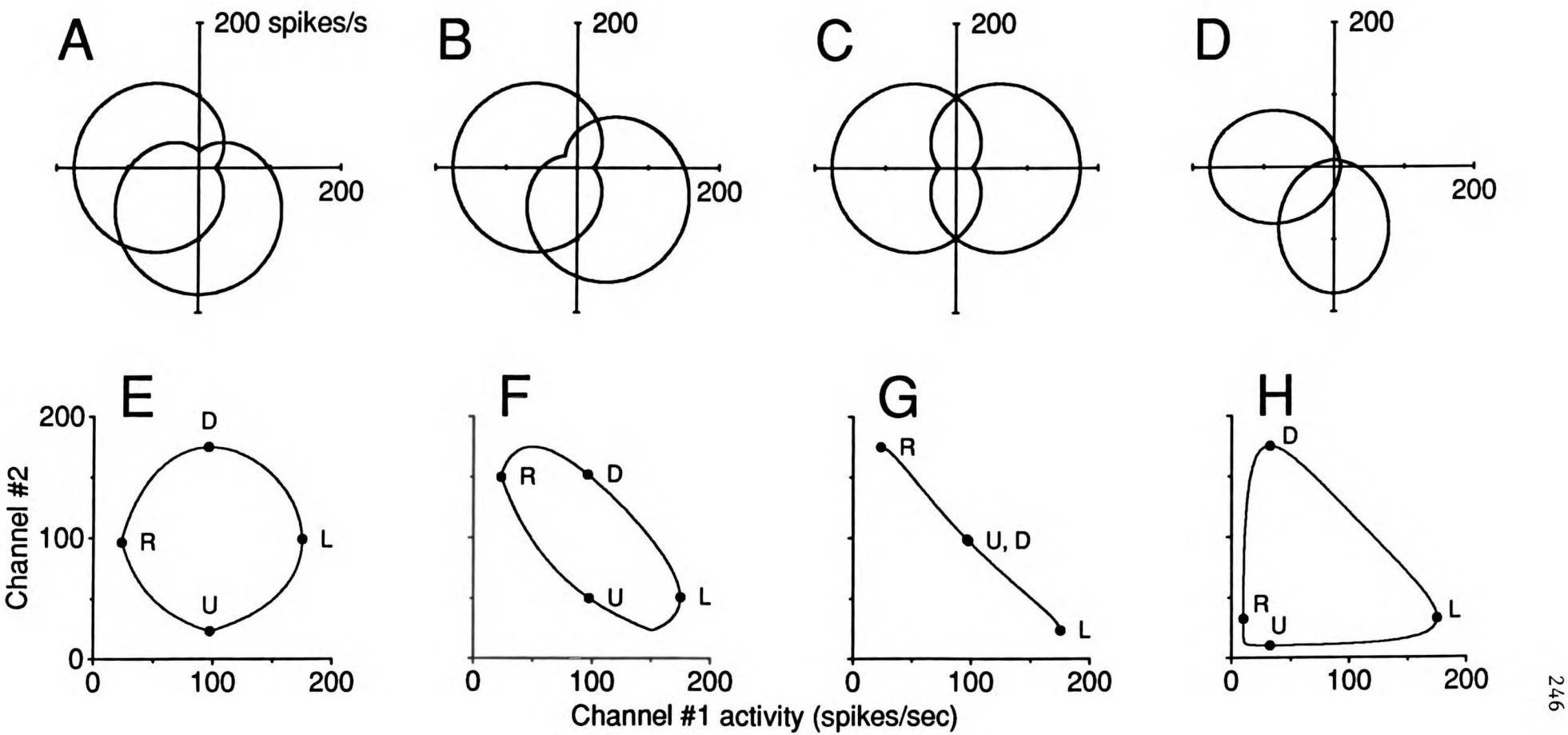
A
200 spikes/s
200
B
200
200
C
200
D
200
200
E
200
100
0
Channel #2
D
R
L
U
0
100
200
F
R
D
U
L
0
100
200
G
R
U, D
L
0
100
200
H
D
R
U
L
0
100
200
Channel #1 activity (spikes/sec)

Chapter Four

Visual motion signals observed on Purkinje cells in the flocculus and ventral paraflocculus during pursuit eye movements in the monkey

Summary and Conclusions

1. Visual inputs to floccular Purkinje cells are believed to play an important role in the generation and control of smooth pursuit eye movements. The identity and function of these visual inputs was the focus of the present study. We recorded from Purkinje cells in the flocculus and ventral paraflocculus while the monkey smoothly tracked several types of target motions. The target motions were selected to provide a range of the visual motion signals that our previous studies have indicated provide important inputs for pursuit.

2. We used a distributed network model to analyze the time-varying averages of firing rate recorded during pursuit. We assumed that the firing rate of each P-cell could be modeled as the sum of one oculomotor input -- eye velocity -- and three visual motion signals -- image velocity, image acceleration, and an image motion transient. Our results show that the hetereogeneity in the firing rate patterns observed across the population of floccular P-cells can be accounted for by variations in the weightings of these four inputs. Also, our analysis indicates that each of the three visual motion signals suggested by our previous results to be important for pursuit is encoded by the output of the flocculus.

3. In a separate experiment, we assessed how the amplitude of the visual signals observed on P-cells changes when the initial motion of the target is placed at different locations in the visual field. In previous behavioral experiments, the largest eye accelerations during the initiation of pursuit

occurred when the target was initially placed 3° eccentric and moved toward the fovea. Our results show that the same conditions caused the largest visual responses on floccular P-cells. This provides further evidence that the visual signals on floccular P-cells are the same visual signals used for pursuit.

4. We also assessed whether the visual signals observed on floccular P-cells occurred at the appropriate time to provide a command for eye acceleration during pursuit. We addressed this question by examining the temporal relationship between the visual component of simple-spike firing rate and the acceleration of the eye. Our results suggest that at least the first portion of the command for eye acceleration during pursuit occurs too early to be conveyed by P-cells in the flocculus.

Introduction

Many regions of the brain have been implicated in the generation and control of smooth pursuit eye movements. As shown in Fig. 1A, most of these regions are stations along anatomical pathways that link sensory areas in the cerebral cortex to motor structures in the cerebellum and brainstem. Visual areas in the cerebral cortex, such as striate cortex (V1), the middle temporal area (area MT), and the medial superior temporal area (area MST), provide signals encoding the motion of the retinal image, as well as extra-retinal signals that may be related to motor aspects of pursuit (Newsome et al. 1985; Newsome et al. 1988). Regions of frontal cortex near the arcuate sulcus (FEF) also show activity related to pursuit eye movements and may contribute signals used to supplement or supplant the inputs provided by occipital and parietal cortex (Lynch 1987, MacAvoy and Bruce 1988; MacAvoy et al. 1988). The strongest anatomical projections from these cortical areas converge onto the lateral, dorsolateral, and dorsomedial portions of the basal pontine nuclei (Brodal 1978; Glickstein et al. 1972, 1980, 1985; May and Andersen 1986; Kunzle and Akert 1977; Leichnetz 1982; Huerta et al. 1986). These pontine neurons, in turn, project to several regions of the cerebellum, including the flocculus, paraflocculus and vermis (Brodal 1979, 1982; Langer et al. 1985). Each of these cerebellar regions can influence smooth eye movements by acting on extraocular nuclei in the brainstem (Langer et al. 1985a, Yamada and Noda 1987, Noda et al. 1990). In addition, there are cortical projections to other nuclei in the brainstem and pretectum that either bypass the cerebellum or provide additional pathways for providing visual inputs to

the cerebellum (Brodal 1980, 1982; Hoffman and Distler 1989; Hoffman et al. 1988; Mustari and Fuchs 1989, 1990).

As a further step toward delineating how individual regions participate in generating pursuit, we have studied the function of the cerebellar flocculus and ventral paraflocculus, the structures which form the most clearly defined nexus of the pursuit system. The anatomical connections of the flocculus are well-suited to mediate the conversion of visual motion information provided by the cerebral cortex into the commands for pursuit eye movements required by motoneurons. One set of inputs to the primate flocculus are related to the motion of the eye and head and arise via mossy fibers projections from the vestibular nuclei and the nucleus prepositus (Langer et al. 1985a, Broussard and McCrea). The flocculus also receives mossy fiber inputs related to visual motion that arise from the dorsolateral portion of the pontine nuclei (DLPN). Additional visual inputs may arise from a dorsomedial portion of the pontine nuclei and the adjacent nucleus reticularis tegmenti pontis (Brodal 1980, 1982; Langer et al. 1985a). The flocculus projects to several portions of the ipsilateral vestibular nucleus and can cause smooth eye movements within 10 ms through inhibition of interneurons in these nuclei (Langer et al. 1985b, Belknap and Noda 1987, Lisberger and Pavelko 1988).

The activity of floccular Purkinje cells (P-cells), the output neurons of the cerebellum, provides the strongest evidence that the flocculus represents an interface between the sensory and motor systems used for pursuit. During continuous smooth movements of the eyes, floccular P-cells show a sustained modulation in their simple-spike firing rate. This tonic modulation of P-cell firing rate is believed to represent a motor component of the command for smooth tracking. Through its reciprocal connections with the vestibular

nuclei, indicated by the feedback pathway in Fig. 1A, the flocculus may form part of a loop that retains a copy of the gaze velocity command provided to the output motor pathways (Lisberger and Fuchs 1978a, Miles et al. 1980, Stone and Lisberger 1990). Continuance of activity around this feedback loop could sustain eye velocity during sustained tracking, eliminating the need for continuous sensory feedback. Experiments in monkeys have provided support both for the idea of eye velocity feedback and for the hypothesis that this feedback is mediated by the flocculus. If visual inputs during pursuit eye movements are eliminated by electronically stabilizing the image of the target on the retina, eye velocity is maintained at its previous value (Morris and Lisberger 1987). When the same experiment was performed while simultaneously recording from floccular P-cells, the tonic modulation of simple-spike firing rate was also maintained (Stone and Lisberger 1990).

In addition to tonic changes in firing rate related to eye velocity, floccular P-cells show phasic changes in simple-spike firing rate related to visual motion. During continuous pursuit of a target that moves alternately rightward and leftward, P-cells show brief bursts or dips in their simple-spike firing rate each time the target changes direction (Lisberger and Fuchs 1978a, Miles et al. 1980). During the initiation of pursuit, when the monkey tracks a target initially at rest that begins to move at a constant speed, floccular P-cells display a directionally-selective pulsatile increase or decrease in firing rate (Stone and Lisberger 1990). These responses follow the occurrence of the visual image motion caused by the motion of the target by about 100 ms and approximately coincide with the large eye acceleration that marks the onset of the eye movement. The transient responses are not related to eye velocity, because their amplitude is much larger than the responses observed during continuous pursuit. The responses also do not appear to be a consequence of

eye acceleration per se, because most P-cells show little or no transient response to eye accelerations evoked by quick movements of the head. Stone and Lisberger (1990) therefore suggested that the transient responses observed on floccular P-cells reflect visual motion inputs used as commands for pursuit.

The current view of how the flocculus participates in the generation of pursuit eye movements is summarized by the diagram in Fig. 1B. The diagram emphasizes the proposal that the flocculus has two distinct functions. First, because the flocculus receives mossy fiber inputs conveying signals related to eye velocity, a component of the output of the flocculus represents a command for eye velocity during pursuit. Second, because the flocculus receives inputs conveying signals related to visual motion, the output of the flocculus is believed to also represent a command for eye acceleration. A virtue of this scheme is that inclusion of the visual command for eye acceleration in the output of the flocculus causes eye velocity to be changed automatically whenever pursuit does not match the motion of the target. The diagram also allows for the possibility that other structures may convey visual signals that are used to accelerate the eye during pursuit. For example, the visual signals causing the earliest eye acceleration during the initiation of pursuit may be conveyed along pathways that bypass the flocculus (Fig. 1A).

The scheme outlined in Fig. 1B is consistent with what is known about the properties of the cerebellar flocculus, but it assigns functions to the flocculus that have not been directly tested. In particular, it has not been shown that the simple-spike firing rate of floccular P-cells conveys visual signals that are adequate or appropriate to provide a command for eye acceleration during pursuit. The identity and function of the visual simple-

spike responses is the focus of the present study. One difficulty in determining the role of the visual responses stems from the fact that different P-cells show different firing rate profiles during tracking of the same target motion. This heterogeneity raises the possibility that only a subset of floccular P-cells provide inputs for pursuit. An alternate possibility is that the diversity of visual signals present on floccular P-cells stems from the diversity of visual signals used for pursuit. Behavioral experiments have provided evidence that the pursuit system uses a combination of visual signals related to the velocity and acceleration of the moving image (chapter one). In the present study, we have used a model which incorporates these visual signals to describe the different types of firing rate profiles observed on floccular P-cells. Our results indicate that the firing rate of each P-cell in our sample can be accounted for by a combination of visual motion signals and eye velocity. The analysis also indicates that each of the visual motion signals used for pursuit is represented in the output of the flocculus.

As a further test of whether the phasic simple-spike responses of floccular P-cells convey visual signals used for pursuit, we performed an experiment to test whether a salient property of the visual signals used for pursuit is also exhibited by the visual signals on P-cells. The property that we studied was the change in the effectiveness of visual motion inputs for pursuit when presented at different locations in the visual field. In behavioral experiments, a given amplitude of image motion elicits the largest eye acceleration during the initiation of pursuit if the target is placed approximately 3^{o} eccentric and moves toward the fovea (Lisberger and Westbrook 1985). We performed similar experiments while recording the simple-spike activity of floccular P-cells and observed comparable changes in the size of the visual component of P-cell firing rate. These results provide

further evidence that the visual signals exhibited by floccular P-cells are the same visual signals that are used for pursuit eye movements.

A final question is whether the visual signals conveyed by the flocculus represent a command for pursuit eye acceleration. As shown in Fig. 1A, there are other pathways through the brainstem that either bypass or operate in parallel with the flocculus that might also be involved in the genesis of pursuit. It is therefore possible that the transient responses of floccular P-cells, although reflecting visual signals used for pursuit, are in fact feedback signals that report the occurrence of activity in more direct pathways. Unfortunately, because of the large variation in the firing rate of P-cells, it has not been possible to use measurements of the latency of P-cell responses to definitively determine whether the transient responses of P-cell precede or follow the onset of pursuit. Also, as suggested by the diagram shown in Fig. 1B, it is possible that the flocculus provides a command for only a portion of the eye acceleration observed during pursuit. If this were the case, measurements of latency might lead to incorrect conclusions concerning the causal relationship between the visual signals on P-cells and eye acceleration. In the present chapter, we have attempted to circumvent these problems by examining the visual responses of P-cells over several hundred milliseconds during the performance of pursuit eye movements. By comparing the profile of the visual component of simple-spike firing rate to the time-course of eye acceleration during pursuit, we examined the temporal relationship between the visual signals on P-cells and the acceleration of the eye. Our results suggest that at least a portion of the command for eye acceleration during pursuit is not conveyed by the flocculus.

Methods

Most of the methods used in the current experiments were identical to those described previously. Detailed information about the preparation of experimental subjects, presentation of visual and vestibular stimuli, and techniques for collecting eye movement and single-unit data can be found in the methods section of chapter three. In this methods section, we will describe the behavioral paradigms employed and the techniques used to analyze the data.

Behavioral paradigms

As in the previous chapter, we first tested the responsiveness of each isolated P-cell with the sinusoidal tracking tasks used previously to identify P-cells in the flocculus (Lisberger and Fuchs 1978a; Miles et al. 1980, Stone and Lisberger 1990). 1) With the head stationary, the monkey tracked a sinusoidally moving target (0.5 Hz, +10^{o}). The monkey was rewarded after each interval of 1500 ms during which his eye position remained within 2^{o} of the moving spot. Recording during sinusoidal pursuit allowed us to measure the eye velocity sensitivity of the unit. 2) The monkey tracked the same sinusoidally moving target, but the turntable was moved exactly with the visual target. This paradigm requires the monkey to cancel his vestibuloocular reflex and allowed measurement of the the vestibular sensitivity of the unit. 3) The monkey fixated a stationary spot. By systematically placing the spot at different locations on the tangent screen, we could assess the eye position sensitivity of the unit.

After assessment of the sensitivities to eye and head velocity, most units were studied in at least one of three additional experiments. In each

experiment, the monkey pursued a target that was initially at rest and then moved either at a constant velocity or smoothly accelerated up to a constant velocity. The presentation of each target motions used a modification of the step-ramp trial originally designed by Rashbass (1961). Each trial started when the monkey fixated a central red spot. After a random interval (500-1000 ms), a white target spot appeared at an eccentric position and remained stationary for an additional random interval (300-500 ms). To initiate pursuit, the fixation spot was extinguished and the target began to move either at a constant velocity or a constant rate of acceleration. If the target motion was an acceleration, it accelerated for 125 ms and then continued moving at a constant velocity equal to the velocity attained after 125 ms of acceleration. The motion of the target lasted 600 - 800 ms. We generated step-ramp target motions with separate stationary and moving spots to avoid unwanted motion that is seen when a single spot is physically stepped away from straight-ahead gaze. The monkey was rewarded with approximately 0.1 ml of water or juice at the end of each trial if he maintained his eye position within 2 degrees of the stationary target and within 3 - 4 degrees of the moving target throughout the trial. If his eye position strayed out of these windows, the trial was aborted and he received no reward. The only exception to the fixation requirement was a 300 - 400 ms grace period allowed at the onset of target motion.

In the first experiment, the set of target motions consisted of constant velocities and accelerations as described above. In addition, for one amplitude of velocity, the target was not visible for the 300-500 ms period prior to the onset of its motion. In these trials, the target simply appeared on the screen already moving at a constant velocity. Slightly different sets of target motions were used in experiments with the two monkeys. For monkey

O, the full set of target motions consisted of targets moving in both the preferred and non-preferred directions at velocities of 5, 10, 20 and 30 °/s, and accelerations of 45, 80, 120, and 180 °/s^2. For monkey U, the set of target motions consisted of targets moving at velocities of 5, 15, and 30 °/s, and accelerations of 80, 120, and 180 °/s^2. For both monkeys, a single velocity of 5 °/s was used for the trial in which the eccentric target appeared already moving. This single velocity was selected, because the MOD effect (chapter one) is most pronounced for low target velocities.

In the second experiment, a single target velocity of 30 °/s was used, but the relative locations of the fixation spot and the eccentric target spot were adjusted so that the initial motion of the target occurred in different portions of the visual field. In each of the eighteen trials used in this experiment, the fixation spot was located at straight-ahead gaze, but the initial position of the eccentric target spot was located at 18 different locations along the horizontal meridian. The combinations of initial target spot locations and target velocity were selected so that the initial 100 ms of target motion were centered at $\pm$3, 6, 9, 12 and 0° in the visual field. For example, when the target moved at 30 °/s to the right, the possible initial locations of the target spot were 1.5, 4.5, 7.5, and 10.5° eccentric in the right visual field, and 1.5, 4.5, 7.5, 10.5, and 13.5° eccentric in the left visual field. When the target motion was directed leftward, complimentary initial locations of the target spot were used. After the target moved for 100 ms at 30 °/s, the target was placed at the straight-ahead gaze position, as determined by the eye position signals monitored by the computer. The target then continued to move at 30 °/s for an additional 700 ms. These experiments were not performed on P-cells that preferred vertical eye movements, because the primate chair blocked the monkey's line of sight for stimuli located more than 10° below the horizontal meridian.

In the third experiment, the target always started its motion with a constant velocity of 15 °/s, but after moving for 500 ms, its speed could either increase to 30 °/s, decrease to 0 °/s, or remain at 15 °/s. In each case, the monkey was required to maintain fixation of the target spot for an additional 500 ms. This experiment was also performed only while recording from horizontal P-cells and consisted of 6 trials, because the target could move either to the left or to the right.

Data analysis

The first step in the analysis of the data obtained from each P-cell during each of the three experiments was the generation of records representing the averaged simple-spike firing rate, eye position and eye velocity which accompanied the performance of each type of trial. As described in the methods section of chapter three, the averaged records were generated by aligning data from individual trials of the same type on the onset of target motion. For the data obtained from the second and third experiments, these averaged records formed the basis of more detailed measurements of firing rate and eye velocity, as will be described in the results section.

Distributed network analysis

For data obtained during the experiment in which targets either moved at constant velocities or smoothly accelerated, each P-cell was further analyzed by describing its firing rate with a separate copy of a model based upon behavioral experiments that we have described in chapters one and two. The model used to analyze each P-cell consisted of four distributed networks, one network for each of the four input signals. The outputs from the four networks were summed linearly to produce a simulated P-cell firing rate. Each network contained three layers of units: "tuned" units, "filter"

units, and a single output unit. The weights assigned to the connections between the tuned units and the filter units, and between the filter units and the output unit determined how each network scaled and filtered its input signal. The input to each network was first activiated by the array of tuned units, which contained eight units for positive and eight units for negative values of the input signal. The output of each tuned unit was a log-Gaussian function of the input signal. The array of 16 tuned units were equally spaced on a log scale over the range of values represented in the input signal. The Gaussian funtions for the tuned units placed at the extremes within each network were centered on values of 60 $^{o}/s$ for the eye velocity, image velocity, and image motion transient signals, and on a value of 500 $^{o}/s^2$ for the image acceleration signal. Each of the sixteen tuned units projected to each member of an array of "filter" units. The output of each filter unit was delayed by a different amount of time (0, 5, 10, 15, 20, 25, 30, or 35 ms) and projected to the single unit that provided the output from the network.

For each P-cell, we presented the model with a set of input and output patterns. Each pair of input and output patterns within the set was based upon data obtained while the monkey tracked on amplitude of one type of target motion. The input patterns were the sets of four signals (eye velocity, image velocity, image motion transient, image acceleration) that were obtained from data during tracking of that target motion. The output patterns were the averaged simple-spike firing rates recorded from the P-cell. Initially, the weights assigned to the connections within each network were randomly assigned. In this state, the model produced an output equal or close to zero for the duration of pursuit of each target motion. Using a gradient descent algorithm, we then adjusted the weights in the model to minimize the sum of the squared differences between the output of the model and the output

pattern for each set of input patterns. For most P-cells, the differences between the outputs of the model and the actual averages of simple-spike firing rate reached a minimum asymptotically after 500 - 1000 iterations of the gradient descent algorithm. Upon completion of the analysis, the values of the final weights assigned to the connections in the model were stored in a file that could be accessed later to reconstruct the solution achieved by the gradient descent algorithm.

Results

The data presented in this chapter were obtained by recording extracellularly from 62 P-cells in both flocculi of two monkeys. Based upon the directionally-selective modulation of their simple-spike firing rate during sinusoidal pursuit (0.5 Hz, +10°) along the horizontal and vertical axes, 45 were classified as horizontal and 27 as vertical P-cells. For each P-cell, we calculated the sensitivity to eye velocity by dividing the amplitude of simple-spike modulation by the amplitude of the change in eye velocity. The horizontal P-cells were also tested while the monkey's head was sinusoidally rotated (0.5 Hz, +10°) and the monkey was required to fixate a spot that moved sinusoidally in phase with the motion of the head. This paradigm required cancellation of the horizontal VOR and allowed us to assess the sensitivity of the P-cell to head velocity. Forty-four of the horizontal P-cells in our sample showed a sensitivity to head velocity that was comparable to their sensitivity to eye velocity and were therefore classified as "gaze velocity" P-cells. Vertical P-cells were not systematically tested for their sensitivity to motion of the head in the horizontal plane, but they were found in regions of the flocculus and ventral paraflocculus that were interspersed among those regions where horizontal gaze velocity cells were found.

Identification of visual motion signals on floccular P-cells

The three columns of traces in Fig. 2 (A, B and C) show the three types of target motions we used to identify the visual signals on each P-cell. For the target motion shown in the first column, the monkey initially fixated a stationary LED located straight-ahead in the visual field while a second target light appeared at an eccentric position. After a random interval no shorter

than 300 ms, the LED was extinguished and the eccentric target moved at a constant velocity toward and through straight-ahead gaze. The target motion shown in the second column was identical, except that the eccentric target was not visible while the monkey fixated the LED. When the LED was extinguished, the eccentric target simply appeared moving at a constant velocity. For the target motion shown in the third column, the eccentric target was once again visible while the monkey fixated the LED. When the LED was extinguished, the target accelerated smoothly from rest for 125 ms and then moved at a constant velocity equal to the velocity obtained after 125 ms of acceleration. In subsequent figures, we will use the three sets of LED and target position traces shown at the top of this figure as icons to represent the three different types of target motions. When shown as icons, the position traces for the smoothly accelerating targets will be shown with dashed lines to distinguish them from the targets moving at a constant velocity.

The three types of target motion elicited different trajectories of eye velocity that can be accounted for by the differences in the visual motion signals associated with each target motion. The averaged eye velocity traces in the upper half of Fig. 4.2 show examples of these differences, and the dashed traces in the lower half of Fig. 4.2 indicate how these differences were associated with different combinations of the three visual signals. When the target was initially stationary and began to move at a constant speed (A), the initial eye velocity was larger than when the target moved at the same speed, but was not visible before the onset of its motion (B). We have attributed this difference to the contribution of an image motion transient signal, which was obtained from the first derivative of image velocity for abrupt changes in target motion. The portion of the response that was shared by the two eye

velocity traces was attributed to a signal encoding image velocity. Finally, an image acceleration signal, derived from the first derivative of image velocity for gradual changes in target motion, contributed synergistically with the image velocity signal during pursuit of the smoothly accelerating target (C). The accelerating target elicited a trajectory of eye velocity that had a larger amplitude than would be predicted based on the contribution of the image velocity signal alone. As was described in chapter two, a model of pursuit eye movements which includes a sensitivity to these three visual motion signals can reproduce many of the observed features of pursuit eye movements in both monkeys and humans. We therefore recorded from isolated P-cells while the monkey tracked a set of target motions consisting of constant velocities and smooth accelerations like those shown in Fig. 4.2 as a means of identifying which of the visual signals were encoded by the firing rate of each P-cell.

The average simple-spike firing rate recorded from five P-cells that illustrate the range of responses that we observed are shown in Fig. 4.3. Each of the traces represents the average simple-spike firing rate obtained during 15-20 presentations of one target motion moving in the P-cell's preferred direction. Each column displays the firing rates obtained during tracking of the target motion indicated by the icon at the top of the column. As these sample traces indicate, the simple-spike firing rates of floccular P-cells in our sample showed a wide range of response profiles when the monkey tracked the three types of target motion. Most P-cells showed both a tonic increase during maintained pursuit and a transient overshoot in firing rate at the initiation of pursuit. A few P-cells in our sample, like P-cell #5 in Fig. 4.3, showed a tonic increase during maintained pursuit with no or only a small overshoot in firing rate at the initiation of pursuit. For some, the amplitude

of the transient response was not affected much by whether the target was visible before it moved or was already moving when it appeared (P-cell #4). For the majority of P-cells, however, the transient response was larger when the target was visible before it moved (P-cells #1-3). For some of these P-cells, there was essentially no transient response if the target was already moving when it appeared (P-cell #1). P-cells that had larger transient responses during pursuit of targets moving at constant velocities also tended to have larger transient responses to targets that accelerated smoothly from rest (P-cells #2-3), but this was not always the case (P-cell #1).

To analyze the data obtained from each P-cell, we assumed that the average simple-spike firing rate recorded during pursuit of each target motion could be described as the sum of four possible input signals: eye velocity, image velocity, image motion transient, and image acceleration. For each P-cell, we developed a separate copy of a model which described how the weighting of the four input signals could account for the simple-spike firing rate of the P-cell as a function of time. The model itself consisted of four distributed networks, one network for each of the four input signals. The weights assigned to the connections between the units in each network determined how the amplitude of the input signal contributed to P-cell firing rate and how its temporal profile was adjusted to match the profile of P-cell firing rate. Using a gradient descent optimization algorithm, we determined a set of weights for the connections in each of the four networks which minimized the squared error between the output of the model and the actual firing rate recorded from each P-cell. The primary reason for using a distributed network to analyze the data was that it provided an unbiased method for adjusting the amplitude of the four input signals. A similar analysis could have been performed by providing equations describing the

scaling of the four input signals and by then using an optimization procedure to determine which parameters provided the best fit to the data. However, because the equations used in such an analysis would be fixed, the properties defined by the equations would impose contraints on how the input signals were be processed. In contrast, the distributed structure of the model made it possible to design a unique nonlinear relationship between each of the four input signals and the firing rate of each P-cell.

The results of applying this analysis to a typical P-cell are shown in Fig. 4.4. Each of the five columns in Fig. 4.4 shows data obtained during pursuit of one target motion, as labeled by the icon at the top of the column. The upper half of the figure shows data obtained during pursuit in the preferred direction of the P-cell; data obtained during pursuit in the non-preferred direction are shown below. The pairs of traces labeled "FR" compare the averaged simple-spike firing rate of the cell (continuous lines) with the output of the model (broken lines). The outputs from each of the four networks in the model are shown below the firing rate traces and are labeled according to which of the four input signals the network processed: image velocity ($\dot{I}$), image motion transient ($\dot{I}'$), image acceleration ($\ddot{I}$), or eye velocity ($\dot{E}$). The sum of the outputs from the four networks equals the total output of the model for each target motion.

Inspection of the outputs from each of the four networks for each target motion revealed how the model weighted the three visual motion signals to provide the best match to the simple-spike firing rate recorded during the initiation of pursuit. As shown by the traces labeled "$\dot{I}$" in Fig. 4.4, the image velocity signal made the largest contribution to the transient overshoots and undershoots in firing rate for this P-cell. The contribution of the image velocity signal to firing rate was not linear with respect to the amplitude of

image velocity. This can be seen most clearly in the non-preferred direction (lower half of Fig. 4.4), where the nonlinear scaling produced an inhibitory contribution of image velocity at 5 °/s that was slightly larger that the contribution at 30 °/s. The network that processed the image motion transient signal made a small contribution to firing rate, as shown by the traces labeled "$\ddot{I}$". The amplitude of this contribution was approximately the same during pursuit of targets moving at different velocities. Finally, the image acceleration signal made only a small contribution to firing rate of this P-cell. Most of the overshoot observed in firing rate at the initiation of pursuit of targets that accelerated smoothly was accounted for by the contribution of the image velocity signal. For this P-cell, the same nonlinear weighting of image velocity that matched the firing rate recorded during pursuit of targets moving at constant velocities also nearly matched the firing rate recorded during pursuit of targets that smoothly accelerated.

An important aspect of the processing accomplished by the model was the nonlinear weighting of the visual and oculomotor inputs that it employed to match the profiles of simple-spike firing rate recorded from this P-cell. For example, during maintained pursuit of a target moving at 30 °/s in the preferred direction (upper middle column of Fig. 4.4), there was a tonic increase in firing rate of about 90 spikes/s. Examination of the outputs from the four networks indicates that almost all of this increase was contributed by the network that processed eye velocity (trace labeled 'E' in upper middle column). The model therefore attributed most of the tonic increase in firing rate to a sensitivity to eye velocity. Likewise, during maintained pursuit of a target moving at 5 °/s in the preferred direction (first two upper columns), most of the tonic increase in firing rate was again attributed to the eye velocity inputs to this cell. However, although eye velocity in these two cases is

approximately 83% lower than during pursuit at 30 °/s, the tonic contribution of the eye velocity signal in the model is approximately 30 spikes/sec, only 67% lower. The network that processed the eye velocity signal therefore used nonlinear weighting of eye velocity to account for the tonic increase in firing rate of the P-cell during maintained pursuit in the preferred direction.

The quality of the fit provided by the model to the recorded simple-spike firing rate shown in Fig. 4.4 was typical of the fits obtained with our sample of P-cells. We measured the standard error of the fit by calculating the sum of the squared differences between the recorded firing rate and the output of the model for each time point, and dividing this sum by the number of time points. For P-cell ul1203b, whose results are shown in Fig. 4.4, the average standard error of the fit was 10.31. The histogram in Fig. 4.5 shows the distribution of average standard errors for the sample of 44 P-cells. The mean value of the average standard error was 11.04 (± 2.99, SD).

To quantify the nonlinear weighting of the eye velocity and visual signals employed by the model, we separately analyzed the four networks used to match the firing rate recorded from each P-cell. For each network, we provided a set of test inputs that consisted of a series of steps of different amplitudes. For each input step, we recorded the output of the model provided by one network. The traces in the upper half of Fig. 4.6 show examples of the outputs obtained from the four networks used to provide the fits to P-cell ul1203b shown in Fig. 4.4. Each column shows the outputs obtained from one network when a step with an amplitude indicated by the numbers to the left was provided as an input. For each input step, we then measured the output of the model at 600 ms, a time point located during the maintained output of the model, as indicated by the dashed vertical lines. By plotting the amplitude of the maintained output of the model against the

known amplitude of each input step, we determined the nonlinear input-output functions described implicitly by the weights in the model. The graphs in the bottom half of Fig. 4.6 show that the model for P-cell ul1203b emphasized the eye velocity and image velocity signals. Furthermore, the scaling of these signals was asymmetric and saturated for higher amplitudes.

Repeating the analysis several times for P-cell ul1203b produced similar outcomes each time. The set of four graphs in Fig. 4.7 show the nonlinear input-output functions described by the four networks in the model used to fit data from unit ul1203b. The four solid lines displayed on each graph represent the four different functions obtained by performing the analysis for unit ul1203b four times. For the networks describing the contribution of the image velocity, eye velocity and image acceleration signals, the functions obtained each time were nearly identical, as shown by the close superimposition of the four functions on each graph. However, there was some variation in the contribution made by the image motion transient signal. There were also small changes in the quality of the final fit produced each time the analysis was performed. The four average standard errors after the four analyses were 10.31, 10.31, 10.44, and 10.38.

For some P-cells, we assessed the importance of the weights assigned to the outputs of the filter units. We repeated the analysis, but removed the filter units from the model and connected each tuned unit directly to the output unit in each network. Repeating the analysis in the absence of the filter units produced similar, but not identical results for the P-cells tested. In particular, the network processing the image motion transient signal was most sensitive to the absence of the filters, because the transient signal was of short duration and occurred at a fixed time. In one case, the analysis used the output of the image motion transient network to reduce the amplitude of the

initial output fromm the image velocity network. In the model with the filter units included, the blunting of the initial contribution of the image velocity network was accomplished by the weights assigned to the outpus of the filter units.

To compare the results from the analyses obtained with different P-cells, it was necessary to summarize how eye velocity and the three visual motion signals contributed to the simple-spike firing rate of each P-cell. We therefore calculated how the firing rate of each P-cell changed as a function of changes in the amplitude of each of the four input signals. The calculation of these sensitivity values was based on the graphs obtained from the analysis of the four networks, like those shown in Figs. 6 and 7. Reducing the information contained in each graph to a single measurement of sensitivity necessarily involved loss of some information about the shape of the functions describing the weighting used by each network. Furthermore, because the functions were nonlinear, there was no straight-forward way to determine sensitivities directly from the graphs. Initially, we estimated the strength of each signal by measuring the peak value of each function. However, this method was strongly biased by the shape of the function, since a function that contained a large and narrow peak produced a larger value with this method than a function that consisted of nearly constant and moderate values. One method we considered to avoid this bias was to measure the average value of the entire function, which would be analogous to measuring the area under each curve. However, both of these methods suffered from the error of considering each value in the functions as equally important in the analysis procedure.

To illustrate this problem, the histograms in Fig. 4.8 show the relative frequency of occurrence for each amplitude of the four input signals. Each

graph shows the relative number of times that each amplitude was present in the set of input signals presented to the model. The histograms shown in Fig. 4.8 are based on the pursuit performance of monkey O, using data obtained while recording from P-cells on four different days. Data obtained on different days produced similar distributions, but there were consistent differences observed in the distributions observed during horizontal (dark bars) and vertical (gray bars) pursuit. In calculating the histograms, we therefore pooled data from two days to calculate the relative frequencies shown here, and calculated separate histograms for data obtained during horizontal and vertical pursuit.

The histograms in Fig. 4.8 show that the amplitudes of the four input signals did not occur with equal frequency. In particular, there are peaks in the histograms that correspond to the values of target velocity and acceleration presented in the experimental trials. Lower values of the image velocity and image acceleration signals occurred more often than higher values, which would be expected since the monkey tracked the target very accurately. In addition, the values for the image velocity signal during horizontal tracking (black bars) tended to be lower than the values observed during vertical tracking (gray bars). The frequency histograms produced with data from the second monkey were similar, except that the peaks in the histograms were at slightly different locations, because the target velocities and accelerations used in the experiments were slightly different.

We used data like that shown by the histograms in Fig. 4.8 to calculate the sensitivity of each P-cell to the four input signals. Using the two frequency histograms obtained for each of the monkeys -- one for horizontal and one for vertical pursuit -- we calculated a weighted average of the values described by each of the four input-output functions in the model. We first

divided both the frequency histograms and the nonlinear functions into discrete bins with a width of either 1 °/s (for eye velocity, image velocity, and image motion transient) or 10 °/s^2 (for image acceleration). For each bin, we multiplied the value given by one of the four input-output functions by the frequency with which the corresponding amplitude of that input signal occurred. These products were then summed over the range of input amplitudes to produce a weighted sum. This weighted sum equaled the average firing rate provided by the network in the model for all of the trials. Dividing the weighted sum by the average value of the input signal provided an estimate of the sensitivity of the P-cell to that signal. Because asymmetric input-output functions were common, we calculated separate values for sensitivities in the preferred and non-preferred directions for each signal.

Across our sample of P-cells, eye velocity and the three visual motion signals made unequal contributions to simple-spike firing rate. The histograms in Fig. 4.9 show the distribution of sensitivities calculated from our sample of P-cells. The distribution of values for motion in the preferred direction of the cell is shown by black bars, the values for the non-preferred direction are shown by the white bars. On average, the P-cells were most sensititive to eye velocity and showed a higher sensitivity for eye velocity in the preferred direction (2.42 spikes/sec per °/s) than for eye velocity in the non-preferred direction (1.18 spikes/sec per °/s). The sensitivity to image velocity (preferred: 1.18 spikes/sec per o/s, non-preferred: 0.69 spikes/s per o/s) was lower, but also showed a directional asymmetry. The average sensitivity to image acceleration was 0.18 spikes/s per °/s^2 in the preferred direction and 0.03 spikes/s per °/s^2 in the non-preferred direction. Finally, the average sensitivity to the image motion transient was 1.69 spikes/s per o/s in the preferred direction and1.17 spikes/s per o/s in the non-preferred

direction. For a few P-cells, the sensitivity to one or more of the three visual signals had the opposite sign as the sensitivity to image velocity. For these P-cells, image motion in the preferred direction decreased or image motion in the non-preferred directed increased the simple-spike firing rate. These sensitivities are shown in the histograms as negative values.

We then assessed whether the sensitivity of a P-cell to one of the four input signals was related to its sensitivity to any of the other three signals. In each graph in Fig. 4.10, the sensitivity of a P-cell to one input signal is plotted as a function of its sensitivity to another input signal. Sensitivities for motion in the preferred direction (open circles) and non-preferred direction (open triangles) were plotted separately. In each of the scatterplots, the data form a cloud in which the circles are further from the origin than the triangles, indicating that there was little correlation between the two sensitivities and that the sensitivities to motion in the preferred direction tended to be higher than the sensitivities to motion in the non-preferred direction.

We next mapped our population of P-cells onto a plot that displays the continuum in the representation of the eye velocity and visual signals. In constructing this plot, we used the weighted sums that were used in calculating the sensitivities to eye velocity and the three visual motion signals. The weighted sums were used, rather than the sensitivities, because they allow direct comparison of the average total contribution made by each signal in our experiments, regardless of the units (e.g., $^{o}/s$ vs $^{o}/s^2$) assigned to the signal. We combined the values of the weighted sums in three different ways to describe the inputs to each P-cell. First, we summed all four values from each P-cell to determine the total average modulation of the simple-spike firing rate. The distribution of these values is shown by the histogram

in Fig. 4.11. We divided this distribution into four nearly equally-sized groups, as indicated by four different shadings. Second, we divided the sum of the values from the three visual signals by the total average modulation. This ratio was used to describe whether the firing rate of the P-cell was driven primarily by visual or by eye velocity inputs. P-cells that were mainly responsive to visual inputs had values near 1; P-cells dominated by eye velocity inputs had values near 0. Finally, we divided the sum of the values from the image motion transient and image acceleration signals by the value of the image velocity signal. This ratio was used to describe which visual inputs contributed to the P-cell. P-cells dominated by the image motion transient or image acceleration signal had values near 1; P-cells dominated by the image velocity signal had values near 0. The scatterplot in the right half of Fig. 4.11 was obtained by plotting the values of these two ratios against each other for each P-cell in our sample. Because the calculation of the two ratios involves losing information about the absolute amplitude of the input signals, the data for P-cells that showed a larger total modulation in their simple-spike firing rate are shown with larger circles. The relationship between the sizes of the circles used in the scatterplot and the amplitude of total modulation is indicated by the four circles placed over the histogram.

To illustrate how the continuum represented by the scatterplot in Fig. 4.11 was related to the profiles of simple-spike firing shown by P-cells in our population, we will present a few examples. The data point highlighted with the square in the scatterplot represents unit ul1203b, the same P-cell shown in Fig. 4.4. Consistent with its position midway along the abscissa, the firing rate of this P-cell was attributed to nearly equal contributions from the eye velocity and the visual inputs. The P-cell was also located midway along the ordinate, indicating that, among the visual inputs, the contribution made by the image

velocity component alone was approximately equal to the sum of the contributions made by the image motion transient and image acceleration components.

The data point highlighted by the triangle in the scatterplot is from P-cell os0917b. This P-cell is represented by a point lying closer to the origin than for P-cell ul1203b, indicating that its firing rate was described by relatively larger contributions from the eye velocity and the image velocity signals. The results of the original analysis of this P-cell are shown by the traces in Fig. 4.12. As was shown in Fig. 4.4 for P-cell ul1203b, each of the five columns in Fig. 4.12 shows data obtained during pursuit of one target motion, inidicated by the icons at the top of the figure. The rows of traces show the averaged simple-spike firing rate of the cell (FR, continuous lines), the output of the model (FR, dashed lines), and the outputs of the four networks in the model ($\dot{I}$, $\ddot{I}'$, $\ddot{I}$, and $\dot{E}$). The model matched the firing rate recorded from this P-cell by a simple combination of the image velocity and eye velocity input signals. The contribution of the image velocity signal accounted for the transient overshoots and undershoots observed at the initiation of pursuit in both the preferred and non-preferred directions, while the eye velocity signal accounted for the tonic increases and decreases in firing rate observed during maintained pursuit. The image motion transient and image acceleration signals contributed very little to the firing rate, as indicated by the flat traces showing the outputs of the networks that processed these signals in the model ($\dddot{I}'$ and $\dddot{I}$).

In contrast to the results from P-cell os0917b, the analysis of P-cell os0629 indicated a large contribution from the image motion transient and image acceleration signals. This P-cell is represented by the data point highlighted with the diamond in Fig. 4.11, located toward the upper left

corner of the scatterplot. The results of the analysis of this P-cell are shown in Fig. 4.13. The traces showing the outputs from the four networks show that all four input signals made important contributions to the firing rate of this cell. As was true for the other two P-cells shown, the tonic increase in firing rate was attributed to a sensitivity to eye velocity. However, matching the transient responses recorded from this P-cell required participation of all three visual signals. During pursuit of targets that moved at a constant velocity (first three columns), the earliest portions of the overshoots and undershoots in firing rate were matched by the combined contribution of the image velocity and the image motion transient signals. After the initial change in firing rate, lasting about 100 ms, the firing rate tended to return toward its resting rate level, but did so at a rate that was faster than the decrease in the image velocity signal. The model attributed this hastened return of firing rate to a contribution of the image acceleration signal, an effect which was especially large for pursuit in the non-preferred direction. The contribution of the image acceleration signal was also evident during the initiation of pursuit of targets that smoothly accelerated (last two columns). Because the firing rate of this P-cell was not very strongly modulated for low values of image velocity (first column), the rapid increase in firing rate during pursuit of accelerating targets was attributed to a large contribution from the network processing the image acceleration signal.

Comparison of visual, oculomotor and vestibular inputs

For the horizontal P-cells in our sample, we compared our description of the visual inputs to each P-cell to the classification of the P-cells as "gaze-velocity" neurons. From data obtained during sinusoidal pursuit and during cancellation of the VOR, we calculated the sensitivities to eye and head velocity for each of the horizontal P-cells. When the sensitivity to eye

velocity was plotted as a function of the sensitivity to head velocity (Fig. 4.14A) all but one of the data points fell close to a line of slope one, indicating that the majority of the horizontal P-cells were "gaze-velocity". Excluding the one outlying point, the average sensitivity to eye velocity was 1.55 spikes/s per °/s (± 0.91, SD) and the average sensitivity to head velocity was 1.61 spikes/s per °/s (± 0.97, SD).

The population of horizontal gaze-velocity P-cells showed a wide range of contributions from the three visual inputs. However, the tendency of horizontal P-cells to be sensitive to visual inputs was not related to any biases in their sensitivities to eye or head velocity. As shown in Fig. 4.14B, we plotted a measure of the visual contribution to each horizontal P-cell as a function of a measure of how strongly the firing rate of the P-cell matched the behavior of an ideal "gaze-velocity" neuron. Along the abscissa is plotted the ratio of the sensitivity to eye velocity over the combined sensitivities to eye and head velocity. A ratio of 0.5, indicated by the dashed vertical line, indicates the behavior of the ideal gaze velocity neuron. Along the ordinate is plotted the total modulation attributed to visual inputs, divided by the total modulation attributed to visual plus eye velocity inputs. This measure is the same quantity that was plotted along the ordinate in the scatterplot in Fig. 4.11. For the population of horizontal P-cells, the data points are equally distributed about the dashed vertical line for the entire range of the variation shown in the strength of the visual inputs. The one outlying point that shows the smallest amplitude of visual inputs is the same P-cell that was identified as a non-gaze velocity P-cell in Fig. 4.14A.

Visual responses to motion presented in different portions of the visual field

In behavioral experiments, it has been shown that moving targets for pursuit evoke the largest eye accelerations when they are placed

approximately 3 degrees eccentric and move toward the fovea. To determine if the same bias was present in the activity of floccular P-cells, we recorded from floccular P-cells while the monkey tracked a target which began its motion at different locations in the visual field.

The traces in Fig. 4.15 show how these trials were presented. The trials started with the monkey fixating a centrally located LED in the presence of target spot placed eccentrically along the horizontal meridian. When the fixation light was extinguished, the target light moved at 30 deg/s either toward (as in the example in Fig. 4.15) or away from straight ahead gaze. After moving for 100 ms, a step in position was superimposed on the target's motion, placing the target directly at the gaze position of the monkey. The amplitude of the step was calculated on-line by the computer during the experiment as the instantaneous difference between the position of the target and the position of the monkey's eyes. The step in target position was necessary to prevent the monkey from making large saccades to acquire the target. The initial eccentricity of the target was adjusted so that the mean position of the moving target over the first 100 ms was located at $\pm$ 3, 6, 9 and 12 degrees relative to straight ahead gaze. For example, the initial eccentricity of the target for the trial shown in Fig. 4.15 was 10.5^{o}. After 50 ms, it passed through a point 9 deg eccentric, as indicated by the double-headed arrow. We refer to the motion presented on this trial as being centered at 9^{o} rightward, or +9.

In our analysis of data from these trials, we concentrated on the first 100 ms after the onset of the pursuit eye movement, the portion of the behavior that is evoked by the first 100 ms of the target motion. The upper set of traces in Fig. 4.15 illustrate the steps in our analysis. To calculate the amplitude of the transient simple-spike response, we first subtracted the

portion of the firing rate that was due to the sensitivity of the P-cell to eye velocity from the total simple-spike firing rate. We measured the average firing rate of the P-cell and the average eye velocity during maintained pursuit, a time interval defined for these trials as 400 - 600 ms after the onset of target motion, as shown by the two arrows in Fig. 4.15. We then calculated the sensitivity to eye velocity by dividing the tonic modulation in firing rate by the value of eye velocity during maintained pursuit. For the trial shown in Fig. 4.15, the sensitivity to eye velocity was -1.41 spikes/s per °/s. Multiplying the averaged eye velocity recorded during the trial by the sensitivity to eye velocity on a millisecond time scale produced an estimate of the component of the simple-spike firing rate that was due to eye velocity inputs. The eye velocity component of firing rate (smoother trace) is shown superimposed on the actual firing rate (noisier trace). The transient simple-spike response was then defined as the average difference between the actual firing rate and the eye velocity component of firing rate during the first 100 ms after the onset of pursuit, an interval indicated by the dashed vertical lines.

Fig. 4.16 shows the full set of total simple-spike firing rate and the eye velocity components of firing rate traces for one P-cell. The left-hand and right-hand columns show results for pursuit in the P-cell's preferred and non-preferred directions, respectively. The numbers between the two columns indicate the location along the horizontal meridian of the initial target motion. The sign of the number indicates whether the initial target motion was located in the hemifield on the same (+) or opposite (-) side as the preferred direction of the P-cell. For pursuit in the preferred direction, the transient response was largest when the initial target motion was located straight ahead (0) or several degrees into the non-preferred hemifield (-3, -6).

The smallest transient response occurred when the initial target motion was centered at 12 degrees in the preferred hemifield. In contrast, for pursuit in the non-preferred direction, the transient responses were largest when the initial target motion was located in the preferred hemifield (+3, +6).

The changes in the size of the transient responses measured for this P-cell are illustrated by the graph in Fig. 4.17A. The symbols plot the amplitude of the transient response as a function of the location in the visual field at which the initial target motion was presented. The filled circles show data for pursuit in the preferred direction; open symbols show data for the non-preferred direction. The transient responses were larger when the initial target motion was placed a few degrees in the non-preferred hemifield, despite the fact that the amplitude of target motion was always 30 °/sec. The effect of visual field location on the amplitude of the transient response was quantified by taking the difference between the largest and the smallest transient responses evoked. As indicated by the double-headed arrow in Fig. 4.17A, the amplitude of the effect for this P-cell was 56.15 spikes/sec.

The distribution of the values obtained by subtracting the smallest transient response from the largest is shown by the histogram in Fig. 4.17B. For the 28 P-cells from which we obtained data for this experiment, the mean change in the size of the transient response was 28.49 spikes/s ($\pm$ 17.13, SD). We subdivided the population by eye into three populations, based upon the amplitude of the effect of visual field location. The eight P-cells most strongly affected (black bars) showed a mean change in firing rate of 50.75 spikes/s ($\pm$11.29, SD). The other two groups showed a modest effect (26.64$\pm$2.67, n = 10) or a weak effect (12.53$\pm$6.83, n=10).

The changes in the amplitude of the transient response for these three groups of P-cells are shown by the three sets of graphs in Fig. 4.18. The lines

in each graph show the amplitude of the transient response plotted as a function of initial location in the visual field, like the graph shown in Fig. 4.18A. The three rows of graphs show data for the strongly affected (top), modestly affected (middle), and weakly affected P-cells (bottom). The righthand and lefthand graphs show data obtained during pursuit in the preferred and non-preferred directions, respectively.

As shown by the graphs in the left half of Fig. 4.19, the largest excitatory transient responses occurred when the initial target motion was located a few degrees in the visual hemifield opposite to the side of the recording site (around -3°, indicated by dashed vertical lines). The largest inhibitory responses occurred when the initial target motion was located a few degrees in the visual hemifield on the same side as the recording site (around +3°). This effect was present in each P-cell that showed a modest or large transient response. Furthermore, the effect of initial visual field location was most pronounced on those P-cells, shown in the top pair of graphs, which showed the largest transient responses.

The changes in simple-spike firing rate shown in Fig. 4.18 are correlated with the changes in the amplitude of the initial eye acceleration observed when the target motion begins at different locations in the visual field. We measured the average eye acceleration over the same 100 ms interval for which we calculated the amplitude of the transient response (as indicated by the vertical dashed lines in Fig. 4.16). The graphs in Fig. 4.19 plot the amplitude of the initial eye acceleration as a function of the amplitude of the transient response for the eight P-cells which showed the largest effect. Each point shows a pair of measurements made from averaged data from a single trial during pursuit in either the preferred (filled circles) or non-preferred direction (open squares). The data from each P-cell indicate that the

amplitude of the initial eye acceleration during pursuit was related to the size of the transient response. Fitting the data by linear regression provided an estimate of the relationship between the transient change in firing rate and the concomitant eye acceleration. The slopes of the best-fit straight lines were consistently higher for pursuit in the preferred direction (0.256 spikes/s per $^{o}/s^{2}$, $\pm$0.062, SD) than for pursuit in the non-preferred direction (0.071 spikes/s per $^{o}/s^{2}$, $\pm$0.039, SD).

Simple-spike responses of floccular P-cells at the termination of pursuit

The trajectory of eye velocity at the termination of pursuit may reflect the properties of the positive-feedback loop used to sustain eye velocity during continuous pursuit. Since the flocculus is believed to represent a component of this feedback loop, we studied the behavior of P-cells during the termination of pursuit.

The traces at the top of Fig. 4.20 show the target motion that the monkey was required to track in these experiments. As in the presentation of constant velocity targets described above, the monkey initially fixated a centrally-located LED while an eccentric target appeared. When the LED was extinguished, the eccentric target moved at 15 $^{o}/s$ toward and through straight-ahead gaze. After moving for 500 ms, the target either continued at the same velocity for an additional 500 ms, increased its velocity to 30 $^{o}/s$, or, as shown by the target position trace in Fig. 4.20, was stepped forward by 2^{o} and then stopped. The final step was used to obviate the need for the monkey to make a corrective saccade to acquire the stationary target.

As shown by the averaged eye velocity trace in Fig. 4.20, the trajectory of eye velocity at the termination of pursuit began with a brief increase in eye velocity in the direction of ongoing pursuit, which was probably caused by the apparent motion caused by the step in target position imposed as the target

stopped. We have used this event to align the average simple-spike activity recorded from four sample horizontal P-cells during tracking of this target motion in their preferred direction. The four P-cells displayed below the eye velocity trace in Fig. 4.20 showed different patterns of activity at the termination of pursuit. For P-cell #1, the sustained increase that it exhibited during continuous pursuit perseverated approximately 100 ms past the start of the decrease in eye velocity at the termination of pursuit. In contrast, other P-cells showed decreases in activity that either approximately coincided with (P-cell #2) or preceded (P-cells #3 and 4) the decrease in eye velocity. The activity of a couple of P-cells, like P-cell #3 shown here, displayed a brief increase in simple-spike firing (indicated by arrow) that preceded the brief increase in eye velocity by approximately 16 ms.

Although individual P-cells varied in their responses, the ensemble activity of the horizontal P-cells closely matched the trajectory of eye velocity observed at the termination of pursuit. The noisier traces in Fig. 4.21A show the results of averaging the activity of the 14 horizontal P-cells recorded from during tracking of this target motion. To generate these averaged traces, we summed the firing rates recorded from each P-cell on a millisecond time scale and then divided the sum for each millisecond by the number of P-cells. The trace on top shows the average activity during tracking in the preferred direction of the P-cells; the non-preferred direction is shown below. Superimposed on the averages of firing rate is the average eye velocity recorded during these experiments. The traces have been scaled by eye so that the tonic simple-spike firing rate is approximately equal to steady-state eye velocity.

As shown by the two pairs of traces in Fig. 4.21, the eye velocity produced by the monkey was symmetric for rightward (top trace) and leftward

(bottom trace) pursuit, but the activity of the ensemble of P-cells was asymmetric. At the initiation of pursuit in the preferred direction, the P-cells showed a transient overshoot followed by a large tonic increase in firing rate. At the termination of pursuit in the preferred direction, however, the activity of the P-cells showed no undershoot in activity and decreased smoothly toward a resting rate level. The left dashed vertical line is aligned with the brief increase in simple-spike activity preceding the termination of pursuit. This brief increase in simple-spike activity preceded the corresponding brief increase in eye velocity by approximately 10 - 20 ms. During pursuit in the non-preferred direction, the P-cells showed no undershoot at the initiation of pursuit, but showed a large overshoot at the termination of pursuit. Comparing the onset of the overshoot with the left vertical line indicates that the overshoot during pursuit in the non-preferred direction occurred about 10 - 20 ms later than the decrease in simple-spike activity observed during pursuit in the preferred direction. The right dashed vertical line is aligned with the peak of the overshoot produced by the P-cells during pursuit in the non-preferred direction. The peak occured approximately 140 ms after the onset of the overshoot and was followed by a smooth decrease toward a resting rate level.

The asymmetries present in the activity of P-cells when studied separately during pursuit in the preferred and non-preferred directions disappeared when the same data were viewed as the concurrent activity of two populations of P-cells, one in each of the two flocculi. We estimated the combined output of the two flocculi by combining the averaged simple-spike firing rates recorded during pursuit in the preferred and non-preferred directions. The noisy trace in Fig. 4.24B shows the result of combining the inhibitory contribution of the P-cells from the "contralateral" side with the

excitatory activity displayed by P-cells on the "ipsilateral" side. In combining the records, we multiplied the trace obtained during pursuit in the non-preferred direction by -1, added it to the trace obtained during pursuit in the preferred dirction, and then divided the sum by 2 on a millisecond time scale. Comparing the combined activity to the superimposed eye velocity trace shows that the asymmetries shown by each side alone were complimentary, so that the combined output from the two sides did not show any asymmetries.

Temporal relationship between the visual responses of P-cells and eye acceleration during pursuit

To assess whether the visual signals observed on floccular P-cells represent a command for eye acceleration, we next examined the temporal relationship between the transient simple-spike responses recorded from P-cells and the concomitant eye accelerations produced during pursuit. The conceptual framework underlying this analysis is illustrated schematically in Fig. 4.22. The visual component of simple-spike firing rate could be related to eye acceleration in several ways. One possibility is that the visual signals displayed on floccular P-cells represent an exclusive command for pursuit eye acceleration. In this case, shown in Fig. 4.22B, all of the visual signals used for pursuit would pass through the flocculus en route to exerting their effect on smooth eye movements. The command for eye acceleration defined by the visual signals (solid lines) would both accelerate the eye and be converted to a command for eye velocity. A copy of this command would be sent back to the flocculus (dashed line) to sustain eye velocity. In this idealized scheme, we can separate the contribution to firing rate made by the visual inputs from the contribution made by the eye velocity feedback signal. Subtracting the eye velocity component (dashed line in Fig. 4.22A) from the total firing rate

isolates the visual component of firing rate (solid line in Fig. 4.22C). Because there are delays in the conduction of signals along the pathways shown in Fig. 4.22B, the visual component of firing rate (Fig. 4.22C, solid line) should precede the acceleration of the eye (Fig. 4.22C, dashed line). A second possibility, shown in Fig. 4.22D, is that some, but not all, of the visual signals go through the flocculus en route to producing eye accelerations during pursuit. For example, it has been suggested that the visual inputs responsible for the first 20 - 40 ms of eye acceleration at the initiation of pursuit may bypass the flocculus. In this case, the increase in the visual component of simple-spike firing rate (Fig. 4.22E, solid line) would be unrelated to an early component of eye acceleration (upper small dashed line), but would provide a command for a later component of eye acceleration (upper dashed line). When the total eye acceleration is considered (lower traces), the visual component would follow the earliest increase in eye acceleration, but precede the later period of eye acceleration. A third possibility is that all of the visual signals providing commands for pursuit eye acceleration bypass the flocculus, but the flocculus receives a copy of the command to accelerate the eye (Fig. 4.22F). In this case, the visual component of simple-spike firing rate would represent a visual corollary signal rather than a command for eye acceleration. The output of the flocculus would still provide a command for eye velocity, but the command for eye acceleration would come from some other source. Depending on the delays associated with each pathway, both the increase and decrease in the visual component of simple-spike firing rate might occur after the corresponding changes are observed in eye acceleration (Fig. 4.22G).

Unlike the idealized firing rate shown in Fig. 4.22, analysis of the simple-spike firing rate recorded from actual P-cells faces two major obstacles.

First, the simple-spike firing rate of individual P-cells is very noisy, even when the data obtained from twenty or more trials are averaged together. The variation in firing rate makes it difficult to assess the temporal relationship between firing rate and eye acceleration. Second, we do not know which component of simple-spike firing rate is driven by eye velocity. It has been shown that most of the tonic increase in simple-spike firing rate during pursuit is due to eye velocity, but the temporal relationship between eye velocity and simple-spike firing rate is not known. Since the visual component of firing rate is obtained by removing the eye velocity component of firing rate, any errors in the temporal assignment of the eye velocity component could cause errors in the millisecond by millisecond estimation of the visual component, rendering dubious any temporal comparisons of the visual component with eye acceleration.

To reduce the noise in our firing rate data, we calculated average simple-spike firing rates for our population of P-cells during pursuit of each target motion. For each target motion, we summed the firing rates recorded from each P-cell on a millisecond time scale and then divided the sum for each millisecond by the number of P-cells. We calculated separate averages for data obtained from the horizontal and vertical P-cells for each of the two monkeys. For example, the traces shown in solid lines in the top row of Fig. 4.23 show the average of the simple-spike firing rates from our sample of 14 horizontal P-cells recorded in monkey U during pursuit of a target that moved at a constant velocity of 30 °/s.

We assessed how shifts in the temporal registration between simple-spike firing rate and the eye velocity component affected the estimation of the visual component. In separate tests, we assumed that the eye velocity contribution to firing rate either followed, was coincident with, or preceded

the externally measured changes in eye velocity. The three estimates of the eye velocity component shown in Fig. 4.23 are distinguished by the number of milliseconds each has been shifted with respect to actual eye velocity. In Fig. 4.23A, the eye velocity contribution to firing rate was shifted in time so that it lagged physical eye velocity by 30 ms. In Fig. 4.23B, the eye velocity component to firing rate was left unshifted, so that it coincided with eye velocity. Finally, in Fig. 4.23C, the eye velocity component to firing rate was assumed to precede eye velocity by 30 ms. The three cases were chosen to cover a temporal range that is consistent with the observed latencies for the effects of electrical stimulation of the flocculus and with the latencies of oculomotor mossy fiber inputs to the flocculus. In each case, the amplitude of the eye velocity component was calculated by multiplying the average eye velocity recorded during the trial by a constant value. This value, which reflects the average sensitivity to eye velocity of the 14 P-cells, was obtained by dividing the average firing rate over an interval 400-600 ms after the onset of the trial by the corresponding average value of the temporally-shifted eye velocity.

The visual components deduced from the three estimates of the eye velocity contribution to P-cell firing rate are shown by the three noisier traces at the bottom of Fig. 4.23. Each of the three traces was produced by subtracting the eye velocity component from simple-spike firing rate and is shown superimposed on a smoother trace that represents eye acceleration. Each of the three estimates of the visual component has been scaled so that the peak of the visual component has the same amplitude as the peak of the eye acceleration trace. Comparison of the three sets of traces shows that the relationship between eye acceleration and the visual component of simple-spike firing rate was relatively unaffected by how the eye velocity component

of firing rate was shifted in time. Regardless of whether eye velocity was shifted by -30, 0 or 30 ms, the peak in the visual component of simple-spike firing rate lagged the peak in eye acceleration by approximately 20 ms. Also, in each case, the transient increase in firing rate persisted beyond the transient increase in eye acceleration. The only differences caused by shifting the relative timing of simple-spike firing rate and eye velocity were the absolute values of the visual component of firing rate and the time at which the visual component began to increase. The earliest possible time of increase for the visual component, achieved when the eye velocity component was made to follow actual eye velocity, made the increase in simple-spike firing rate approximately coincident with the increase in eye acceleration.

The data shown in Fig. 4.23 suggest that simple-spike firing rate can be described as the sum of two signals, eye velocity and eye acceleration, after they have been appropriately scaled and shifted in time. We used a computer program to determine which scaling factors and temporal offsets provided the best match to the average simple-spike firing rate shown in Fig. 4.23. The program adjusted five parameters -- separate temporal shifts and scaling factors for the eye velocity and eye acceleration signals, and an offset. The offset was first adjusted to match the resting rate of the average simple-spike firing rate which, in this case, was 81.67 spikes/s. Then, using the Simplex algorithm, the program determined how eye velocity and acceleration should be scaled and shifted in time to minimize the squared error between the sum of the two processed signals and actual firing rate. The traces at the top of Fig. 4.24 show the results of this analysis and compare actual averaged simple-spike firing rate (solid line) with the sum of scaled and shifted eye velocity and eye acceleration (dashed line). The separate eye velocity and eye acceleration contributions to the fit are shown by the two traces at the bottom

of Fig. 4.24; the sum of these two traces equals the dashed trace above. To achieve this fit, eye velocity was scaled by 2.372 and eye acceleration was scaled by 0.189. These values reflect the average sensitivity of the 14 P-cells included in the average firing rate to eye velocity and eye acceleration, respectively. Furthermore, the fit was achieved by shifting eye velocity forward in time by 26 ms and by shifting eye acceleration backward in time by 30 ms.

We next extended this analysis to the average simple-spike firing rate recorded during pursuit of the same set of five target motions that were included in our analysis of the visual inputs to P-cells. The analysis was performed as described above, except that in addition to the data obtained during pursuit of a target moving at a constant velocity of 30 ^{o}/s, we also included data obtained during pursuit of targets moving at velocities of 5 ^{o}/s, with and without the motion transient, and during pursuit of targets that smoothly accelerated at rates of 80 and 180 $^{o}/s^2$. For each target motion, we considered only the firing rate recorded during pursuit in the preferred directions of the fourteen P-cells. The results of this analysis provided values for the scaling and temporal shifting of eye velocity (scale: 2.501, temporal shift: +22 ms) and eye acceleration (scale: 0.192, temporal shift: -24 ms), that were similar to those obtained for the single target motion considered in Fig. 4.24.

The values produced by the analysis were highly reproducible, but we were concerned that while the values might reflect the best solution, there might be other, quite different, combinations of values that produced results almost as good. For this reason, we repeated the analysis for the set of five target motions, but systematically assessed the quality of the fit produced at fixed temporal shifts of eye velocity and eye acceleration. For each combination of fixed temporal shifts, the Simplex method was used to

determine the best pair of scaling values. The quality of the fit for each combination was measured by calculating the correlation coefficient between the sums of the processed eye velocity and acceleration signals and the actual firing rates recorded during pursuit of each of the five target motions. For each pair of time shifts, we then calculated the average correlation coefficient for the set of five target motions.

The graph shown in Fig. 4.25 shows how the average correlation coefficient changed as a function of imposing fixed temporal shifts on the eye velocity and eye acceleration signals. The graph shows the results of 676 pairings of eye velocity and eye acceleration temporal shifts, covering a range of times from 50 ms preceding (+50) to 50 ms following (-50) actual eye velocity and acceleration. Each of the pairings is represented in the graph by a single box, 4 ms on a side, whose location along the abscissa is defined by the temporal shift of the eye velocity signal and whose location along the ordinate is defined by the temporal shift of the eye acceleration signal. The value of the average correlation coefficient is indicated by the gray level assigned to the interior of the box; darker areas indicate higher values of the average correlation coefficient, as indicated by the scale to the right of the graph.

The peak located in the lower right quadrant of the graph indicates that the highest correlation coefficients were obtained when the eye velocity component of firing rate preceded actual eye velocity by approximately 22 ms and when the eye acceleration component followed actual eye acceleration by about 24 ms. The absence of other peaks in the graph suggests that these time shifts represent the single best values. In particular, regardless of the time shift assigned to the eye velocity component of firing rate, the best time shift for the eye acceleration component always had a negative value.

We were also concerned that the results shown in Fig. 4.25 might be biased by the effects of averaging the data obtained from muliple P-cells. For example, if a minority of P-cells provided an early command for eye acceleration during pursuit, their contribution might be obscured after being averaged together with the firing rate obtained from other P-cells. For this reason, we repeated the analysis on the 14 individual P-cells which were used to produce the averages of simple-spike firing rate shown in Figs. 23 - 25. We started by examining the simple-spike firing rate recorded from the P-cell which showed the shortest latency with respect to the onset of eye motion at the initiation of pursuit. The traces in the upper half of Fig. 4.26 shows the average simple-spike firing rate recorded from this unit (solid lines), superimposed on three estimates of the eye velocity component (dashed lines). The estimates of the eye velocity component were obtained for this single P-cell in the same way that the estimates of the eye velocity component were obtained for the averages of P-cell activity shown in Fig. 4.23. The lower set of traces in Fig. 4.26 compare the three estimates of the visual component of simple-spike firing rate with eye acceleration.

Unlike the data shown for the average simple-spike firing rate obtained from 14 P-cells shown in Fig. 4.23, the visual component of the simple-spike firing rate for the single P-cell shown in Fig. 4.26 did not show a single clear peak. It was therefore difficult to compare the time of the peak in the visual component to the peak in eye acceleration. However, as was seen in the averaged data from the 14 P-cells, the increase in the visual component continued beyond the increase in eye acceleration. Also, regardless of how the eye velocity component was shifted in time, the earliest increase in the visual component was approximately coincident with the increase in eye acceleration.

We next examined the simple-spike firing recorded from this P-cell during pursuit of each of the five target motions. As was done for the firing rate averages from the 14 P-cells, we used a program to determined the best values for the time shifts and scaling factors for the eye velocity and eye acceleration signals. The results of this analysis provided values for the scaling and temporal shifting of eye velocity (scale: 2.374, temporal shift: +29 ms) and for the scaling of eye acceleration (scale: 0.166), that were similar to those obtained for the firing rates pooled from all 14 P-cells. The value determined for the temporal shift of eye acceleration indicated that the firing rate of this P-cell slightly preceded actual eye acceleration (temporal shift: +5 ms).

We repeated this analysis for each of the 14 P-cells that were used to generate the averaged data shown in Figs. 23 - 25. For each P-cell, we allowed the program to determine the best values for both the scaling factors and the time shifts applied to both the eye velocity and eye acceleration signals. The results of this analysis are shown in Fig. 4.27. Each square indicates the pair of temporal shifts that produced the highest correlation between the sum of the processed eye velocity and acceleration signals and the actual firing rate recorded from the P-cell. Most of the data points are located in the right lower quadrant, indicating that the highest correlations were obtained when the eye velocity component preceded physical eye velocity and the eye acceleration component followed physical eye acceleration. The average values of the temporal shifts were +23 ms for they eye velocity component and -25 ms for the eye acceleration component, nearly identical to the values obtained when the analysis was applied to the average data. However, the correlation coefficients obtained when the analysis was applied to single P-cells were

much lower (range: 0.293 - 0.951, mean: 0.743) than when the anlaysis was applied to the average of the 14 P-cells (0.957).

Discussion

We have provided new evidence that P-cells in the flocculus and ventral paraflocculus of the monkey encode visual signals used for pursuit eye movements. First, we have demonstrated that the simple-spike firing rate of P-cells can be accounted for as the sum of eye velocity and visual motion signals used for pursuit. Second, we have shown that the amplitude of the visual responses on P-cells changes in parallel with the amplitude of eye acceleration at the initiation of pursuit. These results suggest that the visual signals exhibited by floccular P-cells are the same visual signals that provide commands for smooth eye movements during pursuit.

Properties of Purkinje cells in the primate flocculus

The first studies of the primate flocculus recognized the convergence of eye velocity, head velocity, and visual signals and suggested that the output of the flocculus may provide a neural signal encoding target velocity (Miles and Fuller 1975). It was subsequently shown that the firing rate of P-cells in the flocculus reflects intrinsic signals related to movements of the eye and head, rather than an extrinsic signal like target velocity. The modulation in simple-spike firing rate during eye and head movements of the same amplitude is approximately equal and the effects of the two signals sum linearly (Lisberger and Fuchs 1978, Miles et al. 1980, Stone and Lisberger 1990). Most floccular P-cells can therefore be identified as "gaze-velocity" cells, since they encode the velocity of changes in gaze accomplished with any combination of eye and head movements.

The additional identification of visual signals on floccular P-cells (Noda and Warabi 1987, Stone and Lisberger 1990) suggested that the flocculus plays an important role as part of the interface between the sensory and motor systems used for smooth pursuit and optokinetic eye movements. The presence of transient visual signals on floccular P-cells indicates that a specific functional term like "gaze velocity" might be replaced with a more general term, such as "visual tracking" P-cells (Miles 1990). In addition, the firing rate of floccular P-cells does not always encode gaze velocity. For example, when presented with the motion of a large-field visual stimulus, primates show nystagmic eye movements consisting of slow eye movements in the direction of the motion of the stimulus and quick resetting eye movements in the opposite direction. Initially, the firing rate of floccular P-cells is modulated during the slow phases of eye movements in a manner that reflects gaze velocity. However, after many seconds of stimulation, the modulation of floccular P-cells wanes, although the smooth eye movements continue. This reduction in the modulation of floccccular P-cells is believed to reflect the complementarity between the functions of the cerebellar flocculus and the neurons in the vestibular nuclei to which the flocculus projects (Buttner and Waespe 1984; Waespe et al. 1981, 1985).

The data presented in the present chapter focus on the possible role of the visual signals on floccular P-cells during the generation of pursuit eye movements. The P-cells in our experiments were identified by their sensitivity to eye velocity and, in the case of horizontal P-cells, by their approximately equal sensitivity to head velocity. In this discussion, we will concentrate on two questions concerning the visual signals recorded from floccular P-cells. Are the visual signals the same signals that are used to

provide inputs for pursuit? What functional role do these visual signals play in the generation of pursuit eye movements?

Use of distributed networks as an analysis tool

We have used a distributed network to analyze the averages of simple-spike firing rate recorded from P-cells during the performance of smooth pursuit eye movements. Network models have been used before to examine the relationship between the activity of single neurons and the performance of specific behaviors or functions (Zipser and Anderson 1988ab, Anderson and Zipser 1988, Lockery et al. 1989, Anastasio and Robinson 1989). In these previous studies, the network was trained to reproduce a facsimile of the function which was believed to involve the neurons under study. After the network was trained, the "hidden units" nested between the input and the output layers of the network were observed to possess properties that were qualitatively similar to the actual neurons. The similarity between the properties of the units in the model and the properties of the neurons was taken as evidence that the neurons may be part of a biological network that implements an algorithm similar to that employed by the network model.

Our use of distributed network models is very different. First, the network was not designed to reproduce a behavior, but was designed to replicate the time-varying averages of firing rate recorded from individual P-cells. Second, the hidden units in our model did not have the freedom to express novel properties -- they were hard-wired so that adjusting the weights of their connections simply scaled the amplitudes of the input signals and shifted the input signals in time. For these reasons, our use of a distributed network model is not very different from the use of other nonlinear optimization procedures. The advantage of using a distributed network is that the model has great flexibility in determining the best set of weights for

each neuron. The model was therefore able to design a unique nonlinear relationship between each input signal and the firing rate of each P-cell.

The primary disadvantage of the analysis we have performed is that it is model-dependent. The strength of our conclusions concerning the representation of visual and oculomotor signals in the simple-spike firing rate is tied to the strength of the model used in the analysis. The particular signals included as inputs to the network model were chosen because those same signals are able to describe the behavior of the entire system. However, if future results indicate that these signals are not used for pursuit in the manner described by our model, then the present analysis will need to be reevaluated. In addition, it is possible that even if these signals are used for pursuit, the particular manner in which they have been described in the model may have been inadequate to fully document their contribution. For example, the signal representing the image motion transient in the network model only approximately resembles the signal identified in our behavioral experiments (chapter one). Also, the eye velocity signal in the model was assumed to contribute to P-cell firing rate with no delay. If there is a delay in the contribution of eye velocity, then we have systematically underestimated the magnitudes of the visual contributions to firing rate. For these reasons, we present these results not as a quantitative documentation of the signals encoded by P-cells, but as a demonstration of how P-cell firing rate can be described with signals important for pursuit.

Visual signals observed on Purkinje cells in the flocculus and ventral paraflocculus

Previous experiments have shown that while P-cells in the flocculus and ventral paraflocculus show only modest responses during passive presentation of moving visual stimuli, they show robust responses if the

moving stimulus is the object of a pursuit eye movement. Only a minority of P-cells can be appreciably modulated by the motion of a large-field visual stimulus (Noda and Warabi 1987, Stone and Lisberger 1990) or the motion of a small spot (Stone and Lisberger 1990), presented while the monkey is required to fixate a stationary target. In contrast, large responses are evoked when the monkey is required to track a target, initially at rest, that then moves at a constant velocity (Stone and Lisberger 1990). Although the simple-spike activity recorded in this situation also reflects the sensitivity of the P-cells to eye velocity, the increase in firing rate occurs too early and is too large to be produced by inputs conveying eye velocity information. The large increase in simple-spike firing rate occurs approximately 100 ms after the onset of target motion, consistent with a latency produced by visual pathways through the cerebral cortex. Stone and Lisberger (1990) therefore suggested that the transient pulse in simple-spike firing rate exhibited by P-cells at the initiation of pursuit encodes visual signals used for pursuit eye movements (Stone and Lisberger 1990).

The data presented in this chapter substantiate the idea that the visual signals on floccular P-cells are related to signals used for pursuit. We have demonstrated that it is possible to describe the time-varying averages of P-cell simple-spike firing rate recorded during pursuit eye movements as the sum of eye velocity and three visual motion signals. The three visual motion signals used in our description of P-cell firing rate are the same signals that we identified in chapter one as underlying the initiation of pursuit. Furthermore, as we have shown in chapter two, a model that includes these three visual signals is able to reproduce several distinctive features of eye velocity produced during smooth pursuit. The demonstration that the firing rate of P-cells in the flocculus can be described as the sum of these particular

visual signals and eye velocity is consistent with the suggestion that the visual signals encoded by floccular P-cells are important for pursuit eye movements. In addition, our analysis indicates that each of the visual signals used for pursuit eye movements is present in the output of the flocculus.

Further evidence that the visual signals observed on P-cells are used for pursuit is provided by the parallel changes observed in the size of the transient visual responses on P-cells and the amplitude of the eye acceleration at the initiation of pursuit. In behavioral experiments with monkeys, measurements of the eye accelerations evoked by different target motions have been used to assess the properties of the visual signals that provide inputs for pursuit. One finding from these studies is that the eye acceleration observed during pursuit depends upon the direction and the retinal location of the moving target. The largest eye accelerations for a given amplitude of target motion is evoked when the target is initially placed approximately 3 degrees eccentric and then moves toward the fovea (Lisberger and Westbrook 1985, Lisberger and Pavelko 1989). The bias for motion directed toward the fovea is present regardless of the direction in which the eye moves, and is believed to reflect a property of motion processing in the visual pathways underlying pursuit. In the present experiments, we have shown that a similar bias is exhibited by the transient visual responses of floccular P-cells. This shared bias suggests that the visual signals on floccular P-cells originate from a source that is shared with the visual signals underlying pursuit.

The role of the flocculus in generating pursuit eye movements

As reviewed in the introduction, floccular P-cells are believed to play two distinct functions in the generation of smooth pursuit eye movements. First, through its reciprocal connections with nuclei in the brainstem, activity in the flocculus is believed to represent a motor command encoding eye

velocity for pursuit eye movements. Second, as suggested by the data and interpretation of Stone and Lisberger (1990), the transient activity of floccular P-cells represents a visually-derived command for eye acceleration during pursuit. The results presented in this chapter suggest a few amendments to this general scheme.

Our examination of the simple-spike activity of P-cells at the termination of pursuit provides new information about the organization of the eye velocity feedback used for pursuit. In particular, our data suggest that eye velocity feedback for pursuit requires the synergistic action of the pair of laterally-placed flocculi. P-cells in one flocculus display a greater sensitivity to both visual motion and eye movements directed to the same side as the recording site. The functional implication of this asymmetry is that the output of one flocculus displays both a transient overshoot and sustained increase in activity during pursuit in one direction, but a smaller sustained decrease with no transient overshoot during pursuit in the other direction. In order for the flocculus to provide a signal that is symmetric for pursuit in both directions, the outputs from the two flocculi need to be combined.

Our analysis of the temporal relationship between the visual component of P-cell simple-spike firing rate and eye acceleration suggests a reconsideration of the idea that the visual signals on P-cells represent commands for eye acceleration. As noted previously (Stone and Lisberger 1990), the latency of P-cell responses during pursuit indicates that the flocculus does not contribute to the earliest acceleration of the eye. The analysis presented in this chapter confirms this idea. Regardless of the delay associated with the eye velocity component of simple-spike firing rate, the visual component occurs too late to drive the first changes in eye velocity at the initiation of pursuit. Furthermore, our analysis cannot exclude the

possibility that none of the eye acceleration observed during pursuit is driven by the output from the flocculus. The salient feature of our analysis in this regard was the observation that both the peak and the decline in P-cell simple-spike activity followed the acceleration of the eye by approximately 25 ms. Therefore, the most parsimonious interpretation of our results is that the flocculus provides only a component of the command to accelerate the eye, the possibility suggested by Stone and Lisberger (1990). However, our data are also consistent with the alternate interpretation that none of the command for eye acceleration during pursuit is provided by the flocculus and that the visual signals for pursuit observed on floccular P-cells are corollary signals used to update the activity in the loop implementing eye velocity feedback.

In summary, our results indicate that the flocculus encodes visual signals used for pursuit and may provide an important, but incomplete, command for smooth pursuit eye movements. Consistent with these results, ablation of the flocculus and paraflocculus causes severe deficits in smooth pursuit (Takemori and Cohen 1974, Zee et al. 1981), but total cerebellectomy is required to completely abolish pursuit (Westheimer and Blair 1973). It would therefore be informative to investigate the activity of neurons in other regions of the cerebellum and brainstem implicated in the generation of pursuit. In particular, the use of target motions like those used in the present chapter would facilitate the examination of how the components of the command for pursuit are parsed among the participating brain structures.

Figure 4.1 Schematic diagram of neural pathways for pursuit eye movements. A: Outline of major pathways underlying the generation of pursuit eye movements. The boxes represent general regions of the brain which consist of more specific areas, as labelled inside each box. Abbreviations used: LGN, lateral geniculate nucleus; V1, primary visual cortex; MT, middle temporal area; MST, medial superior temporal area; FEF, frontal eye fields; LPN, lateral pontine nucleus; DLPN, dorsolateral pontine nucleus; DMPN, dorsomedial pontine nucleus; PT, pretectal nuclei; AOS, accessory optic system; retic. nuc., reticular nuclei; NOT, nucleus of the optic tract; LTN, lateral terminal nucleus; NRTP, nucleus reticularis tegmenti pontis; PARAFLOCC., paraflocculus; VN, vestibular nuclei; NPH, nucleus prepositus hypoglossi; FN, fastigial nucleus; MN, ocular motor neurons. Not all projections between the labelled structures are included in the diagram. For example, the direct projection from the retina to the NOT and LTN has been omitted for clarity. Most feedback projections have also been omitted. B: Schematic diagram summarizing a current view of how the cerebellar flocculus participates in generating pursuit eye movements. Abbreviations used: $\dot{I}$, image velocity; $\dot{E}$, eye velocity; $\ddot{E}$, eye acceleration. Other inputs not directly related to the generation of smooth pursuit, such as mossy fibers conveying head velocity signals, have been omitted for clarity.

Fig. 4.1

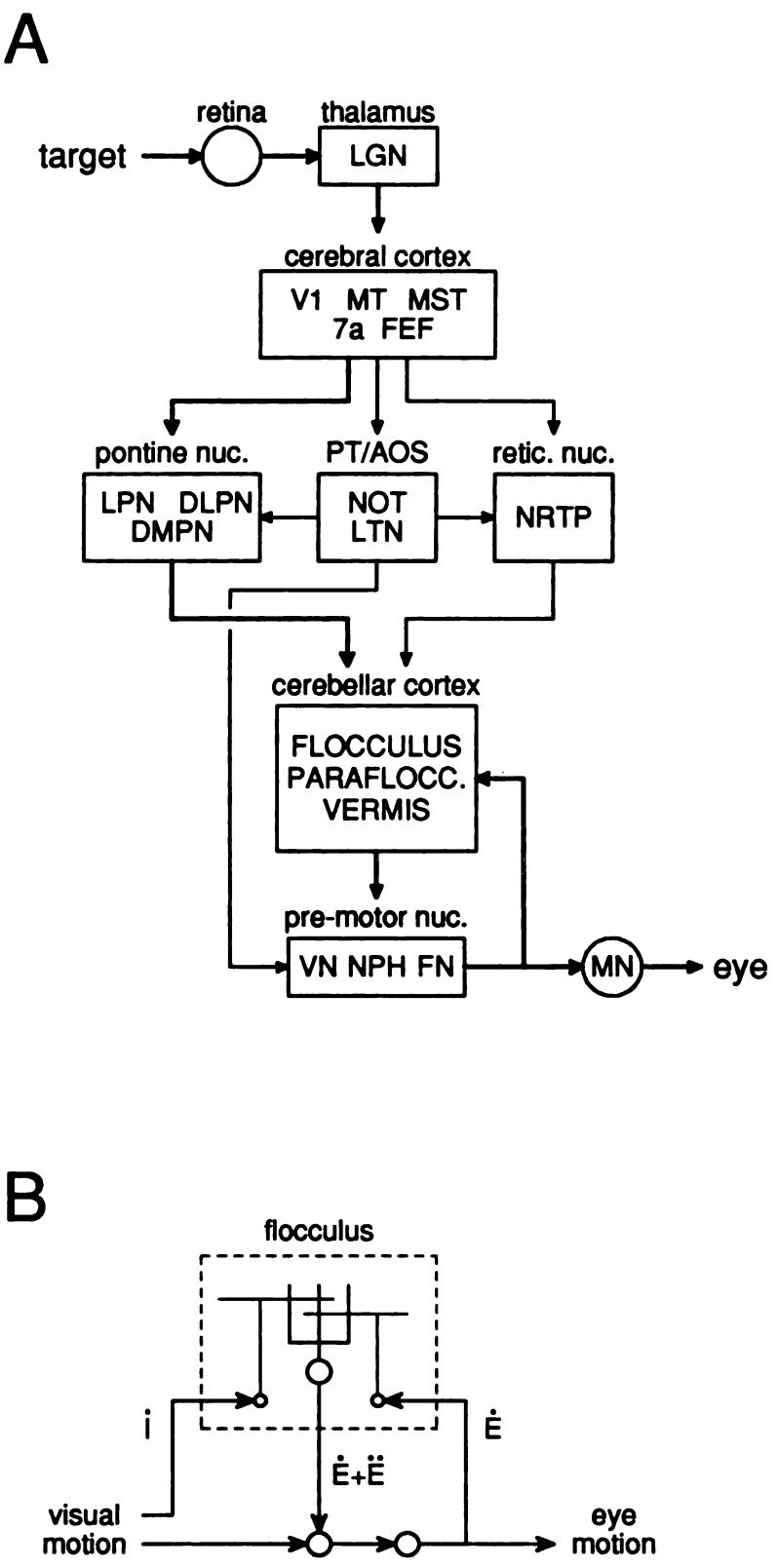
A
retina
thalamus
target
LGN
cerebral cortex
V1 MT MST
7a FEF
pontine nuc.
PT/AOS
retic. nuc.
LPN DLPN
DMPN
NOT
LTN
NRTP
cerebellar cortex
FLOCCULUS
PARAFLOCC.
VERMIS
pre-motor nuc.
VN NPH FN
MN
eye
B
flocculus
i
Ė
Ė+Ë
visual
motion
eye
motion

Figure 4.2 The three target motions used to identify visual signals on P-cells. Each column shows one type of target motion. The different target motions produced different combinations of eye velocity and three visual motion signals. In each case, the monkey initially fixated a central spot (not shown) until an eccentric target (0.5^{o} white spot) began to move. A: The target was visible and stationary for 300 to 500 ms at an eccentric position before it moved at a constant velocity. This variation of the step-ramp paradigm introduced by Rashbass (1961) produces all three signals contained in our behavioral model: image velocity, an image motion transient, and image acceleration. B: The target moved at a constant velocity but was not visible before the onset of its motion. The temporal coincidence of the target's appearance and its motion eliminates the motion transient signal present in A. C: The target accelerated smoothly from rest before achieving a constant velocity. Measured variables (firing rate, target and eye position and velocity) are shown as solid lines, while derived variables (image velocity, image motion transient, and image acceleration) are shown as dashed lines.

Fig. 4.2

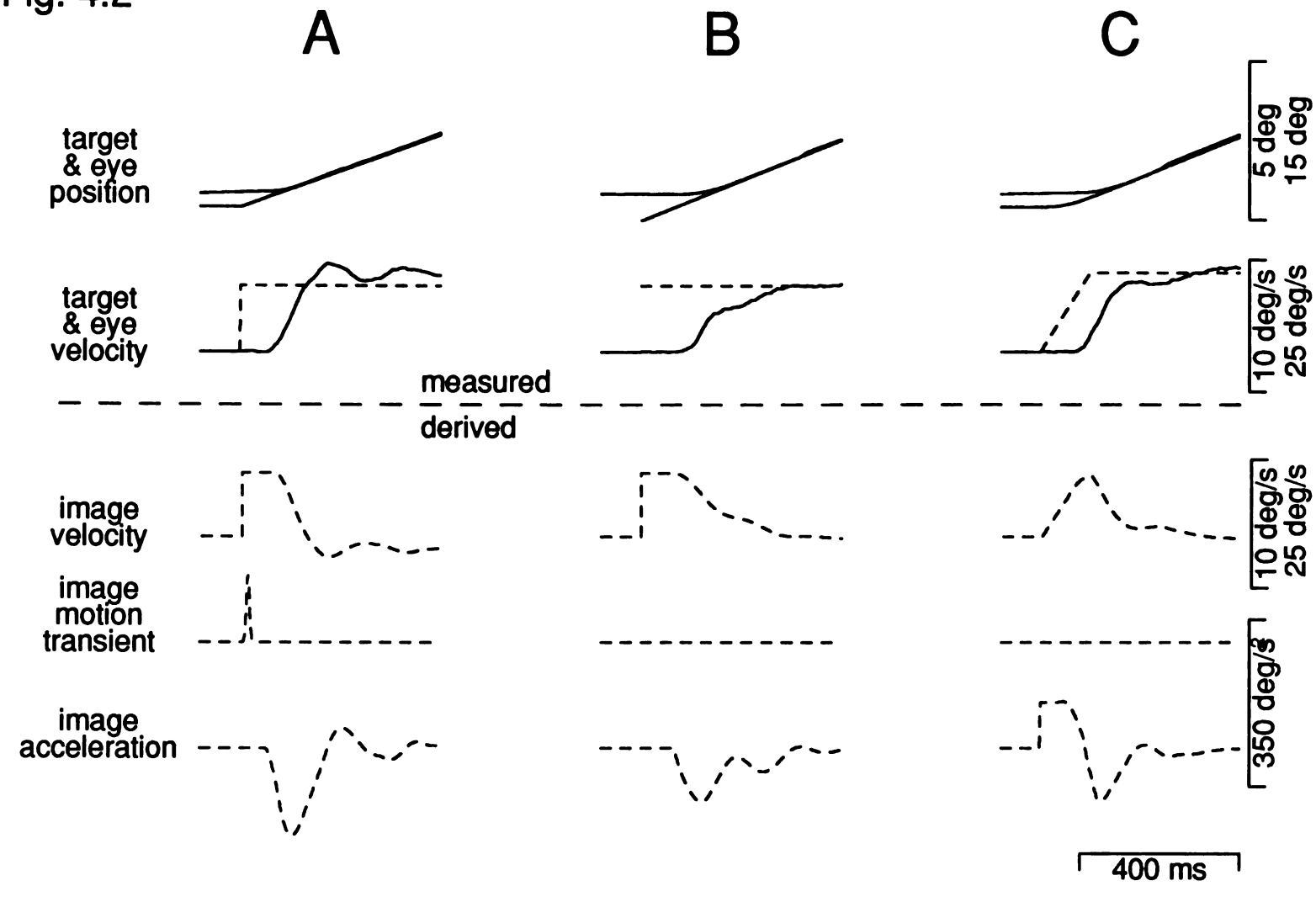
A
B
C
target & eye position
5 deg
15 deg
target & eye velocity
10 deg/s
25 deg/s
measured
derived
image velocity
10 deg/s
25 deg/s
image motion transient
350 deg/s
image acceleration
400 ms

Figure 4.3 Examples of responses recorded from P-cells during pursuit. Each column shows the averaged firing rate recorded during pursuit of one target motion, as indicated by the icon at the head of the column. For data shown in the first column, the target appeared already moving at $5^{o}/s$. In the second and third columns, the target was initially stationary and then moved at 5 and 30 $^{o}/s$, respectively. In the fourth and fifth columns, the target accelerated smoothly from rest at 80 and 180 $^{o}/s^{2}$. Each row shows the data obtained from one P-cell during pursuit in the preferred direction of the neuron.

Fig. 4.3

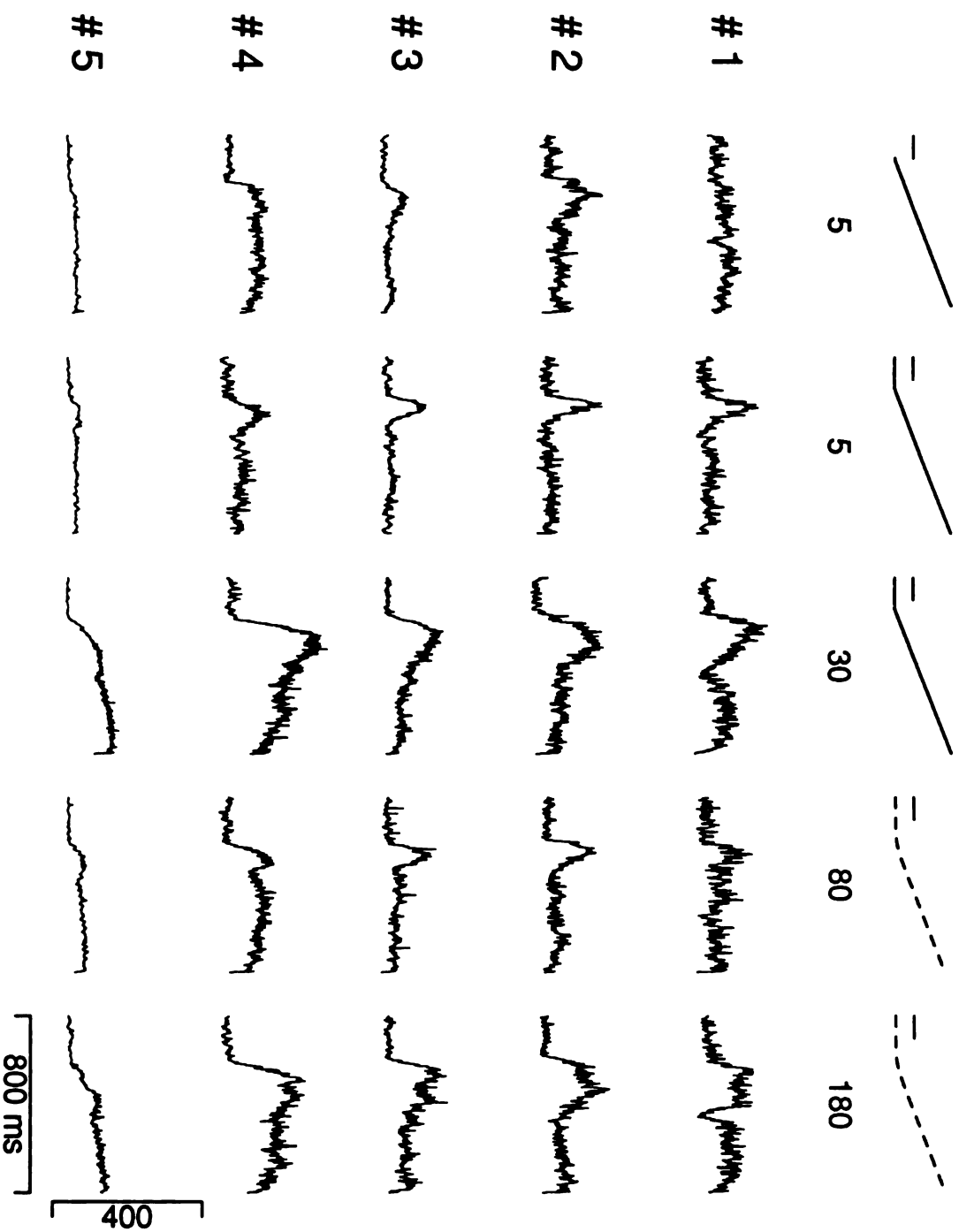

Figure 4.4 Sample fit of model to data from one P-cell. Each column shows the results for one target motion, using the same convention as shown in Fig. 4.3. The top set of five rows show the results during pursuit in the preferred direction of the P-cell; the bottom set of five rows show the results for the non-preferred direction. Within both sets the top pair of traces compare the actual average simple-spike firing rate (noisy trace) with the output of the model (smoother trace). The bottom four traces in each set show the activity of the output units in each of four networks, before being summed at the final unit. Data were obtained from unit ul1203b. Abbreviations used: FR, firing rate; $\dot{I}$, image velocity; $\dddot{I}$, image motion transient; $\ddot{I}$, image acceleration; $\dot{E}$, eye velocity.

Fig. 4.4

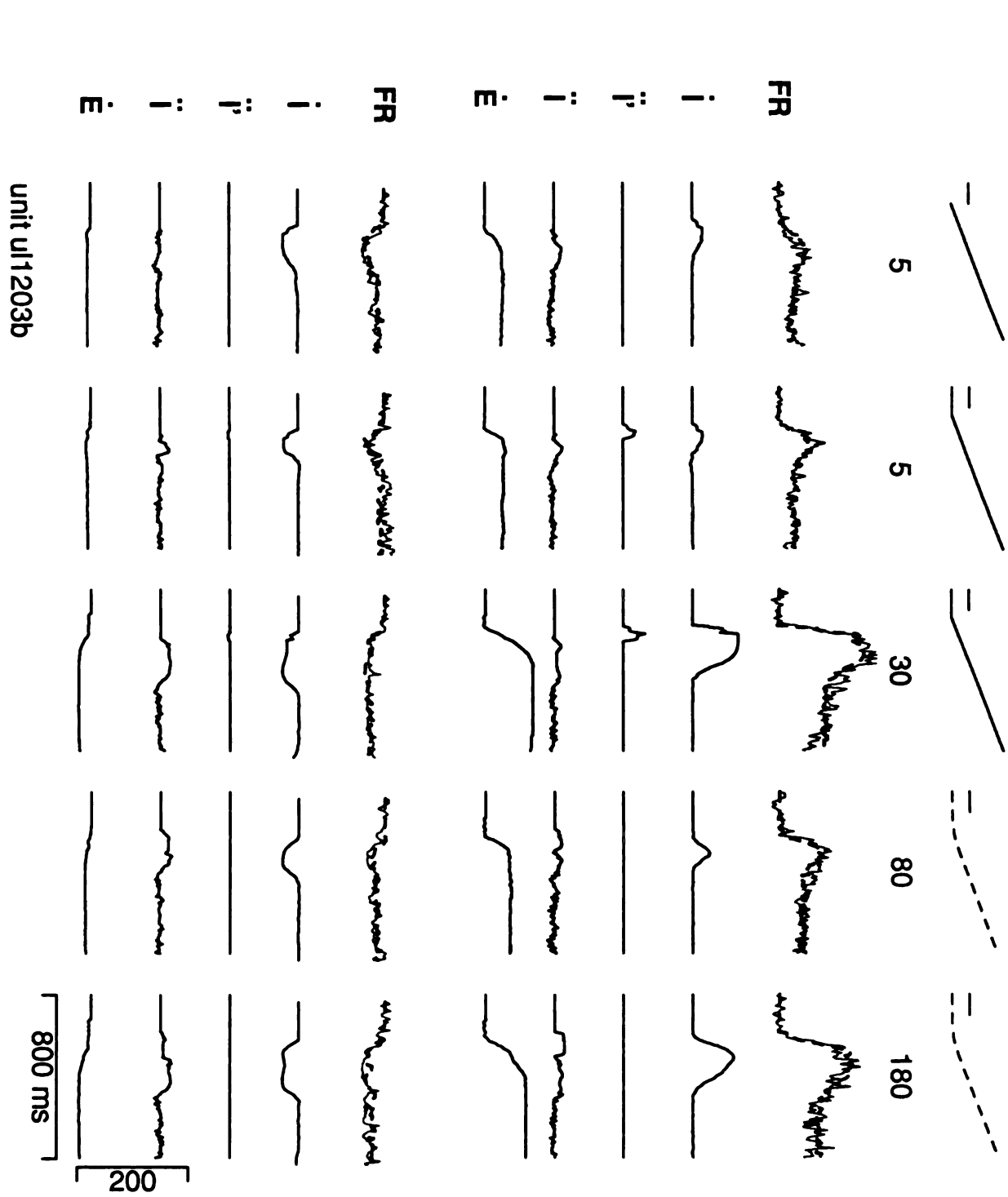

Figure 4.5 Distribution of standard errors.

Fig. 4.5

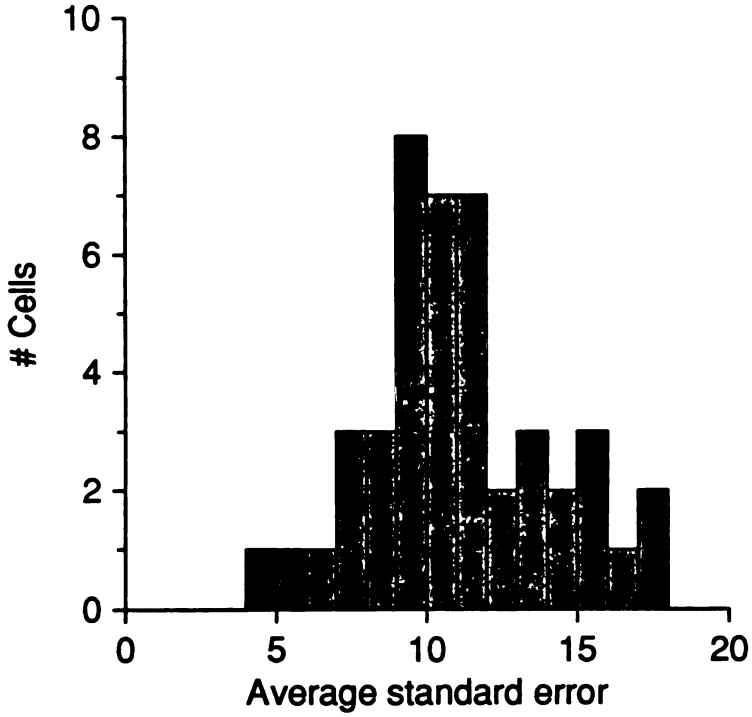

Figure 4.6 Analysis of functions described by networks in the model. Each column shows the results of analyzing one of the four networks. Abbreviations are same as those used in Fig. 4.4. Vertical dashed lines indicate 600 ms after onset of simulation, the point in time used to measure the steady-state output of each of the four networks.

Fig. 4.6

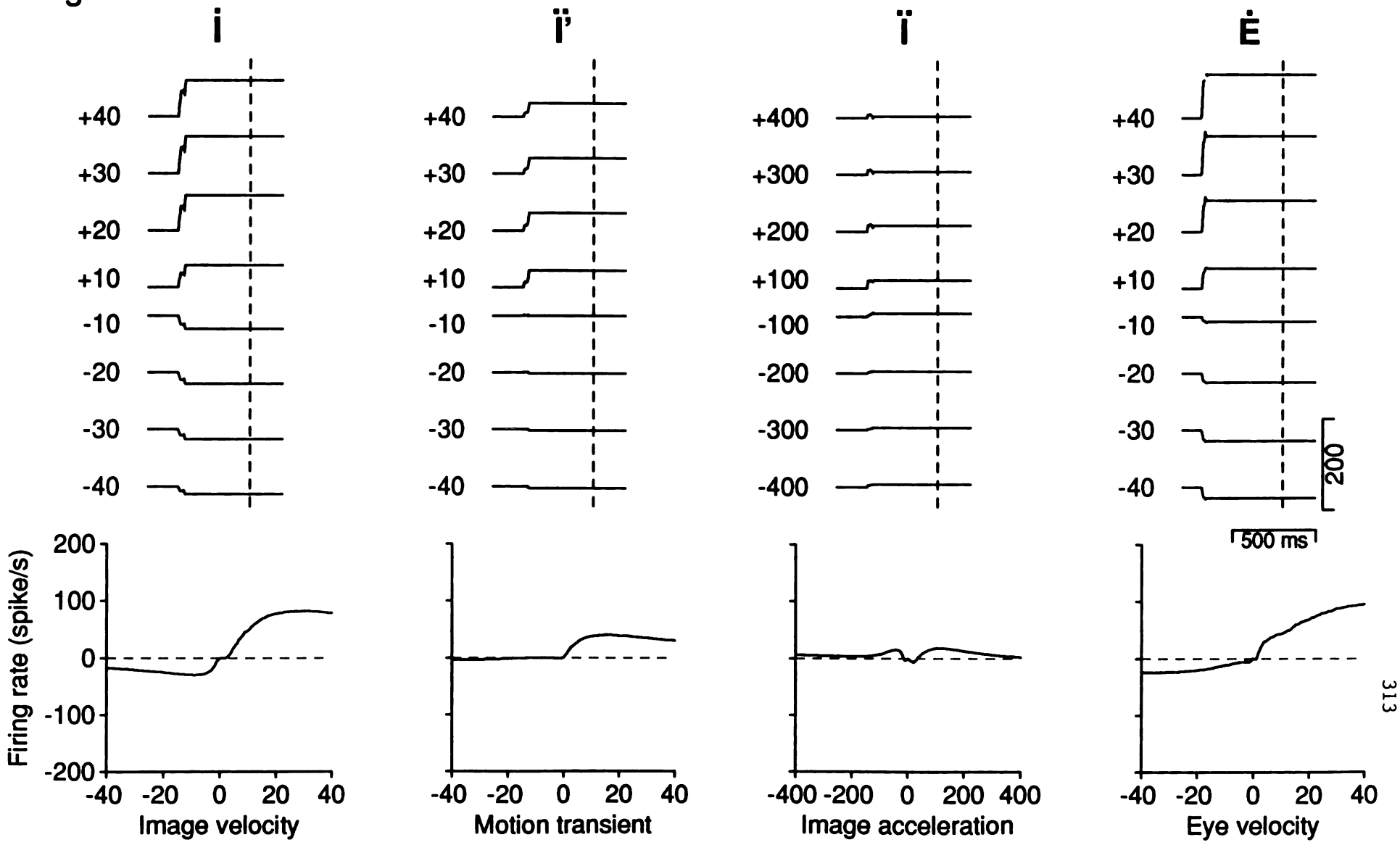
İ
ï'
ï
Ė
+40
+30
+20
+10
-10
-20
-30
-40
+400
+300
+200
+100
-100
-200
-300
-400
200
500 ms
Firing rate (spike/s)
200
100
0
-100
-200
-40 -20 0 20 40
Image velocity
-40 -20 0 20 40
Motion transient
-400 -200 0 200 400
Image acceleration
-40 -20 0 20 40
Eye velocity

Figure 4.7 Results of repeating analysis of unit ul1203b several times.

Fig. 4.7

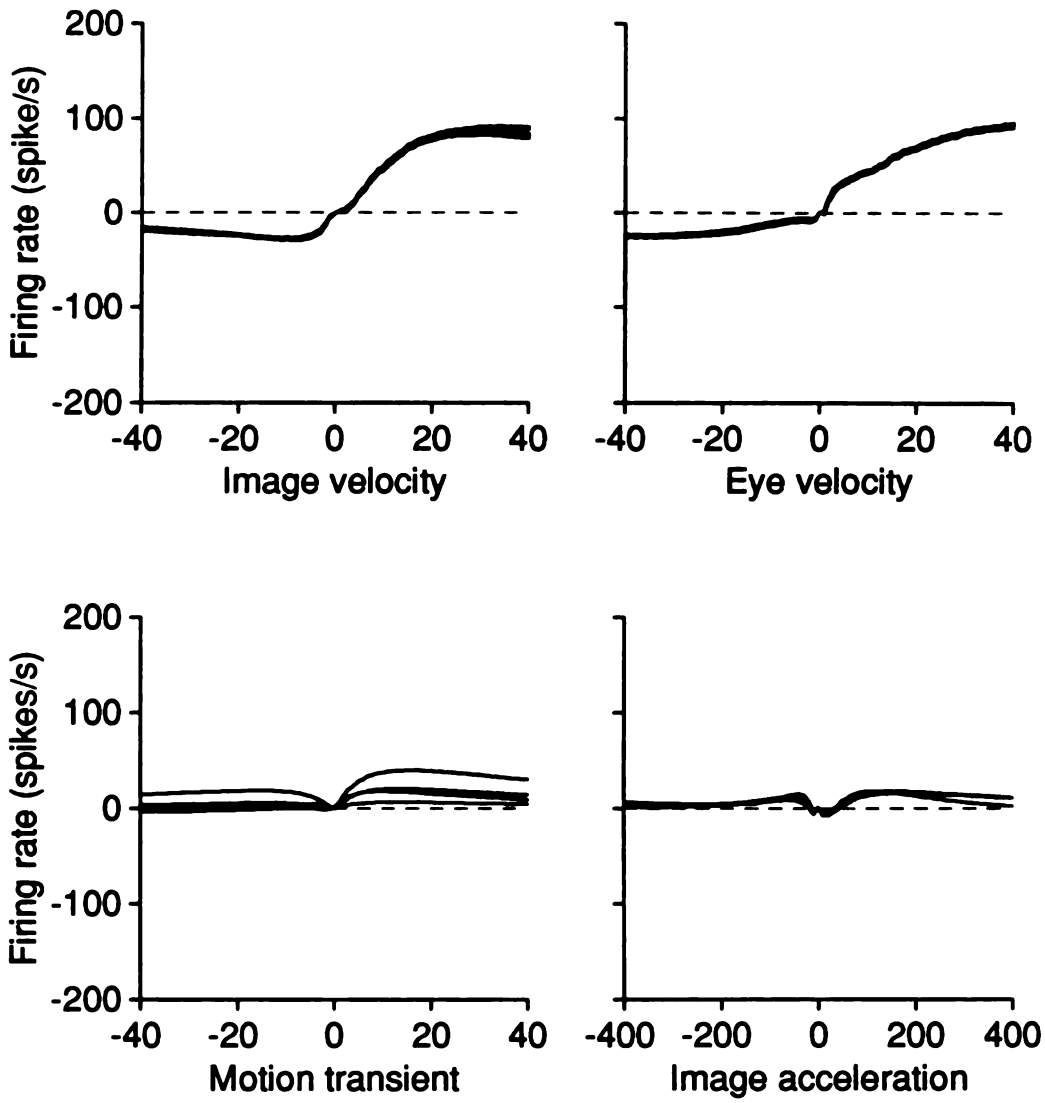
200
100
0
-100
-200
Firing rate (spike/s)
-40
-20
0
20
40
Image velocity
-40
-20
0
20
40
Eye velocity
200
100
0
-100
-200
Firing rate (spikes/s)
-40
-20
0
20
40
Motion transient
-400
-200
0
200
400
Image acceleration

Figure 4.8 Relative frequency of occurrence of each of the four input signals to the model. Histograms are based on data obtained from monkey O while recording from P-cells on two separate days. Dark bars indicate data obtained during horizontal pursuit; gray bars indicate vertical pursuit.

Fig. 4.8

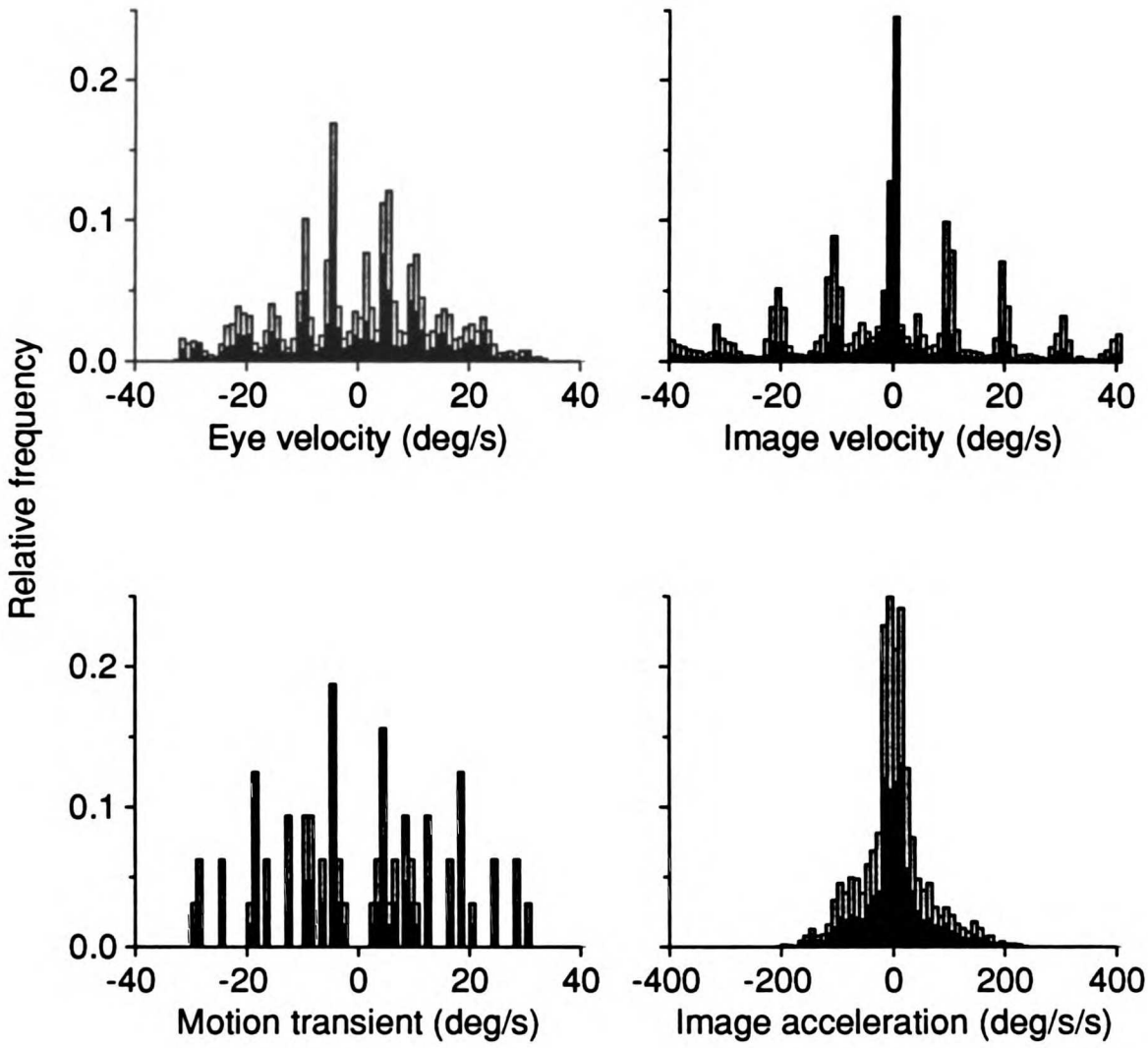
Relative frequency
0.2
0.1
0.0
-40
-20
0
20
40
Eye velocity (deg/s)
Image velocity (deg/s)
Motion transient (deg/s)
-400
-200
200
400
Image acceleration (deg/s/s)

Figure 4.9 Distribution of sensitivities to the four input signals. Filled bars: values obtained during pursuit in the preferred direction of each P-cell. Open bars: values obtained for the non-preferred direction.

Fig. 4.9

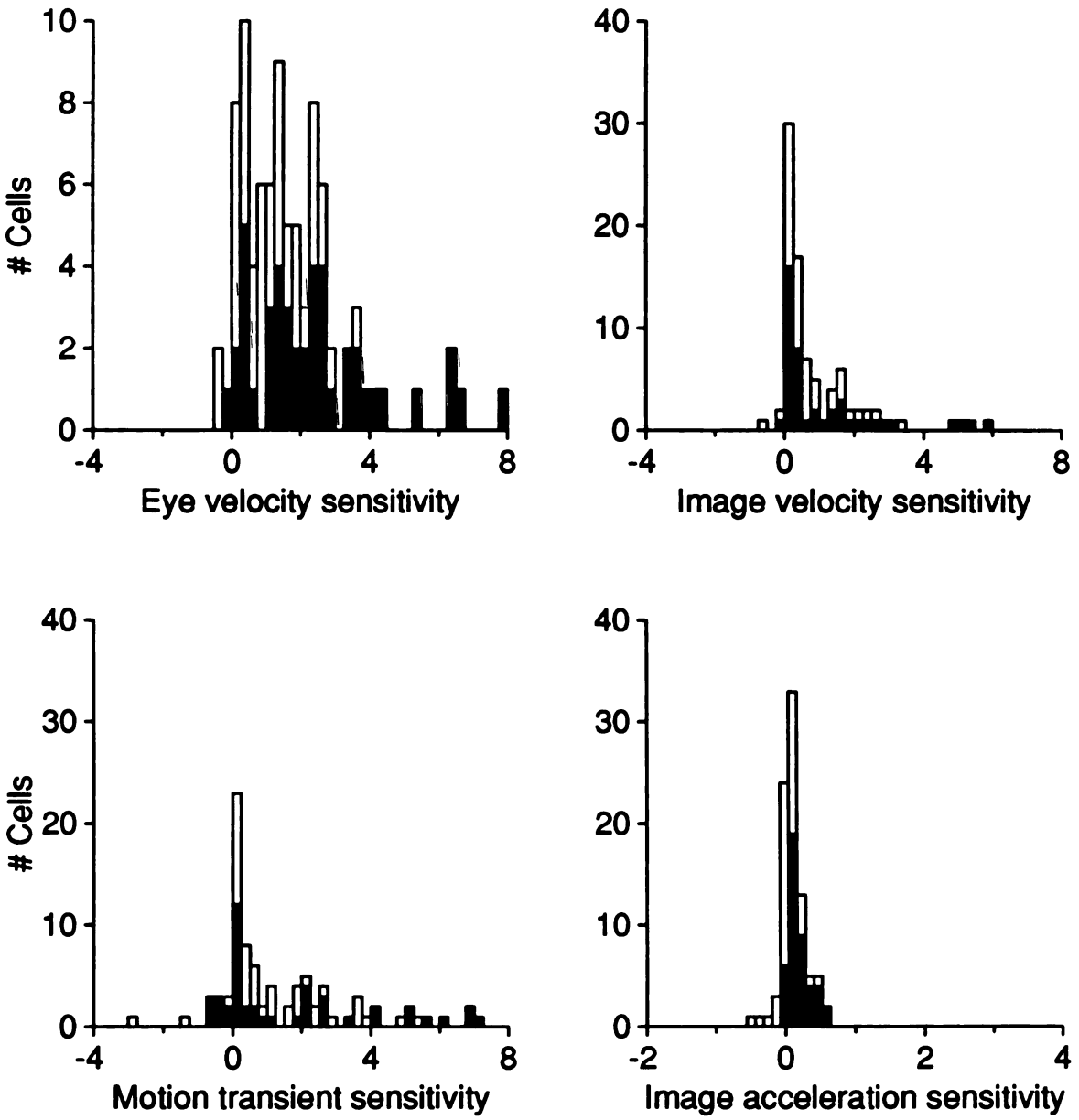
Cells
Eye velocity sensitivity
Image velocity sensitivity
Motion transient sensitivity
Image acceleration sensitivity

Figure 4.10 Correlations between sensitivities to the four input signals. Open circles: values obtained during pursuit in the preferred direction of each P-cell. Open triangles: values obtained for the non-preferred direction.

Fig. 4.10

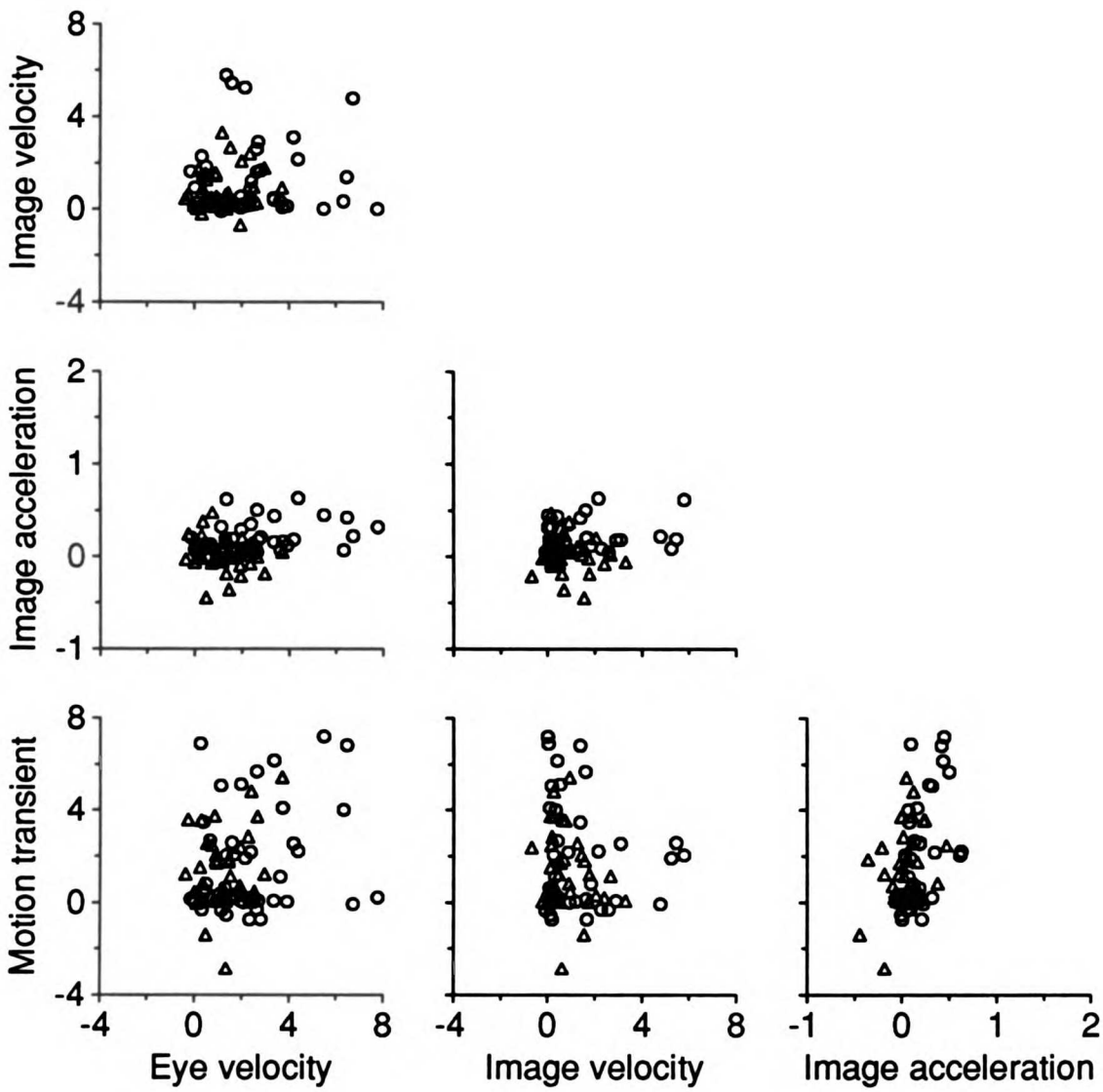
Image velocity
Image acceleration
Motion transient
8
4
0
-4
2
1
0
-1
-4
0
4
8
-1
0
1
2
Eye velocity
Image velocity
Image acceleration

Figure 4.11 Continuum in the representation of eye velocity and visual motion signals. P-cells were placed in one of four groups based upon the total modulation of their simple-spike firing rate during the set of trials (0 - 60, 60 - 100, 100 - 160, or > 160 spikes/s). P-cells in the four groups are distinguished by different shadings in the histogram to the left and by differently sized circles in the scatterplot to the right.

Fig. 4.11

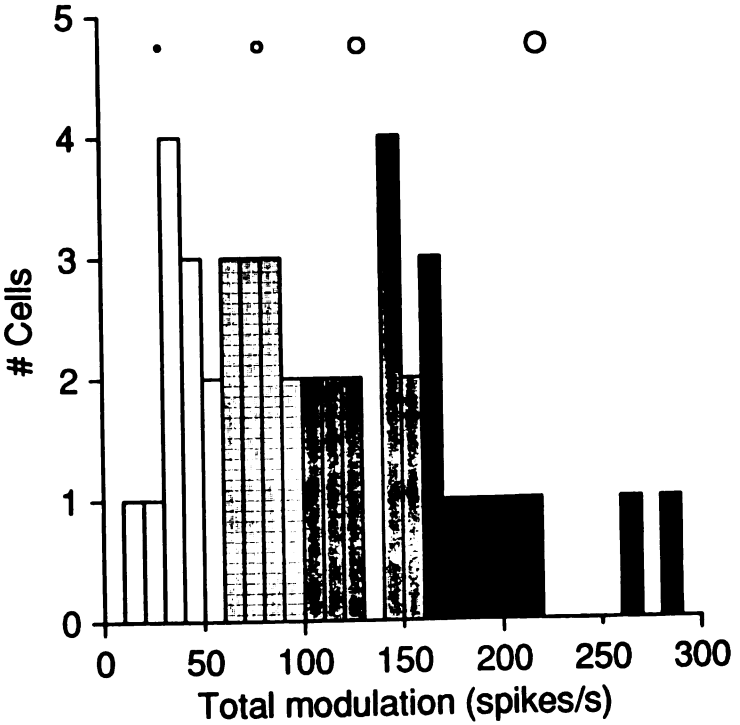
5
4
3
2
1
0
Cells
0
50
100
150
200
250
300
Total modulation (spikes/s)

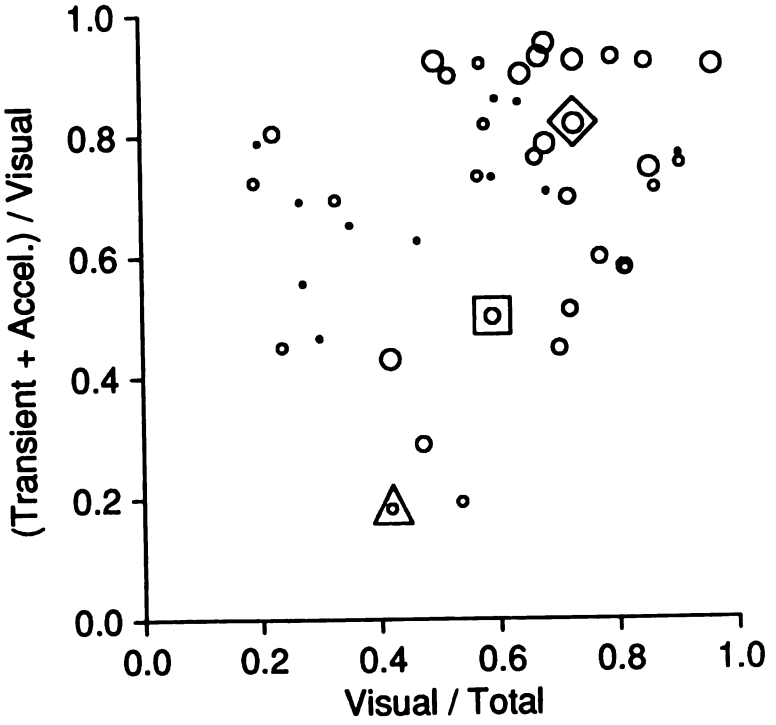
1.0
0.8
0.6
0.4
0.2
0.0
(Transient + Accel.) / Visual
0.0
0.2
0.4
0.6
0.8
1.0
Visual / Total

Figure 4.12 Fit of the model to data from P-cell os0917b. Each column shows the results for one target motion, using the same conventions as shown in Fig. 4.4.

Fig. 4.12

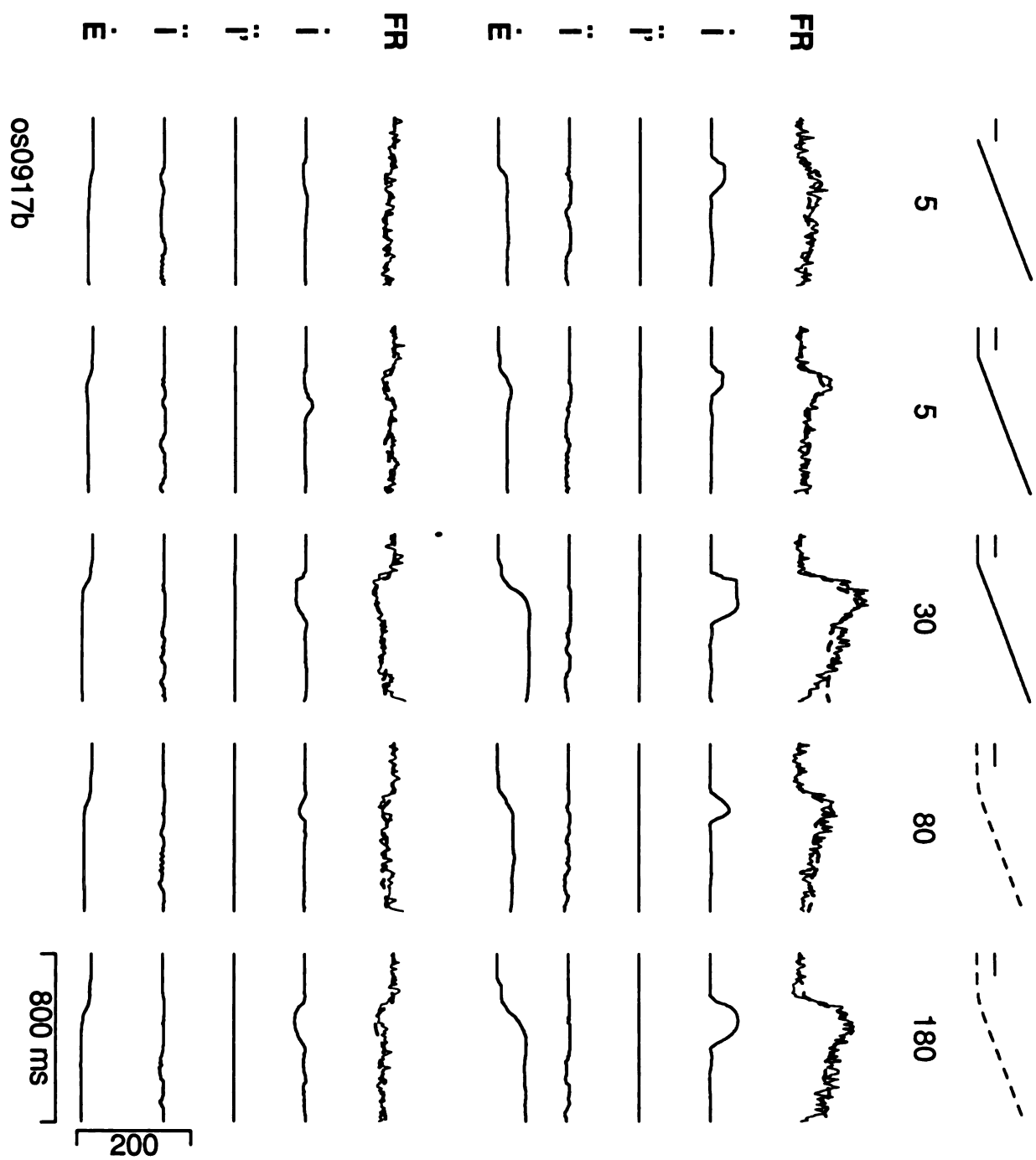

Figure 4.13 Fit of the model to data from P-cell os0629. Each column shows the results for one target motion, using the same conventions as shown in Figs. 4.12 and 4.4.

Fig. 4.13

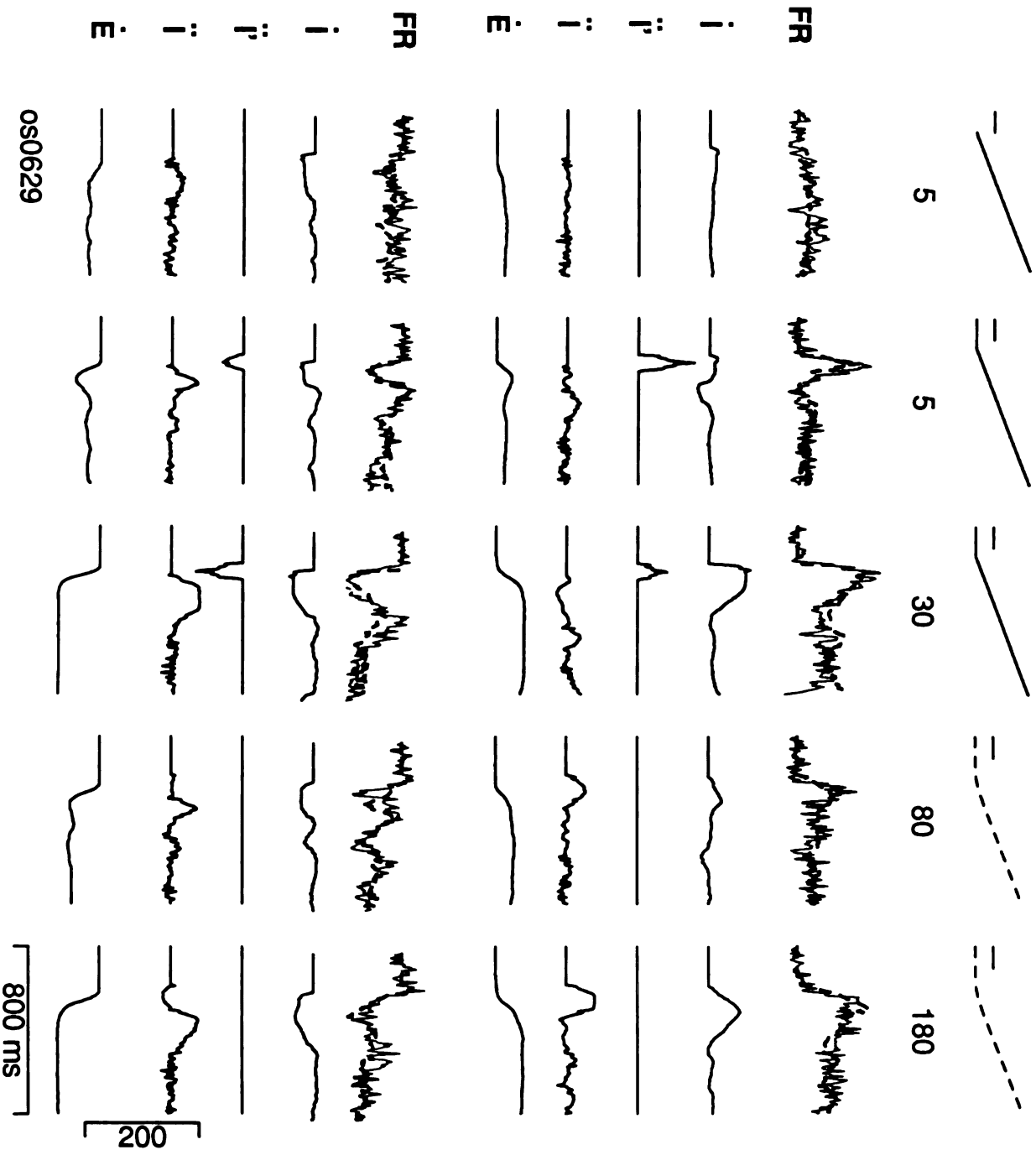

Figure 4.14 Relationship between sensitivities to visual motion signals and sensitivities to eye and head velocity. A: Scatterplot showing sensitivity to eye velocity plotted as a function of sensitivity to head velocity. Dashed line indicates slope of one. B: Index of visual sensitivity plotted as a function of index of relative sensitivity to eye velocity. Dashed vertical line indicates value of 0.5, which indicates the case in which the sensitivities to eye and head velocity are exactly equal.

Fig. 4.14

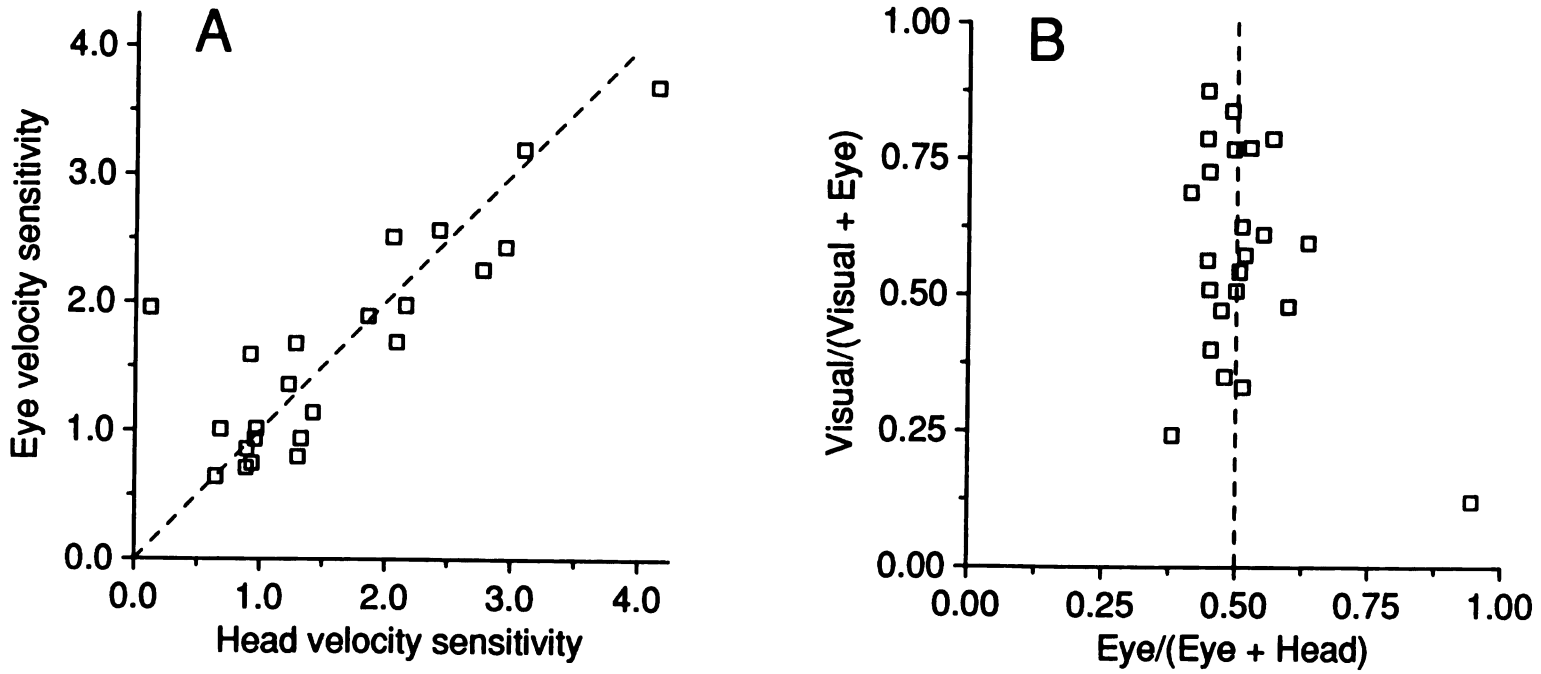
A
Eye velocity sensitivity
Head velocity sensitivity
0.0
1.0
2.0
3.0
4.0
B
Visual/(Visual + Eye)
Eye/(Eye + Head)
0.00
0.25
0.50
0.75
1.00

Figure 4.15 Trial used to present visual motion at different locations in the visual field. Vertical dashed lines indicate the interval from 100 to 200 ms after the onset of target motion. Downward pointing pair of arrows indicate the interval from 400 to 600 ms after the onset of target motion.

Fig. 4.15

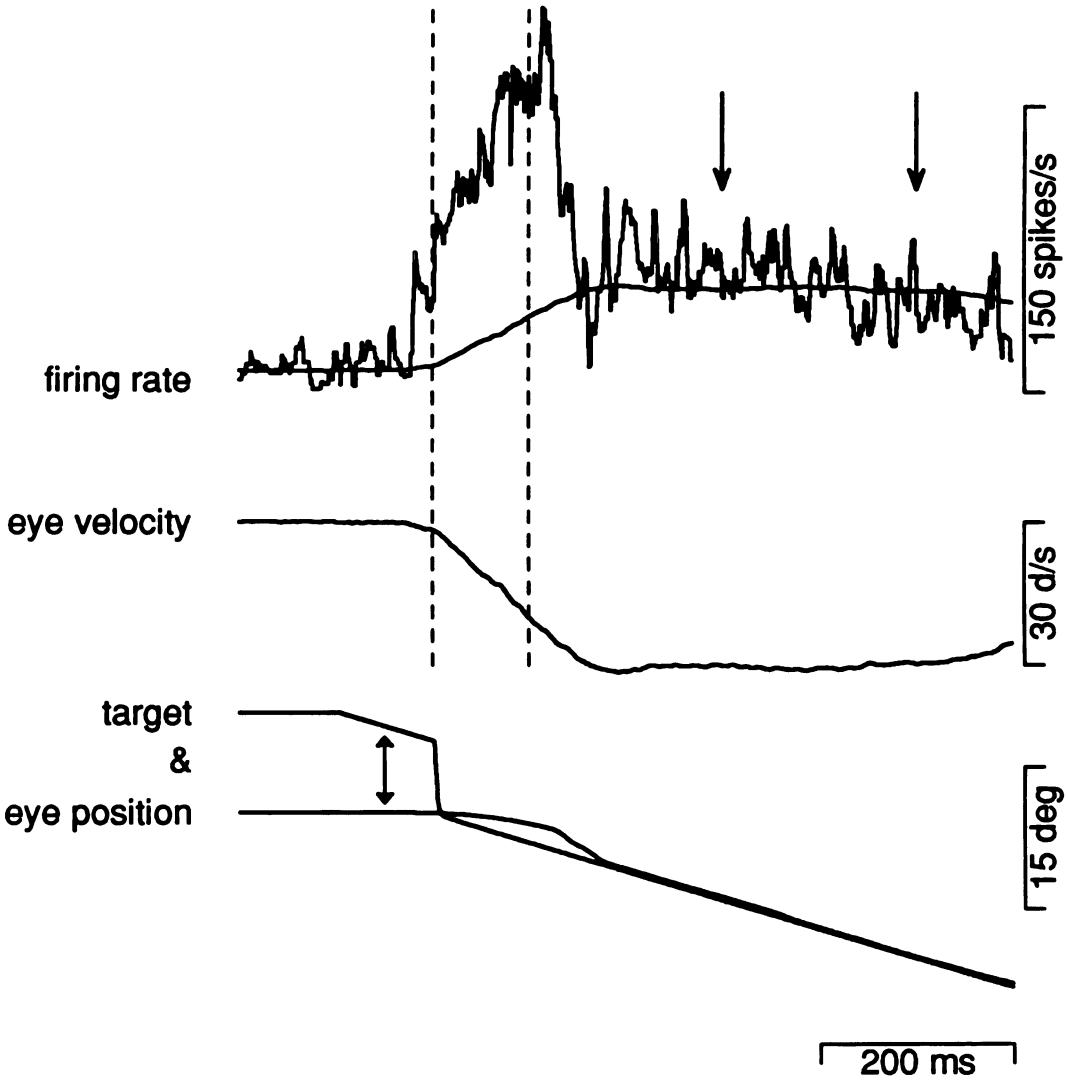
firing rate
eye velocity
target
&
eye position
150 spikes/s
30 d/s
15 deg
200 ms

Figure 4.16 Full set of firing rate traces obtained with one P-cell. Two columns indicate the averaged simple-spike firing rate recorded during pursuit in either the preferred (left column) or non-preferred direction (right column) of the P-cell. The numbers in the center of each row indicate the average location in the visual field of the first 100 ms of motion of the target. Each pair of superimposed traces shows eye velocity (smoother) and visual (noisier) components of simple-spike firing rate. Pairs of vertical dashed lines indicate the interval from 100 to 200 ms after the onset of target motion.

Fig. 4.16

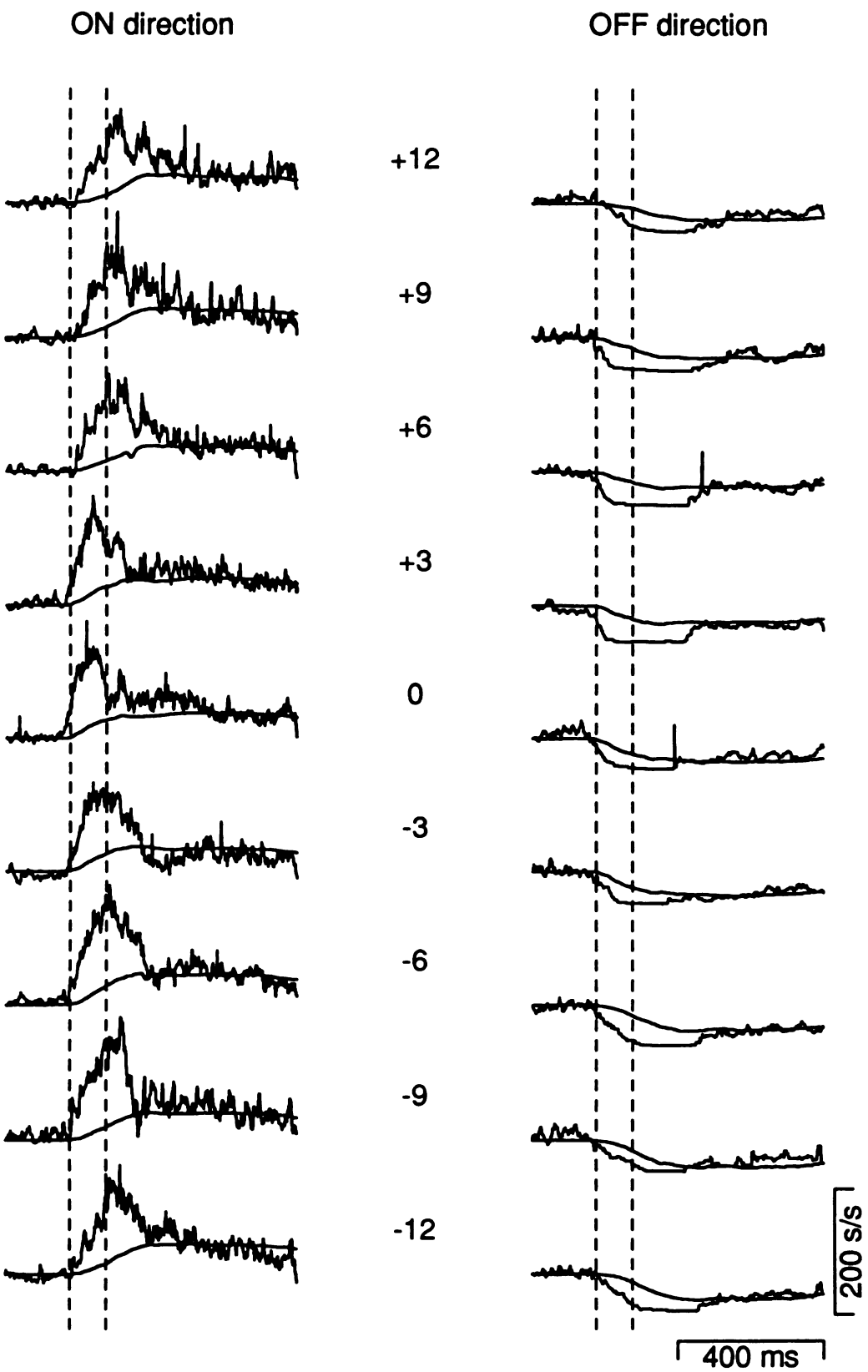

Figure 4.17 Changes in size of visual component for target motion placed at different locations in the visual field. A: Graph plotting size of the visual component as a function of location of the first 100 ms of target motion within the visual field. Data obtained during pursuit in the preferred direction (filled circles) are plotted separately from that obtained in the non-preferred direction (open squares). Double-headed arrow indicates the amplitude of the change in the visual component. B: Distribution of the amplitudes of the changes in the visual component observed in our sample. Three different shadings indicate arbitrary division of the population into three groups.

Fig. 4.17

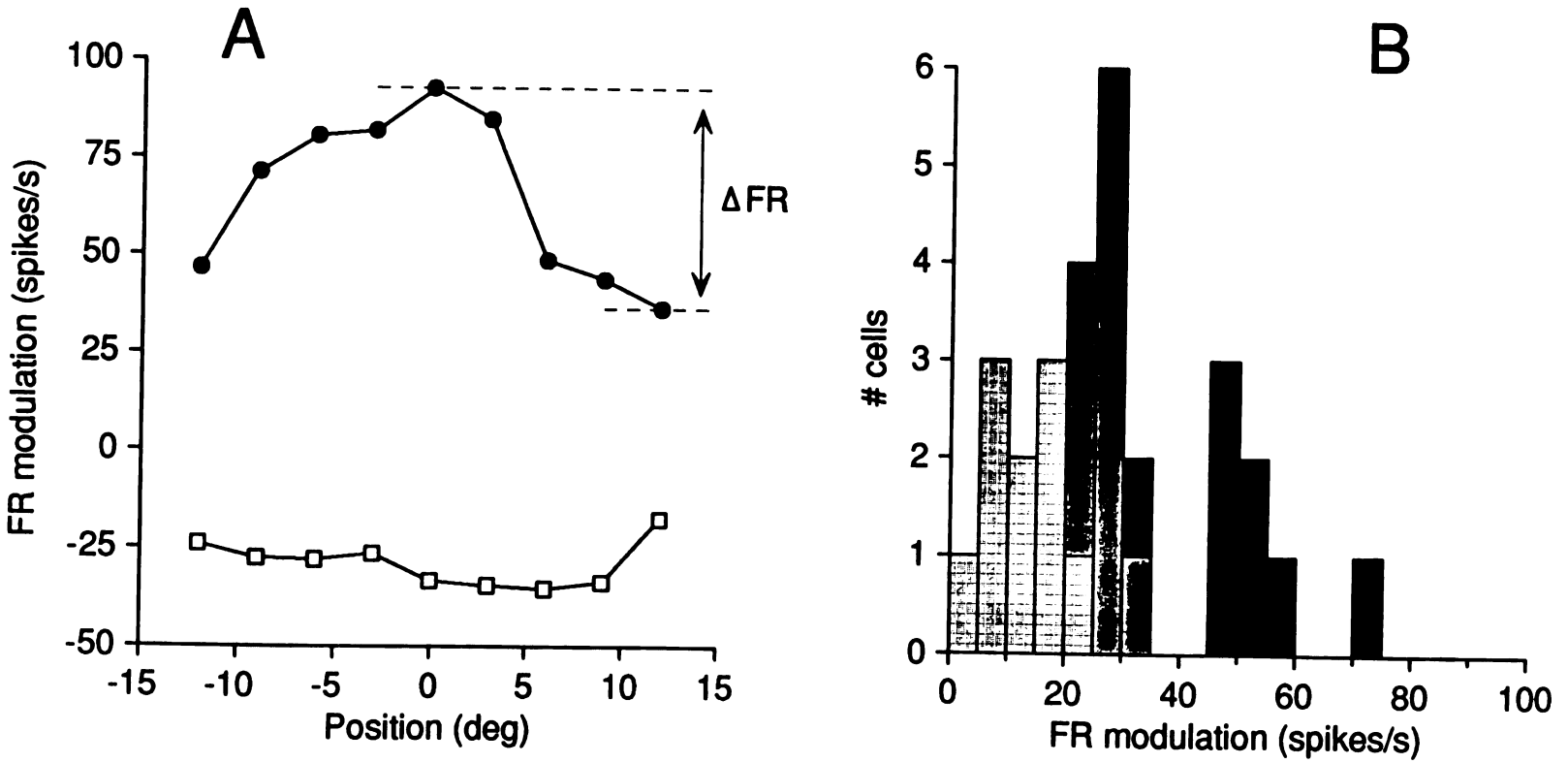
A
100
75
50
25
0
-25
-50
FR modulation (spikes/s)
ΔFR
-15
-10
-5
0
5
10
15
Position (deg)
B
6
5
4
3
2
1
0
cells
0
20
40
60
80
100
FR modulation (spikes/s)

Figure 4.18 Summary of changes in the sizes of the visual components for target motion placed at different locations in the visual field. Graphs plot size of the visual component as a function of location of the first 100 ms of target motion within the visual field, for each P-cell. Three rows of graphs show data from strongly (top), moderately (middle), and weakly (bottom) modulated P-cells. These three groups correspond to the three groups demarcated in Fig. 4.17. Two columns show data obtained during pursuit in the preferred (left) and non-preferred (right) directions for each P-cell. Dashed vertical line indicates 3 degrees in the visual hemifield opposite the recording site.

Fig. 4.18

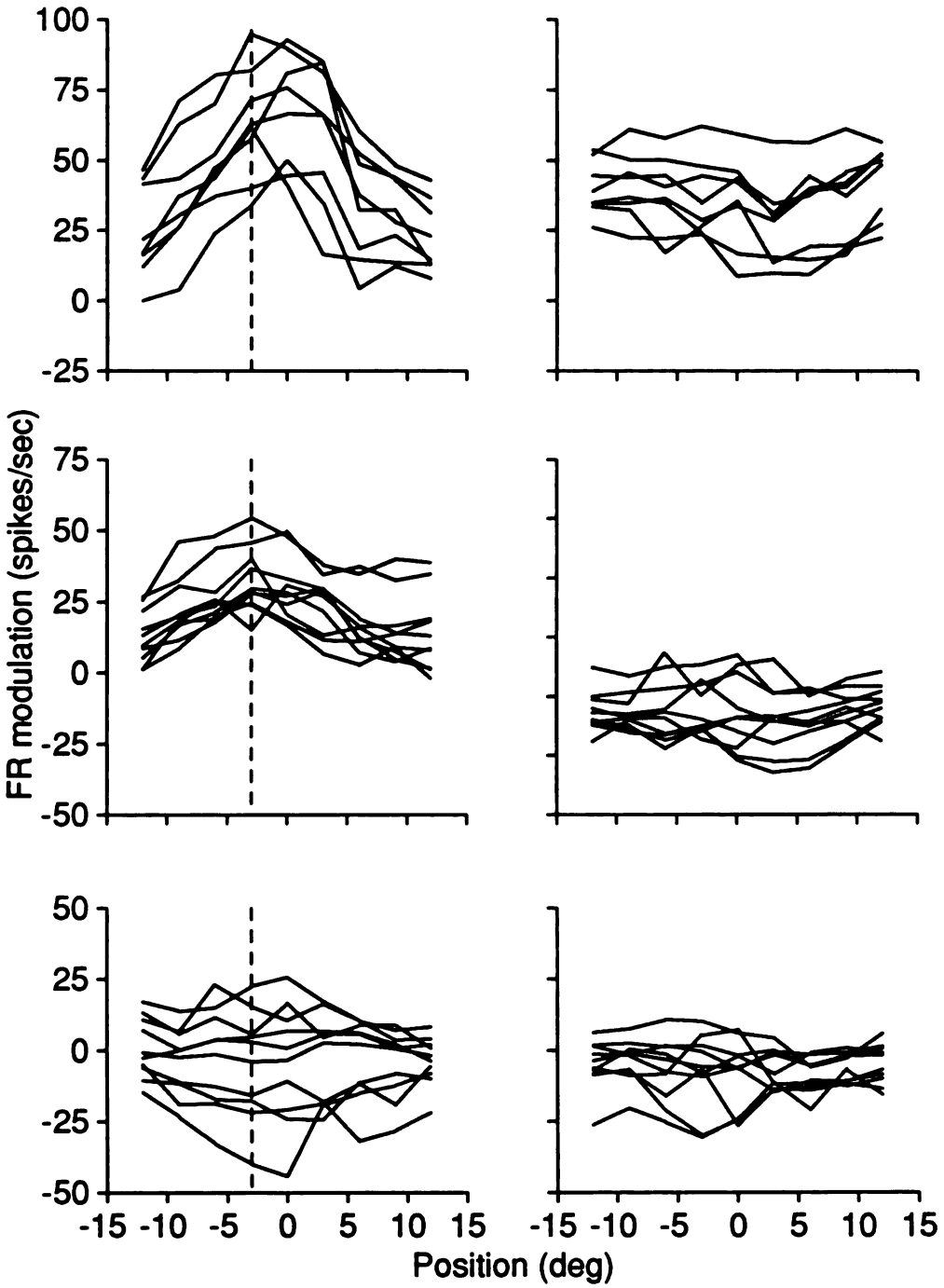
100
75
50
25
0
-25
75
50
25
0
-25
-50
50
25
0
-25
-50
FR modulation (spikes/sec)
-15 -10 -5 0 5 10 15
-15 -10 -5 0 5 10 15
Position (deg)

Figure 4.19 Relationship between size of the visual components and amplitude of eye acceleration at the initiation of pursuit. Each graph plots the size of the visual component as a function of the average eye acceleration during the first 100 ms of the initation of pursuit. Different symbols are used to show data obtained during pursuit in the preferred (filled circles) and non-preferred (open squares) directions for each P-cell. Lines indicate the results of linear regression applied to each set of data. Each graph shows the results from one of the eight strongly modulated P-cells shown in Figs. 4.18 and 4.17.

Fig. 4.19

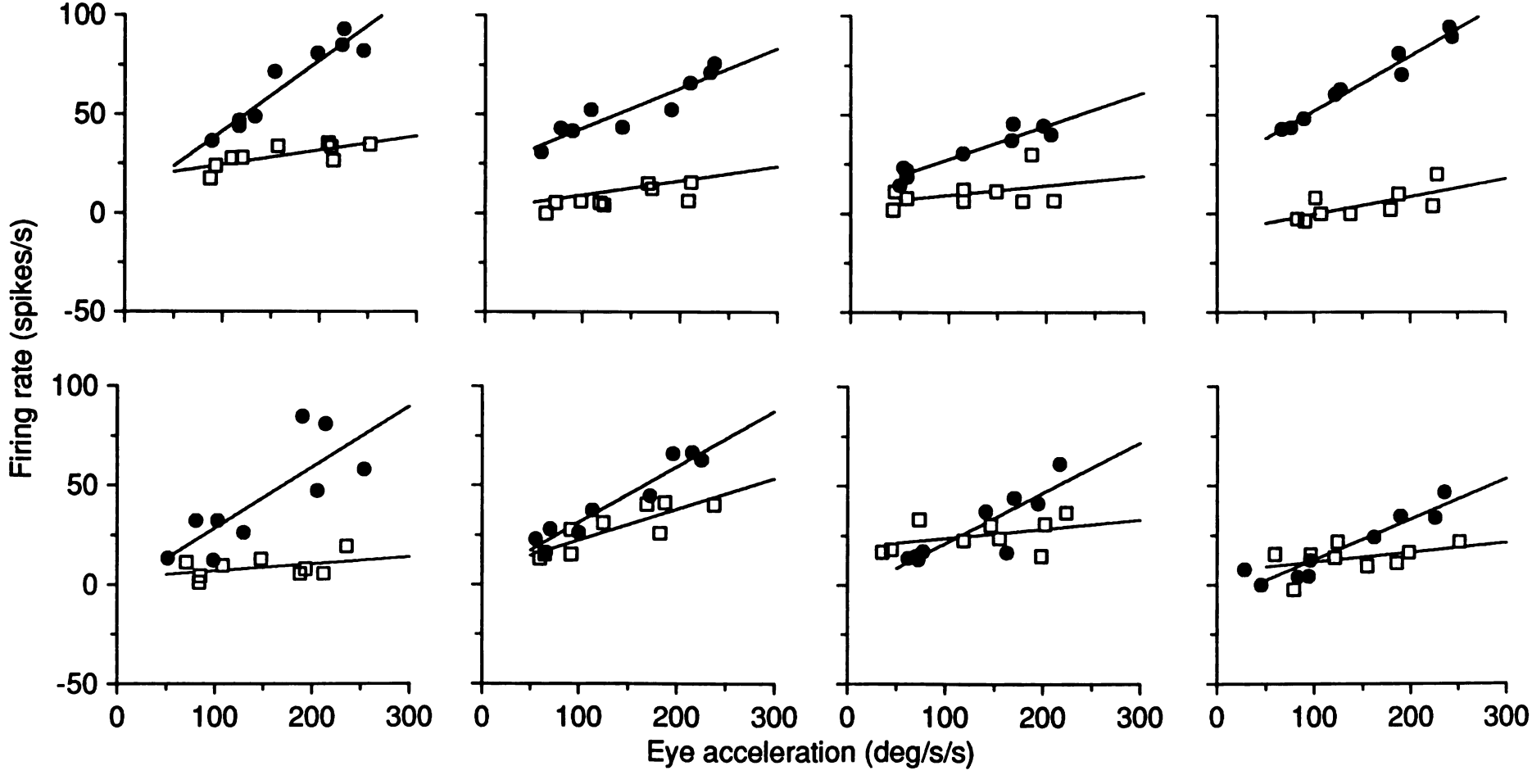
100
50
0
-50
Firing rate (spikes/s)
0
100
200
300
Eye acceleration (deg/s/s)

Figure 4.20 Responses of P-cells at the termination of pursuit. Traces show position of the target and eye as a function of time (top), eye velocity as a function of time (middle), and four examples of the average simple-spike firing rate recorded from P-cells during performance of this behavior. Dashed vertical line indicates the onset of the termination of pursuit and is aligned with the transient increase displayed by the trace representing eye velocity. Arrow indicates transient increase in simple-spike firing rate observed in one P-cell just prior to the termination of pursuit. Similar, but smaller, transient changes were observed in several other P-cells.

Fig. 4.20

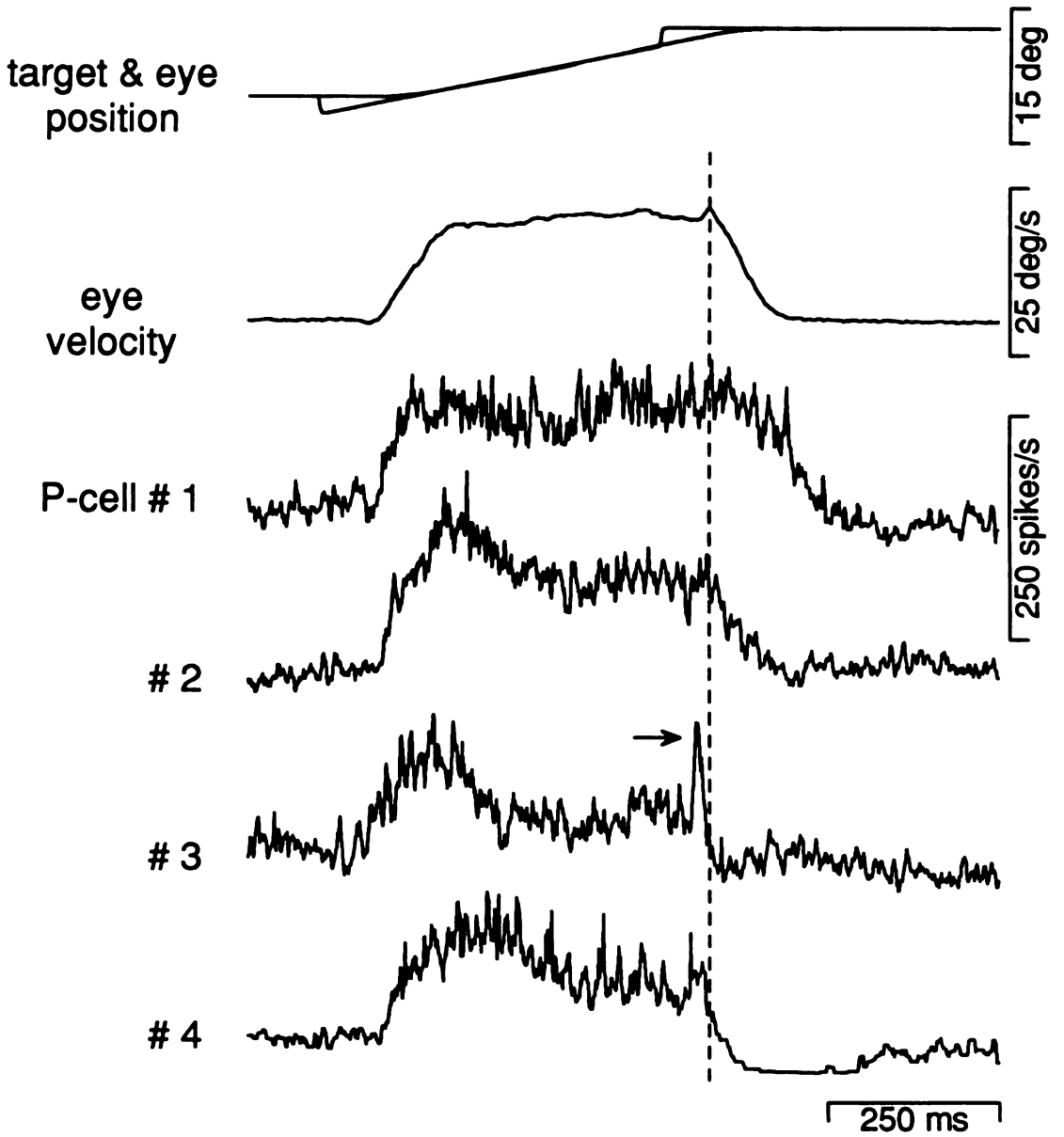
target & eye position
15 deg
eye velocity
25 deg/s
P-cell # 1
2
3
4
250 spikes/s
250 ms

Figure 4.21 Ensemble activity of P-cells at the termination of pursuit. A: Average simple-spike firing rate from 14 horizontal P-cells superimposed on average eye velocity (smoother traces). Two sets of superimposed traces compare responses during pursuit in the preferred (top) and non-preferred (bottom) directions. Left vertical dashed line indicates beginning of the termination of pursuit; right line indicates 140 ms later. B: Result of combining simple-spike responses obtained during pursuit in the preferred and non-preferred directions.

Fig. 4.21

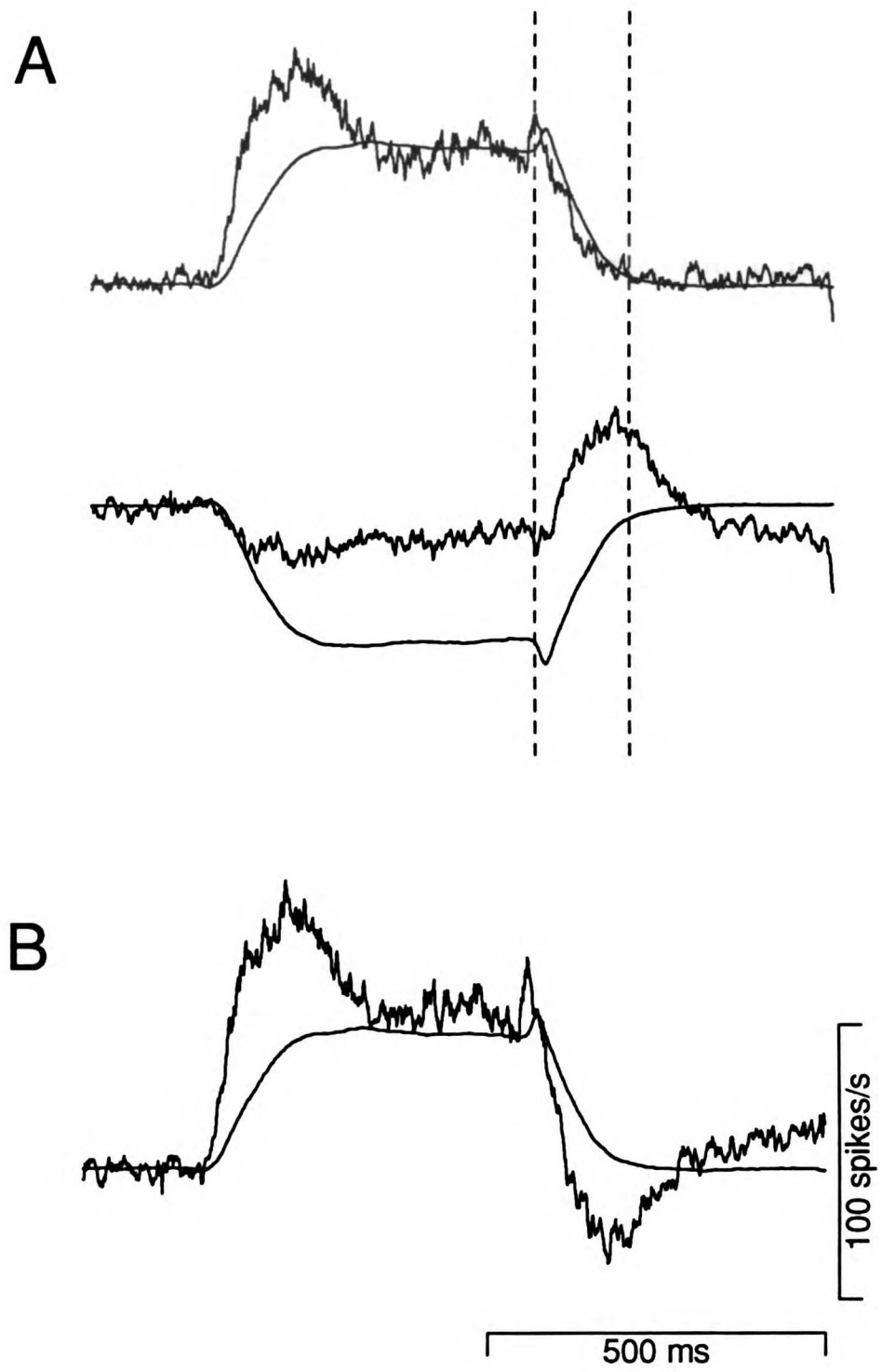

Figure 4.22 Framework underlying analysis of relationship between visual component of simple-spike firing rate and eye acceleration. A: Pair of traces show total firing rate (solid) and hypothetical eye velocity component of firing rate (dashed). The difference between the total and the eye velocity component provides the visual component, shown as the solid traces in C, E and G. The dashed traces in C, E and G show hypothetical eye acceleration. Dashed vertical lines indicate the onset of the visual component. B, D and F: schematic diagrams outlining possible roles visual signals observed on P-cells. B and C: All visual signals for eye acceleration during pursuit go through the flocculus. D and E: Some of the visual signals for eye acceleration go through the flocculus. F and G: Visual signals go through the flocculus, but are not used to accelerate the eye.

Fig. 4.22

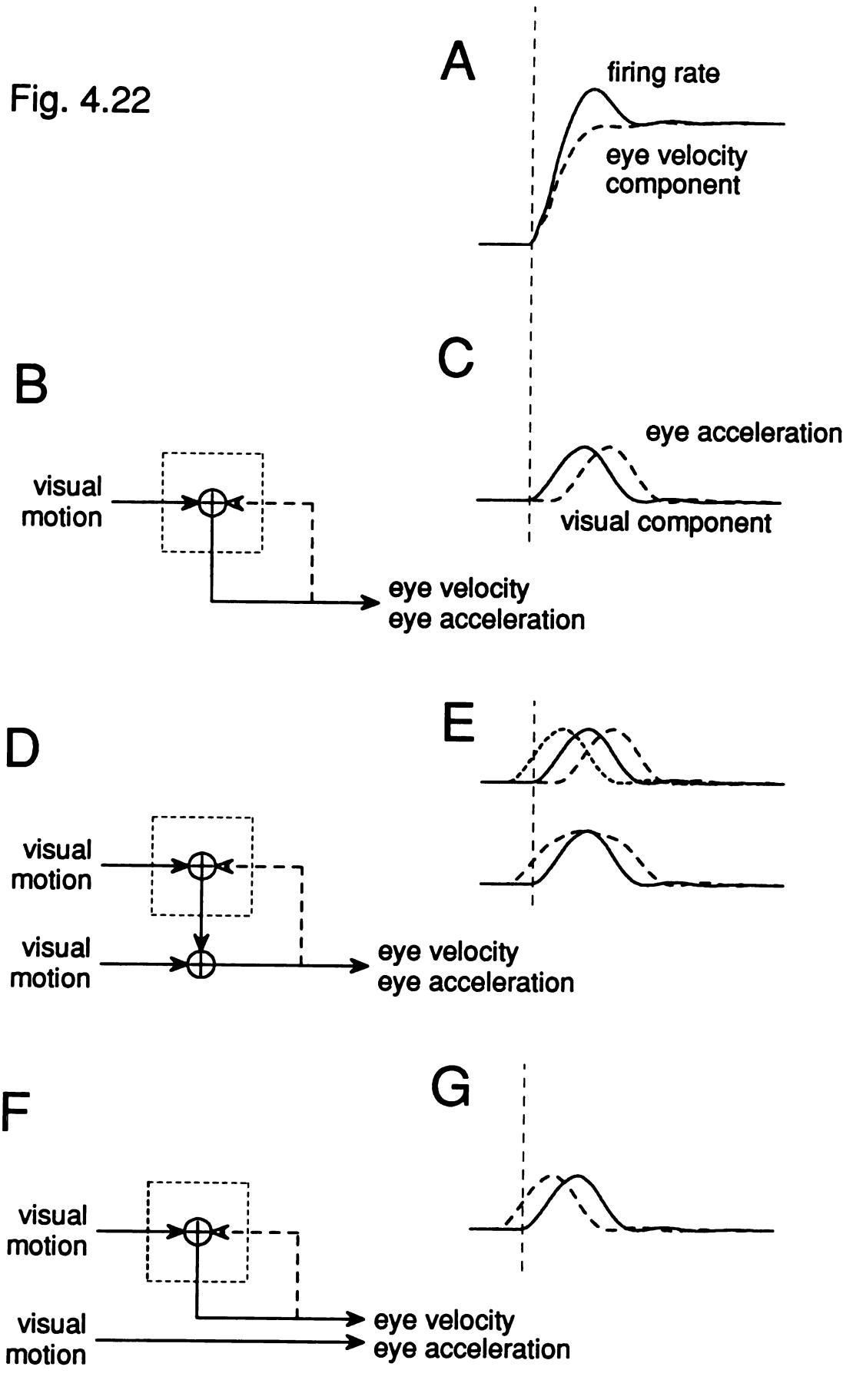
A
firing rate
eye velocity
component
B
visual
motion
eye velocity
eye acceleration
C
eye acceleration
visual component
D
visual
motion
visual
motion
eye velocity
eye acceleration
E
F
visual
motion
visual
motion
eye velocity
eye acceleration
G

Figure 4.23 How temporal shifts affect the temporal relationship between the estimated visual component and eye acceleration, using the ensemble activity of 14 P-cells. Top row shows averaged simple-spike firing rate (noisy traces) during pursuit of a target moving at 30 °/s. Traces represent the average of averaged data obtained from fourteen P-cells. Dashed traces show estimates of the eye velocity component of simple-spike firing rate. Difference between total firing rate and the estimated eye velocity components is shown as "residual firing rate" in lower row. Superimposed on residual firing rate traces are traces showing eye acceleration. Firing rate and eye acceleration traces have not been shifted in time. Eye velocity trace was shifted backward in time by 30 ms (A), forward by 30 ms (C), or left unshifted (B).

Fig. 4.23

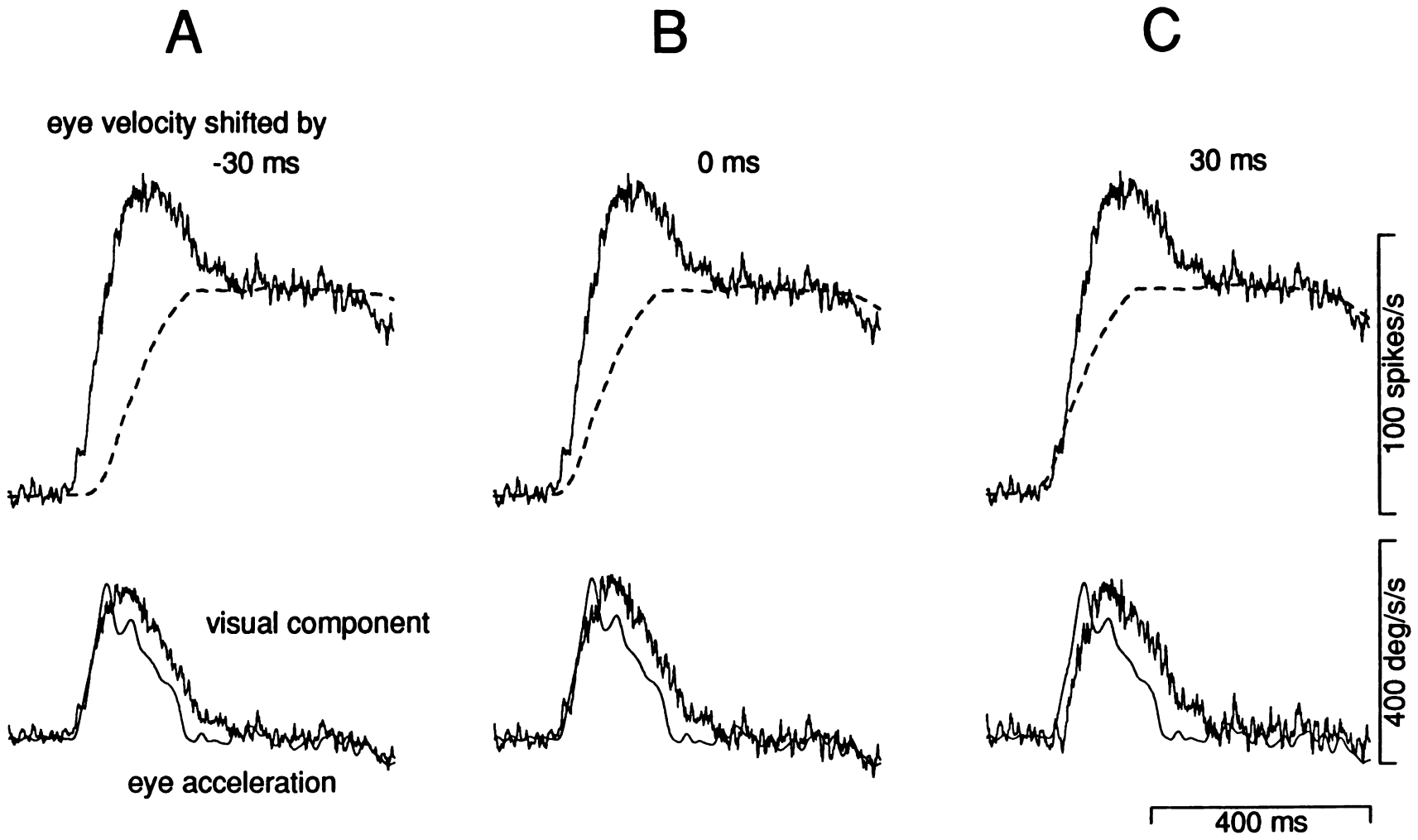
A
B
C
eye velocity shifted by
-30 ms
0 ms
30 ms
visual component
eye acceleration
100 spikes/s
400 deg/s/s
400 ms

Figure 4.24 Description of simple-spike firing rate using weighted sum of time-shifted eye velocity and eye acceleration. Upper pair of traces compare averaged simple-spike firing rate (noisy trace, same as in Fig. 4.23) with output of processed eye velocity and acceleration (dashed trace). Lower pair of traces show the eye velocity (solid) and eye acceleration (dashed) components which produced the fit shown above. The sum of the two traces equals the dashed trace shown superimposed on averaged firing rate.

Fig. 4.24

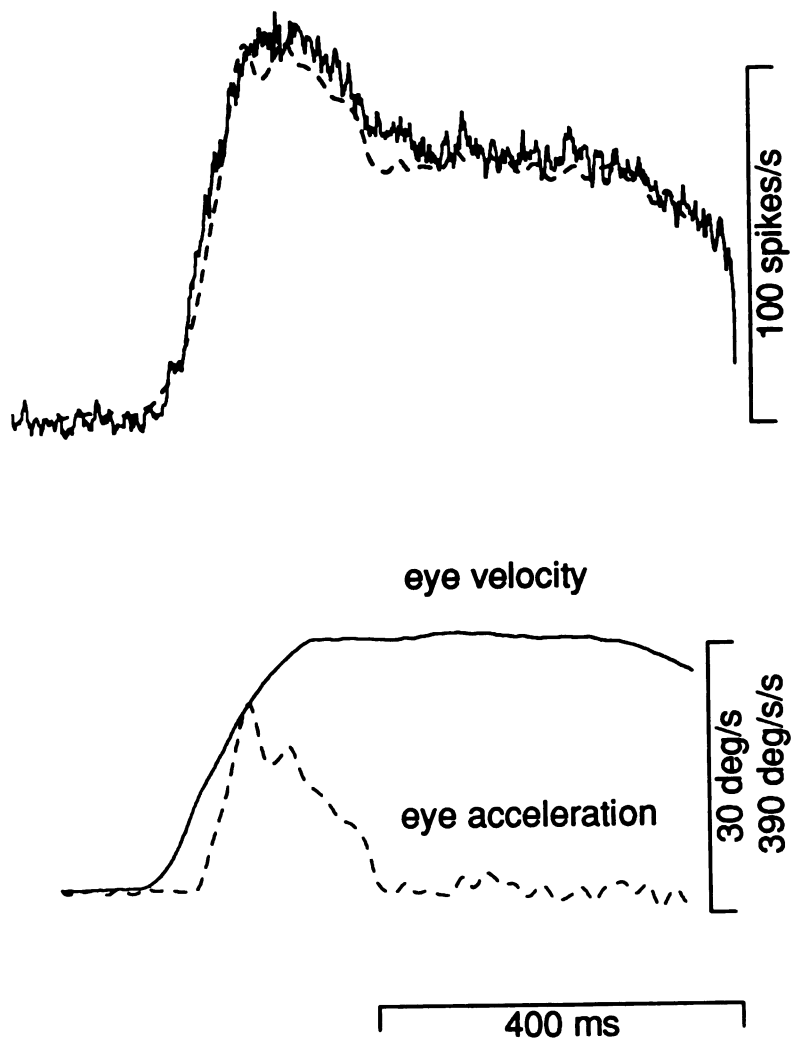
100 spikes/s
eye velocity
eye acceleration
30 deg/s
390 deg/s/s
400 ms

Figure 4.25 The average correlation coefficients associated with fixed temporal shifts in eye velocity and eye acceleration. The graph plots 3 dimensions. Along the abscissa is the temporal shift applied to eye velocity, along the ordinate is the temporal shift applied to eye acceleration, and the gray level indicates the average value of the correlation coefficient (as indicated by the scale to the right). The average correlation coefficient is the average of the correlation coefficients measured for each target motion.

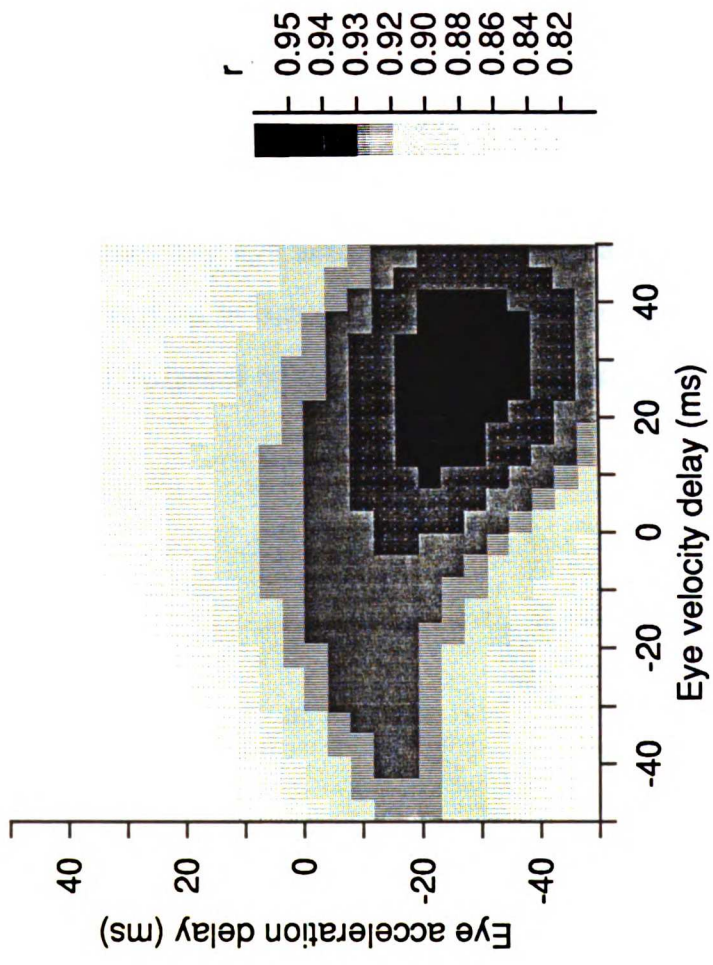
r
0.95
0.94
0.93
0.92
0.90
0.88
0.86
0.84
0.82
Eye velocity delay (ms)
-40
-20
0
20
40
Eye acceleration delay (ms)
-40
-20
0
20
40

Figure 4.26 How temporal shifts affect the temporal relationship between the estimated visual component and eye acceleration, using a single P-cell. Top row shows averaged simple-spike firing rate (noisy traces) during pursuit of a target moving at 30 °/s. Traces represent the averaged data obtained from the P-cell of the fourteen that displayed the shortest latency. Dashed traces show estimates of the eye velocity component of simple-spike firing rate. Difference between total firing rate and the estimated eye velocity components is shown as "visual component" in lower row. Superimposed on the visual components are traces showing eye acceleration. Firing rate and eye acceleration traces have not been shifted in time. Eye velocity trace was shifted backward in time by 30 ms (A), forward by 30 ms (C), or left unshifted (B).

Fig. 4.26

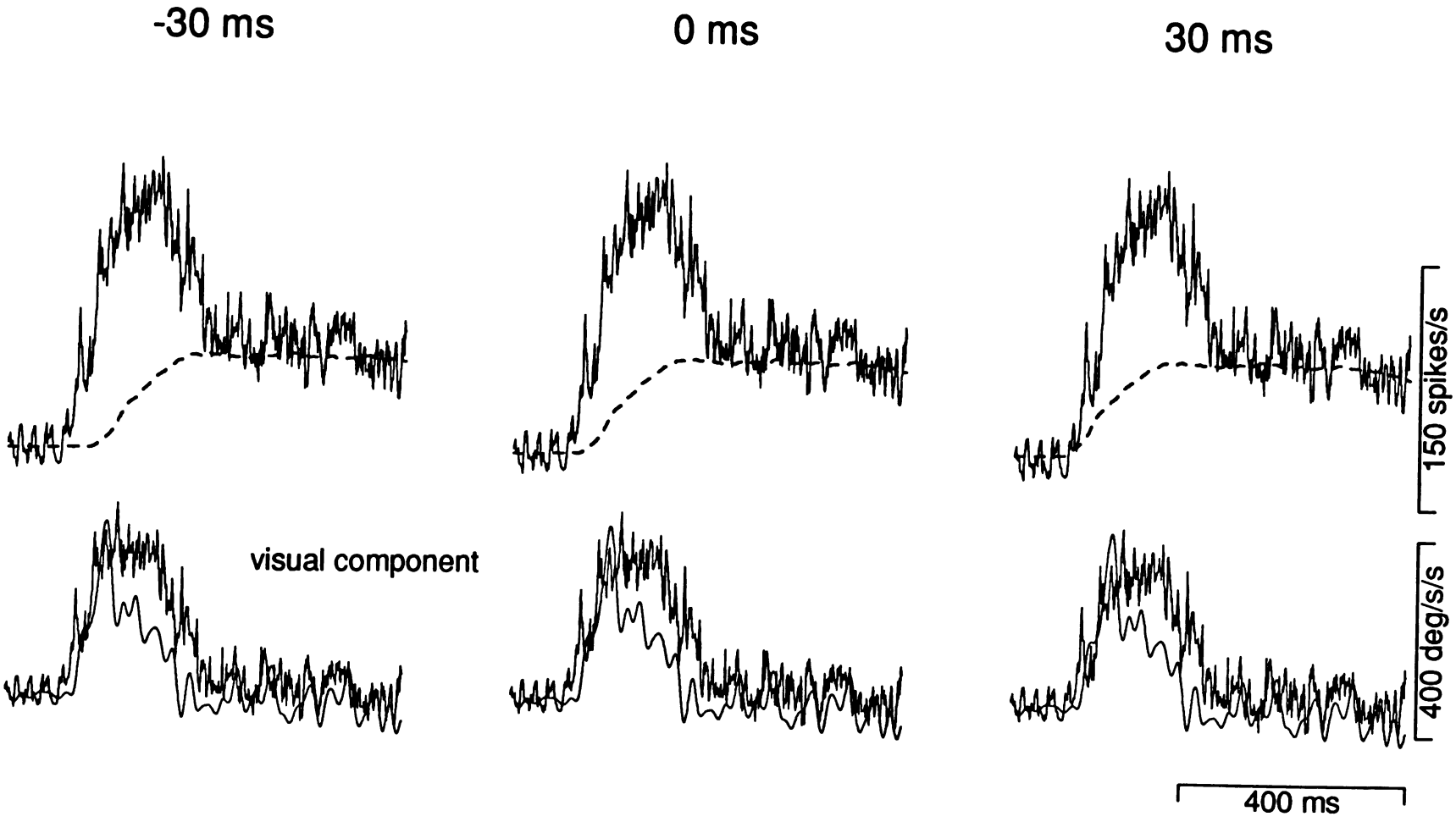

Figure 4.27 Distribution of best temporal shifts for individual P-cells. The graph plots the temporal shifts applied to the eye acceleration traces against the temporal shifts applied to the eye velocity traces which gave the highest correlation coefficients for each of fourteen P-cells. The dashed horizontal and vertical lines indicate temporal shifts of 0 ms.

Fig. 4.27

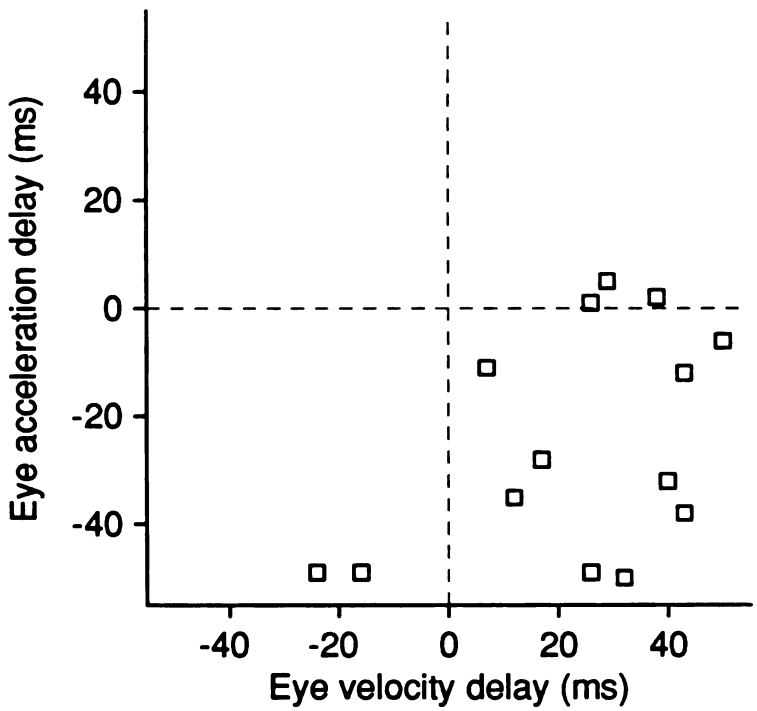
Eye acceleration delay (ms)
40
20
0
-20
-40
-40
-20
0
20
40
Eye velocity delay (ms)

General Conclusions

The results presented in this thesis provide an outline of the signal processing and the circuitry underlying smooth pursuit eye movements. Our study of the visual motion signals underlying pursuit in chapters one and two indicates that much of the details of pursuit behavior can be understood as effects caused by the processing of visual inputs for pursuit. However, some aspects of pursuit performance -- in particular, the termination of pursuit -- suggest that non-visual signals also play an important role. The model we have proposed is capable of reproducing many features of pursuit eye movements and assigns specific functions to visual and non-visual inputs for pursuit.

We have also made an initial attempt to map the conceptual scheme depicted by our model of pursuit eye movements onto the antomical substrates for pursuit in the brain. Our study of the firing rate of Purkinje cells in the flocculus and ventral paraflocculus of the cerebellum have provided several pieces of information about the level of processing achieved at this anatomical stage of the pathways underlying pursuit. First, the results in chapter three suggest that the spatial organization of the outputs of the cerebellum are compatible with the output motor pathways. This implies that the transformation of visual and oculomotor signals into the reference frame defined by the vestibular pathways in the brainstem occurs within or before the cerebellum. Second, our analysis in chapter four indicates that each of the visual motion signals used for pursuit is present in the output of the cerebellar flocculus and ventral paraflocculus. This result is consistent with the view that the flocculus conveys visual signals that are used as commands for smooth pursuit eye movements.

Some unanswered questions

The issues addressed in this thesis also highlight the large number of questions that remain unanswered concerning the control of pursuit eye movements. The following list includes those issues that are most directly related to the results that have been presented here.

How are visual motion signals for pursuit encoded by neurons in visual cortex? In our analysis of pursuit behavior and in the development of the model, we described three pathways that each process a different aspect of visual motion. Visual signals related to image acceleration have been observed on MT cells (Movshon and Lisberger 1990, Movshon et al. 1991, Lisberger and Movshon 1991), but there are several large gaps in our knowledge of how visual motion signals for pursuit are encoded by neurons in visual cortex. For example, the input to the model is assumed to be target velocity, but no attempt is made to describe how individual neurons participate in the encoding of this motion. Also, the model assumes that the target is already defined. How the brain parses the motion contained in complicated visual environments and determines which portions to provide as inputs for pursuit eye movements remains unknown.

What is the role of non-visual signals in area MST? The function of the non-visual signals recorded from neurons in area MST is not known. The interpretation suggested by Newsome et al. (1988) is that these neurons convey an eye velocity signal that is used to construct a neural analogue of target velocity. In contrast, the model we have presented suggests that the non-visual signals may be used to gate the use of visual motion information by other pathways. Experiments designed to quantify the signal conveyed by these neurons would help to determine whether either of these suggestions is correct.

What transformations occur between visual cortex and the cerebellum? The anatomy of the projections from the cortex to the basilar pontine nuclei and from the pontine nuclei to the cerebellum is quite complex (e.g., Glickstein and May 1982). The basilar gray also contains numerous interneurons (Cooper and Fox 19??) which could act to transform the information receives from cerebral cortical areas before this information is provided to the cerebellum. Several important studies have been made of activity in the pontine nuclei, but most experiments have considered the pontine nuclei to be a simple relay.

What roles are played by other regions of the cerebellum in pursuit? Lesions of the flocculus and ventral paraflocculus cause large deficits in smooth pursuit (Takemori and Cohen 1974; Zee et al. 1981), but complete ablation of the cerebellum is required to completely abolish the ability to perform pursuit eye movements (Westheimer and Blair 1973). In addition, other regions of the cerebellum, such as the midline vermis and the fastigial nucleus (Kase et al. 1979, Suzuki and Keller 1988ab, Buttner et al. 1991), have been suggested to play a role in pursuit. Examination of the activity of these regions during pursuit under conditions like those used here would facilitate the examination of how the components of the command for pursuit might be parsed among the participating brain structures

Are smooth pursuit eye movements actually a special case of smooth gaze movements? We have recorded from Purkinje cells during pursuit eye movements in the special case in which the monkey's head is held fixed. However, these same P-cells show a strong sensitivity to head velocity, as is evident in the fact that they are commonly referred to as "gaze-velocity" P-cells. This raises the question as to what role these P-cells might play during

the performance of natural gaze shifts accomplished with a combination of both eye and head movements.

What role do complex spikes play in the control of smooth pursuit? Our studies have focused on the role of simple-spike activity recorded from P-cells. However, these P-cells also display complex spikes that convey visual signals related to the visual motion of small spots and large backgrounds (Stone and Lisberger 1986, 1990b; Gillespie et al. 1991). Although the low frequency of discharge associated with complex spikes would preclude their having a major role in directly controlling pursuit, they could be involved in fine adjustments of P-cell firing rate that could correct small error during pursuit (Stone and Lisberger 1989b). The interaction between the simple-spike and complex-spike discharges of P-cells in the flocculus and ventral paraflocculus is a rich area for study, since we know so much else about the function of this region of the cerebellum.

References

Adelson, E.H., and Bergen, J.R. Spatiotemporal energy models for the perception of motion. J. Opt. Soc. Am. 2: 284-299, 1985.

Albright, T.D. Direction and orientation selectivity of neurons in visual area MT of the macaque. J. Neurophysiol. 52: 1106-1130, 1984.

Anastasio, T.J. and Robinson, D.A. The distributed representation of vestibulo-oculomotor signals by brain-stem neurons. Biol. Cybern. 61: 79-88.

Andersen, R.A. and Zipser, D. The role of posterior parietal cortex in coordinate transformations for visual-motor integration. Can. J. Physiol. Pharmacol. 66: 488-501, 1988.

Baker, R., Precht, W., and Llinas, R. Cerebellar modulatory action on the vestibulo-trochlear pathway in the cat. Exp. Brain Res. 15: 364-385, 1972.

Balaban, C.D., Ito, M. and Watanabe, E. Demonstration of zonal projections from the cerebellar flocculus to vestibular nuclei in monkeys (Macaca fuscata). Neurosci. Lett. 27: 101-105, 1981.

Balaban, C.D. and Watanabe, E. Functional representation of eye movements in the flocculus of monkeys (Macaca fuscata). Neurosci. Lett. 49: 199-205, 1984.

Belknap, D.B. and Noda, H. Eye movements evoked by microstimulation in the flocculus of the alert macaque. Exp. Brain Res. 67: 352-362, 1987.

Brodal, P. The corticopontine projection in the rhesus monkey: origin and principles of organization. Brain 101: 251-283, 1978.

Brodal, P. The pontocerebellar projection in the rhesus monkey: an experimental study with retrograde axonal transport of horseradish

peroxidase. Neuroscience 4: 193-208, 1979.

Brodal, P. The cortical projection to the nucleus reticularis tegmenti pontis in the rhesus monkey. Exp. Brain Res. 38: 19-27, 1980.

Brodal, P. The projection from the nucleus reticularis tegmenti pontis to the cerebellum in the rhesus monkey. Exp. Brain Res. 38: 29-36, 1980.

Brodal, P. Further observations on the cerebellar projections from the pontine nuclei and the nucleus reticularis tegmenti pontis in the rhesus monkey. J. Comp. Neurol. 204: 44-55, 1982.

Brodal, P. and Brodal, A. The olivocerebellar projection in the monkey. Experimental studies with the method of retrograde tracing of horseradish peroxidase. J. Comp. Neurol. 201: 375-393, 1981.

Brodal, P. and Brodal, A. Further observations on the olivocerebellar projection in the monkey. Exp. Brain Res. 45: 71-83, 1982.

Brodal, P. Further observations on the cerebellar projections from the pontine nuclei and the nucleus tegmenti pontis in the rhesus monkey. J. Comp. Neurol. 204: 44-55, 1982.

Broussard, D.M. and McCrea, R.A. The projection from the cerebellar cortex to the rostral medial vestibular nucleus in the squirrel monkey. J. Neurosci., submitted.

Buttner, U. and Waespe, W. Purkinje cell activity in the primate flocculus during optokinetic stimulation, smooth pursuit eye movements and VOR-suppression. Exp. Brain Res. 55: 97-104, 1984.

Buttner, U., Fuchs, A.F., Markert-Schwab, G., and Buckmaster, P. Fastigial nucleus activity in the alert monkey during slow eye and head movements. J. Neurophysiol. 6: 1360-1371, 1991.

Carl, J.R. and Gellman, R.S. Human smooth pursuit: Stimulus-dependent responses. J. Neurophysiol. 5: 1446-1463, 1987.

Chubb, C. and Sperling, G. Drift-balanced random stimuli: a general basis for studying non-Fourier motion perception. J. Opt. Soc. Am. 5: 1986-2007, 1988.

Cohen, B., Suzuki, J.-I., and Bender, M.B. Eye movements from semicircular canal nerve stimulation in the cat. Ann. Otol. Rhinol. Laryngol. 73: 153-169, 1964.

Collewijn, H. Latency and gain of the rabbit's optokinetic reactions to small movements. Brain Res. 36: 59-70, 1972.

Collewijn, H. and Tamminga, E.P., Human smooth pursuit and saccadic eye movements during voluntary pursuit of different target motions on different backgrounds. J. Physiol. (Lond.) 351: 217-250, 1984.

Cooper, M.H. and Fox, C.A. The basilar pontine gray in the adult monkey (Macaca mulatta): a Golgi study. J. Comp. Neurol. 168: 145-174, 19??.

Deno, D.C., Keller, E.I., and Crandall, W.F. Dynamical neural network organization of the visual pursuit system. IEEE Trans. Biomed. Eng. 36: 85-92, 1989.

Dursteler, M.R., Wurtz, R.H., and Newsome, W.T. Directional pursuit deficits following lesions of the foveal representation within the superior temporal sulcus of the macaque monkey. J. Neurophysiol. 57: 1262-1287, 1987.

Dursteler, M.R. and Wurtz, R.H. Pursuit and optokinetic deficits following chemical lesions of cortical areas MT and MST. J. Neurophysiol. 57: 1262-1287, 1987.

Fetter, M. and Buettner, U.W. Stimulus characteristics influence the gain of smooth pursuit eye movements in normal subjects. Exp. Brain Res. 79: 388-392, 1990.

Fluur, E. Influences of semicircular ducts on extraocular muscles. Acta Oto-

Laryngol. Suppl. 149: 1-46, 1959.

Gerrits, N.M. and Voogd, J. The climbing fiber projection to the flocculus and adjacent paraflocculus in thecat. Neuroscience 7: 2971-2991, 1982.

Gerrits, N.M. and Voogd, J. The topographical organization of climbing and mossy fiber afferents in the flocculus and the ventral paraflocculus in rabbit, cat and monkey. Exp. Brain Res. Suppl. 17: 26-29, 1989.

Gillespie, D.C., Krauzlis, R.J., Bronte-Stewart, H.M., and Lisberger, S.G. Properties of visual stimuli that drive complex spikes in monkey flocculus. Soc. Neurosci. Abstr. 17: 462, 1991.

Glickstein, M., Stein, J., and King, R.A., Visual input to the pontine nuclei. Science 178: 1110-1111, 1972.

Glickstein, M., Cohen, J. L., Dixon, B., Gibson, A., Hollins, M., Labossiere, kE., and Robinson, F. Corticopontine visual projections in macaque monkeys. J. Comp. Neurol. 190: 209-229, 1980.

Glickstein, M. and May, J. Visual control of movement. In: Contributions to sensory physiology, vol. 7, pp. 103-145, Academic Press, 1982.

Glickstein, M., May, J., and Mercer, B.E. Corticopontine projection in the macaque: the distribution of labelled cortical cells after large injections os horseradish peroxidase in the pontine nuclei. J. Comp. Neurol. 235: 343-359, 1985.

Goldberg, J.M., and Fernandez, C. The vestibular system. In: Handbook of physiology. QP6 .H25 1977 Williams and Wilkins, Baltimore, 19nn.

Goldreich, D., Krauzlis, R.J., and Lisberger, S.G. Effect of changing feedback delay on spontaneous oscillations in smooth pursuit eye movements of monkeys. J. Neurophysiol., in press.

Grasse, K.L. and Cynader, M. The accessory optic system in frontal-eyed animals. In: Vision and visual dysfunction, Vol. IV, Chapt. 5, Leventhal,

A., (ed.), Macmillan, 1990.

Groenewegen, and Voogd, J. 1977.

Hirai, N. and Uchino, Y. Floccular influence on excitatory relay neurons of vestibular reflexes of anterior semicircular canal origin in the cat. Neurosci. Res. 1: 327-340, 1984.

Hoffman, K.-P. and Distler, C. Quantitative analysis of visual receptive fields of neurons in nucleus of the optic tract and dorsal terminal nucleus of the accessory optic tract in macaque monkey. J. Neurophysiol. 62: 416-428, 1989.

Hoffman, K.-P., Distler, C., Erikson, R.G., and Mader, W. Physiological and anatomical identification of the nucleus of the optic tract and dorsal terminal nucleus of the accessory optic tract in monkeys. Exp. Brain Res. 69: 635-644, 1988.

Huerta, M.F., Krubitzer, L.A., and Kaas, J.H. Frontal eye field as defined by intracortical microstimulation in squirrel monkeys, owl monkeys, and macaque monkeys. I. Subcortical connections. J. Comp. Neurol. 253: 415-439, 1986.

Ito, M., Nisimaru, N., and Yamamoto, M. Pathways for the vestibulo-ocular reflex excitation arising from semicircular canals of rabbits. Exp. Brain Res. 24: 257-272, 1976.

Ito, M., Nisimaru, N., and Yamamoto, M. Postsynaptic inhibition of oculomotor neurons involved in vestibulo-ocular reflexes arising from semicircular canals of rabbits. Exp. Brain Res. 24: 273-283, 1976.

Ito, M., Nishimaru, N. and Yamamoto, Specific patterns of neuronal connexions involved in the control of the rabbit's vestibuloocular reflexes by the cerebellar flocculus. J. Physiol. Lond. 265: 833-854, 1977

Judge, S.J., Richmond, B.J., and Chu, F.C. Implantation of magnetic search

coils for measurement of eye position: an improved method. Vision Res. 20: 535-538, 1980.

Kase, M., Noda, H., Suzuki, D., and Miller, D.C. Target velocity signals of visual tracking in vermal Purkinje cells of the monkey. Science Wash. DC 205: 717-720, 1979.

Komatsu, H. and Wurtz, R.H., Modulation of pursuit eye movements by stimulation of cortical areas MT and MST. J. Neurophysiol. 62: 31-47, 1989.

Kowler, E. and Steinman, R.M. The effect of expectations on slow oculomotor control. II. Single target displacements. Vision Res. 19: 633-646, 1979.

Krauzlis, R.J. and Lisberger, S.G. A control systems model of smooth pursuit eye movements with realistic emergent properties. Neural Comp. 1: 116-122, 1989.

Kunzle, H. and Akert, K. Efferent connections of cortical area 8 (frontal eye field) in *Macaca fascicularis.* A reinvestigation using the autoradiographic technique. J. Comp. Neurol. 173: 147-164, 1977.

Langer, T., Fuchs, A.F., Chubb, M.C., Scudder, C.A., and Lisberger, S.G. Floccular efferents in the rhesus macaque as revealed by autoradiography and horseradish peroxidase. J. Comp. Neurol. 235: 26-37, 1985.

Langer, T., Fuchs, A.F., Scudder, C.A., and Chubb, M.C. Afferents to the flocculus of the cerebellum in the rhesus macaque as revealed by retrograde transport of horseradish peroxidase. J. Comp. Neurol. 235: 1-25, 1985.

Leichnetz, G.R. Inferior frontal eye field projections to the pursuit-related dorsolateral pontine nucleus and middle temporal area (MT) in the monkey. Visual Neurosci. 207: 394-402, 1982.

Leigh, R.J. The cortical control of ocular pursuit movements. Rev. Neurol.

145: 605-612, 1989.

Lisberger, S.G., Evinger, C., Johnamson, G.W., and Fuchs, A.F. Relationship between eye acceleration and retinal image velocity during foveal smooth pursuit eye movements in man and monkey. J. Neurophysiol. 46: 229-249, 1981.

Lisberger, S.G. and Fuchs, A.F. Response of flocculus Purkinje cells to adequate vestibular stimulation in the alert monkey: fixation vs. compensatory eye movements. Brain Res. 69: 347-353, 1974.

Lisberger, S.G. and Fuchs, A.F. Role of primate flocculus during rapid behavioral modification of vestibulo-ocular reflex. I. Purkinje cell activity during visually guided horizontal smooth pursuit eye movements and passive head rotation. J. Neurophysiol. 41: 733-763, 1978.

Lisberger, S.G. and Fuchs, A.F. Role of primate flocculus during rapid behavioral modification of vestibulo-ocular reflex. II. Mossy fiber firing patterns during horizontal head rotation and eye movement J. Neurophysiol. 41: 764-777, 1978.

Lisberger, S.G. and Pavelko, T.A. Brain stem neurons in modified pathways for motor learning in the primate vestibulo-ocular reflex. Science 242: 771-773, 1988.

Lisberger, S.G. and Pavelko, T.A. Topographic and directional organization of visual motion inputs for the initiation of horizontal and vertical smooth-pursuit eye movements in monkeys. J. Neurophysiol. 61: 173-185, 1989.

Lisberger, S.G. and Westbrook, L.E. Properties of visual inputs that initiate horizontal smooth pursuit eye movements in monkeys. J. Neurosci. 5: 1662-1673, 1985.

Lisberger, S.G., Morris, E.J., and Tychsen, L. Visual motion processing and sensory-motor integration for smooth pursuit eye movements. Ann. Rev.

Neurosci. 10: 97-129, 1987.

Lockery, S.R., Wittenberg, G., Kristan, W.B., Jr., and Cottrell, G.W. Function of identified interneurons in the leech elucidated using neural networks trained by back-propagation. Nature 340: 468-471, 1989.

Luebke, A.E., and Robinson, D.A. Transition dynamics between pursuit and fixation suggests different systems. Vision Res. 28: 941-946, 1988.

Lynch, J.C. Frontal eye field lesions in monkey disrupt visual pursuit. Exp. Brain Res. 68: 437-441, 1987.

MacAvoy, M.C. and Bruce, C.J. Oculomotor deficits associated with lesions of the frontal eye field area in macaque monkeys. Soc. Neurosci. Abstr. 15: 1203, 1989.

MacAvoy, M.C., Bruce, C.J., and Gottlieb, J. Smooth-pursuit eye movements elicited by microstimulation in the frontal eye fields region of alert macaque monkeys. Soc. Neurosci. Abstr. 14: 956, 1988.

Maekawa, K., Takeda, T., and Kimura, M. Neural activity of nucleus reticularis tegmenti pontis. The origin of visual mossy fiber afferents to the cerebellar flocculus of rabbits. Brain Res. 210: 17-30, 1981.

Markert, G., Buttner, U., Straube, A., and Boyle, R. Neuronal activity in the flocculus of the alert monkey during sinusoidal optokinetic stimulation. Exp. Brain Res. 70: 134-144, 1988.

Maunsell, J.H.R. and Van Essen, D.C. Functional properties of neurons in middle temporal visual area of macaque monkey. I. Selectivity for stimulus direction, speed and orientation. J. Neurophysiol. 49: 1127-1147, 1983.

May, J.G. and Andersen, R.A. Different patterns of corticopontine projections from separate cortical fields within the inferior parietal lobule and dorsal prelunate gyrus of the macaque. Exp. Brain Res. 63: 265-278, 1986.

May, J.G., Keller, E.L., and Crandall, W.F. Changes in eye velocity during smooth pursuit tracking induced by microstimulation in the dorsolateral pontine nucleus of the macaque. Exp. Brain Res. 63: 265-278, 1986.

Meyer, C.H., Lasker, A.G., and Robinson, D.A. The upper limit of human smooth pursuit velocity. Vision Res. 25: 561-563, 1985.

Mikami, A., Newsome, W.T., and Wurtz, R.H. Motion selectivity in macaque visual cortex. I. Mechanisms of direction and speed selectivity in extrastriate area MT. J. Neurophysiol. 55: 1308-1327, 1986.

Miles, F.A. and Fuller, J.H. Visual tracking and the primate flocculus. Science Wash. DC 189: 1000-1002, 1975.

Miles, F.A. The cerebellum. In: Vision and visual dysfunction (volume 9): eye movements, R.H.S. Carpenter (ed.), Macmillan, London, 1990.

Miles, F.A., Fuller, J.H., Braitman, D.J., and Dow, B.M. Long-term adaptive changes in primate vestibulo-ocular reflex. III. Electrophysiological observations in flocculus of normal monkey. J. Neurophysiol. 43: 1437-1476, 1980.

Morris, E.J. and Lisberger, S.G. A computer model that predicts monkey smooth pursuit eye movements on a millisecond timescale. Soc. Neurosci. Abstr. 11: 79, 1985.

Morris, E.J. and Lisberger, S.G. Different responses to small visual errors during initiation and maintenance of smooth-pursuit eye movements in monkeys. J. Neurophysiol. 58: 1351-1369, 1987.

Mustari, M.J. and Fuchs, A.F. Response properties of single units in the lateral terminal nucleus of the accessory optic system in the behaving primate. J. Neurophysiol. 61: 1207-1220, 1989.

Mustari, M.J. and Fuchs, A.F. Discharge patterns of neurons in the pretectal nucleus of the optic tract (NOT) in the behaving primate. J. Neurophysiol.

64: 77-90, 1990.

Mustari, M.J., Fuchs, A.F., Wallman, J. Response properties of dorsolateral pontine units during smooth pursuit in the rhesus macaque. J. Neurophysiol. 60: 664-686, 1988.

Nelder, J.A. and Mead, R. Computer J. 7: 308, 1965.

Newsome, W.T., Wurtz, R.H., Dursteler, M.R., Mikami, A. Deficits in visual motion processing following ibotenic acid lesions of the middle temporal visual area of the macaque monkey. J. Neurosci. 5: 825-840, 1985.

Newsome, W.T., Wurtz, R.H., and Komatsu, H. Relation of cortical areas MT and MST to pursuit eye movements. II. Differentiation of retinal from extraretinal inputs. J. Neurophysiol. 60: 604-620, 1988.

Noda, H, and Suzuki, D.A. The role of the flocculus in fixation and smooth pursuit eye movements. J. Physiol. Lond. 294: 335-348, 1979.

Noda, H. and Suzuki, D.A. Processing of eye movement signals in the flocculus of the monkey. J. Physiol. Lond. 294: 349-364, 1979.

Noda, H., and Warabi, T. Responses of Purkinje cells and mossy fibers in the flocculus of the monkey during sinusoidal movements of a visual pattern. J. Physiol. Lond. 387: 611-628, 1987.

Noda, H., Sugita, S., and Ikeda, Y. Afferent and efferent connections of the oculomotor region of the fastigial nucleus in the macaque monkey. J. Comp. Neurol. 302: 330-348, 1990.

Pola, J. and Wyatt, H.J. Target position and velocity: the stimulus for pursuit eye movements. Vision Res. 20: 523-534, 1979.

Precht, W., Blanks, R.H.I., Strata, P., and Montarolo, P. On the role of the subprimate cerebellar flocculus in the optokinetic reflex and visual-vestibular interaction. In: Cerebellar functions, pp. 86-108, Bloedel et al. (eds.), Springer-Verlag, Berlin, 1984.

Press, W.H., Flannery, B.P., Teukolsky, S.A., and Vetterling, W.T. Numerical Recipes in C. The art of scientific computing. Cambridge: Cambridge University Press, 1988.

Rashbass, C. The relationship between saccadic and smooth tracking eye movements. J. Physiol. Lond. 159: 326-338, 1961.

Robinson, D.A. The mechanics of human smooth pursuit eye movement. J. Physiol. Lond. 180: 569-591, 1965.

Robinson, D.A. In: Bach-y-Rita P., Collins, C.C., Hyde, J.E. (eds) Control of eye movements. Academic Press, New York, 1971.

Robinson, D.A. A quantitative analysis of extraocular muscle cooperation and squint. Invest. Opthalmol. Vis. Sci. 14: 801-825, 1975.

Robinson, D.A. The use of matrices in analyzing the three-dimensional behavior of the vestibulo-ocular reflex. Biol. Cybern. 46: 53-66, 1982.

Robinson, D.A., Gordon, J.L., and Gordon, S.E. A model of the smooth pursuit eye movement system. Biol. Cybern. 55: 43-57, 1986.

Ron, S. and Robinson, D.A. Eye movements evoked by cerebellar stimulation in the alert monkey. J. Neurophysiol. 36: 1004-1021, 1973.

Sato, Y. and Kawasaki, T. Functional localization in the three floccular zones related to eye movement control in the cat. Brain Res. 290: 25-31, 1984.

Sato, Y., Kawasaki, T., and Ikarashi, K. Zonal organization of the floccular Purkinje cells projecting to the vestibular nucleus in cats. Brain Res. 232: 1-15, 1982.

Sato, Y., Kawasaki, T., and Ikarashi, K. Afferent projections from the brainstem to three floccular zones in cats. II. Mossy fiber projections. Brain Res. 272: 37-48, 1983.

Sato, Y., Kanda, K. and Kawasaki, T. Target neurons of floccular middle zone inhibition in medial vestibular nucleus. Brain Res. 446: 225-235, 1988.

Simpson, J.I. The accessory optic system. Ann. Rev. Neurosci. 7:13-41, 1984.

Simpson, J.I., Soodak, R.E., and Hess, R. The accessory optic system and its relation to the vestibulocerebellum. Prog. Brain Res. 50: 715-724, 1979.

Simpson, J.I. and Graf, W. Eye-muscle geometry and compensatory eye movements in lateral-eyed and frontal-eyed animals. In: Vestibular and oculomotor physiology: international meeting of the Barany Society, Cohen, B. (ed.), New York Academy of Sciences, v. 374, New York, 1981.

Simpson, J.I., Rudinger, D., Reisine, H. and Henn, V. Geometry of extraocular eye muscles and semicircular canals of rhesus monkey. In: Developments in oculomotor research, program of the International Union of Physiological Sciences satellite meeting, p. 53, held July 20-24, 1986, Gleneden Beach, Oregon.

Simpson, J.I., Rudinger, D., Reisine, H. and Henn, V. Geometry of extraocular eye muscles of the rhesus monkey. Soc. Neurosci. Abstr. 12: 1186, 1986.

Stone, L.S. and Lisberger, S.G. Synergistic action of complex and simple spikes in the monkey flocculus in the control of smooth-pursuit eye movements. Exp. Brain Res. Suppl. 17: 299-312, 1989.

Stone, L.S. and Lisberger, S.G. Processing oculomotor information within the monkey cerebellar flocculus. Soc. Neurosci. Abstr. 15: 240, 1989.

Stone, L.S. and Lisberger, S.G. Visual responses of Purkinje cells in the cerebellar flocculus during smooth pursuit eye movements in monkeys. I. Simple spikes. J. Neurophysiol. 63: 1241-1261, 1990.

Stone, L.S. and Lisberger, S.G. Visual responses of Purkinje cells in the cerebellar flocculus during smooth pursuit eye movements in monkeys. II. Complex spikes. J. Neurophysiol. 63: 1262-1275, 1990.

Suzuki, D.A. and Keller, E.L. Visual signals in the dorsolateral pontine nucleus of the alert monkey: their relationship to smooth-pursuit eye

movements. Exp. Brain Res. 53: 473-478, 1984.

Suzuki, D.A., May, J., and Keller, E.L. Smooth-pursuit eye movement deficits with pharmacological lesions in monkey dorsolateral pontine nucleus. Soc. Neurosci. Abstr. 10: 58, 1984.

Suzuki, D.A. and Keller, E.L. The role of the posterior vermis of monkey cerebellum in smooth-pursuit eye movement control. I. Eye and head movement related activity. J. Neurophysiol. 59: 1-18, 1988a.

Suzuki, D.A. and Keller, E.L. The role of the posterior vermis of monkey cerebellum in smooth-pursuit eye movement control. II. Target velocity related Purkinje cell activity. J. Neurophysiol. 59: 19-40, 1988b.

Szentagothai, J. The elementary vestibulo-ocular reflex arc. J. Neurophysiol. 13: 395-407, 1950.

Takemori, S. and Cohen, B. Loss of visual suppression of vestibular nystagmus after floccular lesions. Brain Res. 72: 213-224, 1974.

Their, P., Koehler, W., and Buettner, U.W. Neuronal activity in the dorsolateral pontine nucleus of the alert monkey modulated by visual stimuli and eye movements. Exp. Brain Res. 70: 496-512, 1988.

Tychsen, L. and Lisberger, S.G. Visual motion processing for initiation of smooth pursuit eye movements in humans. J. Neurophysiol. 56: 953-968, 1986.

Ungerleider, L.G., Desimone, R., Galkin, T.W., and Mishkin, M. Subcortical projections of area MT in the macaque. J. Comp. Neurol. 188: 347-366, 1984.

Voogd, J., Gerrits, N.M. and Hess, D.T. Parasagittal zonation of the cerebellum in macaques: an analysis based on acetylcholinesterase histochemistry. In: Cerebellum and neuronal plasticity, Glickstein, M., Yeo C., and Stein, J. (eds.), Plenum, 1987.

Waespe, W. and Henn, V. Visual-vestibular interaction in the flocculus of the alert monkey. Exp. Brain Res. 43: 349-360, 1981.

Waespe, W. and Henn, V. The primate flocculus in visual-vestibular interactions: conceptual, neurophysiological, and anatomical problems. In: Cerebellar functions, pp. 109-125, Bloedel et al. (eds.), Springer-Verlag, Berlin, 1984.

Waespe, W., Buttner, U., and Henn, V. Visual-vestibular interaction in the flocculus of the alert monkey. Exp. Brain Res. 43: 337-348, 1981.

Waespe, W., Rudinger, D., and Wolfensberger, M. Purkinje cell activity in the flocculus of vestibular neurectomized and normal monkeys during optokinetic nystagmus (OKN) and smooth pursuit eye movements. Exp. Brain Res. 60: 243-260, 1985.

Watson, A.B., and Ahumada, A.J.Jr. Model of human visual-motion sensing. J. Opt. Soc. Am. 2: 322-342, 1985.

Westheimer, G. and Blair, S.M. Oculomotor deficits in cerebellectomized monkeys. Invest. Opthalmol. 12: 618-621, 1973.

Westheimer, G. and Blair, S.M. Unit activity in accessory optic system in alert monkeys. Invest. Opthalmol. 13:533-534, 1974.

Wurtz, R.H. Visual receptive fields of striate cortex neurons in awake monkeys. J. Neurophysiol. 32: 727-742, 1969.

Yamada, J. and Noda, H. Afferent and efferent connnections of the oculomotor cerebellar vermis in macaque monkey. J. Comp. Neurol. 265: 224-241, 1987.

Young, L.R. A sampled data model for eye tracking movements. Dept. Aeronautics and Astronautics, MIT, 1962.

Young, L.R., Forster, J.D, and Van Houtte, N. A revised stochastic sampled data model for eye tracking movements. Fourth Ann NASA - University

conference on manual control, University of Michigan, Ann Arbor, Michigan, 1968.

Young, L.R. Pursuit eye movements. In: Bach-y-Rita P., Collins, C.C., Hyde, J.E. (eds) Control of eye movements. Academic Press, New York, pp. 429-443, 1971.

Zee, F.D., Yamazaki, A., Butler, P.H., and Gucer, G. Effects of ablation of the flocculus and paraflocculus on eye movements in the primate. J. Neurophysiol. 46: 878-899, 1981.

Zipser, D. and Anderson, R.A. A back-propagation programmed network that simulates response properties of a subset of posterior parietal neurons. Nature 331: 679-684, 1988.

Zipser, D. and Anderson, R.A. The role of the teacher in learning-based models of parietal area 7a. Brain Res. Bull. 21: 505-512, 1988.

FCC 82-2

ARCHIVE

FOR REFERENCE

NOT TO BE TAKEN FROM THE ROOM

CAT. NO. 23 012

PRINTED IN U.S.A.